

Interaction Processes
and Statistical Properties
of the Propagation of Cosmic Rays
in Photon Backgrounds

Inaugural-Dissertation
zur Erlangung der Doktorwürde
der Hohen Mathematisch-Naturwissenschaftlichen Fakultät
der Rheinischen Friedrich-Wilhelms-Universität
zu Bonn

vorgelegt von
Jörg Paul Rachen
aus Aldenhoven

Bonn 1996

Angefertigt mit Genehmigung der
Mathematisch-Naturwissenschaftlichen Fakultät der Universität Bonn
am Max-Planck-Institut für Radioastronomie, Bonn

1. Referent: Prof. Dr. P.L. Biermann
2. Referent: Prof. Dr. H.-J. Fahr

Termine der mündlichen Prüfungen:

- Philosophie: 6. September 1996
- Astronomie: 11. September 1996

Vorwort

Diese Arbeit behandelt die physikalischen und mathematischen Grundlagen eines Gebiets, das zum gegenwärtigen Zeitpunkt in Deutschland leider einen sehr schweren Stand hat. Man kann es im engeren Sinne als die *Astrophysik kosmischer Strahlung*, im weiteren Sinne aber auch als *hadronische Hochenergie-Astrophysik* bezeichnen. Während diesem Gebiet, das in erster Linie im Grenzbereich von Hochenergie-Astrophysik, Elementarteilchenphysik und Kernphysik angesiedelt ist, fast überall in der Welt zunehmend Beachtung geschenkt wird, insbesondere in den USA und Japan, fristet es hierzulande noch ein Schattendasein. Dies mag zwei Gründe haben: Der erste ist vielleicht der wissenschaftliche Konservatismus in diesem Land, d.h. die generelle Vorsicht gegenüber allem, was neu und ungewohnt ist; der zweite ist mit ziemlicher Sicherheit die "Sättigung", die durch die scheinbar uneingeschränkte Förderung wissenschaftlicher Mammutprojekte besteht, sowohl in theoretischer als auch in experimenteller Hinsicht. Großprojekte wie *HERA*, *LEP-II* oder der geplante *LHC* geben der Elementarteilchenphysik die Gewißheit, in den nächsten Jahrzehnten in der gewohnten Weise fortfahren und noch viele neue Erkenntnisse gewinnen zu können, und in der Astrophysik sonnt man sich noch im Licht erfolgreicher Satellitenmissionen wie *ROSAT* oder *Compton-GRO*, die so viele neue Phänomene zu Tage förderten, deren Interpretation auch die Theoretiker noch lange beschäftigen kann. In einem solch sonnigen Klima ist, verständlicherweise, für andere Ansätze oder gar "revolutionäre" Ideen wenig Platz.

In den USA dagegen wurde spätestens auf dem APS Treffen in Snowmass 1994 klar, daß sich das Blatt dort gewendet hat: Die geplatzten Träume elementarteilchenphysikalischer Gigantomie (kurz: die Streichung des SSC durch den amerikanischen Kongreß), haben eine Aufbruchstimmung erzeugt, die sich nun in einem verstärkten Interesse an beobachtbaren, teilchenphysikalischen Phänomenen im Universum äußert. Das *Auger-Projekt* zur Beobachtung kosmischer Strahlung bei höchsten Energien, das zur Zeit immer mehr an Struktur gewinnt, und bezeichnenderweise gerade von dem renommierten "Beschleuniger-Institut" *Fermilab* in Chicago propagiert wird, ist sicher nur eine der Konsequenzen dieser Tatsache.

Diese Arbeit wurde, sowohl in ihrer Anfertigung als auch in ihrer Konsequenz, stark von diesen unterschiedlichen Einschätzungen des behandelten Gebietes geprägt. Da eine Förderung des eigentlichen Themas dieser Dissertation in Deutschland nicht möglich war, konnte ich sie nur unter Inkaufnahme einer zeitaufwändigen (wenn auch nicht uninteressanten) Nebentätigkeit in einem "anerkannten" Gebiet der Astronomie und Astrophysik, sowie im Rahmen eines achtmonatigen Auslandsstipendiums in den USA anfertigen; nicht überraschend führt sie mich nun in auch wieder die USA zurück. Es ist daher nur konsequent, daß sie durchgehend in *englischer Sprache* abgefaßt ist; ich sehe diese Arbeit als ein, hoffentlich nützliches, Hilfsmittel für die zukünftige hadronische Hochenergie-Astrophysik an, und es sollte daher für diejenigen gefertigt sein, die es mitunter auch benutzen wollen. Nicht zuletzt sind damit auch meine Betreuer in den USA, Prof. Todor Stanev und Prof. Tom Gaisser gemeint, die hier gleichberechtigt neben den eigentlichen Referenten dieser Dissertation genannt werden sollen.

Jörg Rachen, Bonn, August 1996

Contents

Introduction	3
Cosmic ray physics and astrophysics	3
High energy astronomy and radiative processes	4
Hadronic radiation processes as a new task for cosmic ray physics	5
A basic toolkit for photonuclear and photohadronic astrophysics	6
1 Photonuclear interactions	7
1.1 Photonuclear reactions in astrophysics	8
1.1.1 Classification and basic concepts	8
1.1.1.1 Coherent and incoherent interactions	8
1.1.1.2 Interaction of charged particles with electromagnetic fields	10
1.1.1.3 Large scale magnetic scattering	12
1.1.2 Coherent electromagnetic processes	16
1.1.2.1 Inverse Compton scattering	16
1.1.2.2 Synchrotron Radiation	17
1.1.2.3 Inverse pair production	18
1.1.3 Incoherent reactions	22
1.1.3.1 Resonances	22
1.1.3.2 The substructure of the interaction system	24
1.1.3.3 The phenomenological approach to high energy interactions	25
1.2 Photomeson production at free nucleons	32
1.2.1 Basic physics of photohadronic interactions	32
1.2.1.1 Classification of final states	32
1.2.1.2 Resonances and direct scattering	34
1.2.1.3 Final state angular distributions and branching ratios	37
1.2.1.4 Kinematics	40
1.2.2 Astrophysical application of photomeson production	44
1.2.2.1 The role of photomeson production in astrophysics	44
1.2.2.2 Classification of energy regions in the NRF	45
1.2.2.3 Cross section fits	46
1.2.2.4 Efficiency functions and hadronic radiation processes	52
1.3 Photodisintegration of nuclei	59
1.3.1 Low energy nuclear reactions	59
1.3.1.1 Binding energy and shell structure	59
1.3.1.2 Electromagnetic excitation of nuclei	62
1.3.1.3 Statistics of nucleon emission	64
1.3.2 High energy nuclear reactions	66
1.3.2.1 Nuclear fragmentation and the abrasion-ablation approximation	66
1.3.2.2 High energy interactions of photons and nucleons	69

1.3.3	Photodisintegration processes	71
1.3.3.1	Photon absorption by bound nucleons	71
1.3.3.2	The giant dipole resonance	73
1.3.3.3	The quasi-deuteron process	74
1.3.3.4	Photodisintegration in the baryon resonance region and beyond	77
1.3.4	Photodisintegration of cosmic ray nuclei	79
1.3.4.1	Inverse photodisintegration in astrophysics	79
1.3.4.2	Photodisintegration cross sections of light nuclei	81
1.3.4.3	Photodisintegration yield functions in the mass scaling regime	84
1.3.4.4	Total efficiency and astrophysical applications	88
2	Statistics of cosmic ray interactions	95
2.1	Notes on probability theory and Markov chains	96
2.1.1	Probability distribution functions	96
2.1.1.1	Random variables and distributions	96
2.1.1.2	Generating functions and the cumulants	99
2.1.1.3	Some special distributions	101
2.1.1.4	Operational definition of distributions	106
2.1.2	Multidimensional probability spaces and joint distributions	108
2.1.2.1	Uncorrelated random variables and the probability space	108
2.1.2.2	Random vectors and probability propagation	110
2.1.2.3	Markov chains with independent increments	113
2.1.2.4	Asymptotic expansion of compound distributions	115
2.1.2.5	Products of distributions	117
2.2	The point process approach to cosmic ray transport	121
2.2.1	Random point processes	121
2.2.1.1	Definition and classification of point processes	121
2.2.1.2	Markov processes	122
2.2.1.3	Counting processes	124
2.2.1.4	Marked point processes	126
2.2.2	Random processes and particle transport	129
2.2.2.1	Transport theory: the physical language of random processes	129
2.2.2.2	Classification of transport processes	131
2.2.2.3	Simplified approaches to cosmic ray transport	134
2.2.2.4	Cosmic ray transport as a marked point process	138
	Outlook — no Conclusion	141
	Contemplations about life, the universe and everything	141
	About life: writing and finishing PhD theses	141
	About the universe: the hot questions of cosmic ray astrophysics	141
	About everything: here in particular about the way of science	143
	List of publications	145
	References	146

Introduction

Cosmic ray physics and astrophysics

When VICTOR HESS discovered the *Höhenstrahlung*¹ in 1911, he was not looking for cosmic phenomena — he was investigating the ionization of the atmosphere, and realized that the degree of ionization increases with altitude. Quickly it became clear that Hess' discovery must be connected to a radiation of cosmic origin, and the term *cosmic rays* was introduced. Nevertheless, the following investigation of this radiation was mainly motivated by the properties of the *radiation itself* — *cosmic ray physics* marked the starting point of experimental elementary particle physics, which made use of cosmic rays as a natural laboratory to investigate the structure of matter. Later, when particle accelerators had been built, and thus a technical source of high energy particles was available, the interest in cosmic rays moved to continually increasing energies, which were not yet accessible by accelerators. Since the cosmic ray flux decreases strongly with energy, a direct detection of the radiation was no longer possible, and the physicists started to investigate particle *air showers* induced by primary cosmic rays. Again, understanding the physics of these air showers was the main task, and a very interesting subject by itself. Today, air shower experiments cover detector areas of up to 100 km², and use extraordinary detection techniques like atmospheric scintillation to observe cosmic rays in the atmosphere up to a few hundred EeV [Sok89] — the highest energy event ever detected had an energy of 51 Joule, comparable to a full bottle of water smashing on the ground. The interaction energies involved in the primary collision of such a particle with an atmospheric nucleus is far beyond the limits of experimental particle physics, and so the investigation of the highest energy cosmic rays can still bring new insights in the structure of matter. Recently, physicists started to plan a giant air shower array, called the *Pierre Auger Project*, which proposes to observe many more events of this kind. But, all in all, we may state that the main interest of most physicists investigating cosmic rays is directed to the *atmospheric phenomenon* of cosmic ray interactions, giving a late justification to Hess' term “Höhenstrahlung”, which is still officially used in the German linguistic area.

Clearly, there has always been the question on the origin of cosmic rays; the research for cosmic ray sources may be called *cosmic ray astrophysics*, and is certainly one of the most speculative branches of astrophysics. The reason can be found in the property of cosmic rays to consist of *charged particles*, which do not contain any information about their origin since they are deflected in ambient magnetic fields. Thus, there is no possibility for a *cosmic ray astronomy*, which opens the field of cosmic ray astrophysics to all kind of speculations: whenever other branches of astronomy discovered new, enigmatic objects with extraordinary features — whether it were quasars, pulsars or, most recently, gamma-ray bursts, or whenever theoreticians invented new speculative objects which may inhabit the universe — magnetic monopoles, cosmic strings, anti-matter worlds or wormholes; there have always been models quickly by hand which connect them to the origin of cosmic rays, in particular of the cosmic rays at the highest (and thus most enigmatic) energies. The theoreticians proposing such models are on the safe side — it is not so easy for an experimentalist to prove their predictions wrong, because cosmic rays

¹ “High-altitude radiation”

contain so little information about their origin. While some theoreticians may consider this as a strength of their theories, it is in fact an awful weakness: To speak in POPPER'S terms about scientific testability [Pop94], we may even come to the radical conclusion that the whole field of cosmic ray *astrophysics* should be subsumed under the subject of *metaphysics* rather than physics, because the predictions derived from it can hardly be falsified by experiment; they have no empirical predictability.

Clearly, the situation is not quite as radical; there have been theories developed to explain the origin of cosmic rays which have got a strong impact on other physical and astrophysical branches. FERMI'S theory of stochastic acceleration and its application in the theory of diffusive shock acceleration may be considered as benchmarks here. They are meanwhile successfully used to explain not only the origin of cosmic rays, but also many heliospheric phenomena as well as the radio spectra of supernovae and extragalactic jets. It is funny to note that these theories, if they are applied to cosmic rays, predict that the highest energy particles are more likely to be produced in the *largest*, and thus probably least spectacular objects, in contrast to the common connection to compact energetic objects. Of course, shock acceleration and powerful compact objects do not exclude, but rather complement each other; we just have to keep in mind that the most compact objects are *in this picture* less likely to be the sources of the highest energy cosmic rays. The theory of shock acceleration has established the connection of cosmic ray physics to observational astronomy, mainly to radio astronomy; nevertheless, the cosmic rays themselves are still unobservable inside their putative sources, so the speculative smell is not quite removed. This problem is probably responsible for the fact that cosmic ray astrophysics has been kept a relatively small field compared to other branches of astrophysics, which are closer connected to direct observational astronomy.

High energy astronomy and radiative processes

When the first X-ray imaging satellite, *Uhuru*, was launched in late 1970 and discovered a plenty of point sources of energetic radiation in the sky, the new field of *high energy astronomy* was born. Only a few years later, the *COS-B* satellite extended the energy range into the MeV gamma-ray regime. Energetic photons, formerly connected to cosmic rays in the widest sense, have been drawn into their own life as carrier of astronomical information, which allow for a direct observation of their sources. Exploring higher and higher photon energies with imaging telescopes may be considered as the main task of contemporary astronomy: *ROSAT* shifted X-ray astronomy onto a level of spatial and spectral resolution almost comparable to optical astronomy, and the *Compton-GRO* observatory opened the field of high precision imaging astronomy to the GeV gamma-ray energy range. The energetic front line of imaging astronomy is now constituted by atmospheric Cherenkov telescopes, which are about to explore the TeV sky. The recent discovery of the quasar Mkn421 by *HEGRA*, at photon energies above 1 TeV, may be considered as the preliminary summit of this development [PBK⁺96].

When the first images of the high energy sky were taken, radiative processes of energetic particles did already play a role in astrophysics, because of their elementary connection to radio astronomy; radio emission was found to be mostly of non-thermal origin, and explained as synchrotron radiation from energetic electrons in magnetic fields. It was therefore natural to try to explain the X-ray emission of astrophysical objects by similar processes, namely the interaction of energetic electron and positron populations with ambient magnetic fields and photons. The application of *synchrotron-self-inverse-Compton models* to the known sites of energetic radiation has been quite successful, so there seemed to be no need to consider possible contributions of other high energy processes. It was quickly realized, however, that the existence of cosmic rays in sources of energetic radiation can have a strong impact on their electromagnetic spectrum, because they provide a *unique* process producing gamma radiation: the production and subsequent decay of mesons in photonuclear or internuclear collisions. The impact of such *hadronic radiation processes* has to be considered as increasing with gamma-ray

energy; while they are generally neglected in most models of X-ray origin, and controversially discussed in GeV gamma-ray astronomy, the observations of TeV gamma-ray sources might set a clear case that at least not *all* energetic radiation observed in cosmic sources is of “conventional” leptonic origin; it may even be assumed that *most* of it is not.

Hadronic radiation processes as a new task for cosmic ray physics

If cosmic rays are responsible for the energetic radiation from compact objects, our rather pessimistic view on cosmic ray astrophysics changes drastically: We may now consider the *observable cosmic rays* only as the small tip of a much bigger iceberg, whose underwater part is called *hadronic radiation processes*. If we succeed to establish the connection of cosmic ray physics to GeV and TeV gamma-ray astronomy, also the models for the directly observable cosmic rays lose their “metaphysical” character — because we now have methods to *observe* cosmic ray sources at least indirectly through the secondary radiation. When we emphasize the connection to gamma-ray astronomy, we should not forget that there is another particle principally allowing for imaging astronomy — the *neutrino*, which can *only* be produced in hadronic interaction processes. The only astronomical sources of neutrinos discovered so far are the sun and the supernova 1987a — but there is no prophet needed to predict that imaging *neutrino astronomy* might be one of the frontiers of physics and astrophysics in the next century; the first experiments are already under construction.

However, entering the field of “exact” astrophysics and precise astronomical data also means some changes for the *methodology* of cosmic ray astrophysics. In the more or less qualitative discussion of cosmic ray observations and their possible astrophysical explanation, it is often sufficient to argue on a very rough level — the motto to discuss physical processes of cosmic rays may be stated as: “One process, one threshold, one cross section”. This is good for order of magnitude estimates, and this is what cosmic ray physicists mostly did so far. But considering the competition to the theoretically highly developed “conventional” methods in high energy astrophysics, we feel that it is not good enough for the new tasks we are confronted with. Clearly, the basic physics of cosmic ray interactions is well known; most interactions happen at energies which are already well explored by accelerator experiments. This is in particular true when we consider that in most astrophysical environments cosmic rays interact dominantly with low energy photons, which are the most abundant “particles” in the universe. The task is rather, to bring this physics into a useful form for the astrophysical application, which is exact enough to produce quantitatively reliable results, and simple enough to be used in analytical or semi-analytical² calculations; it may be considered as one of the main drawbacks of hadronic astrophysics so far, that almost all quantitatively serious calculations are performed on a highly numerical basis, which makes them difficult to communicate and give only a small scope to apply results known for one special case to other, similar cases.

But not only the physical foundations, also the mathematical methods to describe the evolution of spectra have to be reconsidered; cosmic rays which are subject to interactions develop essentially discontinuously in their energy, which does not allow the conventional diffusion or continuous energy loss approximations, as frequently used in astrophysical transport theory. The transport of cosmic rays can only be described by considering the full *Ginzburg-Syrovatskii-equation* [GS64, HS85], which is the appropriate form of the *Boltzmann equation* for cosmic ray physics. To bring this integro-differential equation into a form which allows a treatment by semi-analytical methods may be considered as one of the main mathematical tasks in cosmic ray physics. So far, detailed transport calculations of cosmic rays have been performed only numerical, mostly using Monte-Carlo methods.

²With *semi-analytical* we mean the reduction to ordinary differential equations, which can be solved by standard numerical methods.

A basic toolkit for photonuclear and photohadronic astrophysics

In this work, we propose to take a step towards a more detailed treatment of cosmic ray induced processes and cosmic ray transport. We will restrict ourselves to the discussion of *cosmic ray transport in photon backgrounds*. This restriction is justified because internuclear reactions are (i) less important in most astrophysical situations (ii) much better investigated because of their connection to the cosmic ray physics in the atmosphere (see, e.g. [Hay69]). The work is divided into two main parts:

1. A thorough discussion of the basic physics of photonuclear interactions, and the development of parametrized representations for the astrophysical application.
2. A mathematical discussion of cosmic ray transport, based on the theory of Markov point processes.

These two parts seem to be fairly independent; but in fact they are closely connected. The detailed treatment of particle physics in Sect. 1.2 is not only done for the application to hadronic radiation processes, but also in front of a more detailed treatment of cosmic ray transport. One of the largest parts of this work is dedicated to the discussions of the interactions of complex cosmic ray nuclei with photon backgrounds; there has been only one relevant astrophysical paper on this subject presenting numerical results so far [PSB76], and an improvement of the situation is highly desirable. The extensive introduction into basic statistics in Sect. 2.1 should be considered not only with respect to the following discussion of point processes and transport theory, but also as a guide to a somewhat more precise use of statistics in cosmic ray astrophysics generally — which we found to be necessary in particular in view of the discussion about the highest energy events.

It is the main line of this work to connect the astrophysical tools we develop here to their physical and mathematical foundations; therefore we give a brief discussion of all the relevant methods of particle physics, nuclear physics and statistics we have made use of. The suffering part of this physical and mathematical completeness is clearly the astrophysics itself: the reader may miss some direct applications, some answers on the “hot” questions of contemporary astrophysics. But noting that the extent of this work *already* exceeds that of a usual PhD thesis, and that there are currently *so many* hot questions in this field, we have decided to restrict the scope of this work to the development of the tools: their application has to follow in subsequent work. To prevent that the astrophysical connection gets lost completely, we have “spiced” the work with some numerical examples which are — not accidentally — always somehow connected to a direct astrophysical application. A more thorough treatment is generally necessary, but also straightforward using the toolkit developed here.

Chapter 1

Photonuclear interactions

Photons are the most abundant “particles” in the universe, even though their energy content in the present universe is negligible; this means that most dense astrophysical photon fields contain low energy photons, strongly decreasing in density to higher photon energies. Therefore, high energy photonuclear reactions find an application in astrophysics mostly when considering *inverse reactions*, where an energetic nucleus interacts with low energy photon fields. Moreover, when comparing different photonuclear processes, the low energy processes are generally more important than the high energy processes, because they happen more often. Thus, the emphasis set by astrophysicists considering photonuclear reactions is somewhat different from that set by most nuclear and particle physicists, who are more interested in high energy reactions to investigate the structure of matter.

Photonuclear reactions can essentially be divided into two parts: (i) coherent electromagnetic interactions and (ii) incoherent interactions of photons with the nuclear structure. In the first kind of processes, the nucleus just acts as a classical charge, and the results are merely charge and mass scalings of the corresponding physics for electrons. In the second, the substructure of the nucleus is essential, and the typical and distinct features of hadronic and nuclear astrophysics show up. For complex nuclei, the lowest energy incoherent interaction is the removal of single nucleons out of the nuclear unit, which is called *photodisintegration*. The nucleons itself can interact incoherently with photons of energies comparable to the mesonic mass scale, leading to *photomeson production*. The latter process is more important in astrophysics because of the high abundance of hydrogen nuclei, i.e. protons, in the universe. However, in specific contexts complex nuclei can play an important role, so that a detailed treatment of photodisintegration is required.

In this chapter, we will give an outline of photonuclear interactions, in view of their astrophysical application. Sect. 1.1 presents the basic astrophysical approaches to particle transport, including the coherent reactions which can be treated without reference to the nuclear structure. Sect. 1.2 describes the physics of photomeson production in great detail, with the aim to give a useful parametrization of all relevant processes. Sect. 1.3 gives a description of the photodisintegration of complex nuclei in terms of a parametric approach, allowing to treat the subsequent photodisintegration of nuclei as the evolution of *one* particle with variable mass number A .

1.1 Photonuclear reactions in astrophysics

In this section, the basic astrophysical concepts of particle transport are presented. We classify photonuclear interactions and describe the most basic reaction types, which do not refer to the nuclear structure. We subsume the general reaction of charges with electromagnetic fields under the topic of photonuclear interactions, by means of the virtual photon concept (Sect. 1.1.1 and Sect. 1.1.2). In Sect. 1.1.3 we give a brief outline of the basics of incoherent reactions and present a concept for the treatment of nuclear transport phenomena, which allows to describe the relevant physical quantities by parametrization functions developed from simple models and experimental data in nuclear and particle physics. We call this the *phenomenological approach to cosmic ray transport*.

Throughout this section, references are only given when we refer to special models or ideas; the general concepts presented here can be found in the books of JACKSON [Jac75], and RYBICKY & LIGHTMAN [RL79]. For details on QED processes we refer to JAUCH & ROHRLICH [JR76].

Notation: In this and the following sections, we distinguish between quantities given in the laboratory frame (LF: unmarked symbols), the nuclear rest frame (NRF: dashed symbols) and the center of momentum frame (CMF: symbols marked with an asterisk) of an interaction. We use the symbols “ $\underline{\quad}$ ” and “ $\underline{\quad}^*$ ” to mark equations referring explicitly to the NRF or the CMF, respectively. General symbols introduced here and used subsequently in this meaning are: cosmic ray Lorentz factor in the LF, γ_{CR} ; nucleon mass, \hat{m} ; nuclear charge, Z , and mass number, A . In vector equations, we write the scalar product as $\mathbf{x} \cdot \mathbf{y}$ and the vector product as $\mathbf{x} \times \mathbf{y}$; the symbol \times is also used as a simple multiplication sign when writing numbers in scientific notation; this should not cause any confusion. The same applies to the symbol c , which is used as a symbolic index variable for “reaction channel”, and in formulae of course in its common meaning of the velocity of light. Units, or numbers with units, are generally enclosed in square brackets when occurring in displayed equations, to avoid confusion with physical symbols.

1.1.1 Classification and basic concepts

1.1.1.1 Coherent and incoherent interactions

Nuclear structure and energy scales: Seen from a distance, the atomic nucleus is just a massive point charge, and the photon is just the quantized representation of an electromagnetic wave, which can be treated in the classical way of electrodynamics — quantum-effects may occur as correction in the formulae. Going closer, the essential quantum-electrodynamical (QED) structure of the photon shows up; it is no longer just a electromagnetic wave, but a cloud of virtual particles, which can themselves interact with the nucleus, resulting in the production of real electron-positron pairs. On the same scale, the nucleus reveals its inner structure of nucleons, which are themselves charged particles; the nucleus no longer behaves like a point charge, but like a system of point charges, which can absorb the photon while transforming to an excited state. On smaller scales, the single nucleons themselves can be excited, and baryonic resonances occur. Proceeding to still smaller scales, the electromagnetic picture breaks down altogether: the photon reveals a virtual hadronic core, and can therefore undergo strong interactions with the quark-gluon structure of the nucleons. On this quantum-chromodynamical (QCD) scale, the photon behaves like a superposition of mesons carrying the same quantum numbers as the photon, which are called *vector mesons*; one speaks about the *hadronic photon* [BSYP78].

To quantify those different scales of photonuclear interactions, it is more convenient to use a scale of energy rather than size. In the rest system of the nucleus, the QED structure of the photon becomes important for a photon energy $\epsilon > 2m_e c^2 \sim 1 \text{ MeV}$. The structure of the nucleus becomes important for energies larger than the average nucleon binding energy, $\epsilon \gtrsim 8 \text{ MeV}$. The QCD structure of the nucleons shows up for photon energies in the mesonic mass scale, $\epsilon \gtrsim 140 \text{ MeV}$, while the hadronic structure of the photon starts to dominate above $\epsilon \sim 1 \text{ GeV}$. For larger energies, photonuclear interactions become very similar to other hadronic interactions, and we may therefore apply results derived from interactions between nuclei as well. For energies below all these thresholds, $\epsilon < 1 \text{ MeV}$, we can treat the nucleus as an ordinary electric point charge.

With respect to the behavior of the nucleus, we may distinguish two groups of interactions: The first are *coherent interactions*, in which the nucleus interacts as a whole, the second are *incoherent interactions*, where the photon interacts with parts of the nuclear structure. This classification is independent of the appearance of the photon; elastic photon scattering is of course a coherent interaction, but the QED process of Bethe-Heitler pair production is as well. Even the so-called diffractive production of vector mesons, clearly a QCD process, is coherent with respect to the interaction nucleon, and at high energies even with respect to the whole nucleus. On the other hand, the incoherent giant dipole resonance excitation of heavy nuclei is a classical electrodynamical process, and baryon resonance excitation can be understood without referring to the QED or QCD structure of the photon. Generally, we will find that the *momentum transfer* in the interaction is the relevant quantity to distinguish coherent and incoherent interactions; coherent interactions correspond to momentum transfers smaller than the energy scale on which the system can be excited.

Inverse photonuclear scattering: In most experimental setups, an energetic photon collides with a nucleus at rest, therefore most data are parameterized with the photon energy ϵ' *nuclear rest frame* (NRF). The total energy of the system in the *center of momentum frame* (CMF) is generally expressed in the quantity

$$s = M_{\text{int}}^2 c^4 = m^2 c^4 + 2mc^2 \epsilon' , \quad (1.1.1)$$

where M_{int} can be called the total mass of the interaction. The energy amount available for secondary reaction products, or the total kinetic interaction energy, is thus

$$E_{\text{kin}}^* = M_{\text{kin}} c^2 = \sqrt{s} - mc^2 \approx (1 - 2x) \epsilon' + O(x^2) \quad (1.1.2)$$

with $x = \epsilon'/mc^2$, giving $E_{\text{kin}}^* \sim \epsilon'$ for $\epsilon' \ll mc^2$. We can therefore take the NRF photon energy ϵ' as the relevant energy scale for the interaction. In cosmic ray astrophysics we have the situation that an energetic nucleus interacts with low energy photons or electromagnetic fields. So, in the astrophysical *laboratory frame* (LF) we have a nucleus with Lorentz factor $\gamma_{\text{CR}} \gg 1$ colliding with a photon of energy ϵ . Because of the Lorentz boost the photon energy seen in the NRF is $\epsilon' \sim \gamma_{\text{CR}} \epsilon$; low energy photons therefore appear as high energy gamma rays for the cosmic ray nucleus, and may therefore induce high energy interactions.

In nuclear and particle physics, photonuclear interactions are investigated to gain knowledge about the structure of matter. Therefore, emphasis is given to the detailed description of the *exclusive* differential cross sections of specific interaction channels. In cosmic ray astrophysics, the point of interest is the energy emitted from the nucleus in the LF in form of particles or radiation. In classical electrodynamics, this is given by the power P_{rad} emitted in form of radiation from the particle. With a more general understanding of “radiation”, this term may also be used if heavy particles are emitted. From the point of view of two-particle interaction physics, the only relevant quantities determining P_{rad} are the total cross section σ and the average CMF scattering angle $\langle \chi^* \rangle$. We will discuss the classical and the interaction approach in more detail in the next section.

To compare radiation loss processes among themselves and with other processes determining an astrophysical system, the *radiation time scale*

$$\tau_{\text{rad}} = \frac{E}{P_{\text{rad}}} \quad (1.1.3)$$

is introduced; τ_{rad} is the time over which the particle suffers a considerable energy loss, and it may be compared to other time scales, e.g. the lifetime of a system under consideration. For intergalactic particle transport over cosmological scales, the comparison of τ_{rad} with the Hubble time $\tau_h = 1/H_0$ can give a first idea whether a process is relevant or can be neglected. In systems where particles are accelerated, the acceleration time τ_{acc} can be defined similarly to Eq. (1.1.3), and the comparison of τ_{acc} and τ_{rad} generally gives a first idea about the limiting energy of an acceleration process.

1.1.1.2 Interaction of charged particles with electromagnetic fields

Relativistic dipole radiation: In classical electrodynamics, any accelerated charge emits radiation, mainly *electric dipole radiation*. In an electromagnetic field, (\mathbf{E}, \mathbf{B}) , the total power emitted by dipole radiation of a particle with charge e and mass m , moving with a relativistic velocity $\beta_{\text{CR}} = \mathbf{v}/c$ is given by

$$P_{\text{rad}} = \frac{2e^4\gamma_{\text{CR}}^2}{3m^2c^3} \left\{ (\mathbf{E} + \beta_{\text{CR}} \times \mathbf{B})^2 - (\beta_{\text{CR}} \cdot \mathbf{E})^2 \right\} . \quad (1.1.4a)$$

If we split the \mathbf{E} and \mathbf{B} vectors in components parallel and perpendicular to β_{CR} , and introduce the partial energy densities $U_{\mathbf{E}} = \mathbf{E}^2/8\pi$ and $U_{\perp} = (\mathbf{E}_{\perp}^2 + \mathbf{B}_{\perp}^2)/8\pi$, we can rewrite this equation as

$$P_{\text{rad}} = \frac{16\pi e^4}{3m^2c^3} \left\{ U_{\mathbf{E}} + \gamma_{\text{CR}}^2 \left(\beta^2 U_{\perp} + 2\mathbf{E}_{\perp} \cdot (\beta_{\text{CR}} \times \mathbf{B}_{\perp}) \right) \right\} , \quad (1.1.4b)$$

which shows more clearly the influence of the particles motion: The electrostatic acceleration or deceleration power $P_{\text{stat}} = e[\mathbf{E} \cdot \mathbf{v}]$ causes a radiation loss P_{rad} independent of β_{CR} , which is however, unimportant compared to the P_{stat} for all realistic field strengths and particle velocities. For highly relativistic particles ($\gamma_{\text{CR}} \gg 1$), the second component dominates the radiation loss with $P_{\text{rad}} \propto \gamma_{\text{CR}}^2$; for arbitrary field configurations, there is no simple connection of P_{rad} to the energy density of the perpendicular field component U_{\perp} because of the orientation term $\mathbf{E}_{\perp} \cdot (\beta_{\text{CR}} \times \mathbf{B}_{\perp})$; for $\beta_{\text{CR}} \times \mathbf{B}_{\perp} = -\mathbf{E}_{\perp}$ and $\mathbf{E}_{\parallel} = 0$ we even have $P_{\text{rad}} = 0$, i.e. the particle moves without energy loss. This configuration corresponds to the situation where an ultrarelativistic particle ($\beta = 1$) moves *with* an electromagnetic wave in the same direction.

Thomson scattering: Another manifestation of dipole radiation is the scattering of a classical electromagnetic wave a charged particle. The particle, oscillating with the frequency ω_0 of the wave, emits in its rest system dipole radiation into a solid angle element $d\Omega = (\sin \theta d\theta d\varphi)$ with

$$\frac{dP_s}{d\Omega} = \frac{cE_0^2}{8\pi} \frac{d\sigma_{\text{T}}}{d\Omega} = \frac{e^4 E_0^2}{8\pi m^2 c^3} \sin^2 \theta , \quad (1.1.5)$$

where E_0 is the amplitude of the wave. Integrating over solid angle yields

$$\sigma_{\text{T}} = \frac{8\pi}{3} \frac{e^4}{m^2 c^4} , \quad (1.1.5a)$$

which is called the *Thomson cross section* of the particle; for an electron $\sigma_{\text{T}e} \simeq 0.665$ barn and for a proton $\sigma_{\text{T}p} \simeq 0.197 \mu\text{barn}$.¹ For a nucleus of charge Ze and mass $m = A\hat{m}$ we obviously have

$$\sigma_{\text{T}}(A, Z) = \hat{\sigma}_{\text{T}} \frac{Z^4}{A^2} , \quad (1.1.5b)$$

where $\hat{\sigma}_{\text{T}} \approx 0.2 \mu\text{barn}$ is the Thomson cross section per proton in the nucleus; it differs slightly from $\sigma_{\text{T}p}$ due to the mass defect of bound nucleons. Obviously, σ_{T} is independent of the frequency ω_0 of the incoming wave. Since the charge oscillates in resonance with the wave, the frequency of the scattered wave is $\omega = \omega_0$; this is called *Thomson scattering*. Changing to the quantized picture of photon scattering, Thomson scattering

¹In the literature the Thomson cross section is generally defined for an electron, $\sigma_{\text{T}} \equiv \sigma_{\text{T}e}$. However, since we will mostly discuss protons and nuclei, it is helpful to overcome this constraint and define σ_{T} without reference to a specific particle; for electrons and protons we will therefore write $\sigma_{\text{T}e}$ and $\sigma_{\text{T}p}$, respectively.

obviously corresponds to the case of elastic scattering at a rigid scattering center, which means that the energy transfer from the photon to the particle can be neglected. Thus we have $\epsilon_f = \epsilon_i$, but we note that there is still a non vanishing momentum transfer due to the directional change of the photon. The condition of the rigid scattering center can be written as

$$\epsilon'_0 \ll mc^2 \quad (1.1.6)$$

and is called the *Thomson limit*. For $\epsilon'_0 \gtrsim mc^2$, elastic photon-charge scattering cannot be treated as simple Thomson scattering and is generally called *Compton scattering*; for composite particles like protons and nuclei, however, the appearance of incoherent processes in this energy regime is more important than the corrections to the elastic scattering.

In the astrophysical scenario, we will mostly consider charged particles which move with relativistic velocities, $\beta \simeq 1$, and interact with photons of much lower energy $\epsilon_i \ll m\gamma_{\text{CR}}c^2$. Now, the component of the momentum transfer parallel to the direction of motion of the nucleus, $q_{\parallel} = (\epsilon'/c)(1 - \cos\theta)$, transforms into an energy loss in the LF. For the relation between LF and NRF energies of incoming and scattered photons we find

$$\frac{\epsilon'_i}{\epsilon_i} \sim \frac{\epsilon_f}{\epsilon'_f} \sim \gamma_{\text{CR}} \quad \text{and} \quad \epsilon'_i \sim \epsilon'_f \quad (1.1.7)$$

In the Thomson limit, $\epsilon'_i = \epsilon'_f$, one can easily find the expression for the radiated power of the particle, which means here the amount of particle energy per unit time converted into photon energy, as

$$P_{\text{rad}} = c\sigma_{\text{T}}\gamma_{\text{CR}}^2 \int_{4\pi} d\Omega \left[\frac{dU_{\gamma}}{d\Omega} \right] \left\{ \beta^2(1 + \cos^2\theta) - 2\beta \cos\theta \right\} \quad , \quad (1.1.8)$$

where $dU_{\gamma}/d\Omega$ is the differential photon energy density per unit solid angle in the LF. We will discuss the astrophysical consequences of Eq. (1.1.8) in Sect. 1.1.2.1.

The virtual photon concept: A close view on Eqs. (1.1.4b) and (1.1.8) reveals some interesting similarities between the interaction of a relativistic charge with a static electromagnetic field and a photon background. We consider a monochromatic photon beam, i.e. all photons have the same energy ϵ_0 and direction θ_0 relative to the charged particle velocity in the LF, and evaluate Eq. (1.1.8) for the cases $\theta_0 = 0^\circ, 90^\circ$ and 180° . Furthermore, we assume $\gamma_{\text{CR}} \gg 1$, so that the U_{E} term can be neglected in Eq. (1.1.4b). We immediately find the following correspondence with respect to the emerged radiation power between the orientation of a classical (\mathbf{E}, \mathbf{B}) field and an oriented photon beam

$$\theta_0 = 0^\circ \quad \longleftrightarrow \quad |\mathbf{E}_{\perp}| = |\mathbf{B}_{\perp}| \quad \text{and} \quad \mathbf{E}_{\perp} = -\mathbf{e}_{\beta} \times \mathbf{B}_{\perp} \quad (1.1.9a)$$

$$\theta_0 = 90^\circ \quad \longleftrightarrow \quad |\mathbf{E}_{\perp}| = 0 \quad \text{or} \quad |\mathbf{B}_{\perp}| = 0 \quad (1.1.9b)$$

$$\theta_0 = 180^\circ \quad \longleftrightarrow \quad |\mathbf{E}_{\perp}| = |\mathbf{B}_{\perp}| \quad \text{and} \quad \mathbf{E}_{\perp} = \mathbf{e}_{\beta} \times \mathbf{B}_{\perp} \quad , \quad (1.1.9c)$$

if we identify U_{\perp} with U_{γ} . Clearly, this correspondence does not really surprise us, because the special (\mathbf{E}, \mathbf{B}) configurations we have chosen correspond to a classical electromagnetic wave scattering moving in the direction θ_0 . However, also for any other field configuration it will be possible to find a photon distribution $dU_{\gamma}/(d\Omega d\epsilon)$ corresponding to it in the relativistic limit. We also note that, if $\mathbf{E}_{\parallel} = 0$, Eq. (1.1.4b) would *exactly* correspond to Eq. (1.1.8) if we would have defined P_{rad} as the total radiated energy per time including the energy taken from the incoming photons (and not just as the energy of the moving charge converted into radiation).

We can therefore split Eq. (1.1.4b) into a nonrelativistic contribution of a static \mathbf{E} -field and a term expressing the scattering of a photon beam with energy density U_{\perp} , which dominates in the ultrarelativistic limit. The

picture behind it is the QED interpretation of electromagnetic interactions by the exchange of *virtual photons*. The analogy shown here expresses the fact that for the interaction of a relativistic particle with an electromagnetic field, those exchange quanta behave exactly like *real photons*, which are scattered at the charged particle; note that for a pure \mathbf{B} -field this is true for all particle velocities, because $U_{\mathbf{E}}$ vanishes in Eq. (1.1.4b). We therefore can conclude that the Thomson limit and the threshold energies for incoherent reactions apply in the classical case as well. To give an order of magnitude estimate of the virtual photon energy, we may use the inverse Compton scaling relation Eq. (1.1.7): If a certain electromagnetic radiation process leads to the emission of photons of a characteristic frequency ω_c , we can estimate the energy of the scattered virtual photon to be $\epsilon_{\text{virt}} \sim \hbar\omega_c/\gamma_{\text{CR}}$. So, the Thomson limit for this process reads $\hbar\omega_c \ll m\gamma_{\text{CR}}c^2$ — which also expresses the physical limit for the energy of the scattered photon, visualizing that in the LF this is taken almost entirely from the moving charge. For relativistic nuclei, we have already argued that incoherent processes can set in at even lower energies E_{th} , so photodisintegration or pion production in electromagnetic field is possible if $\epsilon_{\text{virt}} \gtrsim E_{\text{th}}$.

1.1.1.3 Large scale magnetic scattering

Radiation-free scattering by magnetic clouds: We consider a region of an enhanced magnetic field with limited size, called a *magnetic cloud*, which we may think of as being surrounded by a field-free environment. A charge moving into this cloud will remain there for a certain time, T , and then be emitted in a different direction; the charge is scattered at the cloud. A kind of opposite case to Thomson scattering of photons on charged particles is given if the scattering of the charge at the cloud happens *radiation-free*, i.e. the scattering happens on time scale much shorter than the energy loss by radiation. This can be written as $T \ll \tau_{\text{rad}}$, or

$$P_{\text{rad}}T \ll m\gamma_{\text{CR}}c^2 \quad . \quad (1.1.10)$$

The scattering time T depends, of course, on the details of the geometry of the magnetic field in the cloud and the initial conditions of the scattering system. However, we may ask for the minimum scattering time τ_{scat} for a given \mathbf{B} -field, in order to find a limit for the particle Lorentz factor still allowing radiation-free scattering, finding

$$\tau_{\text{scat}} = \frac{\pi r_g}{c} = \frac{\pi m\gamma_{\text{CR}}\beta c}{eB_{\text{eff}}} \quad (1.1.11)$$

for the case of a particle moving through the cloud in a gyration half-circle of radius r_g before being emitted in the opposite direction, where $B_{\text{eff}} \sim B$ is the effective magnetic field strength used for scattering, i.e. the average strength of the component perpendicular to the particle motion. Inserting Eqs. (1.1.4) and $T = \tau_{\text{scat}}$ in Eq. (1.1.10), we get

$$\gamma_{\text{CR}} \ll \sqrt{\frac{12e}{\sigma_{\text{T}}B}} \quad (1.1.12)$$

assuming that this limit occurs in the ultrarelativistic regime ($\beta = 1$). For a nucleus of charge Ze and mass $A\hat{m}$ this leads to

$$\gamma_{\text{CR}} \ll \left[1.7 \times 10^{11}\right] \frac{A}{Z^{3/2}} \left(\frac{B}{[\text{G}]}\right)^{-\frac{1}{2}} \quad . \quad (1.1.12a)$$

It is important to note that the maximum Lorentz factor allowing radiation free scattering depends inversely on the magnetic field; elastic magnetic scattering for very high energies works best in weak magnetic fields, requiring very large structures because of the increasing gyration radius. This has a strong impact on particle acceleration models, as we will see in the next paragraph.

The Fermi mechanism: We now consider radiation-free scattering from magnetic clouds in motion. This means, that in the rest frame of the cloud the particle energy remains unchanged in the scattering event. We call β_{cl} the relativistic velocity of the cloud and γ_{cl} its Lorentz factor, and assume $\gamma_{\text{cl}} \sim 1$, i.e. the motion of the cloud is not highly relativistic. From simple kinematical considerations (see [Gai90]) we obtain the relative energy change of the particle in a scattering event as

$$\frac{\Delta E}{E} = \gamma_{\text{cl}}^2 \beta_{\text{cl}}^2 \left\{ 1 - \cos \theta_1 \cos \theta'_2 + \frac{\cos \theta'_2 - \cos \theta_1}{\beta_{\text{cl}}} \right\} , \quad (1.1.13)$$

where θ_1 is the angle between the velocity vectors of the incoming particle and the cloud in the LF and θ'_2 the angle between cloud and outgoing particle velocity in the rest frame of the cloud. The distribution of $\cos \theta_1$ and $\cos \theta'_2$ are dependent on the details of the physical system; however, there are two special configurations commonly assumed:

a) A system of clouds moving all with the same velocity β_{cl} , but randomly in all directions with equal probability. The internal magnetic configuration of the clouds is assumed to give a uniform distribution of emission angles θ'_2 , which, of course, requires

$$B_{\text{cl}} L_{\text{cl}} \gg \frac{mc^2}{e} \gamma_{\text{CR}} , \quad (1.1.14)$$

i.e. we assume that the particle gyration radius is considerably smaller than the size of the cloud. We then have the probability of hitting a cloud with angle θ_1 of $\frac{1}{2}(1 - \beta_{\text{cl}} \cos \theta_1)$, leading to

$$\langle \cos \theta_1 \rangle = -\frac{1}{3} \beta_{\text{cl}} \quad (1.1.15a)$$

$$\langle \cos \theta'_2 \rangle = 0 \quad (1.1.15b)$$

and thus

$$\left\langle \frac{\Delta E}{E} \right\rangle = \frac{4}{3} \gamma_{\text{cl}}^2 \beta_{\text{cl}}^2 . \quad (1.1.15c)$$

Therefore, the particle receives a net acceleration over time, which is in the nonrelativistic limit proportional to the square of the cloud velocity. This acceleration mechanism was originally proposed by Fermi [Fer49] and is called *second order Fermi* or *stochastic acceleration*.

b) A system of magnetic clouds moving all in the same direction with the same velocity, β_{cl} , which falls instantaneously to zero at a *parallel shock front*, i.e. a plane discontinuity with its *normal* pointing in the direction of the cloud velocity. This is a basic representation of a shocked plasma flow with a tangled turbulent magnetic field frozen in it, seen from the downstream rest frame. We consider as a scattering event one back-and-forth crossing of the shock front, and the one-dimensional geometry of the system implies

$$\langle \cos \theta_1 \rangle = -\frac{2}{3} \quad (1.1.16a)$$

$$\langle \cos \theta'_2 \rangle = \frac{2}{3} . \quad (1.1.16b)$$

Note that we do not assume that a single cloud is able to scatter the particle by an arbitrary angle, therefore, Eq. (1.1.14) does not necessarily apply. The average net energy gain per scattering event is here

$$\left\langle \frac{\Delta E}{E} \right\rangle = \gamma_{\text{cl}}^2 \beta_{\text{cl}} \left(\frac{4}{3} + \frac{13}{9} \beta_{\text{cl}} \right) . \quad (1.1.16\text{c})$$

We note that Eq. (1.1.16c) depends on β_{cl} to the first power, while the dependence in Eq. (1.1.15c) is only to the second power; for $\beta_{\text{cl}} \ll 1$, first order Fermi acceleration is much more efficient than second order Fermi acceleration.

Diffusive shock acceleration: Basing on the principle of first order Fermi acceleration, a theory of particle acceleration at strong shock fronts in astrophysical plasmas has been developed, which is meanwhile one of the most important theories for cosmic ray acceleration; it is called *diffusive shock acceleration*. We will not present this theory here in detail, but just quote the most important results because of their relevance to cosmic ray physics (for an introductory review of diffusive shock acceleration theory see [Dru83]).

A shock front in a linear plasma flow can be described approximately by an instantaneous jump in the flow velocity of $U_{\text{d}} - U_{\text{u}}$, where U_{u} and U_{d} are called the *upstream* and *downstream* velocity, respectively. For a gas with a specific heat index $\tilde{\gamma}$ the compression ratio $r = U_{\text{u}}/U_{\text{d}}$ at the shock is given by

$$r_c = \frac{\tilde{\gamma} + 1}{\tilde{\gamma} - 1 + 2M_{\text{S}}^{-2}} , \quad (1.1.17)$$

where M_{S} is the Mach number of the shock, thus $r \rightarrow 4$ (with $r_c < 4$) for $\tilde{\gamma} = \frac{5}{3}$ (i.e. a nonrelativistic, monoatomic ideal gas) in the limit of strong shocks ($M_{\text{S}} \rightarrow \infty$). In this plasma, a tenuous component of energetic particles shall be embedded, which can diffuse across the shock front in any direction, where the upstream and downstream diffusion coefficients are denoted as κ_{u} and κ_{d} , respectively. The time scale for energy gain of an energetic particle crossing back-and-forth the shock due to first order Fermi acceleration can then be found as

$$\tau_{\text{acc}} = \frac{3r_c}{r_c - 1} \frac{\beta}{U_{\text{u}}^2} (\kappa_{\text{u}} + r_c \kappa_{\text{d}}) . \quad (1.1.18)$$

The diffusion coefficients are generally functions of the particle energy; in the most simple case, we may assume a magnetic field which is completely turbulent on all scales, which implies that $\kappa_{\text{d}} \sim \kappa_{\text{u}} = \kappa_{\text{B}}$, where $\kappa_{\text{B}} = r_{\text{g}} \beta c / 3$ is the *Bohm diffusion coefficient*, which gives $\tau_{\text{acc}} \propto E$. A more realistic assumption in plasma physics, however, is that the magnetic field is governed by an ordered component, and that the particle diffusion proceeds over scattering at plasma waves, changing the pitch angle of the particle gyrating over the main field. Here, the geometry of the system in terms of the orientation of the shock normal to the main field direction is important, and the diffusion coefficients in Eq. (1.1.18) have to be replaced by their parallel components; a theory of diffusion in oriented fields with arbitrary orientation angle, which considers the possibility of the particle to be accelerated just by gyrating back-and-forth the shock in highly oblique geometries, has been developed by JOKIPII [Jok87]: he finds

$$\tau_{\text{acc}} = \frac{r_c}{r_c - 1} \frac{\eta_{\text{B}} r_{\text{g}} \beta c}{U_{\text{u}}^2} \mathcal{J}(\theta; r_c, \eta_{\text{B}}) \quad (1.1.18\text{a})$$

with

$$\mathcal{J}(\theta; r_c, \eta_{\text{B}}) = \left[\cos^2 \theta_{\text{u}} + \frac{\sin^2 \theta_{\text{u}}}{1 + \eta_{\text{B}}^2} \right] + \frac{r_c \cos^2 \theta_{\text{u}} + r_c^3 \sin^2 \theta_{\text{u}} / (1 + \eta_{\text{B}}^2)}{[\cos^2 \theta_{\text{u}} + r_c^2 \sin^2 \theta_{\text{u}}]^{3/2}} ,$$

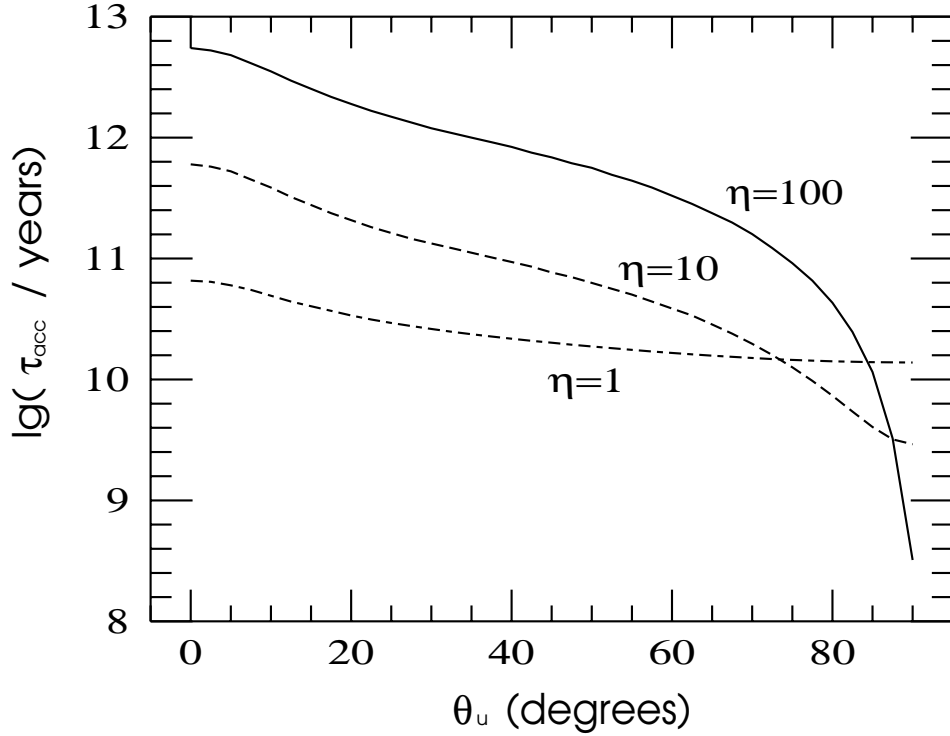


Figure 1.1: Acceleration timescales for Jokipii diffusion, Eq. (1.1.18a), for $\eta_B = 1, 10, 100$, as a function of shock obliquity angle θ_u , calculated for protons with energy $r_g = 43$ kpc, and shock parameters $r_c = 4$ and $U_u = 1000$ km sec $^{-1}$ (taken from [KRB96]).

where $\kappa_d = \kappa_{\parallel} \cos^2 \theta_u + \kappa_{\perp} \sin^2 \theta_u$, $\kappa_{\parallel} = \frac{1}{3} \eta_B r_g \beta c = (1 + \eta_B^2) \kappa_{\perp}$, and θ_u is the upstream angle between shock normal and main magnetic field direction. The factor η_B may depend on energy; a famous case is $\eta_B \propto E^{-2/3}$, corresponding to a Kolmogorov spectrum of plasma waves (see [BS87] for an astrophysical application). The dependence of τ_{acc} on η_B and θ_u is shown in Fig. 1.1; we see that acceleration at parallel shocks is generally slower for $\eta_B > 1$ than in the Bohm diffusion case, but it can be much faster in highly oblique shocks. The limiting case, $\eta_B \gg 1$ and $\theta_u \approx 90^\circ$ can be considered as acceleration by ideal mirrors, i.e. the particle is reflected just by doing half a gyration circle on each side on the shock. In this case, Eq. (1.1.12a) immediately applies to determine the energy limit of the particle due to synchrotron losses; this limit is generally much lower for Bohm or parallel pitch-angle diffusion. In most astrophysical applications, however, other processes determine the energy limit of shock acceleration; most important are limitations due to the size R of the system ($r_g < R$), the time scale of evolution T of the system ($\tau_{\text{acc}} < T$), or interaction losses with ambient photon fields ($\tau_{\text{acc}} < \tau_{\text{rad}}$).

The most important feature of diffusive shock acceleration is the prediction of a unique particle spectrum, which is determined by the shock properties. For a planar shock front, one obtains a power law in momentum, $f(p) \propto p^{-a}$, with

$$a = \frac{3r_c}{r_c - 1} \quad , \quad (1.1.19)$$

which gives $a \geq 4$ for $r_c \leq 4$, and $a = 4$ for the limiting case of a strong, nonrelativistic shock wave.

For ultrarelativistic particles and an isotropic momentum distribution this is equivalent to an energy spectrum $F(E) = E^{-2}$. This result is independent of shock obliquity, but may be modified if relativistic effects or influences of second order Fermi acceleration (due to the moving plasma waves) are considered [Krü92]. For nonplanar shocks, in particular spherical shocks, other spectral indices are obtained [Dru83, Bie93]. We will, however, not go deeper here.

1.1.2 Coherent electromagnetic processes

1.1.2.1 Inverse Compton scattering

Differential cross section: Compton scattering is the general term for the scattering of real photons on charged particles. In the particles rest frame, the energy of a photon coming in with energy ϵ'_i after scattering is

$$\epsilon'_f = \epsilon'_i \left[1 + \frac{\epsilon'_i}{mc^2} (1 - \cos \theta) \right]^{-1}. \quad (1.1.20)$$

The differential cross section found from evaluating the Born contribution terms of the process, corresponding to the classical plane-wave approximation, is

$$\frac{d\sigma_C}{d\Omega} = \frac{3\sigma_T}{16\pi} \left(\frac{\epsilon'_f}{\epsilon'_i} \right)^2 \left(\frac{\epsilon'_f}{\epsilon'_i} + \frac{\epsilon'_i}{\epsilon'_f} - \sin^2 \theta \right), \quad (1.1.21)$$

known as the *Klein-Nishina* formula. In the nonrelativistic limit Compton scattering reduces to Thomson scattering, while in the extreme relativistic limit $\epsilon'_i \gg mc^2$ the total cross section is reduced with energy by

$$\sigma_C = \frac{3\sigma_T mc^2}{8\epsilon'_i} \left(\ln \frac{2\epsilon'_i}{mc^2} + \frac{1}{2} \right). \quad (1.1.22)$$

This decrease of the cross section is, however, only relevant if there are no incoherent processes due to the photon or particle structure on energy scales *below* the rest mass of the particle. The process with lowest threshold energy is pair production in the Coulomb field of the charge, which sets in at $\epsilon'_i \sim 2m_e c^2$, thus much below the Thomson limit for nuclei. We note that both photodisintegration and pion production are also below this limit. Therefore, for the inverse Compton interaction of cosmic ray nuclei with photon backgrounds we can assume to be in the Thomson limit for all relevant cases.

Inverse Compton loss time scale: According to Eq. (1.1.8), a relativistic nucleus of mass $A\hat{m}$, charge Ze and Lorentz factor γ_{CR} , moving through an isotropic photon background satisfying $\gamma_{\text{CR}} \langle \epsilon \rangle \ll mc^2$, loses energy due to inverse Compton scattering on a time scale

$$\tau_{\text{IC}} = \frac{3\hat{m}c}{4\hat{\sigma}_T U_\gamma} \frac{A^3}{Z^4} \frac{\gamma_{\text{CR}}}{\gamma_{\text{CR}}^2 - 1} \approx \left[1.16 \times 10^{29} \text{ sec} \right] \frac{A^3}{Z^4} \left(\frac{\gamma_{\text{CR}} U_\gamma}{[\text{eV cm}^{-3}]} \right)^{-1}, \quad (1.1.23)$$

This equation is mostly used for estimating inverse Compton losses in any photon background, but it has to be noted that τ_{IC} can be much larger if the photons are anisotropically distributed and irradiate the particles mainly from the back.

In the isotropic case, the photon background energy density must be of order $\sim \text{eV cm}^{-3}$ or more, to make τ_{IC} shorter than the Hubble time scale even for the highest known particle energies. The dependence on nuclear mass is weak, since $A^3/Z^4 \sim 0.1-1$ for all nuclei. For typical astrophysical photon background densities, the energy loss by inverse Compton scattering can therefore be neglected; in dense photon regions around compact objects, it is mostly dominated by incoherent reactions.

1.1.2.2 Synchrotron Radiation

Radiation time scale: Radiation emitted by a relativistic particle moving through a pure magnetic field is called *synchrotron radiation*. In an oriented field, the radiation power is given by Eq. (1.1.4) by setting $\mathbf{E} = 0$ and $U_{\perp} = U_{\mathbf{B}} \sin \vartheta$, where ϑ is the angle between particle velocity and field direction, called the *pitch angle* of the particle. Averaging over pitch angle, as for instance appropriate in a turbulent magnetic field, gives an energy loss time scale exactly as given by Eq. (1.1.23), just by replacing U_{γ} by $U_{\mathbf{B}}$, which may be expressed by the relation

$$U_{\mathbf{B}} \tau_{\text{sync}} = U_{\gamma} \tau_{\text{IC}} \quad . \quad (1.1.24)$$

This relation is useful because whenever $U_{\mathbf{B}} \neq 0$ we also have $U_{\gamma} \neq 0$, *because* of the synchrotron radiation. Radiation produced by inverse Compton scattering of particles at synchrotron photons produced by themselves (i.e. particles from the same population) is called Synchrotron-Self-Inverse-Compton (SSIC) radiation; it is very important for electrons, but less for cosmic ray nuclei. For the latter, a rather indirect synchrotron-self scattering variation, i.e. the scattering of synchrotron photons radiated by relativistic *electrons* moving along with the nuclei through the \mathbf{B} field, may play a role. However, not inverse Compton but incoherent photon scattering interactions will dominate here.

Energy limits on the classical approach: The strong similarity between synchrotron radiation and inverse Compton scattering has already been mentioned in the discussion of the virtual photon concept. To apply this concept here, we need the characteristic frequency of the emitted synchrotron radiation. From the classical theory we have

$$\omega_c = \frac{3eB\gamma_{\text{CR}}^2 \sin \vartheta}{2mc} \quad , \quad (1.1.25)$$

which marks the center of gravity of the frequency distribution by order of magnitude. Averaging over pitch angle and dividing by γ_{CR} following Eq. (1.1.7), we find the typical energy of virtual photons as

$$\epsilon_{\text{virt}} \sim \frac{\hbar\gamma_{\text{CR}}eB}{mc} \approx [6.35 \times 10^{-12} \text{ eV}] \frac{Z\gamma_{\text{CR}}}{A} \frac{B}{[\text{G}]} \quad . \quad (1.1.26)$$

Since Z/A is of order one, we notice that the factor $\gamma_{\text{CR}}B$ expresses basically the energy range of the virtual scattering, and therefore also the classical limit of synchrotron radiation. Thus we find $\gamma_{\text{CR}}B \gtrsim (A/Z)10^{17} \text{ G}$ for the threshold of pair production, for $\gamma_{\text{CR}}B$ one order larger photodisintegration of nuclei is possible and for $\gamma_{\text{CR}}B \gtrsim 3 \times 10^{19} \text{ G}$ pionic synchrotron radiation will dominate. Above the Thomson limit for nuclei,

$$\gamma_{\text{CR}}B \gtrsim [10^{20} \text{ G}] \frac{A^2}{Z} \quad , \quad (1.1.27)$$

the whole approach breaks down and has to be replaced by an exact quantum mechanical treatment [LAQ89]. It is important to point out that, if Eq. (1.1.27) applies, processes starting at lower threshold energies cannot work either; rather, the particle will damp all its motion perpendicular to the magnetic field on quantum mechanical time scales and move along the field lines. The only surviving radiation process in this case is *curvature radiation*, which will not be treated here. Eq. (1.1.27) may apply for UHE cosmic rays in neutron star magnetospheres, and maybe to Gamma Ray Bursters (GRBs); for most astrophysical applications synchrotron radiation of nuclei can be treated classically, and may be even neglected for large scale background magnetic fields of low energy density.

1.1.2.3 Inverse pair production

Bethe-Heitler scattering: In the framework of QED electromagnetic interactions are completely reduced to the interactions of photons and charges. Interactions between charges are represented by the exchange of virtual photons. On the other hand, photons can interact with each other by the exchange of virtual charges, which allows processes like photon-photon scattering. Clearly, charged particles in QED, i.e. electrons and positrons, can only be produced in pairs because of charge conservation; the most elementary interaction process between photons is therefore the process $\gamma\gamma \rightarrow e^+e^-$, as shown in the Feynman diagram Fig. 1.2. This process gives important limitations to the mean free path of UHE gamma rays in the universe; it gains importance for the transport of nuclei if the second scattering photon is thought as a virtual photon from the Coulomb field around a nucleus. In this case, the process is called *Bethe-Heitler scattering* of a photon at a nucleus, $N\gamma \rightarrow Ne^+e^-$.

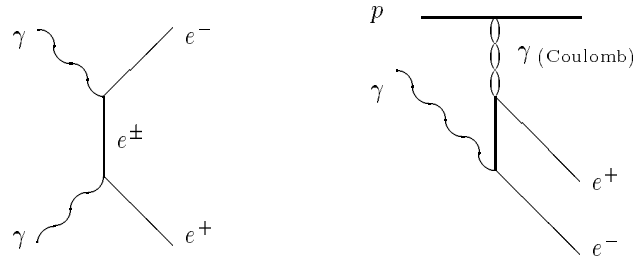


Figure 1.2: Diagrams for pair production in interactions of real photons, and of a photon in a nuclear Coulomb field (Bethe-Heitler process).

To first order, the Bethe-Heitler process may be considered as elastic scattering, which may be written as

$$\gamma_+ + \gamma_- \stackrel{\prime}{=} k \quad (1.1.28)$$

with $k' = \epsilon'/m_e c^2$ is the photon energy in units of electron masses, and γ'_\pm the Lorentz factor of the electron and the positron, respectively, all given in the NRF. With this condition, the momentum transfer in the NRF is given by

$$|\mathbf{q}|^2 \stackrel{\prime}{=} |\mathbf{q}_\parallel|^2 + |\mathbf{q}_\perp|^2 \stackrel{\prime}{=} m_e^2 c^2 \left\{ (q_{\parallel+} + q_{\parallel-})^2 + q_{\perp+}^2 + q_{\perp-}^2 + 2q_\perp^\pm \cos \phi \right\} , \quad (1.1.29)$$

where we introduced the notations $q_{\parallel\pm} \stackrel{\prime}{=} \gamma_\pm (1 - \beta_\pm \cos \chi_\pm)$, $q_{\perp\pm} = \gamma_\pm \beta_\pm \sin \chi_\pm$, and $X^\pm \equiv X_+ X_-$ for any pair-related quantity X ; χ'_\pm and ϕ' are the scattering angle of the electron and the positron to the direction of the photon, and their relative azimuth angle, respectively. Introducing $q^2 = |\mathbf{q}|^2/m_e^2 c^2$, the cross section for unpolarized photons can be written as

$$\frac{d\sigma_{\text{BH}}}{d\gamma d\chi^\pm d\phi} \stackrel{\prime}{=} -\frac{3Z^2 \alpha_e \sigma_{T_e}}{(4\pi)^2} \frac{q_\perp^\pm}{k^3 q^4} \times \left\{ \frac{q_{\perp+}^2}{q_{\parallel+}^2} (4\gamma_-^2 - q^2) + \frac{q_{\perp-}^2}{q_{\parallel-}^2} (4\gamma_+^2 - q^2) - \frac{2k^2}{q_\parallel^\pm} (q_{\perp+}^2 + q_{\perp-}^2) + \frac{2q_\perp^\pm}{q_\parallel^\pm} (4\gamma^\pm + q^2 - 2k^2) \cos \phi \right\} . \quad (1.1.30)$$

The dependence $\sigma_{\text{BH}} \propto q^{-4}$ indicates that Bethe-Heitler scattering is strongly forward peaked, i.e. the differential cross section is maximal for small scattering angles. The total cross section cannot be expressed in closed

form, but approximations can be given near threshold and in the ultrarelativistic case,

$$\sigma_{\text{BH}} \stackrel{!}{=} \frac{\alpha_e \sigma_{\text{T}e}}{32} Z^2 (k-2)^3 \quad \text{for } k-2 \ll 1 \quad (1.1.31\text{a})$$

$$\sigma_{\text{BH}} \stackrel{!}{=} \frac{7\alpha_e \sigma_{\text{T}e}}{6\pi} Z^2 \left(\ln 2k - \frac{109}{42} \right) \quad \text{for } k \gg 2. \quad (1.1.31\text{b})$$

An important point for the comparison with Compton scattering is, that the mass of the nucleus does not enter into σ_{BH} ; in fact, the particle properties of the nucleus play no role at all, it is just a source for virtual photons in this process. Compared to Compton scattering at an electron, Bethe-Heitler scattering is suppressed by a factor of the fine-structure constant $\alpha_e \simeq 1/137$, due to the additional vertex for the virtual pair splitting in Fig. 1.2. For protons and nuclei, however, the suppression of Thomson scattering due to the mass factor $(m_e/A\hat{m})^2$ is much bigger, thus $\sigma_{\text{BH}} \gg \sigma_{\text{T}}(Z, A)$. Looking at the k -dependence of σ_{BH} , we see that $\sigma_{\text{BH}} \sim Z^2 \alpha_e \sigma_{\text{T}e}$ for $k \gg 2$, but $\sigma_{\text{BH}} < \sigma_{\text{T}p}$ at threshold. Therefore, Bethe-Heitler scattering is *the dominant elastic photon scattering process* for high energy photons with $\epsilon' \gg 2m_e c^2$, while of minor importance in its threshold region.

Inverse Bethe-Heitler scattering: For the moving nucleus, Bethe-Heitler scattering looks very much like Thomson scattering; the process is coherent with respect to the nucleus, and elastic with respect to the photon energy in the NRF. The effective energy loss per interaction in the LF is of order ϵ'/mc^2 , as for inverse Compton scattering in the Thomson limit; differences occur only in the magnitude of the cross section and the dependence on photon energy and scattering angles. Considering that the energy change of the nucleus in the LF transforms in the NRF to the momentum transfer component parallel to the nucleus velocity, it is easy to see that the loss time scale *in the NRF* may be written as

$$\tau_{\text{BH}} \stackrel{!}{=} \frac{2A\hat{m}c}{m_e} \left[\int_2^\infty dk n(k) \int_1^{k-1} d\gamma_- \frac{d\sigma_{\text{BH}}}{d\gamma_-} \langle q_{\parallel-} \rangle_{(\chi^\pm, \phi)} \right]^{-1}, \quad (1.1.32)$$

using the assumption that all photons hit the nucleus *head-on* in the NRF, which is justified by the Lorentz beaming for ultrarelativistic nuclei with $\gamma_{\text{CR}} \gg 1$. The loss time scale in the LF is then given by $\tau_{\text{BH}} = \gamma_{\text{CR}} \tau'_{\text{BH}}$. $n'(k)$ is the photon number distribution with energy as seen in the NRF, and $\langle q_{\parallel-} \rangle_{(\chi^\pm, \phi)}$ is the parallel momentum transfer averaged over angles. The impact of Bethe-Heitler scattering on the transport of UHE cosmic rays has been pointed out first by Blumenthal, who expressed Eq.(1.1.32) in terms of the LF photon distribution $n(\epsilon)$ and gave an analytic expression for $\langle q_{\parallel-} \rangle_{(\chi^\pm, \phi)}$ [Blu70].² We will give a brief discussion of the integral Eq. (1.1.32) within a more general context in Sect. 1.1.3.3.

We realize immediately that Eq. (1.1.32) does not lead to a simple connection of loss time scale and photon energy density. Rather, the inner integral in Eq. (1.1.32) determines which region of photon energy k contributes most to the process, leading to the definition of the *efficiency function*

$$\eta_{\text{BH}}(k) \stackrel{!}{=} \frac{m_e}{A\hat{m}} \int_1^{k-1} d\gamma_- \frac{d\sigma_{\text{BH}}}{d\gamma_-} \langle q_{\parallel-} \rangle_{(\chi^\pm, \phi)}. \quad (1.1.33)$$

At threshold, the efficiency is obviously given by $\eta_{\text{BH}}(2) = (2m_e/A\hat{m})\sigma_{\text{BH}}(2)$. Comparing the efficiency function, $\eta_{\text{BH}}(k)$, with the total cross section scaled with the threshold efficiency, $(2m_e/A\hat{m})\sigma_{\text{BH}}(k)$, we see that the cross section grows steadily for $k' \rightarrow \infty$, while the efficiency has a broad maximum around $k' \sim 20$

²The relation to Blumenthals function $A(k, \gamma_-)$ is given by $3Z^2 \alpha_e \sigma_{\text{T}e} A = 8\pi k \langle q_{\parallel-} \rangle_{(\chi^\pm, \phi)}$.

²The formula for the total cross section is taken from [JLS50] (after correcting some typos), the formula given in [JR76] seems to contain a mistake.

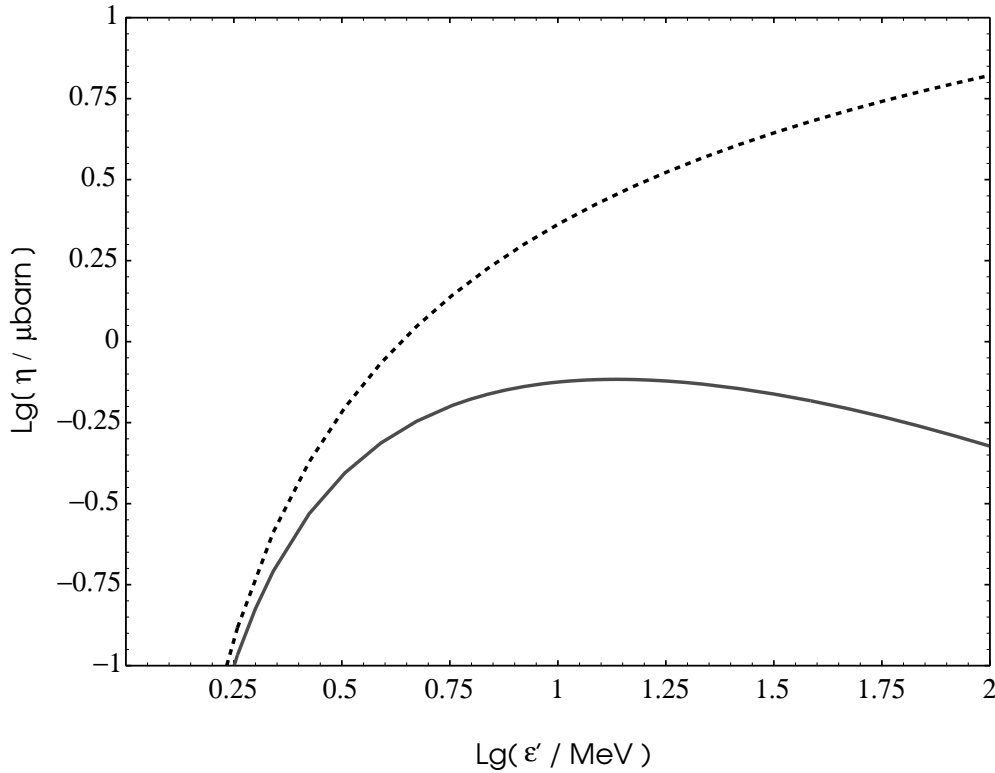


Figure 1.3: Cross section (dashed line) and efficiency function (solid line) for the Bethe-Heitler process. The cross section is scaled with the threshold efficiency, which is $(2m_e/A\hat{m}) \approx 10^{-3}A^{-1}$ for nuclei.⁴

(Fig. 1.3). Thus, both the threshold region and the extremely high energy region contribute little to the energy loss in inverse Bethe-Heitler scattering. Transforming to LF photon energies, we see that photons with $\epsilon \sim (10/\gamma_{CR})$ MeV contribute most to the Bethe-Heitler process.

Dependence on nuclear charge: A general assumption which has been presupposed in all the discussion so far is that electrons and positrons can be treated as quantum-mechanical plane waves and do not interact with the nuclear Coulomb field after production. In the framework of perturbation theory, this corresponds to the consideration of only the first term of the Born series, represented by the Feynman diagrams shown in Fig. 1.2. This is known as the *Born approximation*, which is, of course, not strictly correct since the e^\pm pair carries charge and therefore *must* interact with the Coulomb field in which it was produced. The higher order terms correspond to diagrams containing additional vertices due to the exchange of virtual photons between the pair and the nucleus. Numerically, these terms enter to an order of $(Z\alpha_e/\beta_\pm)^n$, when n is the number of interactions with the field. Thus, since $\alpha_e \ll 1$, the Born approximation can be considered as good for $Z \sim 1$ and $\beta_\pm \approx 1$. Near threshold ($\beta_\pm \ll 1$) or for very heavy nuclei ($Z \gg 1$), however, we can expect that the Bethe-Heitler formula Eq. (1.1.30) will no longer give an appropriate description of the cross section, and that the symmetry between electron and positron breaks down.

An exact treatment of pair production in a Coulomb field is very difficult; however, for the nonrelativistic limit, and for large Z in the extreme relativistic limit, approximate solutions have been found. The nonrelativistic

adaptation is performed by multiplying the Bethe-Heitler cross section Eq. (1.1.30) with the *Sommerfeld factor*

$$f_{\text{SOM}}(\beta_{\pm}) = \frac{x_+ x_-}{[\exp(x_+) - 1][1 - \exp(-x_-)]} \quad \text{with} \quad x_{\pm} = \frac{2\pi Z\alpha_e}{\beta_{\pm}} \quad . \quad (1.1.34)$$

From our discussion of the efficiency function we know that the threshold region contributes little to the Bethe-Heitler loss time scale of nuclei. Therefore, we can neglect the factor f_{SOM} in the integral Eq. (1.1.32).⁵

A theory of pair production in the Coulomb field in the extreme relativistic limit has been developed by BETHE & MAXIMON [BM53, DBM53]. In this limit, the scattering angles χ'_{\pm} can be assumed to be small, and the differential Bethe-Heitler cross section simplifies to

$$\frac{d\sigma_{\text{BH}}}{d\gamma_+} \stackrel{!}{=} \frac{3Z^2\alpha_e\sigma_{\text{T}e}}{2\pi k^3} \left(\gamma_+^2 + \gamma_-^2 + \frac{2}{3}\gamma^{\pm} \right) \left(\ln \frac{2\gamma^{\pm}}{k} - \frac{1}{2} \right) \quad . \quad (1.1.35a)$$

The result of the calculation performed in [DBM53] in the extreme relativistic limit reads

$$\frac{d\sigma_{\text{BH}}}{d\gamma_+} \stackrel{!}{=} \frac{3Z^2\alpha_e^2\sigma_{\text{T}e}}{2\pi k^3} \left(\gamma_+^2 + \gamma_-^2 + \frac{2}{3}\gamma^{\pm} \right) \left(\ln \frac{2\gamma^{\pm}}{k} - \frac{1}{2} - f_{\text{BM}}(Z\alpha_e) \right) \quad (1.1.35b)$$

with

$$f_{\text{BM}}(x) \equiv \sum_{n=1}^{\infty} (-1)^n \zeta(2n+1) x^{2n} \quad , \quad (1.1.35c)$$

where $\zeta(x)$ is the Riemann Zeta-function. For the total cross section this leads to an asymptotically energy independent reduction of the cross section

$$\sigma_{\text{BH}}^{\text{C}}(k) = \sigma_{\text{BH}}(k) - \frac{7\alpha_e\sigma_{\text{T}e}}{6\pi} Z^2 f_{\text{BM}}(Z\alpha_e) \quad \text{for} \quad k \gg 2 \quad . \quad (1.1.36)$$

Comparison with data for lead confirm this theoretical result in the ultrarelativistic limit; however, for the transrelativistic regime, which is most important for τ_{BH} due to its large efficiency, the data suggest that there is a constant *relative correction* of the cross section,

$$\sigma_{\text{BH}}^{\text{C}}(k) \approx \varphi_{\text{C}}(Z\alpha_e)\sigma_{\text{BH}}(k) \quad \text{for} \quad k \gtrsim 2 \quad , \quad (1.1.37)$$

rather than an absolute correction as suggested by Eq. (1.1.36). Since the Coulomb correction has no influence on the energy distribution of the pair, as suggested by Eq. (1.1.35b) (see also discussion in [DBM53]), we can assume that the same correction factor applies to τ_{BH} after performing the integral Eq. (1.1.32), i.e.

$$\tau_{\text{BH}}^{\text{C}} \approx \frac{\tau_{\text{BH}}}{\varphi_{\text{C}}(Z\alpha_e)} \quad .$$

From comparison of Eq. (1.1.37) and Eq. (1.1.36) we define

$$\varphi_{\text{C}}(x) \equiv 1 - \frac{f_{\text{BM}}(x)}{\ln 2k_0 - \frac{1}{2}} \quad ,$$

⁵BLUMENTHAL [Blu70] has proposed to apply a symmetrized Sommerfeld factor to σ_{BH} in Eq. (1.1.32) to adopt it to the Coulomb corrections at threshold *and* for large Z . This method has to be rejected, since f_{SOM} is only valid in the nonrelativistic limit, while the largest part of the integral in Eq. (1.1.32) is carried out over the extreme relativistic regime. Numerically, Blumenthals correction is negligible for protons (therefore his published results are still correct), but leads to a reduction of the pair production rate for heavy nuclei which is much too large compared to experiment.

and note from [DBM53, Fig.3] that the data are well represented for $k_0 \sim 500$. Setting $k_0 \equiv 500$, we get the numerical result

$$\varphi_C(x) = 1 - 0.29x^2 + 0.25x^4 - 0.25x^6 \quad , \quad (1.1.38)$$

and defining $\hat{\tau}_{\text{BH}}$ as the Bethe-Heitler loss scale of a proton, we can write the explicit Z dependence of the loss time scale for nuclei as

$$\tau_{\text{BH}}^C(Z, \gamma_{\text{CR}}) = \frac{A}{Z^2 \varphi_C(Z\alpha_e)} \hat{\tau}_{\text{BH}}(\gamma_{\text{CR}}) \quad , \quad (1.1.39)$$

which we will use subsequently. We stress that the factor φ_C arises from a crude phenomenological approximation, and that the magnitude of correction caused by it, $1 - \varphi_C$, cannot be regarded as more accurate than about 30%. Therefore, for nuclei up to Fe ($Z = 26$) we may disregard this factor, or use the expansion Eq. (1.1.38) only to order x^2 .

1.1.3 Incoherent reactions

1.1.3.1 Resonances

The classical oscillator in electrodynamics: Thomson scattering is the classical scattering of an electromagnetic wave on a free particle, i.e. which is free to oscillate with an incoming wave of any frequency. A charged particle which is bound to a potential well can, for small excitations, be described as a classical oscillator with a characteristic frequency ω_0 . An oscillating charge will, of course, radiate; the fractional energy radiated during one oscillation cycle can be written as $\Delta E/E = \omega_0/\omega_*$ with

$$\omega_* = \frac{3mc^3}{2e^2} \quad (1.1.40)$$

for a particle of mass m and charge e . Therefore, the oscillator loses its energy over a typical time scale $\tau_{\text{rad}} = \omega_*/\omega_0^2$; since for an electron $\omega_{*e} \simeq 1.6 \times 10^{23}$ Hz, and $\omega_{*p} \simeq 2.93 \times 10^{26}$ Hz (corresponding to the photon energy $\epsilon_{*p} = \hbar\omega_{*p} \simeq 193$ GeV), we can assume that $\omega_0 \ll \omega_*$ for all oscillators under consideration, thus $\tau_{\text{rad}} \gg \omega_0^{-1}$. We note that the oscillator picture is in general applicable only for limited energy transfers, corresponding to amplitudes small or comparable to the size of the oscillating system.

If the oscillator is irradiated by an electromagnetic wave of frequency ω , the wave acts as an excitation force, while $\Gamma_\gamma = \omega^2/\omega_*$ acts as a damping parameter in the equation of motion. The relation of the scattered to the incoming electromagnetic flux, i.e. the scattering cross section, is found as

$$\sigma_{\text{el}}(\omega) = 6\pi\lambda^2 \frac{\omega^2 \Gamma_\gamma^2(\omega)}{(\omega^2 - \omega_0^2)^2 + \omega^2 \Gamma_\gamma^2(\omega)} \quad , \quad (1.1.41a)$$

where $\lambda = c/\omega$ is the wavelength of the incident wave. The scattering amplitude has a maximum at $\omega = \omega_0$, where we find $\sigma_{\text{el}}(\omega_0) = 6\pi\lambda_0^2$, and approaches asymptotically the free particle cross section $\sigma_{\text{T}} = 6\pi\lambda_*^2$. Therefore we have $\sigma_{\text{el}}(\omega_0) \gg \sigma_{\text{T}}$ for $\omega_0 \ll \omega_*$, showing that the cross section of the bound oscillator greatly exceeds that of the free particle for frequencies close to ω_0 .

Resonant reactions: The situation described above is well resembled by an atomic nucleus, in which every nucleon can act as an oscillator, bound by the joint potential well of all nucleons. With respect to the nucleus, the resonant scattering is *incoherent*, although elastic with respect to the scattered wave (photon). The importance of incoherent processes, however, arises rather from the fact that the oscillating system has in general some

additional decay modes other than the re-emission of the photon. If the resonant absorption of the photon leads to the emission of a particle (e.g. a nucleon), the process is called a *reaction*. The reaction cross section can be found as (see, e.g. [Jac75])

$$\sigma_c(\omega) = 6\pi\lambda^2 \frac{\omega^2 \Gamma_c \Gamma_\gamma(\omega)}{(\omega^2 - \omega_0^2)^2 + \omega^2 \Gamma^2} \quad , \quad (1.1.41b)$$

where Γ_c is the decay parameter for the reaction channel c , and $\Gamma = \sum_c \Gamma_c + \Gamma_\gamma(\omega)$ the total decay parameter of the resonant state, considering *all* possible decay channels; Γ^{-1} is obviously the lifetime of the resonance. In general, the reaction decay parameters are independent of the frequency of the incident wave, leading to a vanishing cross section for $\omega \rightarrow \infty$. Replacing Γ_c by Γ in the numerator of Eq. (1.1.41b), we get the expression for the *total absorption cross section* $\sigma_{\text{ab}}(\omega)$ of the wave; clearly we have $\sigma_{\text{ab}}(\omega) = \sum_c \sigma_c(\omega) + \sigma_{\text{el}}(\omega)$. For inelastic reactions we generally have a threshold energy $\hbar\omega_{c,\text{th}}$, given by the minimum energy necessary to remove the corresponding particle from the system, which gives a low energy limit to $\sigma_c(\omega)$.

Resonances in quantum theory: In the view of quantum mechanics, some changes have to be applied to the classical picture: The incident wave is now represented by an incoming photon of energy $\epsilon = \hbar\omega$, scattering at a system of charges X with total mass M . The resonance, which has a total energy $Mc^2 + \epsilon$ in the NRF, has itself the properties of a quantum mechanical state and is described by a set of quantum numbers (like angular momentum, parity, etc.); it can be treated as a particle in the same sense as X and will be called X^* , an *excited state* of X . The rest frame of X^* is the center of momentum frame of the interaction, and the characteristic frequency transforms to a mass $M_{\text{res}} \leftrightarrow \hbar\omega_0/c^2$; obviously, the CMF is the appropriate frame to describe the scattering process and to apply the classical results, with ω transformed to the total energy of the system in the CMF, $E^* = \sqrt{s}$. The decay parameter Γ is transformed into units of energy by multiplication with \hbar ; now the relation to the lifetime τ of the resonance reads $\Gamma\tau = \hbar$, expressing Heisenbergs uncertainty principle for energy and time.

A significant change to the classical formula arises from the fact that every resonance of a specific mass M_{res} carries a specific angular momentum, $J\hbar$, and a specific parity Π . Thus, only photons with the right parity and a suitable impact parameter $l\lambda \leq b < (l+1)\lambda$, corresponding to a quantized orbital angular momentum $l\hbar$, can contribute to the interaction. The classical counterpart to the quantum mechanical photon state (J, Π) is the radiation multipole momentum; here, electromagnetic waves are analyzed into electric and magnetic 2^l -pole contributions, which are denoted by El and Ml , respectively. The El pole carries a parity $\Pi = (-1)^l$, while the Ml pole has $\Pi = (-1)^{l+1}$. In analogy to the classical situations, one speaks about El and Ml photons also in quantum theory to characterize their quantum numbers l and Π . The possible polarizations of the photon correspond to the angular orientation quantum number, which can take the values $l_z = \pm 1$. From the rules for the combination of angular momenta it follows that we have to rescale the amplitude $6\pi\lambda^2$ in the classical formula with a spin-multiplicity factor, i.e.

$$6\pi\lambda^2 \longrightarrow 4\pi\lambda^2 \frac{2J+1}{4J_0+2} \quad (1.1.41c)$$

for the interaction of an El or Ml photon with a particle with spin J_0 . As expected, the classical formula expresses dipole photon scattering at spinless particles.

Also the meaning of λ in Eq.(1.1.41b) changes due to kinematical considerations; in the classical case, a rigid scattering center is assumed, allowing to set λ equal to the wavelength of the photon. Here, it is the *de Broglie wavelength* of the scattering particles in the CMF, which is for photonuclear reactions given by

$$\lambda = \frac{\hbar}{mc} \frac{\sqrt{s}}{\epsilon'} , \quad (1.141d)$$

when m is the mass of the unexcited nucleon (or nucleus).

The dipole sum rule: An important constant in resonant electromagnetic interaction is the integrated total absorption cross section, Σ , for the photon. Assuming that $\Gamma \gg \Gamma_\gamma$, i.e. that photon scattering is unimportant compared to the reaction channels, one obtains for $E1$ absorption by a single oscillator

$$\hat{\Sigma}_{E1} \equiv \int_0^\infty \sigma_{ab}(\omega) d\omega = \frac{2\pi^2 e^2}{mc} , \quad (1.142)$$

where m is the mass of the oscillating particle; we see that $\hat{\Sigma}_{E1}$ is independent of ω_0 and Γ . This is called the *dipole sum rule* of an oscillator. In a system of particles moving in a fixed potential, Σ_{E1} is obviously the sum over all single oscillator cross sections; if the particles are bound in a potential formed by mutual interactions, one can show that a term corresponding to the center of mass motion has to be subtracted, yielding

$$\Sigma_{E1} = \frac{2\pi^2}{c} \left[\sum_j \frac{e_j^2}{m_j} - \frac{Q^2}{M} \right] \quad (1.143)$$

with

$$Q = \sum_j e_j \quad \text{and} \quad M = \sum_j m_j .$$

This relation is particularly important for electromagnetic interactions of nuclei, but we note that it is restricted to electric dipole absorption (see Sect. 1.3.1.2).

1.1.3.2 The substructure of the interaction system

Direct interactions with constituent particles: Resonance scattering usually occurs only in a limiting energy range; the photon energy ϵ' must be of the order of the binding energy of the system E_b , such that oscillations can be excited. For lower energy, the scattering is coherent; for higher energy, the photon interacts only with the constituent particles of the system, which behave almost like free particles. In atomic physics, this is known as Compton scattering with shell electrons. We will generally call it *direct interactions* in the following.

A parallel case to atomic physics is given when high energy photons scatter on bound protons in a nucleus, called *direct photodisintegration*. If the momentum transfer q from the photon to the proton is larger than the binding energy, $cq \gtrsim E_b$, the nucleon is immediately kicked out of the nucleus. In this case, the momentum transfer to the rest nucleus is of order $q(E_b/\hat{m}c^2) \ll q$. Therefore, in nuclear physics, the momentum transfer to the residual nucleus is negligible; for inverse scattering, this means that there is no energy loss in the lab frame for the residual *nucleons*. Of course, the total energy of the *nucleus* is reduced due to the mass loss, $\Delta E/E = \Delta M/M$, but the Lorentz factor is conserved. We will discuss direct interactions in photodisintegration in greater detail in Sect. 1.3.2.

On smaller scales, i.e. $p\gamma$ interaction, we may still speak of direct interactions with constituents; the photon is then thought to interact with the quark-structure of the proton. However, since the quark mass $m_q c^2 \sim E_b$ in this case, we can not make arguments so simple as in nuclear physics. Rather, the condition for being outside

the resonance region, $\epsilon' \gg E_b$, is now equivalent to $\epsilon' \gg m_q c^2$, which means that the transferred energy can be transformed into mass by production of a statistical mixture of quark-antiquark pairs, i.e. mesons (mainly pions). Therefore, the equivalent process to direct photodisintegration on the sub-hadronic scale is *statistical multipion production*, which we will discuss in Sect. 1.2.

Direct particle production: Another kind of direct processes, which occur in the energy range $\epsilon' \sim m_\pi c^2$, is the direct scattering on virtual pions around a baryon. Similarly to Bethe-Heitler pair production, which is the scattering of a virtual photon from the nuclear Coulomb field on a virtual $e^+ e^-$ pair “in” the photon, a photon can directly interact with charged pions from the virtual pion cloud around a nucleon. In the language of quantum field theory, this is expressed by the exchange of a pion between photon and nucleus through the spacelike t -channel (see Sect. 1.2.1.2). This means that the absolute square of the 4-momentum exchange is $|t| \sim m_\pi^2 c^2$, while the total energy in the timelike s -channel is not constrained. Reactions of this type are called t -channel-interactions, for the special case of $|t| = m_\pi^2 c^2$ *one-pion-exchange (OPE)* interactions. We may also call it *direct pion production*, because a virtual pion is materialized in the scattering event.

Since the momentum transfer in direct pion production peaks around the mass of the exchange particle, one may call this a t -channel resonance [Fey72]; to distinguish it from “real” (s -channel) resonances, it is called a *pole*. For a specific pole, the total momentum transfer remains always in the same order of magnitude, independent of the photon momentum; thus, in the high energy limit, the exchanged momentum is small compared to the total momentum, leading strongly forward peaked differential cross sections. A special situation is given if the exchange particle is a photon, which has no massive poles; here, the scattering is forward peaked at all interaction energies. We have already discussed an interaction of this type, the Bethe-Heitler process; the hadronic analogy to this QED process, i.e. quark pair production, is called *Primakoff effect*. A similar process is the production of vector mesons, which carry the same quantum numbers of the photon. Here, one even can say that the photon consists of a superposition of electromagnetic and hadronic constituents; this is known as the *vector meson dominance model*, VDM. This model assumes a direct coupling between the photon and neutral vector mesons $V = \rho^0, \omega, \phi, \dots$ without referring to the QCD structure, assuming coupling constants, $\alpha_\rho, \alpha_\omega, \dots$. Neglecting the small contribution of the ω , the $\gamma N \rightarrow N \rho^0$ cross section is related to the elastic photon cross section by

$$\frac{d\sigma_\rho}{dt} = \frac{4\alpha_\rho}{\alpha_e} \frac{d\sigma_c}{dt} \quad , \quad (1.1.44)$$

From storage ring experiments one finds $\alpha_\rho \simeq 0.6$, leading to $\sigma_\rho \sim 330\sigma_c$, which gives roughly the right order of magnitude. However, we point out that Eq. (1.1.44) should not be taken too literally in connection to Eq. (1.1.22), because there is no strong decrease of the ρ^0 photoproduction cross section observed in the limit to high energies.

We want to point out the most important difference between direct and resonant interactions with respect to cosmic ray transport: direct interactions have generally a very low momentum transfer, and lead therefore to a small energy loss of the cosmic ray. Since the particle is not excited, one can call them *coherent reactions* on the hadronic scale. We will see that this is not only true for interactions with protons, but even for complex nuclei, which are mostly not disintegrated in such processes at high photon energies (see Sect. 1.3.2.2).

1.1.3.3 The phenomenological approach to high energy interactions

Phenomenological modeling: In Sect. 1.1.2.3 we have given an exercise of a method to treat transport phenomena of high energy particles in astrophysical environments, which we want to generalize now. There, we have taken the *theory* of Bethe-Heitler scattering, based on quantum electrodynamics, to obtain the efficiency

function for pair production losses of protons. This treatment was exact in the first Born approximation, therefore a valid description of the real situation (i.e. confirmed to a high degree in experiments) in the limit of small charges and high energies. To apply the results also to heavy nuclei, we again used a theory, which is, however, only valid in the high energy limit which is less important for the astrophysical application. We then found, by inspection of data, a simple *heuristic* modification of the theory, which allowed a simple modification of the astrophysically relevant quantities. The result is, of course, no longer a strict theoretical result; it is an *empirically motivated modification of a theoretical model*.

There is a clear difference between this type of heuristical extensions and empirical data fits, as published in many articles of experimental or observational physics. These fits are generally performed using *mathematically simple functions*, which have no physical meaning at all. The drawback is, that these functions fit the data *in the physical regime where the data have been taken*, and nowhere else. In general, they cannot be used for extrapolation to regions which have not yet been investigated. On the other hand, a theoretical model always contains the feature of predictability; however, in nuclear and particle physics, theoretical models have the drawback to be often either complicated and of limited applicability, or of poor *quantitative* correspondence with the data.

The approach we will follow, which is settled between quantitatively exact theoretical results and empirical data fits, will be called the *phenomenological approach to cosmic ray transport* in the following. It is based on more or less simple theoretical models, which are only required to resemble the *qualitative behavior* of the data;⁶ quantitative deviations are then corrected by applying empirical fudge factors, or by modifying the poorly known parameters used in the derivation of the theory. We will see in Sect. 1.2 and Sect. 1.3 how this works out in practice.

The general form of the loss function: The general form of the *loss time scale* of cosmic ray nuclei due to photonuclear interaction processes, τ_{loss} , is quite close to that already introduced in Eqs. (1.1.32) and (1.1.33): we can write

$$\tau_{\text{loss}}^{-1} = c \int_{\epsilon'_{\text{th}}}^{\infty} d\epsilon' \left[\frac{dN_{\epsilon'}}{d\epsilon'} \right]_{\gamma_{\text{CR}}} \eta(\epsilon') \quad , \quad (1.1.45)$$

where N_{ϵ}' is the LF number density of photons with NRF energy less than ϵ' , and η is the efficiency function of the interaction process, expressing the energy loss per LF time caused by interactions with photons of NRF energy ϵ' ; The function τ_{loss}^{-1} is also called the *loss function* of cosmic rays. We note that we argue simultaneously in two different reference systems; this is because the *astrophysics* is generally given in the LF, while the *interaction physics* is described in the NRF. Clearly, we have to perform consistent transformations of the quantities to develop Eq. (1.1.45) in a useful form. We will divide this task into two steps: (i) the astrophysical part, i.e. determination of the function $dN_{\epsilon}'/d\epsilon'$, and (ii) the interaction physics part, i.e. determination of $\eta(\epsilon')$. The general definition of the efficiency function can be written as

$$\eta(\epsilon) \equiv \int_{\mathcal{F}} d\varphi_1 \dots d\varphi_n \left[\frac{d^n \sigma(\epsilon', \varphi)}{d\varphi_1 \dots d\varphi_n} \right] K(\epsilon', \varphi) \quad , \quad (1.1.46)$$

where $\varphi = (\varphi_1, \dots, \varphi_n)$ are variables determining the *final state space*, \mathcal{F} , of the interaction, and $K(\epsilon', \varphi)$ is the *inelasticity* of the interaction. The inelasticity is defined as the energy loss of the cosmic ray particle in the LF in an interaction determined by the set of variables, ϵ' and φ . Therefore, the task in our treatment of nuclear and particle physics can be summarized as follows:

⁶This is obviously equivalent to confine ourselves to models which are at least partially accepted by the community, because models which do not explain the data at least qualitatively are generally rejected!

1. Separate the total cross section into individual reaction channels c , whose final state can be described by as few variables $\varphi_{c,1}, \dots, \varphi_{c,n}$ as possible.
2. Find for each channel an expression for the inelasticity function $K(\epsilon', \varphi_c)$.
3. Determine the differential cross sections $d^n \sigma_c / (d\varphi_{c,1} \dots d\varphi_{c,n})$ for all channels.

Now we can determine η_c for every channel; since efficiency functions are obviously additive, we have

$$\eta(\epsilon') = \sum_c \eta_c(\epsilon') \quad . \quad (1.1.47)$$

We will now discuss the details of determining photon spectrum, differential cross section and inelasticity functions.

The photon spectrum: In general we will have to deal with photon spectra which are given as functions of LF photon energy, ϵ , and LF interaction angle, θ , with respect to the direction of the cosmic ray velocity. We will introduce the notations $n(\epsilon) = dN_\epsilon/d\epsilon$ for the energy spectrum of the photons in the LF (i.e. the number density per unit energy interval), and the phase space density $f(\epsilon, \Omega)$ in the LF correlated to $n(\epsilon)$ by

$$\frac{n(\epsilon)}{\epsilon^2} = \int_{4\pi} d\Omega f(\epsilon, \Omega) \quad ;$$

Thus we have obviously $n(\epsilon) = 4\pi\epsilon^2 f(\epsilon)$ in the case of an isotropic photon distribution. We note that the phase space density is Lorentz invariant, as is the differential $(\epsilon d\epsilon d\Omega)$, and that the relation between ϵ , θ and ϵ' is given by

$$\epsilon' = \gamma_{\text{CR}} \epsilon (1 - \cos \theta) \quad , \quad (1.1.48)$$

assuming that the cosmic ray nucleus is moving with a Lorentz factor $\gamma_{\text{CR}} \gg 1$, i.e. $\beta_{\text{CR}} = 1$. Then we easily find

$$\left. \frac{dN_{\epsilon'}}{d\epsilon'} \right|_{\gamma_{\text{CR}}} = \frac{2\pi\epsilon'}{\gamma_{\text{CR}}^2} \int_{\epsilon'/2\gamma_{\text{CR}}}^{2\epsilon'\gamma_{\text{CR}}} d\epsilon \bar{f}(\epsilon, \epsilon'/\gamma_{\text{CR}}) \quad , \quad (1.1.49)$$

where $\bar{f}(\epsilon, \epsilon'/\gamma_{\text{CR}})$ is the phase space density averaged over azimuth and with θ expressed in terms of ϵ' and ϵ using relation (1.1.48). For $\gamma_{\text{CR}} \gg 1$, the upper limit of the integral can be set to infinity, because in almost all cases $2\epsilon'\gamma_{\text{CR}} \gg \epsilon_{\text{max}}$, the maximum photon energy available in the LF. We give the analytical result of the integral (1.1.49) for two special cases: (a) an isotropic blackbody spectrum with temperature T ,

$$n(\epsilon) = 4\pi\epsilon^2 f(\epsilon) = \frac{\epsilon^2}{\pi^2 \hbar^3 c^3} \left[\exp\left(\frac{\epsilon}{kT}\right) - 1 \right]^{-1} \quad , \quad (1.1.50a)$$

and (b) an anisotropic power-law spectrum

$$f(\epsilon, \theta) = \frac{N_0}{4\pi\epsilon_0} \frac{(a-1)(b+1)}{2^b} \left(\frac{\epsilon_0}{\epsilon}\right)^{a+2} (1 - \cos \theta)^b \quad \text{for } \epsilon > \epsilon_0 \quad , \quad (1.1.50b)$$

where we call $a \geq 2$ the energy index and $b > -1$ the anisotropy index, θ is defined as the LF angle of the hitting photon with the particle velocity. N_0 is total volume density of photons with $\epsilon_0 < \epsilon < \infty$. Then we obtain

$$\left. \frac{dN_{\epsilon'}}{d\epsilon'} \right|_{\gamma_{\text{CR}}} = \frac{-kT}{2\pi^2 \hbar^3 c^3} \frac{1}{\gamma_{\text{CR}}^2} \ln \left[1 - \exp \left(\frac{-\epsilon'}{2\gamma_{\text{CR}} kT} \right) \right] \quad (1.1.51a)$$

and

$$\left. \frac{dN_{\epsilon'}}{d\epsilon'} \right|_{\gamma_{\text{CR}}} = \frac{N_0}{\gamma_{\text{CR}} \epsilon_0} \frac{(a-1)(b+1)}{a+b+1} \left(\frac{2\gamma_{\text{CR}} \epsilon_0}{\epsilon'} \right)^a \quad \text{for } \epsilon' > 2\gamma_{\text{CR}} \epsilon_0, \quad (1.1.51b)$$

respectively; the low energy limit in Eq.(1.1.51b) is obviously irrelevant for Eq.(1.1.45) if $\epsilon'_{\text{th}} > 2\gamma_{\text{CR}} \epsilon_0$. Eq.(1.1.51a) is well known from many papers on extragalactic UHECR transport, because it determines the losses in the universal microwave background if we set $T = 2.73$ K. Eq.(1.1.51b) may describe the situation near particle accelerators, where the background radiation is dominated by synchrotron photons emitted from a power-law spectrum of electrons. We note that the range $-1 < b < 0$ describes an anisotropic spectrum irradiating the cosmic rays mainly from the back, while $b > 1$ describes irradiation mainly from the front (see Fig. 1.4). The mean value of $\cos \theta$ is connected to the power law index by

$$b = -\frac{2 \langle \cos \theta \rangle}{1 + \langle \cos \theta \rangle} ; \quad (1.1.52)$$

we may consider Eqs.(1.1.50b) and (1.1.51b) as an analytical sample spectrum for any given $\langle \cos \theta \rangle$ if b is determined following Eq. (1.1.52). We see that $b = -1$ leads to $dN_{\epsilon'}/d\epsilon' = 0$, because photons from the back have zero energy in the NRF, while $b \rightarrow \infty$, corresponding to irradiation completely from the front, enhances $dN_{\epsilon'}/d\epsilon'$ by a factor $(a+1)$ compared to the isotropic case. However, the anisotropy of the photon background plays only a role if also the cosmic ray distribution is anisotropic, otherwise we may average over cosmic ray direction and set $b = 0$.

Kinematics and inelasticity: The inelasticity is a function which explicitly refers to the LF, no matter in which Lorentz system the independent variables are given, because it expresses the non-invariant energy loss of the particle in this frame. The energy loss may be most generally expressed in the form $\Delta E = \Delta(m_{\text{CR}} \gamma_{\text{CR}})$; therefore, the inelasticity expresses a combination of mass and Lorentz factor changes of the particles. For cosmic ray protons, this can be reduced to a pure Lorentz factor change, if we define an ‘‘interaction’’ as everything what happens between the collision with the photon, and the recovery of the proton of a, possibly multistep, baryon decay chain. For complex nuclei, we have to consider both mass and Lorentz factor changes, but as we will see in Sect. 1.3.4.1 the possible reactions are separable between both cases, i.e. they cause either mass or Lorentz factor changes, but not both.

If pure mass change has to be considered, the inelasticity can generally be expressed in a *discrete quantity* $\Delta A/A$, which is obviously independent of the reference frame. To treat Lorentz factor changes, we have to consider the *kinematics* of the interaction, which is frame dependent. It is, of course, desirable for practical use to give an expression for the function K in terms of quantities related to the interaction process without knowing about LF. There are two ways to do that:

1. If the energy transfer to the nucleus in the NRF is small, the inelasticity is given by the *parallel momentum transfer* q_{\parallel} in the NRF. The variable in this case are generally the energies and scattering angles of the final state particles in the NRF; because of the conservation of energy we have $2n - 1$ final state variables for n particles produced by the photon.

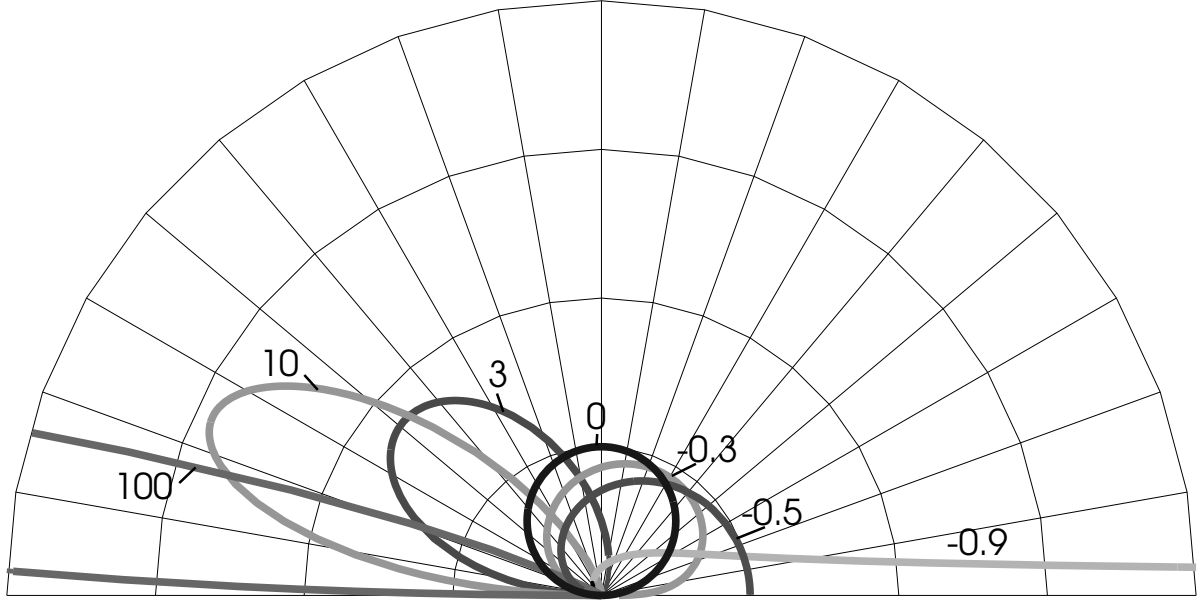


Figure 1.4: Anisotropy distribution for photon spectrum given in Eq.(1.1.50b). The radius of the curves corresponds to the LF probability density that the cosmic ray is hit from this direction, $d\mathcal{P}/d\theta$, for anisotropy indices b as labeled at the curves.

2. In a final state containing only two particles with masses m_1 and m_2 , the inelasticity with respect to m_1 (identified with the cosmic ray particle) is most easily described in the CMF, where it is given as a function of scattering angle χ^* and total interaction mass M_{int} by

$$K_{f2}(M_{\text{int}}, \chi^*) = 1 - \frac{m_1}{M_{\text{int}}} \gamma_1^*(M_{\text{int}}) (1 + \beta_1^* \cos \chi^*) \quad , \quad (1.1.53a)$$

with

$$\gamma_1^*(M) = \frac{M^2 + m_1^2 - m_2^2}{2m_1 M} \quad (1.1.53b)$$

being the Lorentz factor of the particle with mass m_1 in the rest system of the interaction mass M , and β_1^* its velocity. Note that M may be set to M_{int} in a collision, as well as to the mass of a decaying particle. M_{int} is given as a function of NRF photon energy by Eq.(1.1.1), and often expressed in the quantity $s = M_{\text{int}}^2$. We note that we can *not* use the simplification $\beta_1^* \simeq 1$; at production threshold, we will even have $\beta_1^* = 0$. We note that this expression does not assume that the energy transfer to the nucleus (mass m_1) in the NRF is small.

The first method is generally only useful if elaborated theories allow to determine the complicated expression for the differential cross section with respect to the $2n - 1$ final state variables; we have made use of this method in determining the efficiency function for the Bethe-Heitler process, Eq.(1.1.33). The second method

is quite general; all we need are the differential cross sections $d\sigma/d\chi^*$, which are known from experiment for many reactions. Unfortunately, there is no useful expression in the general case for the inelasticity of reaction channels with more than two outgoing particles; therefore, we should try to choose our reaction channels in a way that Eq. (1.1.53) can be applied; we will discuss this in detail in Sect. 1.2.

Cross section parametrizations: When we have found a suitable classification of a photonuclear reaction into reaction channels, we need to parametrize the differential cross section of the reaction. The first step is to separate initial and final state variables by writing

$$\frac{d^n \sigma_c(\epsilon', \boldsymbol{\varphi})}{d\varphi_1, \dots, d\varphi_n} = \sigma_c(\epsilon') \Phi_c(\boldsymbol{\varphi}) \quad , \quad (1.1.54)$$

where $\sigma(\epsilon')$ is the total photon absorption cross section of the reaction channel c , and the function Φ_c described its final state probability distribution. In the case of two particle kinematics, this is a function of only one parameter, χ^* , which generally expressed as a superposition of Legendre polynomials.

The remaining task is to parametrize the total cross section. We have seen that bound systems of particles generally will show resonant behavior in interactions with photons; since nuclei and even baryons are composite particles, we have to expect that resonances play a dominant role in the description of reaction cross sections. If we know the mass M , the width Γ and the angular momentum quantum number J of the resonance, it is uniquely described by the Breit-Wigner cross section curve, which is given in terms of photon NRF energy and related CMF quantities as

$$\sigma_{\text{BW}}(\epsilon') = \frac{2\pi(\hbar c)^2}{(mc^2)^2} \frac{2J+1}{2J_0+1} \frac{s}{\epsilon'^2} \frac{b_\gamma b_c \Gamma^2}{[(s-M^2)^2/s] + \Gamma^2} \quad , \quad (1.1.55)$$

where m and J_0 are the mass and spin of the unexcited nucleus. Note that the only free parameter in this formula are the *branching ratios* b_γ and b_c for radiative decay of the resonance, and the decay into the chosen reaction channel c , respectively. These parameters are often well determined by experiment (see Sect. 1.2.2.3). However, in many cases we will be confronted with the situation that the cross section is given by a superposition of overlapping resonances, whose properties are not all well known; in this case, it may be sufficient to express the cross section by the approximate Lorentz-shape description of a resonance,

$$\sigma_{\text{L}}(\epsilon') \equiv \sigma_0 \hat{\sigma}_{\text{L}}(\epsilon'; E_0, \Gamma) = \frac{\sigma_0 \Gamma^2}{(\epsilon' - E_0)^2 + \Gamma^2} \quad , \quad (1.1.56a)$$

and then to determine the resonance energy E_0 , width Γ and maximum cross section σ_0 by fitting the cross section to experimental data. We note that the total integrated cross section resulting from Eq. (1.1.56) is

$$\Sigma_{\text{L}} = \frac{\sigma_0 \Gamma}{2} \left(\frac{\pi}{2} + \arctan D_{\text{th}} \right) \quad \text{with} \quad D_{\text{th}} = \frac{E_0 - \epsilon_{\text{th}}}{\Gamma/2} \quad , \quad (1.1.56b)$$

where ϵ_{th} is the reaction threshold; thus we may express σ_0 in terms of the total integrated cross section.

Clearly, there are reactions which do not proceed over resonance excitation; in such cases, there should be, at least, some models available which predict the asymptotic behavior of the cross section — we may then fit the data with a curve showing the predicted asymptotic behavior, and assume that we have found at least an approximate description of the cross section. For this purposes, we define the special functions

$$\text{Pl}(x; x_{\text{th}}, x_{\text{max}}, \alpha) = \left(\frac{x - x_{\text{th}}}{x_{\text{max}} - x_{\text{th}}} \right)^{A-\alpha} \left(\frac{x}{x_{\text{max}}} \right)^{-A} \quad \text{with} \quad A = \alpha \left[\frac{x_{\text{max}}}{x_{\text{th}}} \right] \quad (1.1.57a)$$

and $\text{Pl}(x; x_{\text{th}}, x_{\text{max}}, \alpha) = 0$ for $x < x_{\text{th}}$, and

$$\text{Ef}(x; x_0, w) = \frac{1}{2} \left[1 + \text{erf} \left(\frac{3}{\sqrt{2}} \frac{2x - 2x_0 - w}{|w|} \right) \right] \quad . \quad (1.1.57b)$$

The functions $\text{Pl}(x)$ show a power law behavior both at threshold and in the asymptotic limit, where $\text{Pl}(x; x_{\text{th}}, x_{\text{max}}, \alpha) \propto x^{-\alpha}$, and have a maximum at x_{max} . $\text{Ef}(x)$ are a kind of smooth step functions, which rise from $\text{Ef}(x) \approx 0$ to $\text{Ef}(x) \approx 1$ in the region $x_0 < x < x_0 + w$; note that $\text{Ef}(-x; -x_0, -w)$ is a cutoff function dropping from 1 to 0 between x_0 and $x_0 + w$. Of course, other simple mathematical functions may find use if appropriate; we will only always make sure to use functions with a predictable (and reasonable) asymptotic behavior.

1.2 Photomeson production at free nucleons

This section presents a detailed treatment of astrophysically relevant photomeson processes, following the phenomenological approach described in Sect. 1.1.3.3. The approach followed here is guided by the phenomenological concept of mixing experimental data with simple theoretical ideas to obtain a most useful parametrization of the various processes. Sect. 1.2.1 discusses the relevant concepts of elementary particle physics, and in Sect. 1.2.2 we develop the parametrization to be used in astrophysical applications.

Basic concepts of particle physics are described, e.g., in the books of PERKINS [Per82] and CHENG & O'NEILL [CO79]. A good description of the properties of baryon resonances is given by BRANSDEN & MOORHOUSE [BM73]. An overview about the physics of photohadronic interactions can be found in a monograph of FEYNMAN [Fey72], and in the proceedings *Hadronic Interactions of electrons and photons* [CO70]; specific references are given in the text. The *Review of Particle Properties* (Edition 1994) [Par94] has been used extensively.

Notation: The notation of the last section applies unchanged. The symbols s , t and u denote mandelstam variables throughout this section. We make use of the special functions $Ef(x)$ and $Pl(x)$, defined in Eqs. (1.1.57). The reader should never be confused by denoting both the η -meson and the efficiency function with the same symbol, η .

1.2.1 Basic physics of photohadronic interactions

1.2.1.1 Classification of final states

On the definition of “final state”: The determination of the efficiency function for cosmic ray transport is based on the analysis of the interaction kinematics. This is clearly dependent on the number and type of the mesons produced in the interaction, so any kinematical analysis has to start with a separation into different final states. But what should we call the “final state” of an interaction?

A convenient way often used in particle physics is to distinguish the *number of pions* produced; pions are the lightest mesons and undergo only weak and electromagnetic decay, thus they have a relatively long lifetime compared to strong decaying particles. Therefore, final state is here defined as that which can be observed in a particle detector (e.g. a bubble chamber). We would therefore start the analysis by determining the differential cross sections of the reactions $\gamma N \rightarrow N\pi$, $\gamma N \rightarrow N\pi\pi$, $\gamma N \rightarrow N\pi\pi\pi$ etc., with respect to the energy and momentum transfer to the nucleon in the NRF. This could be conveniently performed using particle event generator programs. Finally, we would have to parametrize both cross section and inelasticity as functions of photon energy. However, several problems of this method must be considered: First, some reactions as η or strange particle production do not simply fit into a classification in pion multiplicity, because these particles have additional decay channels not involving pion production; this could, of course, easily be considered by a good event generator. More care has to be taken about *experimental selection effects* due to the bad observability of neutral particles. Final states containing more than one neutral particle can not be completely analyzed in general; therefore, they are often missing in standard data collections, which however does not mean that they are nonexistent. Therefore, we have to consider the way of modeling efficiency functions from *mere* interpolation and extrapolation of empirical data as problematic; using event generators which consider basic symmetry principles may solve this problem.

In our phenomenological approach, we will go a different way: first, we separate the final state space into *quasi-two-particle* channels, which means that we consider the *first* products of the interaction, which are generally strong-decaying particles of very short lifetimes. We find that almost the entire γN cross section below $\epsilon' \sim 500$ MeV and still a large fraction up to $\epsilon' \sim 1$ GeV is dominated by quasi-two-particle final states. The differential cross sections of these reaction channels are generally well treated in particle data collections. As we have seen, the inelasticity of such reactions is completely determined by the CMF scattering angle χ^* . Furthermore, we can use simple symmetry concepts to discern the contribution of not or badly detectable reactions.

The remaining part of the γN cross section, which does not fit into the quasi-two-particle picture, can then be approximated by a statistical model of multipion production, which dominates for $\epsilon' \gtrsim 1$ GeV.

Quasi-two-particle channels: The most important photohadronic two-particle channel is, of course, is single pion production. However, also two- and three-pion production proceeds largely through two particle intermediate states. The main contribution is by the channels

$$\gamma N \rightarrow N \pi \quad (1.2.1)$$

$$\gamma N \rightarrow \Delta(1232) \pi \quad (1.2.2)$$

$$\gamma N \rightarrow N \rho \quad (1.2.3)$$

$$\gamma N \rightarrow N \eta \quad (1.2.4)$$

$$\gamma N \rightarrow N \omega \quad (1.2.5)$$

$$\gamma N \rightarrow B_S K \quad , \quad (1.2.6)$$

where we have denoted the nucleon with N , and B_S stands for *strange baryon*, i.e. the particles Λ and Σ ; heavier baryons are disregarded because of their negligible contribution. The channels are enumerated in the order of increasing threshold energy, and decreasing contribution to the total cross section. Reactions (1.2.2) and (1.2.3), together with a 37% contribution of the η -decay from (1.2.4) make up almost the whole $\gamma N \rightarrow N \pi \pi$ cross section. Reactions (1.2.3) and (1.2.5) contribute substantially to three-pion production.

Reactions (1.2.1) and (1.2.2) are subdivided into different charge distributions on the outgoing particles, which are connected by isospin symmetry (see Sect. 1.2.1.3). We can distinguish the reactions

$$\gamma p \rightarrow p \pi^0 \quad \gamma n \rightarrow n \pi^0 \quad (1.2.1a)$$

$$\gamma p \rightarrow n \pi^+ \quad \gamma n \rightarrow p \pi^- \quad (1.2.1b)$$

and

$$\gamma p \rightarrow \Delta^{++} \pi^- \quad \gamma n \rightarrow \Delta^- \pi^+ \quad (1.2.2a)$$

$$\gamma p \rightarrow \Delta^+ \pi^0 \quad \gamma n \rightarrow \Delta^0 \pi^0 \quad (1.2.2b)$$

$$\gamma p \rightarrow \Delta^0 \pi^+ \quad \gamma n \rightarrow \Delta^+ \pi^- \quad (1.2.2c)$$

corresponding to the isospin multiplets of N and Δ baryons (see below). We have explicitly distinguished between photo-proton and photo-neutron reactions; these are in general *not* connected by isospin symmetry, because the electromagnetic interaction does not conserve isospin. However, one finds experimentally that the total cross sections of γp and γn reactions are almost equal, except for some special cases which will be pointed out.

The strange channel (1.2.6) splits up into the reactions

$$\gamma p \rightarrow \Lambda K^+ \quad \gamma n \rightarrow \Lambda K^0 \quad (1.2.6a)$$

$$\gamma p \rightarrow \Sigma^0 K^+ \quad \gamma n \rightarrow \Sigma^0 K^0 \quad (1.2.6b)$$

$$\gamma p \rightarrow \Sigma^+ K^0 \quad \gamma n \rightarrow \Sigma^- K^+ \quad . \quad (1.2.6c)$$

Reactions (1.2.6b) and (1.2.6c) are connected by isospin symmetry, while (1.2.6a) is not. However, the Λ and the lowest mass Σ baryons belong to the ($J^P = \frac{1}{2}^+$) SU(3) octet of baryons in the quark model, which also makes

predictions for their relative contributions to strong interactions. The total contribution of the strange channel to the γN cross section is almost negligible, it only could play a role if the properties of the strange particles are important, in particular their long lifetime $\tau \gtrsim 10^{-8}$ sec which corresponds at highest energy cosmic ray Lorentz factors, $\gamma \gtrsim 10^{11}$, to a mean path length $L \gtrsim 3$ AU. Moreover, the Λ and Σ baryons have almost equal mass; we will therefore treat Eqs. (1.2.6) as just one reaction channel in photohadronic interactions and assume SU(3) symmetry as valid.

Statistical multi-pion production: At high energies, photomeson production will generally not fit any more into the simple picture of quasi-two-particle final states. Rather, the number of possible reactions possible in every energy bin increases so fast, that we can assume a kind of *statistical mixture* of processes, all leading to the production of two or more pions. This kind of models are called *fireball models*, or more specifically in the context of pion production, *statistical multipion production*; pion production is here considered as the mass fragmentation of an energy cloud.

An important feature of high energy pion production is the *leading particle effect*: It expresses the experimental finding that most of the longitudinal CMF momentum in the final state of a fireball reaction is carried by particles which have the quantum numbers of the incident particles. Simply speaking, we might say that the fireball is produced “at rest” in the CMF by two particles flying “through each other”, interacting only peripherally. Recalling our earlier description of this process as direct photon scattering at the quark scale (Sect. 1.1.3.2), we may use the quark model to determine a quantitative estimate of the total energy available for mass production (cf. [Erw71]): Adopting the hadronic picture of a photon as a superposition of vector mesons, we would expect that the main interaction takes place between one nucleon quark and one (virtual) photon quark, while all the other (spectator) quarks keep their momentum. Therefore, we would naively expect that about $\frac{2}{5}$ of the total kinetic energy is converted into mass production — which is in good correspondence with experimental results. Hence, the leading particle effect finds a natural explanation in a participant-spectator model of inter-quark collisions (see also Sect. 1.3.2.1 for similar ideas in nuclear physics).

The fragmentation of the fireball into pions can be treated in terms of simple thermodynamics, leading to a pion multiplicity distribution as a function of total CMF energy. The first approach in this direction was done by FERMI [Fer51]; modifying his ideas to comply with the leading particle effect and the inter-quark collision picture, we may write

$$\overline{N}_{(\pi)} \propto M_{\text{kin}}^{1/2} \propto s^{1/4} \quad ,$$

which is in fair agreement with the data for $s \lesssim 10^4 \text{ GeV}^2$ [DS72]. More detailed models of multipion fragmentation of fireballs are currently under discussion, but involve complicated physics of the quark-gluon-plasma; for our purposes we will consider it as sufficient to use the numerical approximation

$$\overline{N}_{(\pi)}(\epsilon') \approx 2.4 \left(\frac{\epsilon}{[\text{GeV}]} \right)^{\frac{1}{4}} \quad (1.2.7)$$

and assume the multiplicity distribution to be Poissonian around $\overline{N}_{(\pi)}$, which is roughly consistent with the data [Wan69].

1.2.1.2 Resonances and direct scattering

Spacelike and timelike exchange diagrams: The quasi-classical view on resonances and direct scattering events, as presented in Sect. 1.1.3, may help to imagine the processes happening in quantum-mechanical photohadronic scattering processes. The corresponding picture of relativistic quantum theory is expressed by the

concept of *spacelike and timelike trajectories*, which considers the “wholeness” of quantum mechanical states:⁷ *Timelike* means, that the exchange particle has distinct time of production and decay, and a well defined lifetime; this corresponds to the classical picture of the formation and decay of a resonance. The mass of the resonance appears as a Breit-Wigner peak in the total interaction energy, called the *s*-channel. *Spacelike* means that there is no causal connection between the emission and absorption of the exchange particle, the exchange happens *simultaneously*. As already assumed, the mass of the exchange particle appears as a *pole* (one might say: a spacelike resonance) in the 4-momentum transfer. One distinguishes between the *t*-channel, through which a meson is exchanged, and the *u*-channel corresponding to the exchange of the baryon. The lowest order terms of single pion production may therefore be depicted as

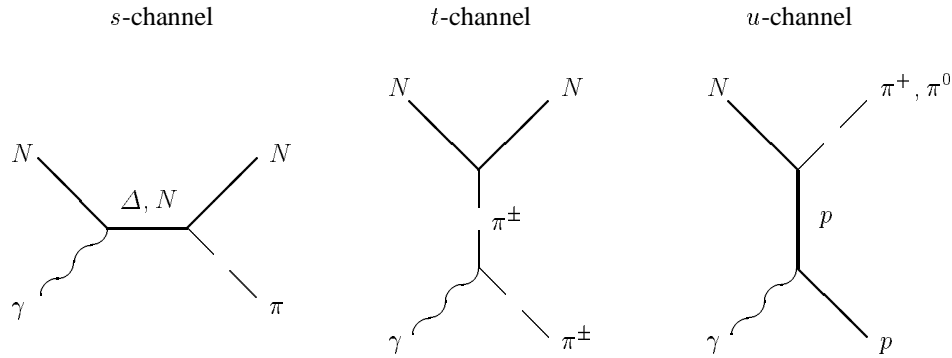


Figure 1.5: Lowest order photohadronic Feynman diagrams

The main difference of these reaction types with respect to the astrophysical application is the different behavior in cross section and kinematics: Timelike (*s*-channel) reactions, i.e. resonant scattering, shows a pronounced peak around the resonance mass in the total cross section, but is in good approximation structureless in the momentum transfer distribution (i.e. isotropic in the CMF). Spacelike (*t* and *u*-channel) interactions are almost structureless in their *s*-dependence, but show a strong correlation of the final state and initial state particle momentum directions; *t*-channel reactions correspond to small scattering angles (i.e. they are *forward-peaked*), *u*-channel reactions are *backward peaked*. *t* and *u*-channel correspond not equally to the cross section of direct scattering, but depend on the mass of the exchange particle approximately as $\sigma \propto m^{-2}$; *u*-channel exchange ($m \gtrsim m_p$) may therefore be disregarded in comparison to low mass poles ($m \lesssim m_\pi$) in the *t*-channel.

Baryon resonances: The baryon is a composite particle. Similar to the situation in atomic and nuclear physics, we therefore expect a shell structure of the baryon, and the existence of excited states of well defined quantum numbers, called *baryon resonances*. They have first been discovered as resonances in elastic pion-nucleon scattering, and are thus described by spectroscopic terms of the pion-nucleon system: a capital letter, *S, P, D, F, ...*, for the orbital angular momentum of the πN system, $L = 0, 1, 2, 3, \dots$, and indices for the isospin *I* and the total angular momentum *J*, in the way $L_{[2I][2J]}$; e.g., a resonance with $L = 1$, $I = \frac{3}{2}$ and $J = \frac{3}{2}$, is denoted as P_{33} . The parity of a baryon resonance is given by $P = (-1)^{L+1}$, and the its angular momentum can only take values $L - \frac{1}{2} \leq J \leq L + \frac{1}{2}$; thus an alternative, unique notation for a resonance is $I(J^P)$. Additionally, every resonance state $L_{[2I][2J]}$ can exist in different radial excitation modes (i.e. on different shells), thus with different masses. However, the mass differences between resonances due to radial and rotational excitation are

⁷A Capraesque statement, but nevertheless true!

comparable. The possible excitation states of the nucleon can only have the isospin values $I = \frac{1}{2}$ or $I = \frac{3}{2}$; the former are called N -resonances, the latter Δ -resonances. So, another way of denoting baryon resonances is by calling their isospin and mass in the form $N(M_{[\text{MeV}]})$ or $\Delta(M_{[\text{MeV}]})$, which may be completed by notation of J^P .

Of the parameters determining a baryon resonance, their mass M , total width Γ , angular momentum J , and radiative decay width Γ_γ , determine *completely* their contribution to the total γN cross section. For the πN decay channel, the spectroscopic classification of the resonance determines the angular distribution of the resonance decay. Finally, the isospin of the resonance, and the isospin of the final state particles, determine the branching ratios within charge multiplets.

Spacelike trajectories and photon vertices: In our naive picture of direct scattering discussed in Sect. 1.1.3.2, virtual mesons are scattered out of the strong field around the nucleon. Clearly, to be scattered by a photon, a particle must carry charge. In the quantum-relativistic picture, this corresponds to the restriction that the photon vertex in diagram 2 of Fig. 1.5 is electromagnetic. The second vertex, between baryon and meson, is assumed to be strong, therefore fulfills isospin symmetry. Since the electromagnetic scattering cannot change the properties of the particle, the mass of the exchange particles may be assumed to be that of the charged meson in the final state, corresponding to direct π^\pm , K^\pm , . . . production.

Clearly, the vertex between the photon and the meson may be not purely electromagnetic. In this case, it must be possible to “resolve” the photomesonic vertex into a set of vertices in the quark picture, where all direct photon vertices are electromagnetic. Primakoff production of quark-pairs in the Coulomb field of the nucleus can be resolved in a way shown in diagram 2 of Fig. 1.6, similarly to the Bethe-Heitler diagram (Fig. 1.2). Since it contains two electromagnetic vertices, we may assume that it is suppressed by roughly two orders of magnitude compared to direct production of charged pions. The Primakoff effect is expected to be important in the production of mesons which show strong electromagnetic ($\gamma\gamma$) decay channels, as the π^0 and η mesons. On the other hand, the production of *vector mesons*, which carry the same spin-parity quantum numbers as the photon, $J^{PC} = 1^{--}$, requires the exchange of a particle with quantum numbers $J^{PC} = 0^{++}$. These are the quantum numbers of the vacuum, and the corresponding exchange trajectory is generally depicted as the *Pomeranchuk particle* or *pomeron*. However, there are also a number of massive mesons carrying these quantum numbers, which may therefore contribute as massive poles to vector meson production. The lightest vector mesons are the ρ^0 and the ω , corresponding to superpositions of $u\bar{u}$ and $d\bar{d}$ quark states; heavier vector mesons, as the $\phi = s\bar{s}$ play no role for our considerations. The general diagram for vector meson production

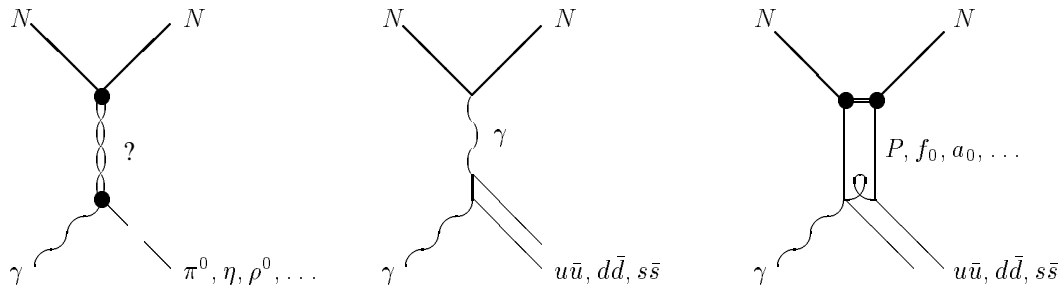


Figure 1.6: Second order direct meson production diagrams in the QCD picture

in the quark picture would therefore be a quark-pair exchange (diagram 3 of Fig. 1.6). The Pomeron exchange term could be probably depicted as a double gluon exchange between the virtual quarks in the hadronic photon and proton quarks [DW88].

1.2.1.3 Final state angular distributions and branching ratios

Radiative excitation of resonances: Since baryon resonances have specific quantum numbers for angular momentum and parity, J^P , we can constrain the possible contribution of photon multipoles to the excitations of the resonance. A photon with orbital angular momentum $l\hbar$ ($l \neq 0$) and parity Π , interacting with a nucleon with spin $\frac{1}{2}$, can create resonances with total angular momenta $l - \frac{1}{2} \leq J \leq l + \frac{1}{2}$ and parity $P = -\Pi$; therefore, for given J the possible L values are $J - \frac{1}{2} \leq l \leq J + \frac{1}{2}$, which means that there always exist *two* possible l values for the excitation of a resonance with $J \geq \frac{3}{2}$, and *one* for $J = \frac{1}{2}$. The parity constraint determines for each of the possible l one electric and/or one magnetic excitation mode. Averaging over the possible spin orientations of the nucleon, $S_z = \pm\frac{1}{2}$, and polarization of the photon, $l_z = \pm 1$, one can obtain the distribution of J orientations, J_z , of the resonance. For the $N^* \rightarrow N\pi$ decay channel, we can immediately take the orbital angular momentum of the $N\pi$ system from the spectroscopic classification of the resonance, and calculate the distribution coefficients C_{LL_z} of L_z from the J_z by using the Clebsch-Gordan coefficients. The angular distribution of the decay in the CMF is then given in terms of spherical harmonics by

$$\left(\frac{d\sigma}{d\chi}\right)_L \stackrel{*}{=} \sum_{m=-L}^L C_{Lm} |Y_{Lm}(\chi)|^2 \quad . \quad (1.2.8)$$

It is convenient to introduce the electric and magnetic multipole transition amplitudes, $E_{L\pm}$ and $M_{L\pm}$, respectively, where $L\pm$ refers to the resonance states (L, J) with $J = L \pm \frac{1}{2}$. Obviously, $E_{L\pm}$ amplitudes correspond to El transitions with $l = L \pm 1$, $M_{L\pm}$ amplitudes to Ml transitions with $l = L$. One can then find that

$$\frac{d\sigma}{d\chi^*} \propto 1 \quad \text{for } E_{S+}, M_{P-} \quad (1.2.8a)$$

$$\frac{d\sigma}{d\chi^*} \propto 5 - 3 \cos^2 \chi^* \quad \text{for } E_{D-}, M_{P+} \quad (1.2.8b)$$

$$\frac{d\sigma}{d\chi^*} \propto 1 + \cos^2 \chi^* \quad \text{for } E_{P+}, M_{D-} \quad (1.2.8c)$$

$$\frac{d\sigma}{d\chi^*} \propto 5 + 6 \cos^2 \chi^* + 5 \cos^4 \chi^* \quad \text{for } E_{F-}, M_{D+} \quad (1.2.8d)$$

$$\frac{d\sigma}{d\chi^*} \propto 1 + 6 \cos^2 \chi^* - 5 \cos^4 \chi^* \quad \text{for } E_{D+}, M_{F-} \quad (1.2.8e)$$

Higher excitations involve $\cos^{2n} \chi^*$ terms with $n \geq 3$. Experimentally, the radiative excitation amplitudes are commonly expressed in terms of the *helicity amplitudes* $A_{3/2}$ and $A_{1/2}$, which correspond to a parallel and anti-parallel spin coupling of the photon-nucleon system, respectively. The multipole amplitudes can be calculated from the helicity amplitudes using the formulae in Ref. [BM73, App. B]; more important here is the connection to the total radiative decay width of the resonance, which is given by

$$\Gamma_\gamma = \frac{k_0^2}{\pi} \frac{2m_N}{(2J+1)M_{\text{res}}} \left(|A_{1/2}|^2 + |A_{3/2}|^2 \right) \quad , \quad (1.2.9)$$

where k_0 is the decay momentum of the photon in the rest frame of the resonance. Γ_γ determines the total cross section for the radiative excitation of a baryon resonance, following Eq. (1.1.55).

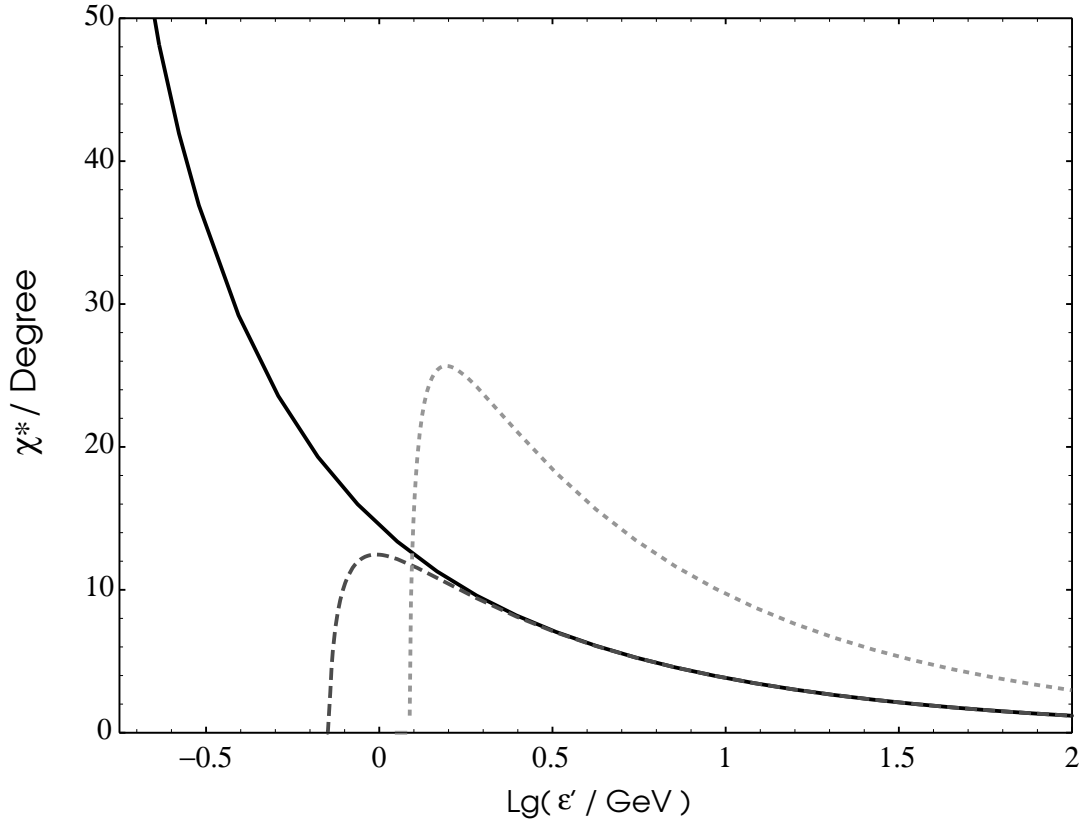


Figure 1.7: Average CMF scattering angle for t -channel reactions, as derived from Eq. (1.2.10) with $t = -(m_t c)^2$, for: $\gamma N \rightarrow N\pi$ (solid line, OPE, $m_t = m_\pi$), $\gamma N \rightarrow \Delta\pi$ (dashed line, OPE, $m_t = m_\pi$), and $\gamma N \rightarrow N\rho^0$ (dotted line, diffractive, $m_t = 350$ MeV, see text).

Angular distribution of t -channel reactions: The Lorentz invariant quantity t is connected to the CMF scattering angle by

$$t \doteq (\Delta E)^2 - [p_i^2 + p_f^2 - 2p_i p_f \cos \chi^*] c^2 \quad (1.2.10)$$

with

$$\frac{\Delta E^*}{c^2} = \frac{m_1^2 - m_2^2 - m_N^2}{2M_{\text{int}}} \quad , \quad \frac{p_i^*}{c} = \frac{M_{\text{int}}^2 - m_N^2}{2M_{\text{int}}} \quad \text{and} \quad \frac{p_f^*}{c} = m_1 \gamma_1^* \beta_1^* \quad ,$$

where m_1 and m_2 are the masses of the baryon and the meson in the final state, respectively, and γ_1^* and β_1^* can be determined using Eq. (1.1.53b). ΔE^* is the CMF energy transfer due to mass production, in elastic interactions is $\Delta E^* = 0$. In the limit of large $s = M_{\text{int}}^2$, this leads to

$$\cos \chi^* \rightarrow 1 + \frac{2t}{s} \quad . \quad (1.2.10a)$$

In the picture of a definite t -exchange particle, corresponding to a constant $t = -m_t^2 c^2$, we see that $\cos \chi^* \rightarrow 1$ for $M_{\text{int}} \rightarrow \infty$, which means that t -channel scattering is increasingly forward peaked for high energies. In the special case of OPE reactions, i.e. direct pion production in the $\gamma N \rightarrow N\pi$ and $\gamma N \rightarrow \Delta\pi$ channels, we have

Table 1.1: Branching ratios within isospin multiplets

Final state:		$N\pi$		$\Delta\pi$		
I	I_3	$\Delta I_3 = \pm 1$	$\Delta I_3 = 0$	$\Delta I_3 = +1$	$\Delta I_3 = 0$	$\Delta I_3 = -1$
$\frac{1}{2}$	N^+	$\frac{2}{3} \rightarrow N^0\pi^+$	$\frac{1}{3} \rightarrow N^+\pi^0$	$\frac{1}{2} \rightarrow \Delta^{++}\pi^-$	$\frac{1}{3} \rightarrow \Delta^+\pi^0$	$\frac{1}{6} \rightarrow \Delta^0\pi^+$
	N^0	$\frac{2}{3} \rightarrow N^+\pi^-$	$\frac{1}{3} \rightarrow N^0\pi^0$	$\frac{1}{6} \rightarrow \Delta^+\pi^-$	$\frac{1}{3} \rightarrow \Delta^0\pi^0$	$\frac{1}{2} \rightarrow \Delta^-\pi^+$
$\frac{3}{2}$	Δ^+	$\frac{1}{3} \rightarrow N^0\pi^+$	$\frac{2}{3} \rightarrow N^+\pi^0$	$\frac{2}{5} \rightarrow \Delta^{++}\pi^-$	$\frac{1}{15} \rightarrow \Delta^+\pi^0$	$\frac{8}{15} \rightarrow \Delta^0\pi^+$
	Δ^0	$\frac{1}{3} \rightarrow N^+\pi^-$	$\frac{2}{3} \rightarrow N^0\pi^0$	$\frac{8}{15} \rightarrow \Delta^+\pi^-$	$\frac{1}{15} \rightarrow \Delta^0\pi^0$	$\frac{2}{5} \rightarrow \Delta^-\pi^+$

assumed that $\overline{m}_t = m_\pi$, where the distribution of m_t is given by a Breit-Wigner curve. There is no definite mass assigned to the t -channel in Pomeron exchange; for high energy reactions one finds

$$\frac{d\sigma}{dt} \propto e^{-t/t_0} \quad \text{with} \quad t_0 \sim -\frac{1}{8} \frac{\text{GeV}}{c}, \quad (1.2.11)$$

which leads to an average value of $\overline{m}_t \sim 350$ MeV. Adopting this value for diffractive vector meson $m_t = m_\pi$ for OPE reactions, we obtain $\langle \cos \chi^* \rangle$ as a function of photon NRF energy ϵ' as shown in Fig. 1.7.

We should point out that the assumption of constant exchange mass is quite crude, and definitely wrong for OPE reactions in the high energy limit. Rather, one finds that *every* reaction shows a t -dependence as given by Eq. (1.2.11) for large ϵ' , thus we have to expect that the OPE curves in Fig. 1.7 approach the diffractive curve at high energies. However, we will see that the effect of t -channel reactions on inverse $p\gamma$ scattering is negligible far from threshold, so that we only have to assume that $\langle \chi^* \rangle$ as shown in Fig. 1.7 is a reliable estimate close to threshold.

Isospin symmetry: In the same way as the distribution of J_z determines the angular distribution of decay particles, the distribution of isospin orientations, I_3 , gives the charge distribution of the particles within an isospin multiplet. We will call these numbers *iso-branching ratios*. Obviously, N -resonances exist in a charge doublet (N^+ , N^0), as the nucleon itself, while Δ -resonances form a charge quadruplet (Δ^{++} , Δ^+ , Δ^0 , Δ^-). Like the geometrical spin, the isospin follows rotational symmetry principles, which allows to determine decay branching ratios by use of Clebsch-Gordan coefficients. We note that isospin symmetry is fulfilled only in strong interactions, thus the decay of resonances, but not in their electromagnetic formation (for this reason Δ resonances can be excited in a photonuclear reaction). Of course, electromagnetic interactions conserve I_3 , i.e. the charge of the particle.

The iso-branching ratios following from the Clebsch-Gordan coefficients are summarized for the possible resonance excitation states of photonuclear interactions in Tab. 1.1. Simply speaking, they give the probabilities for a certain isospin flip, ΔI_3 , of the baryon in the interaction. In s -channel reactions, every reaction has to be energetically allowed, i.e. the sum of masses in the final state must be below the mass of the decaying resonance. This constraint does not apply in t -channel reactions; here the branching ratios do still apply, but we have to consider electromagnetic constraints on the “decay” channels, as the deletion of the π^0 branch in direct pion production. On the other hand, t -channel reactions obey isospin symmetry between neutron and proton, because they contain no direct vertex between the photon and the nucleon (see diagram 2 in Fig. 1.5).

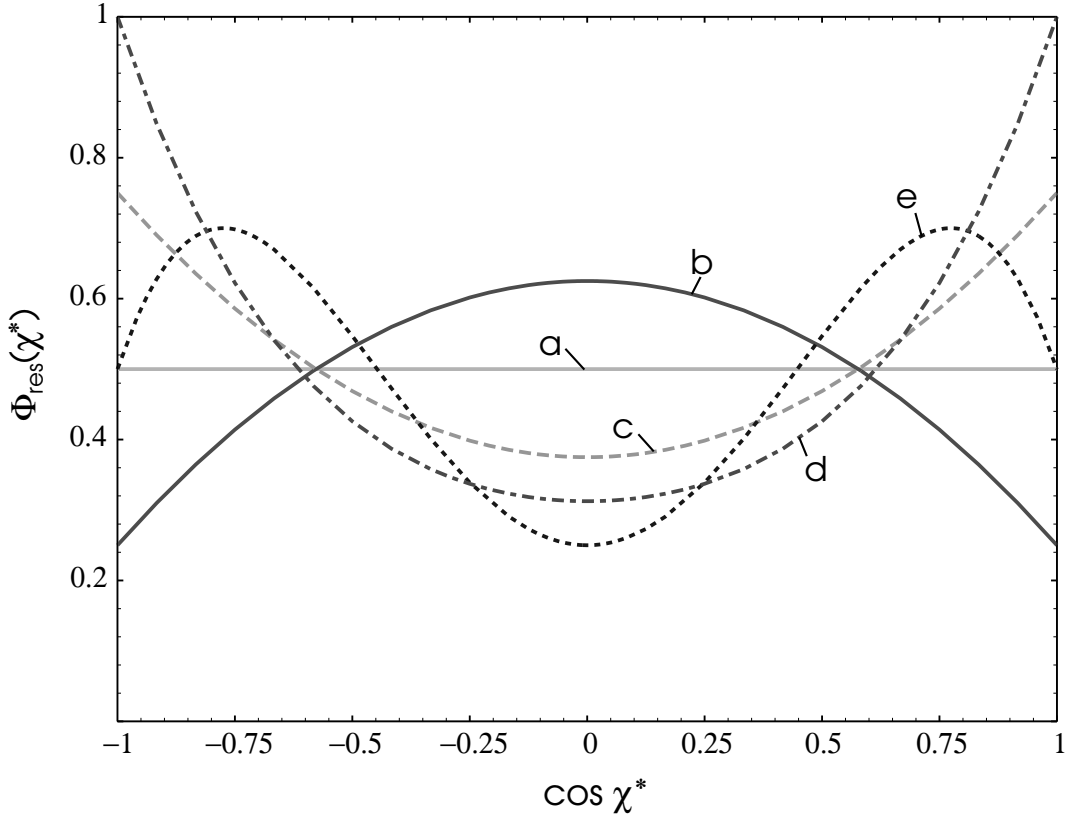


Figure 1.8: Angular distribution of resonance decay, following Eqs. (1.2.8)

1.2.1.4 Kinematics

Resonance decay: The angular distribution of the decay of resonances has been found to be a function of the angular momentum J , radiative excitation mode and the orbital momentum L of the final state particles. From Eq. (1.2.8) we immediately see that the final state probability distribution function can be written as a polynomial in $\cos \chi^*$,

$$\Phi_{\text{res}}(\chi^*) = \sum_{\nu=0}^L \tilde{c}_{\nu} [\cos \chi^*]^{2\nu} \quad , \quad (1.2.12)$$

where the coefficients \tilde{c}_{ν} are calculated from the C_{LL_z} . As we already have mentioned, resonances are classified by the partial waves of πN scattering, thus for πN decay L can immediately be taken from the resonance spectroscopic notation. For other decay channels, other dominant partial waves can be expected, and a “clean” resonance in $N\pi$ scattering may appear as a superposition of partial waves in this case. Assuming $N\pi$ decay, which is the dominant decay channel of most light resonances, $\Phi_{\text{res}}(\chi^*)$ can be taken from Eqs. (1.2.8), if the excitation mode is known. Fig. 1.8 shows that there is an increasing tendency to prefer decay into forward and backward directions of the reaction axis with increasing L .

The average inelasticity of an s -channel reaction, however, is found to be completely independent on angular

momentum parameters. Since $\Phi_{\text{res}}(\chi^*)$ contains only even powers of $\cos \chi^*$, we have

$$\overline{K}_{\text{res}}(M_{\text{int}}) = \int_{-1}^1 d \cos \chi^* \Phi_{\text{res}}(\chi^*) K_{f2}(M_{\text{int}}, \chi^*) = \frac{1}{2} \left(1 - \frac{m_{\text{N}}^2 - m_{\text{mes}}^2}{M_{\text{int}}^2} \right) , \quad (1.2.13)$$

where m_{N} and m_{mes} are the masses of the nucleon and the meson, respectively, in the final state. We assume that the nucleon immediately reappears after the resonance decay; otherwise, we have to consider a decay chain as discussed below.

Direct meson production: Considering the inelasticity of OPE and diffractive meson production, the only difference to resonance decay is the angular distribution, thus the value of $\langle \cos \chi^* \rangle$ given by Eq. (1.2.10) when setting $t = -m_t^2 c^2$. The inelasticity is then given by

$$\overline{K}_{\text{dir}}(M_{\text{int}}, m_t) = 1 - \frac{1}{2} \left(1 + \frac{m_{\text{N}}^2 - m_{\text{mes}}^2}{M_{\text{int}}^2} \right) \left(1 + \beta_{\text{N}}^* \langle \cos \chi^* \rangle_{(M_{\text{int}}, m_t)} \right) , \quad (1.2.14)$$

where we again assume that the nucleon appears immediately in the final state and postpone decay chains to the next paragraph. An important point to note is here, that the final state cannot be separated from the initial state even if all masses including m_t are fixed by the reaction channel, because M_{int} appears explicitly in the determination of $\langle \cos \chi^* \rangle$. However, we note from Fig. 1.7 that χ^* takes considerable values only near threshold, where $\beta_{\text{N}}^* \ll 1$, while $\langle \cos \chi^* \rangle \approx 1$ when $\beta_{\text{N}}^* \sim 1$; thus, the impact of $\langle \cos \chi^* \rangle$ in Eq. (1.2.13) is large only in the range where the reaction is strongly forward peaked. We may therefore set

$$\langle \cos \chi^* \rangle_t = 1 \quad \text{for all } M_{\text{int}} , \quad (1.2.15)$$

for all t -channel reactions. The error in $\overline{K}_{\text{dir}}$ introduced by this simplification is shown in Fig. 1.9, we see that it is generally of order 10% or less, and becomes largest in the high energy region, where both cross section and inelasticity of the reactions decrease strongly. We may therefore regard t channel reactions as *strictly forward peaked* in the following; the final state space has thus no free parameter, and the inelasticity is fixed for every M_{int} .

Decay chains: We have defined the inelasticity as the fractional LF energy loss a nucleon suffers in an interaction. In the two-particle channel picture, however, the final state is defined by the *first* particles which are produced; in this state, the baryonic particle may be in an excited state, i.e. a Δ or N resonance rather than a nucleon. To keep the meaning of the term ‘‘inelasticity’’, we therefore have to include the whole baryonic *decay chain*, whose end is defined by the recovery of the nucleon. The basic assumptions in our treatment of decay chains are

1. The direction of the baryon (cosmic ray) velocity in the LF does not change in decays, which requires $\gamma_{\text{CR}} \gg 1$. This means that all scattering and baryon resonance decay angles, generally taken in the CMF of the decaying particle and therefore with respect to its velocity direction, refer to the same axis in the LF.
2. Every intermediate baryon resonance in the chain has only one dominant two-particle decay channel, which contains again a baryon resonance or a nucleon

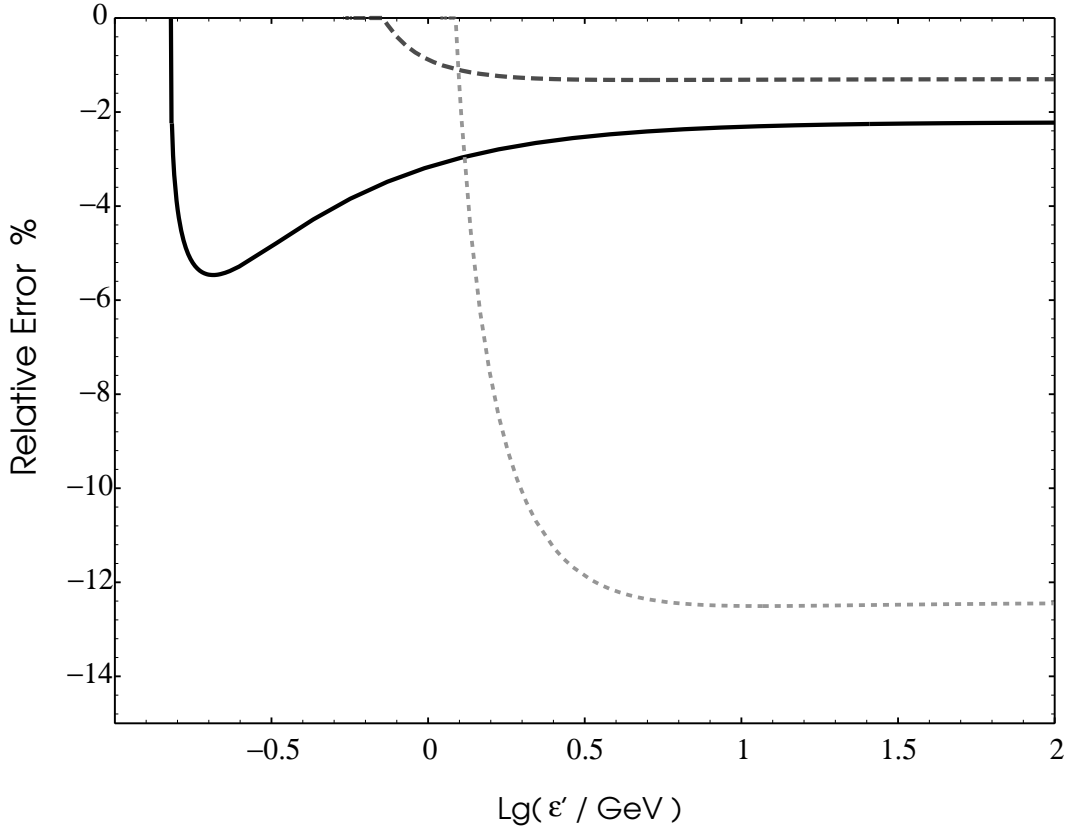


Figure 1.9: Error estimate for the inelasticity of t -channel reactions calculated using the $\langle \cos \chi^* \rangle_t = 1$ assumption. Linestyles correspond to Fig. 1.7.

Then, we can easily show that the total inelasticity is given by

$$K_{\triangleright n}(M_{\text{int}}, \chi^*, \mathbf{M}, \chi_{\text{d}}^*) = 1 - \left[1 - K_{f2}(M_{\text{int}}, \chi^*) \right] \prod_{i=1}^n \left[1 - K_{f2}(M_i, \chi_{\text{d}i}^*) \right] . \quad (1.2.16)$$

The final state of the interaction is described by the set of masses $\mathbf{M} = M_1, \dots, M_n$ and decay angles $\chi_{\text{d}}^* = \chi_{\text{d}1}^*, \dots, \chi_{\text{d}i}^*$ of the n secondary resonances in the decay chain. However, to simplify the task we will generally average over the mass distribution of the resonance (given by a Lorentz-curve) and use for M_i the *nominal masses* of the secondary resonances. Then, only the vector of decay angles χ_{d}^* determines the inelasticity of the decay chain.

The initial assumption that during the decay chain every state has only one dominant decay channel seems to be an oversimplification. However, it is clearly true in reactions where the (first) secondary resonance is the $\Delta(1232)$, which is also the only important application of decay chains; we therefore restrict ourselves to this case in the following. The final state variables are noted as χ^* and χ_{Δ} , the latter being the decay angle of the Δ resonance relative to the CMF velocity of the incident nucleon. As a further simplification, we may assume that secondary baryon resonances decay isotropically, which is motivated by the necessity of averaging of different excitation mechanisms arising from the decay of the heavier resonance, and which is in good correspondence with experimental data [Cam67, ABB68]. Therefore, the average of the $\gamma p \rightarrow \Delta \pi : \Delta \rightarrow N \pi$ decay chain

inelasticity is given by

$$\overline{K}_\Delta(M_{\text{int}}) = 1 - \frac{m_N}{M_{\text{int}}} \gamma_N^\Delta(M_\Delta) \gamma_\Delta^*(M_{\text{int}}) \left[1 + \beta_\Delta^* \langle \cos \chi^* \rangle \right] \quad (1.2.17)$$

The first interaction in a decay chain may proceed either over the s -channel, i.e. be again described as a resonance decay, or over the t -channel. Hence, the angular distribution of the respective reaction type, as discussed above, has to be inserted to obtain the averaged inelasticity.

Kinematics of statistical multi-pion production: The key to a simple treatment of multi-pion production within our framework of two particle final state interactions is the leading particle effect; for the nucleon this means that it carries on most of its longitudinal CMF momentum through the interaction. Considering energy, we may express this as an approximately constant fraction of the CMF kinetic energy of the interaction going into secondary particles. It is also known from experiment that the transversal momenta of the produced pions are small; therefore, and because of the statistical mixture of scattering angles of the produced pions, we can expect that the transversal momentum transfer to the nucleon is negligible compared to its total momentum, which in turn means that the reaction is *strictly forward peaked*. This removes the CMF scattering angle of the nucleon from the degrees of freedom in the final state space.

We may consider the *multipion system* produced in the interaction as *one particle* with an unknown mass, $M_{\langle\pi\rangle} = f_{\langle\pi\rangle} M_{\text{kin}}$. $M_{\langle\pi\rangle} c^2$ is obviously equivalent to the total energy of the pion system in its own center of mass frame. Then, the kinematics of multipion production is equivalent to that of a two particle final state with strict forward scattering, and the inelasticity can then be written as $\overline{K}_{\langle\pi\rangle}(M_{\text{int}}, f_{\langle\pi\rangle}) = K_{f2}(M_{\text{int}}, \chi^*=1)$, cf. Eq. (1.1.53a), with

$$\gamma_1^*(M_{\text{int}}, f_{\langle\pi\rangle}) = 1 + \frac{1}{2} \frac{M_{\text{kin}}^2}{M_{\text{int}} m_N} (1 - f_{\langle\pi\rangle}^2) \quad , \quad (1.2.18)$$

where m_N is the mass of the incident nucleon. We see that

$$\overline{K}_{\langle\pi\rangle}(M_{\text{int}}, f_{\langle\pi\rangle}) \rightarrow f_{\langle\pi\rangle}^2 \quad \text{for } M_{\text{int}} \rightarrow \infty . \quad (1.2.18a)$$

Since M_{int} and M_{kin} are functions of initial state variable ϵ' , the variable $f_{\langle\pi\rangle}$ determines completely the final state of multipion production. The task is therefore to find the distribution function $\Phi_{\langle\pi\rangle}(f_{\langle\pi\rangle})$. We may again adopt the idea of a quasi-free interaction on the quark scale, and take $\langle f_{\langle\pi\rangle} \rangle = \frac{2}{5}$ from the participant-spectator quark number relations. To estimate the width of the distribution, we consider the nucleon as a relativistic Fermi gas of three massless quarks (i.e. $m_q \ll m_N$, see [Par94]) with a total energy $E_F = 6.23 (\hbar c/r_p) = m_N c^2$; we stress that this relation is naturally achieved for a proton radius $r_p \simeq 1.3$ fm. Considering then the momentum distribution of the three quarks within this model, and repeating the participant-spectator counting game (we assume that the virtual photon quarks carry exactly $\frac{1}{2}$ of the photon CMF momentum), we easily obtain

$$f_{\langle\pi\rangle} = 0.4 \pm 0.25 \quad (1.2.19)$$

The simplicity of our assumptions does certainly not allow a more definite prediction of $\Phi_{\langle\pi\rangle}$; we may thus take any convenient simple distribution function which complies with Eq. (1.2.19). Clearly, we may also use the exact momentum distribution of a relativistic Fermi gas. Unfortunately, there seem to be no reliable data of multipion mass distributions *regardless of multiplicity* which would allow to confirm, or even improve, Eq. (1.2.19) empirically.

1.2.2 Astrophysical application of photomeson production

1.2.2.1 The role of photomeson production in astrophysics

The Greisen-Zatsepin-Kuzmin-cutoff: Photomeson production is the most effective energy loss mechanism for protons and neutrons of ultra high energies. In the NRF, the interaction threshold is approximately given by the pion mass, $m_\pi c^2 \approx 140 \text{ MeV}$. Hence, extreme Lorentz factors of the cosmic ray particle are required if we have to deal with ordinary, low energy background photons as the target field: With a typical intergalactic LF photon energy $\epsilon_{\text{ref}} \sim 10^{-4} - 10^{-2} \text{ eV}$, a cosmic ray Lorentz factor $\gamma_{\text{CR}} \gtrsim 10^{10} - 10^{12}$ is necessary to induce photopion production.

Shortly after the discovery of the cosmic microwave background (CMB) by Penzias and Wilson in 1965, the photomeson loss time scale for cosmic ray protons in this universal background field was calculated by GREISEN [Gre66], and independently by ZATSEPIN & KUZMIN [ZK66]. The photon density of the cosmic microwave background (CMB) is about $400/\text{cm}^3$, and multiplication with the efficiency in the Δ -region of about $100 \mu\text{barn}$ yields an attenuation length $\lambda_{\text{att}} = c\tau_{\text{loss}} \sim 10 \text{ Mpc}$. The characteristic photon energy of the CMB is about $\epsilon_{\text{ref}} \sim 6 \times 10^{-4} \text{ eV}$, thus photomeson production most efficient at $\gamma \sim 3 \times 10^{11}$, corresponding to a proton energy of about 300 EeV . Thus it was concluded that, if cosmic rays originate mainly at cosmological distances $D \gg 10 \text{ Mpc}$, the spectrum should cut off in the sub-ZeV regime; this is commonly called the *Greisen-Zatsepin-Kuzmin-cutoff*, or short *GZK-cutoff*.

It is worth to note that the GZK cutoff is in fact not connected to a specific source distance, but rather to the time of flight of the extragalactic cosmic rays. For diffusive transport models of extragalactic cosmic rays, even sources with $D \lesssim 10 \text{ Mpc}$ may show the GZK cutoff. Another application of photoproduction at the CMB radiation was recently found as the limiting process for the shock acceleration at very large shock structures, when $\tau_{\text{acc}} \gtrsim 10^{15} \text{ sec}$ [KRJ96, KRB96]. Recent observations of cosmic rays with energies above the GZK limit have drawn photomeson production at the CMB into the center of interest again, and it is one of the main subjects of this work to improve the treatment of cosmic ray transport in the trans-GZK regime. A detailed derivation of the photomeson *efficiency function* is required for this purpose.

Secondary gamma and neutrino production: Photomeson production at lower cosmic ray energies can happen in the vicinity of strong IR-to-UV sources. In dense UV fields around AGN ($\epsilon_{\text{ref}} \sim 10 - 100 \text{ eV}$) photomeson processes set in at $\gamma_{\text{CR}} \gtrsim 10^6$, which corresponds to proton energies in the PeV regime. Here, not the protons themselves, but the decay products produced mesons are of interest; considering only the lightest meson products, the π^\pm and the π^0 , we have a source of energetic gamma rays by the dominant decay mode

$$\pi^0 \rightarrow 2\gamma \quad (1.2.20a)$$

of the neutral pion, while the charged pions are a source of neutrinos by

$$\pi^+ \rightarrow \mu^+ \nu_\mu \quad : \quad \mu^+ \rightarrow e^+ \nu_e \bar{\nu}_\mu \quad (1.2.20b)$$

$$\pi^- \rightarrow \mu^- \bar{\nu}_\mu \quad : \quad \mu^- \rightarrow e^- \bar{\nu}_e \nu_\mu \quad . \quad (1.2.20c)$$

We see that the ratio $\nu_\mu : \bar{\nu}_\mu : [\nu_e / \bar{\nu}_e]$ is 1:1:1 in any case, while the ratio $\nu_e : \bar{\nu}_e$ is determined by the $\pi^+ : \pi^-$ production ratio. The primary gamma rays from the π^0 decay have generally energies above about 10 PeV , but will cascade down to TeV energies in ambient radiation fields (due to $\gamma\gamma$ scattering and subsequent leptonic radiation processes). This kind of gamma ray origin in energetic astrophysical objects is completely different from pure leptonic (e^\pm) radiation processes, which are usually considered in astrophysics; we may thus call them *hadronic*

Table 1.2: Baryon resonances in γN reactions, arranged by resonance mass

Name	$L_{[2J][2J]}$	Modes	Γ/MeV	$10^3 b_\gamma$	ϵ_0/GeV	$\sigma_0/\mu\text{barn}$
$\Delta(1232)$	P_{33}	$M1, E2^*$	110	5.9	0.34	437.5
$N(1440)$	P_{11}	$M1$	350	0.5	0.64	7.2
$N(1520)$	D_{13}	$E1, M2$	120	4.5	0.76	101.0
$N(1535)$	S_{11}	$E1$	150	4.5	0.79	48.3
$N(1650)$	S_{11}	$E1$	150	1.0	0.98	8.0
$N(1680)^\dagger$	F_{15}	$E2, M3$	140	2.8	1.03	62.4
$\Delta(1700)$	D_{33}	$E1, M2$	300	2.1	1.07	29.8
$\Delta(1905)$	F_{35}	$E2, M3$	350	0.3	1.46	4.3
$\Delta(1950)$	F_{37}	$M3, E4$	300	1.4	1.56	24.8

* $E2$ contribution negligible, $\sigma_{E2}/\sigma_{M1} \sim 10^{-4}$

† Appears only in γp scattering; instead, $N(1675)/D_{15}$ contributes to γn scattering with $10^3 b_\gamma = 0.6$. This is the only considerable difference between the γp and γn cross sections, and will be called $N(1680)/N(1675)$ asymmetry in the following.

radiation processes. The application of hadronic radiation processes to AGN and other energetic astrophysical sources has been suggested first by PROTHEROE & KAZANAS [PK83] on the basis of energetic pp collisions, and was extended to photohadronic pion origin by MANNHEIM [Man93] who introduced the term *Proton Initiated Cascade (PIC)*. An observational confirmation of PIC processes could give direct evidence for the origin of cosmic rays. More decisive would be a clear observational evidence for energetic neutrino radiation from astrophysical objects, but experiments are not sensitive enough yet. The detailed treatment of hadronic radiation processes is outside the scope of this work; however, we can derive some useful results on the first step of these processes, the production of pions and their charge ratio.

1.2.2.2 Classification of energy regions in the NRF

The Δ -resonance region: The dominant feature in the total γN cross section is the $\Delta(1232)$ resonance, which has a spectroscopic classification P_{33} . The resonance occurs in the NRF at a photon energy $\epsilon' = 340$ MeV, approximately double the threshold energy; the energy regime marked by this prominent resonance is called the *first resonance region*, or often just the *Δ -resonance region*⁸.

Because it is the lightest baryon resonance, the $\Delta(1232)$ can only decay into an (unexcited) nucleon and a pion; the branching ratio of radiative decay is about 0.6%. The decay branching ratios of the different isospin orientations of the $\Delta(1232)$ resonances are given by:

$$\begin{array}{c|cccccc}
 & p\pi^+ & p\pi^0 & p\pi^- & n\pi^+ & n\pi^0 & n\pi^- \\
 \hline
 \Delta^{++} & 1 & & & & & \\
 \Delta^+ & & \frac{2}{3} & & \frac{1}{3} & & \\
 \Delta^0 & & & \frac{1}{3} & & \frac{2}{3} & \\
 \Delta^- & & & & & & 1
 \end{array} \tag{1.2.21}$$

It can be deduced from the quark model that the only possible radiative excitation mode of the $\Delta(1232)$ is the $M1$ transition; since it is a P -wave resonance in the pion nucleon system, the differential cross section is proportional to $5 - 3 \cos^2 \theta$, which is confirmed by observations of the $N\pi^0$ decay of the resonance. The properties of the $\Delta(1232)$ are listed in Tab. 1.2.

⁸Even though, of course, the $\Delta(1232)$ is not the only Δ resonance in the cross section!

The second resonance region: Above the Δ -resonance region, the total γN cross section shows two or three resonance peaks between $500 \text{ MeV} \lesssim \epsilon' \lesssim 1.5 \text{ GeV}$, which is called the *second resonance region* (SRR). Of the baryon resonances known from πN scattering, only a few have considerable radiative decay branching ratios and therefore contribute to the photohadronic cross section; they are listed in Tab. 1.2. Most of them have large angular momenta, and particularly the heavier ones decay predominantly over channels other than πN . Experimental results suggest that the differential cross section for all decay channels can be assumed as roughly isotropical, which is used as an approximation henceforth. The most important decay channel in this second resonance is the decay chain $\gamma N \rightarrow \Delta\pi : \Delta \rightarrow N\pi$, but also single pion channels and the production of heavier mesons contribute.

The high energy region: At $\epsilon' \gtrsim 1.5 \text{ GeV}$, the total photohadronic cross section becomes roughly constant above 1 GeV with a value of about $125 \mu\text{barn}$. The most important channel is here the statistical multipion production. About 15% of the cross section is contributed by diffractive vector meson production. In this energy region, photohadronic reactions are completely analogous to other hadronic interactions, as πp , pp or $p\bar{p}$ scattering, therefore the findings from such interactions may be applied to photohadronic interactions. To very high energies, models expect a slight increase of the cross section as

$$\frac{\sigma_{N\gamma}}{[\mu\text{barn}]} = 67.7x^{0.08} + 129x^{-0.45} \quad , \quad (1.2.22)$$

with $x = (M_{\text{int}}/[\text{GeV}])^2$.

1.2.2.3 Cross section fits

General procedure: We extrapolate the cross sections of the quasi-two-particle channels given in Eqs. (1.2.1) to (1.2.6) from fits to data taken from published tables [BFMM73]. The main task is to discern the contributions of resonant and direct reaction for every channel separately, because they behave quite different in the efficiency functions. To achieve this, we make use of the fact that the resonance contributions are *completely* determined from the resonance parameters listed in Tab. 1.2, and their branching ratios to the respective decay channels, which have been experimentally determined by particle physicists on the basis of partial wave analysis techniques, and are given in [Par94]. Then we can use the residual data to obtain the contribution of direct interactions to every channel. For this we define the dimensionless function $\zeta(x)$ by

$$\sigma_t(\epsilon'; c) \equiv \zeta(\epsilon'/[\text{GeV}]) [\mu\text{barn}] \quad , \quad (1.2.23)$$

and express $\zeta(x)$ for every channel in terms of simple fit functions, e.g. $\text{Pl}(x)$ or $\text{Ef}(x)$. Our procedure to obtain cross sections may thus be summarized as follows:

1. Determine the resonances contributing to every channel and their branching ratios into this channel.
2. Calculate the resonance contribution from Eq. (1.1.55).
3. Determine the residuals of the specific cross section data relative to the resonance contribution.
4. Find a suitable expression for $\zeta(x)$, and obtain the free parameters from fitting to the residuals.
5. In cases where only data to one part of a reaction iso-multiplet exist, derive the other branches by applying isospin symmetry.

6. Finally, sum up all quasi-two-particle contributions, and determine the residuals of the total γp cross section. These are fitted by a simple function showing the correct high energy behavior (see Eq. (1.2.22)), and treated as statistical multipion production.

For our fits, we use only data on γp reactions, with one exception in the reaction (1.2.1b), where γp and γn data are used. The differences expected for between proton and neutron are briefly discussed.

Single pion channels: From isospin symmetry, we expect that the branching ratio of single pion production with and without isospin flip is 1:2 in the Δ -resonance region, while it is just the opposite in the second resonance region, where predominantly N -resonances contribute. The resonances in the SRR which contribute significantly to single pion production are

	$N(1440)$	$N(1520)$	$N(1535)$	$N(1650)$	$N(1680)$	$\Delta(1700)$	$\Delta(1950)$
b_π	0.7	0.6	0.55	0.6	0.6	0.1	0.4

For the $\Delta(1232)$ we already have stated that $b_\pi \simeq 1$. The contribution of resonances to the $\gamma p \rightarrow p\pi^0$ and $\gamma N \rightarrow n\pi^+$ channels are shown in Fig. 1.10(a)&(b). For π^0 production there exist only second order direct production effects, as Primakoff scattering; we see that there is no evidence in the data for a considerable contribution of this effect, and neglect it henceforth. In contrast, for the $\gamma p \rightarrow n\pi^+$ channel we find a strong background overlaid to the resonance contribution, which we can assign to direct pion production. We fit the underlying background with a function

$$\tilde{\xi}_\pi(x) = 53.3 \text{Ef}(x; 0.15, 0.15) \text{Ef}(-x; -0.65, -0.2) + 16.3 \text{Pl}(x; 0.15, 0.3, 6) \quad (1.2.24)$$

The abrupt cutoff of the direct pion production cross section at $\epsilon' \sim 650$ MeV can readily be explained by the takeover of the direct $\Delta\pi$ channel, as shown below. The data above 750 MeV shown in Fig. 1.10(b) are taken from the $\gamma n \rightarrow p\pi^-$ reaction; in the region of the $N(1680)$ resonance at $\epsilon' \approx 1$ GeV the γn cross section is considerably smaller than the γp cross section because of the $N(1680)/N(1675)$ asymmetry (see Tab. 1.2).

Secondary baryon resonance production: Two-pion production below $\epsilon' \sim 1$ GeV proceeds to a large fraction over the quasi-two-particle channels $\gamma N \rightarrow \Delta(1232)\pi$: $\Delta(1232) \rightarrow N\pi$ and $\gamma N \rightarrow N\rho^0$: $\rho^0 \rightarrow \pi^+\pi^-$. The former channel is subdivided into the isospin multiplet given by Eqs.(1.2.2a) to (1.2.2c). These reactions are connected by isospin symmetry, which predicts $\Delta^{++}:\Delta^+:\Delta^0$ branching ratios of 3:1:2 for N resonance decay, and 6:8:1 for Δ resonance decay (see Tab. 1.1). Experimentally, reaction (1.2.2b) comprises the difficulty that it has mostly two neutral particles in the final channels (except for $\gamma n \rightarrow \Delta^0\pi^0$: $\Delta^0 \rightarrow p\pi^-$), and is therefore badly to detect. In fact, almost no data exist for this reaction. On the other hand, for reaction (1.2.2a) the data situation is excellent, and for (1.2.2c) it is good enough to confirm approximately isospin symmetry; we will assume that isospin symmetry holds to determine the total cross sections for reaction (1.2.2b) and (1.2.2c) from the data on reaction (1.2.2a).

The resonances which show a significant contribution to the $\gamma N \rightarrow \Delta\pi$ channel are

	$N(1440)$	$N(1520)$	$N(1680)$	$\Delta(1700)$	$\Delta(1950)$
b_Δ	0.3	0.25	0.25	0.6	0.3

Using the isospin branching factors to determine the contribution to the $\gamma p \rightarrow \Delta^{++}\pi^-$ reaction, we find that only an insufficient part of the measured cross section can be due to the decay of heavier resonances. We obtain

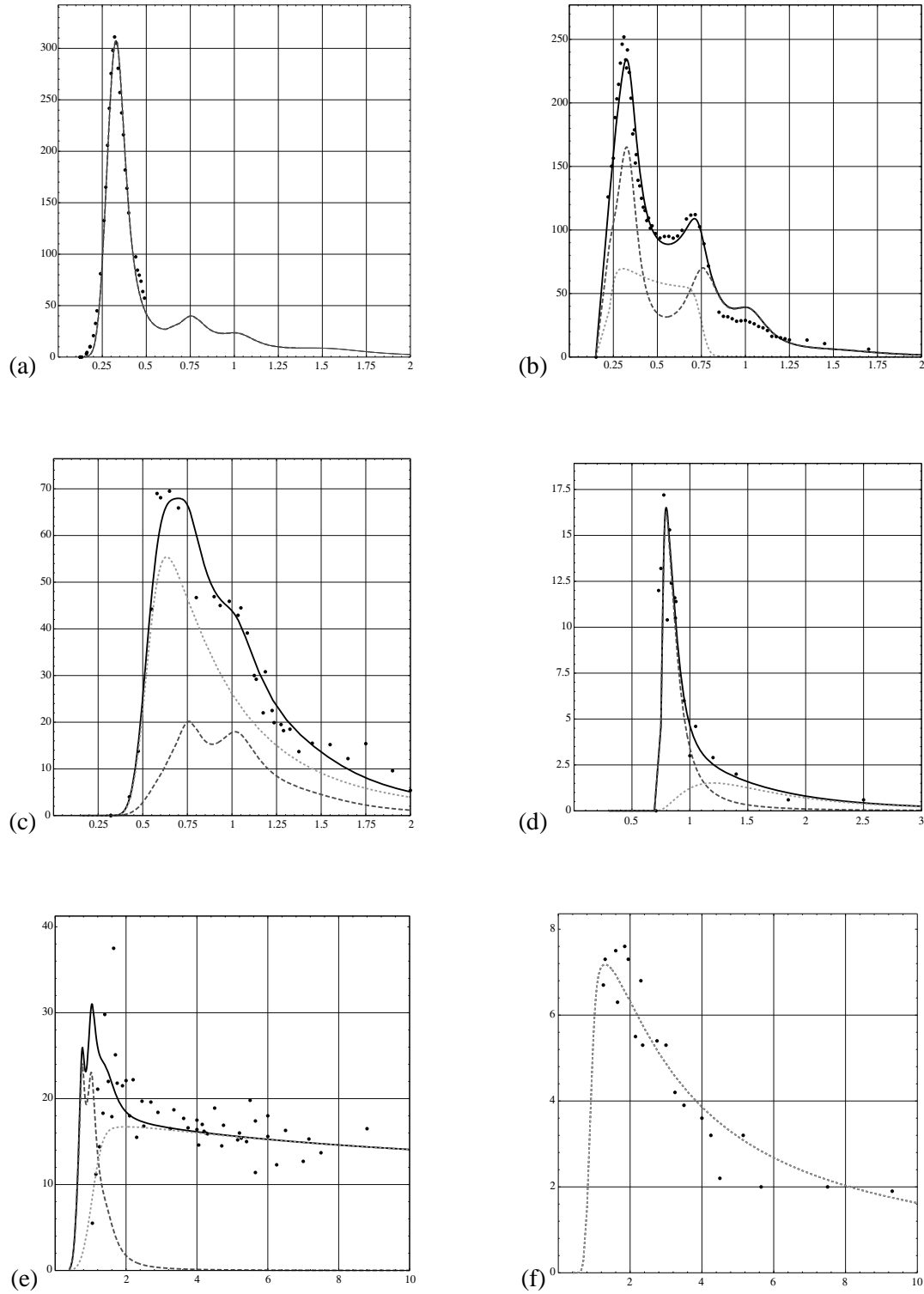


Figure 1.10: Cross section fits of specific $p\gamma$ interaction channels: (a) $\gamma p \rightarrow p\pi^0$, (b) $\gamma p \rightarrow n\pi^+$, (c) $\gamma p \rightarrow \Delta^{++}\pi^-$, (d) $\gamma p \rightarrow p\eta$, (e) $\gamma p \rightarrow p\rho^0$, (f) $\gamma p \rightarrow p\omega$. See next page for further explanation.

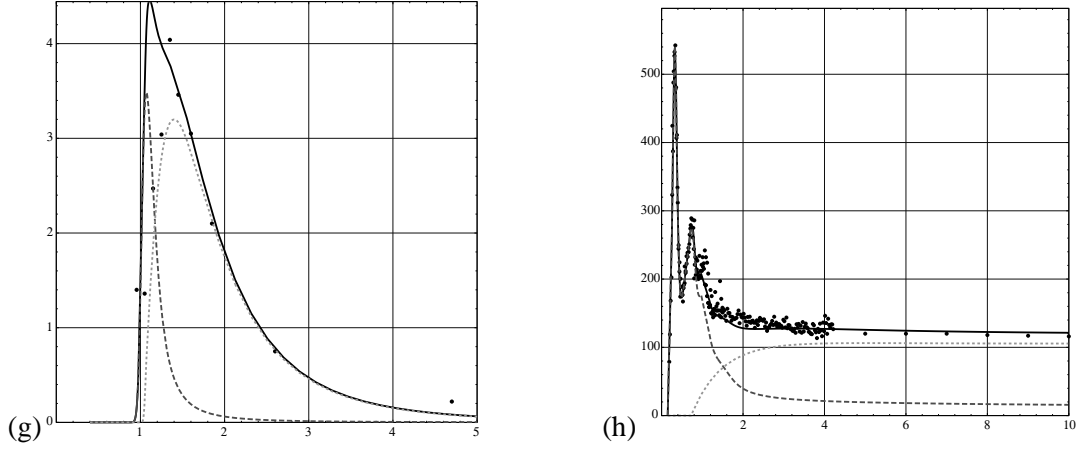


Figure 1.10: (cont'd) Cross section fits of specific $p\gamma$ interaction channels: (g) $\gamma p \rightarrow B_S^0 K^+$, (h) total γp cross section, with multipion channel. Plotted are cross section in μbarn vs. NRF photon energy in GeV. Solid lines show total cross sections, dashed line contributions from resonance decay (no fits!), and dotted lines the direct (t -channel) contributions obtained from fitting the data. Data are taken from [BFMM73]. Plotted is $\sigma(\epsilon')$ in μbarn vs. ϵ' in GeV.

a good fit if we underly a background

$$\tilde{\zeta}_\Delta(x) = 62.4 \text{Pl}(x; 0.321, 0.55, 3.5) \quad (1.2.25)$$

which can be attributed to the direct (OPE) pion production with Δ excitation. The fit to the $\gamma p \rightarrow \Delta^{++} \pi^-$ data is shown in as shown in Fig. 1.10 (c).

We can now use Tab. 1.1 for the determination of the mirror-reactions within the iso-multiplet. We expect no big difference between γp and γn reactions in this channel, because the suppression of the $N(1680)/N(1675)$ contribution is partially compensated by a higher reaction width, $b_\Delta = 0.6$, of the $N(1675)$ resonance. For the OPE production of secondary Δ^{++} and Δ^0 resonances isospin symmetry predicts a cross section ratio of 3:1, and no difference between γp and γn reactions. The total cross section for secondary baryon resonance production is shown in Fig. 1.11.

The η channel: An important channel for neutral particle production is $\gamma N \rightarrow N\eta$. The η meson decays mainly electromagnetically over $\eta \rightarrow 2\gamma$ (39%) and $\eta \rightarrow 3\pi^0$ (32%). The dominant charged decay channels are $\eta \rightarrow \pi^+\pi^-\pi^0$ and $\eta \rightarrow \pi^+\pi^-\gamma$. The electromagnetic decay properties are the only thing which makes this channel interesting, its contribution to the total photohadronic cross section is quite low. The only resonance which contributes to η production is $N(1535)$ with $b_\eta = 0.35$. A slight contribution of direct, presumably Primakoff production can be seen at higher energies, and is fitted by an underground function

$$\tilde{\zeta}_\eta(x) = 1.5 \text{Pl}(x; 0.7, 1.2, 4) \quad (1.2.26)$$

For rough calculations which do not refer to the η decay products, photo- η -production may readily be neglected.

Vector meson production: The reaction $\gamma N \rightarrow N\rho$ is the dominant vector meson production channel. The ρ^0 decays to 100% into a $\pi^+\pi^-$ pair, the decay into neutral pions is forbidden by C -parity conservation. Diffractive

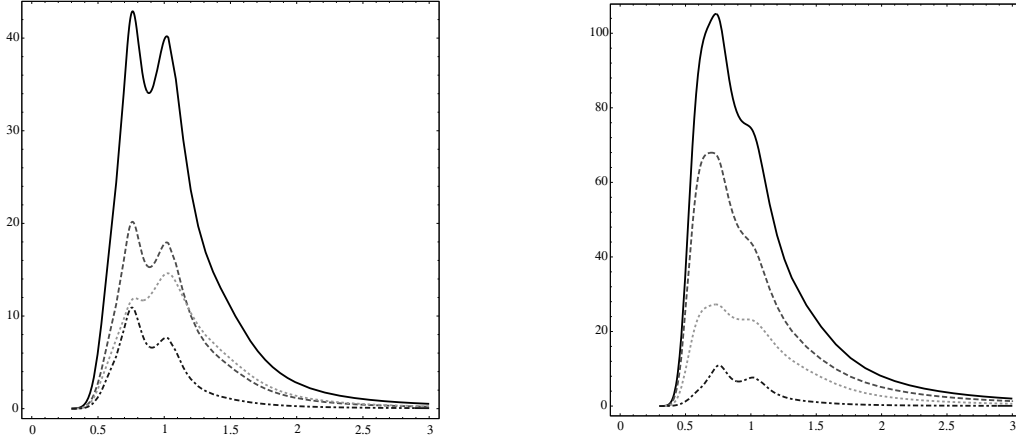


Figure 1.11: Total contribution of all $\gamma p \rightarrow \Delta\pi$ channels (solid lines), as derived from isospin symmetry from the data on $\gamma p \rightarrow \Delta^{++}\pi^-$ (dashed lines). Chain lines show $\gamma p \rightarrow \Delta^+\pi^0$, dotted lines $\gamma p \rightarrow \Delta^0\pi^+$. Left: Contribution from resonance excitation; Right: Total cross section; The cross section of direct $\Delta^0\pi^+$ production is $\frac{1}{3}$ of that shown for the $\Delta^{++}\pi^-$ channel in Fig. 1.10 (c). Axes labels are the same as in Fig. 1.10.

ρ^0 production sets in at about $\epsilon'_{\text{th}} = 1.08$ GeV, and shows an almost constant cross section of $12 \mu\text{barn}$ above this energy. However, the channel plays also a role *below* this threshold, because of the large ρ^0 -width $\Gamma_\rho \simeq 150$ MeV. Thus we find ρ^0 production as a considerable decay channel of the resonances:

	$N(1520)$	$N(1650)$	$N(1680)$	$\Delta(1700)$	$\Delta(1905)$
b_ρ	0.15	0.1	0.15	0.3	1.0

Subtracting the resonance contribution from the data, we obtain a fit function for diffractive ρ^0 production as

$$\tilde{\zeta}_\rho(x) = 16.7 \text{Pl}(x; 0.321, 2.0, 0.2) \quad . \quad (1.2.27)$$

The threshold was set to that of the $\gamma p \rightarrow p\pi^+\pi^-$ reaction. In the high energy limit, we do not apply the possible rise of the diffractive cross section. This is justified by the crude treatment of the multipion channel, which does not justify the detailed treatment of a second channel at high energies, which only contributes to a few percent.

The second vector meson, ω , is only produced in diffractive scattering for $\epsilon' \gtrsim 1$ GeV. The dominant decay channel is $\omega \rightarrow \pi^+\pi^-\pi^0$, with a 10% contribution of $\omega \rightarrow \pi^0\gamma$. The nominal threshold energy of this reaction is $\epsilon'_{\text{th}} = 1.11$ GeV, but as for the ρ^0 the process is possible also at lower energies; a definite threshold is given by the 3π production threshold. We obtain a fit of the data with

$$\tilde{\zeta}_\omega(x) = 7.2 \text{Pl}(x; 0.512, 1.3, 1.1) \quad . \quad (1.2.28)$$

The cross sections for photohadronic ρ^0 and ω production are shown in Fig. 1.10 (e)&(f), respectively. The cross section for production of the ϕ meson is about an order of magnitude below that of ω production and is disregarded in our analysis.

Strange particles: Even less important than η or ω production is the production of strange particles. Nevertheless we quote this channel, because the long lifetime of the strange particles may be of interest for specific

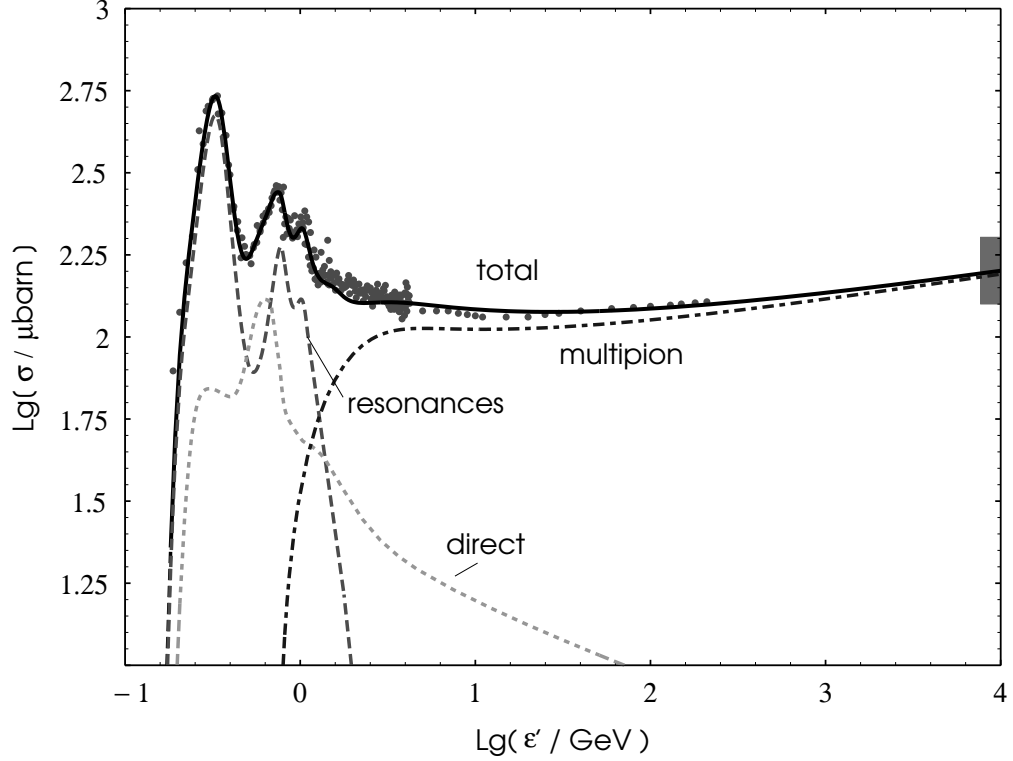


Figure 1.12: Total γp cross section, with contributions of resonant two particle channels, direct particle production and statistical multipion production. Low energy data are taken from [BFMM73], the shaded area at the right border marks the cross section range obtained by the ZEUS and H1 detectors at HERA, at $\epsilon' \sim 2 \times 10^4$ GeV [Lev93].

hadronic radiation processes. It is, however, disregarded for the derivation of the photohadronic cosmic ray loss function.

The nonstrange baryon resonances showing a detectable branch to the channel $N^* \rightarrow AK$ are $N(1650)$, $N(1710)$ and $N(1720)$, with $b_A \approx 0.1$ and $b_A \approx 0.2$, respectively. We note that the $N(1710)/P_{11}$ resonance does not belong to the resonances with strong radiative excitation; from the measured helicity amplitudes we obtain $b_\gamma \lesssim 5 \times 10^{-4}$; its total contribution is therefore negligible compared to the neighboring $\Delta(1700)$. The $N(1720)$ shows similar branching ratios b_γ and b_A , so we do not treat these two resonances separately; we just sum up their contributions to $b_\gamma b_A \sim 1.6 \times 10^{-5}$, guided by the limits set by the data.

The data situation on strange photohadronic channels is also quite poor; data are given only for the channels (1.2.6a) and (1.2.6b). However, we can use the SU(3) symmetries to derive that $b_A/b_{\Sigma^0} \approx 1$, and isospin symmetry to obtain $b_{\Sigma^+} = 3b_{\Sigma^0}$. We then bin the data on Λ and Σ^0 photoproduction and put them together to obtain better statistics; subtracting the resonance contribution, we see that most of the strange channel is probably dominated by direct interactions. We find a fit with

$$\tilde{\zeta}_S(x) \approx 3.2 \text{Pl}(x, 1.0, 1.4, 4.6) \quad (1.2.29)$$

Because of the large uncertainties in the determination of the resonance contribution, these may also be omitted and the cross section can be fitted using only Eq. (1.2.29), as obvious from Fig. 1.10 (g). Since direct K^0

production is strongly suppressed, Eq. (1.2.29) is also the total cross section of the reaction (1.2.6).

The statistical channel and the total γp cross section: Summing up all total cross sections of the quasi-two particle channels treated so far for the γp reaction, we find that we obtain an excellent fit to the total γp cross section for $\epsilon' \lesssim 0.8$ GeV. This confirms that the selected quasi-two-particle channels are quite complete. Above the 4π threshold, $\epsilon'_{\text{th}} = 727$ MeV, we assume that statistical multipion production sets in. The residuals of the total γp cross section data are fitted by

$$\tilde{\zeta}_{(\pi)}(x) = \left[1 - \exp\left(-\frac{x - 0.727}{0.8}\right) \right] \left[69.8s^{0.081} + 64.3s^{-0.453} \right] \quad \text{for } x > 0.727, \quad (1.2.30)$$

with $s = 0.88 + 1.88x$; the total fit is shown in Fig. 1.10 (h). Fig. 1.12 shows the summed contributions of resonant, direct, and multipion channels on a logarithmic scale, also showing the slight increase of the cross section and the high energy limits set at the HERA accelerator.

1.2.2.4 Efficiency functions and hadronic radiation processes

Treatment of inelasticity functions: The efficiency functions are obtained by multiplying the cross section with the inelasticity function, separately for s and t -channel reactions. Following our discussion in the preceding section, we use the following results and approximations:

1. For resonance decay we have $\langle \cos \chi^* \rangle_s = 0$, thus the inelasticity is given by Eq. (1.2.13).
2. Particles produced in resonance decay below their nominal mass, i.e. below the nominal threshold for their production, are assumed to be produced *at threshold* with $m = M_{\text{kin}}$.
3. For t -channel reactions we assume strict forward scattering, and use Eq. (1.2.14) with $\langle \cos \chi^* \rangle_t = 1$.
4. The decay chain in the $\gamma N \rightarrow \Delta\pi$ channel is treated using Eq. (1.2.16), again using the isotropy relation for an initial s -channel reaction, and strict forward scattering for direct production of the Δ .
5. For the multipion channel we use Eq. (1.2.18) with $f_{(\pi)} = 0.4$.

We consider here only average values to obtain the efficiency function; methods for a statistical treatment are discussed in in Sect. 2.2. The efficiency functions for γp reactions obtained this way are shown in Fig. 1.13, indicating the relative contributions of s -channel and t -channel reactions. In this figure, we compare the result for each specific channel with the common estimate of an average inelasticity of 20%, which turns out to be acceptable for the most relevant channels. Fig. 1.14 shows the total efficiency with the relative contributions of different channels, including multipion production.

Energy loss time scale in power law spectra: The evaluation of energy loss time scales in general background spectra for different γ_{CR} must in be performed by numerical calculations. However, for an important type of astrophysical spectra, the anisotropic power law Eq. (1.1.50b), we find that all the particle physics can be reduced to a set of simple coefficients, dependent only on the spectral index. If we insert Eq. (1.1.51b) into Eq. (1.1.45), we see that we can obtain a very simple expression of the loss time scale if we introduce the reference Lorentz factor scale

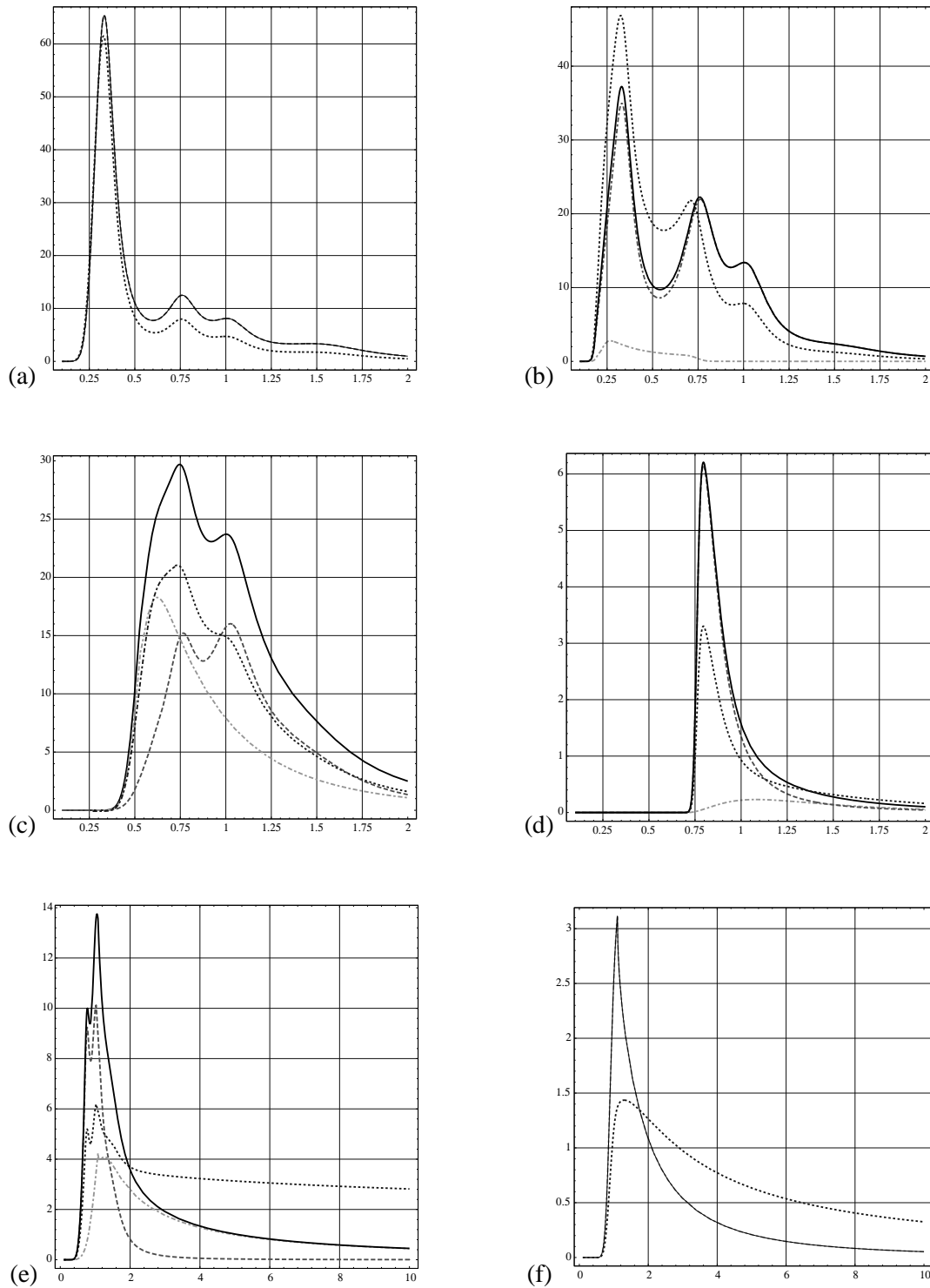


Figure 1.13: Efficiency functions for specific channels, separated according to: total efficiency (solid lines), s -channel efficiency (dashed lines), t -channel efficiency (light chain lines). Plotted is $\eta(\epsilon')$ in μbarn vs. ϵ' in GeV. Also shown is $0.2\sigma(\epsilon')$ (dotted lines) for comparison. Channel labels are the same as in Fig. 1.10.

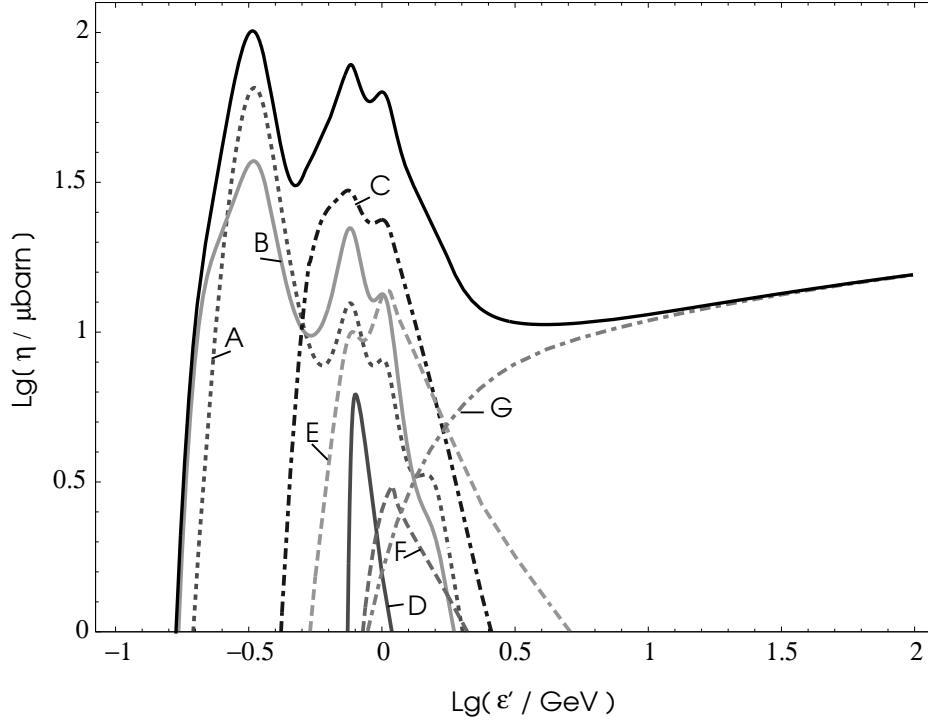


Figure 1.14: Total efficiency function for γp reactions. For neutrons, the resonance peak at about $\epsilon' \approx 1$ GeV is less pronounced, otherwise the function looks similar. Channel labels A, . . . , F correspond to labels (a) . . . (f) in Fig. 1.10, G marks multipion production.

$$\hat{\gamma}_{\text{CR}} = \frac{\gamma_{\text{CR}}}{\gamma_0} \quad \text{with} \quad \gamma_0 = \frac{\epsilon'_{\text{th},0}}{2\epsilon_0} \quad , \quad (1.2.31a)$$

where ϵ_0 is the lower limit of validity of Eq. (1.1.50b), and $\epsilon'_{\text{th},0}$ is the lowest threshold energy of all photomeson production processes (i.e. $\gamma p \rightarrow p\pi^0$, $\epsilon_{\text{th}} = 145$ MeV). Then, the validity of Eq. (1.1.51b) is limited to $\gamma_{\text{CR}} < \gamma_0$, or $\hat{\gamma}_{\text{CR}} < 1$. If we now introduce the *total weighted efficiency*

$$H_{ab}^{(c)} = \frac{2(a-1)(b+1)}{a+b+1} \int_1^\infty dx x^{-a} \eta_c(x\epsilon'_{\text{th},0}) \quad , \quad (1.2.31b)$$

where a and b are the energy and anisotropy index, respectively, we can simply write

$$\tau_{\text{loss}}^{-1} = cN_0 H_{ab} \hat{\gamma}_{\text{CR}}^{a-1} \quad (1.2.31)$$

with $H_{ab} = \sum_c H_{ab}^{(c)}$; they will be called the *efficiency coefficients* of the photon spectrum henceforth. For isotropic power law photon spectra, the efficiency coefficients $H_{a0}^{(c)}$ are shown as functions of a for all photomeson channels in Fig. 1.15; here, we realize best which channels are really important in power law spectra and which can be neglected in rough calculations.⁹ Spectra with $a \leq 2$ correspond to so-called *inverse spectra*,

⁹We stress that the power law index here refers to a global property of the spectrum rather than to a local. It expresses the relative weight of high and low energy interactions.

which are not energy normalized; we thus have to assume a cutoff somewhere, which affects the applicability of our results. We therefore confine ourselves to the case $a > 1.5$, and recommend for flatter spectra to evaluate the integral Eq. (1.2.31b) with an upper limit corresponding to the cutoff energy. The lower panel of Fig. 1.15 shows the total weighted photomeson efficiency for various anisotropy indices b .

Pion multiplicities and secondary ν/γ ratios: Besides deriving efficiency functions for proton energy losses, our detailed analysis of various photomeson channels allows to derive some general results on the secondary $\pi^+:\pi^-:\pi^0$ multiplicity relation. This is, as we have discussed in Sect. 1.2.2.1, important for the gamma-ray to neutrino ratio produced in hadronic radiation processes. We introduce the average pion numbers $N_{\pi^+}^{(c)}(\epsilon')$, $N_{\pi^-}^{(c)}(\epsilon')$ and $N_{\pi^0}^{(c)}(\epsilon')$ produced by a photon with NRF energy ϵ' in a reaction channel c . For quasi-two-particle channels, we derive from the decay channels of heavy baryons and mesons:

$$\begin{array}{c|cccccccc}
 \gamma p \rightarrow & p\pi^0 & n\pi^+ & \Delta^{++}\pi^- & \Delta^+\pi^0 & \Delta^0\pi^+ & p\eta & p\rho^0 & p\omega \\
 \hline
 N_{\pi^+}^{(c)}(\epsilon') & 0 & 1 & 1 & \frac{1}{3} & 1 & \frac{1}{4} & 1 & 1 \\
 N_{\pi^-}^{(c)}(\epsilon') & 0 & 0 & 1 & 0 & \frac{1}{3} & \frac{1}{4} & 1 & 1 \\
 N_{\pi^0}^{(c)}(\epsilon') & 1 & 0 & 0 & \frac{5}{3} & \frac{2}{3} & \frac{6}{5} & 0 & 1
 \end{array} \tag{1.2.32a}$$

For multipion production, we make use of Eq. (1.2.7) and assume charge equipartition in the multipion system, leading to

$$N_{\pi^+}^{(c)}(\epsilon') = N_{\pi^-}^{(c)}(\epsilon') = N_{\pi^0}^{(c)}(\epsilon') = 0.8 \left(\frac{\epsilon}{[\text{GeV}]} \right)^{\frac{1}{4}}. \tag{1.2.32b}$$

We then define the pion production functions for every channel c by

$$\varpi_{\pm 0}^{(c)}(\epsilon') = N_{\pi^{\pm 0}}^{(c)} \sigma_c(\epsilon') \quad \text{and} \quad \varpi_{\pm 0} = \sum_c \varpi_{\pm 0}^{(c)}(\epsilon'). \tag{1.2.32}$$

The total pion production function is shown in Fig. 1.16. In γn reactions, the π^+ and π^- curves are interchanged, and the little peak in the cross sections around $\epsilon' \approx 1$ GeV is partially removed, due to the $N(1680)/N(1675)$ asymmetry.

As a general example for the astrophysical application, we can now try to express the pion production rate $\psi_{\pm 0}(\gamma_\pi)$ of pions $\pi^{\pm 0}$ with Lorentz factor γ_π in an anisotropic power law photon spectrum. The problem is here, that the determination of the pion LF Lorentz factor requires in principle a detailed analysis of the final state reaction kinematics, in the same way as for the determination of the efficiency function. However, it is possible to use a very simple approximation here because of two facts valid in *most* reaction channels: (i) the Lorentz factor of the CMF in the LF is very large, and (ii) the pion CMF velocity is small, $\beta_\pi^* \ll 1$; this allows us to write $\gamma_\pi \approx \gamma_{\text{CR}}$. The latter assumption is only true close to the threshold of a specific channel, and for most pions produced by fireball-fragmentation, but in fact most pions are produced in one of these two ways. We can then write the approximate pion production rate in the same way as Eq. (1.2.31), that is

$$\bar{\psi}_{\pm 0}(\gamma_{\text{CR}}) = cN_0 \Pi_{ab}^{\pm 0} \hat{\gamma}_{\text{CR}}^{a-1} \tag{1.2.33}$$

with

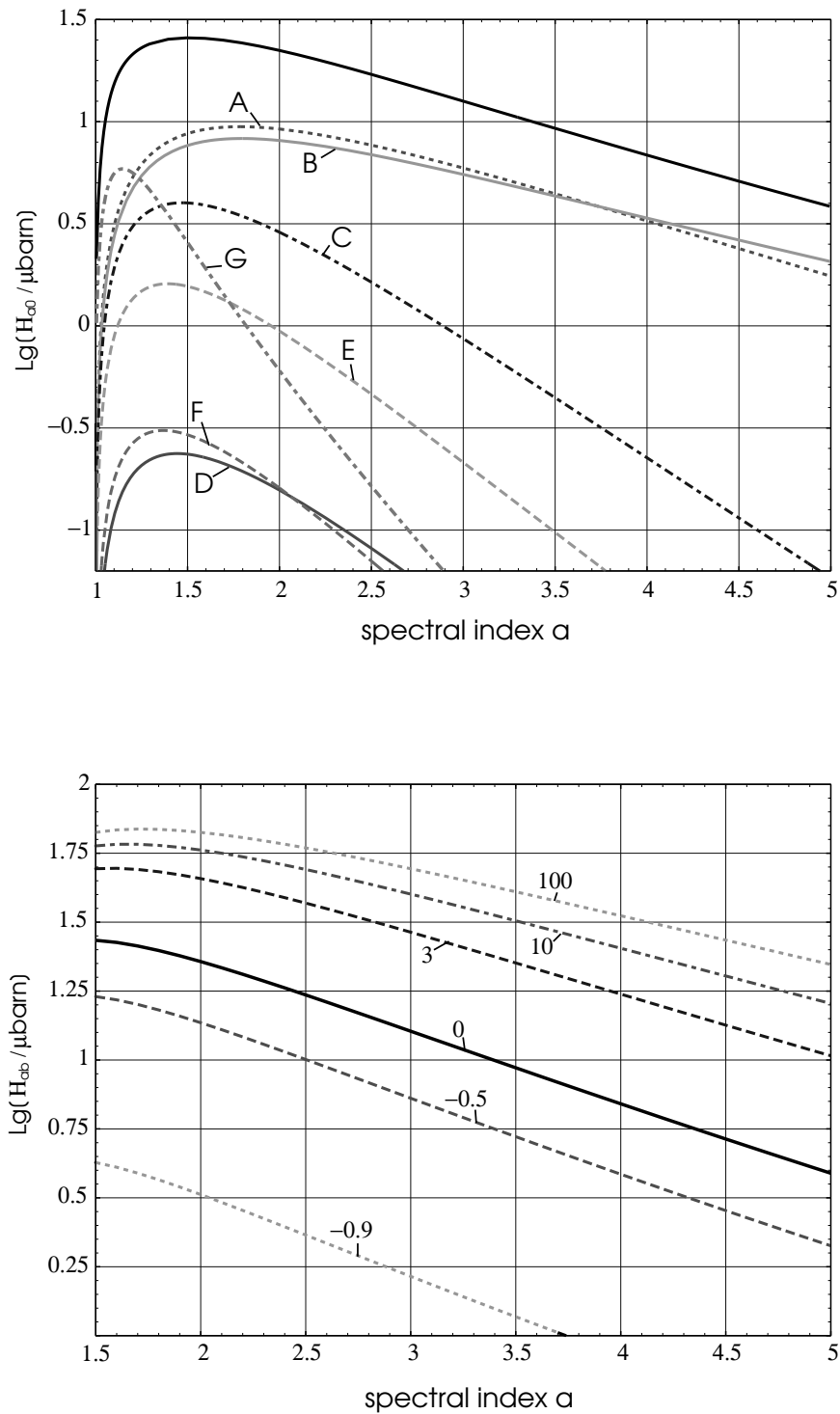


Figure 1.15: Efficiency coefficients in power-law photon spectra. Upper panel: contribution of different reaction channels, labeled as in Fig. 1.14. Lower panel: dependence on the anisotropy index b , marked at the curves.

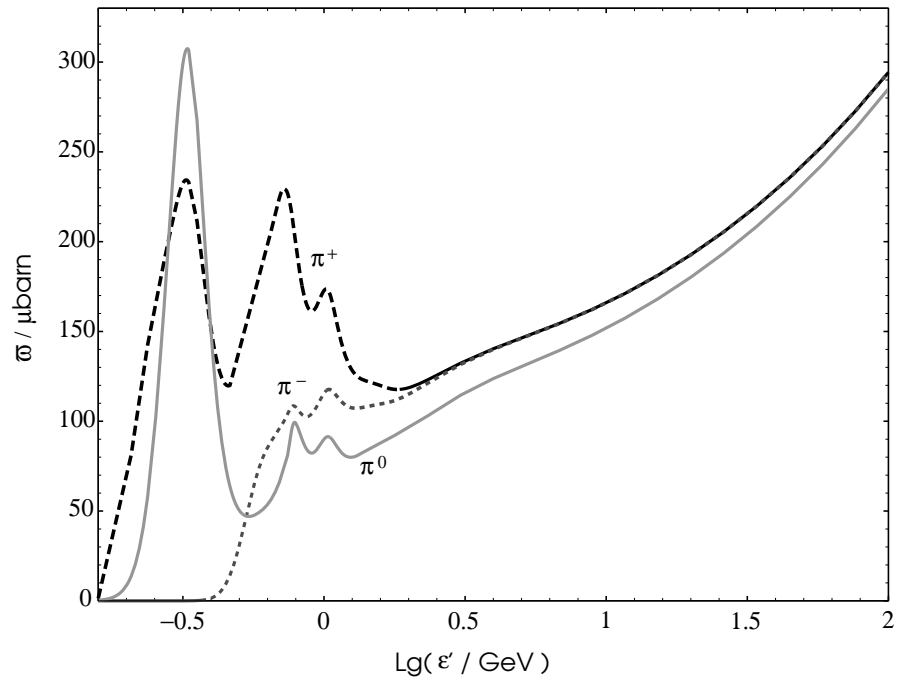


Figure 1.16: Production functions of π^+ , π^- and π^0 in γp reactions.

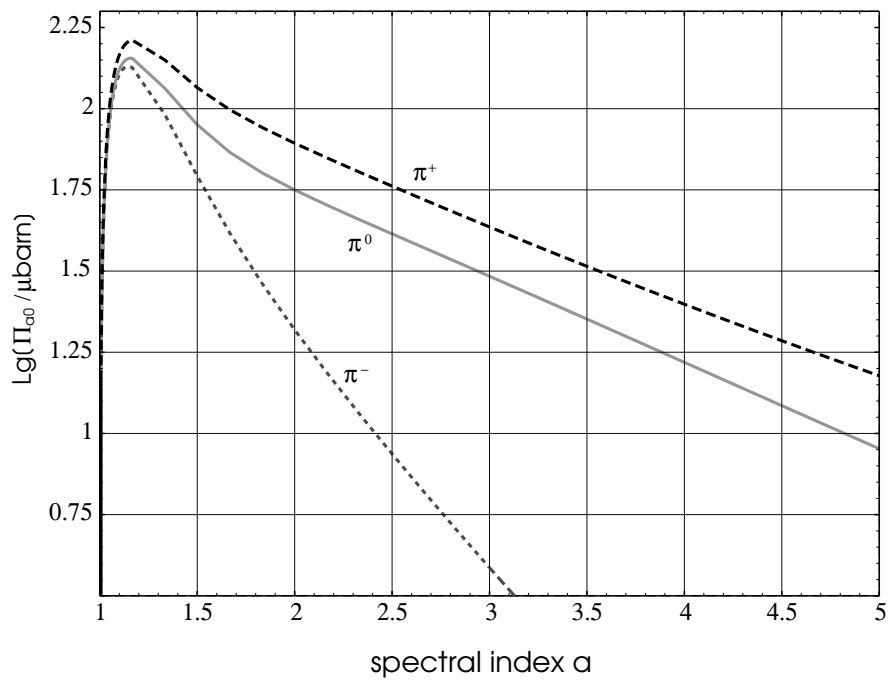


Figure 1.17: Total integrated pion production functions in isotropic power law photon spectra.

$$H_{ab}^{\pm 0} = \frac{2(a-1)(b+1)}{a+b+1} \int_1^\infty dx x^{-a} \varpi_{\pm 0}(x \epsilon'_{\text{th},0}) \quad . \quad (1.2.33a)$$

The resulting production functions for isotropic spectra are shown in Fig. 1.17; the scaling relation for nonvanishing anisotropy is simple, hence we omit a figure.

Clearly, both the assumed spectral shape and the simplification $\gamma_\pi \approx \gamma_{\text{CR}}$ limit the applicability of our results to real hadronic radiators in astrophysics (e.g. AGN); the purpose of this investigation is rather to show up the influence of the severe differences in the pion charge ratio in the first and second resonance regions of photohadronic interactions. We stress that these differences may even be more pronounced if pion production at “sharp” black-body peaks is considered. Looking at Eqs. (1.2.20), we see that the $\pi^\pm:\pi^0$ ratio reflects essentially the power going into neutrinos relative to the power going into gamma rays. Even though the detailed PIC physics of is complicated [MKB91, Man93], we can state here that the common assumption of equipartition between charged and neutral pions is not quite correct in spectra with global power law behavior (and maybe even less in other spectra). Rather, the ratio $\pi^\pm:\pi^0$ is close to 2:1 — the same as at high energy interaction due to isospin equipartition, with the only difference that at low energies the initial isospin of the nucleon causes an anisotropy in the pion charge-ratio, $\pi^+:\pi^-$.

1.3 Photodisintegration of nuclei

Photodisintegration of nuclei can be considered as the nuclear analogy to the atomic photoeffect, or more general, the photoionization of atoms. In contrast to photomeson production, it is not the production of massive particles causing an energy loss of the cosmic ray nucleus, but a mass loss of the nucleus itself. In this section, we give a phenomenological classification of the processes leading to photodisintegration, and develop suitable efficiency functions for the application to cosmic ray physics. Sect. 1.3.1 gives an outline of low energy nuclear physics, which is determined by the binding forces between nucleons, while Sect. 1.3.2 describes the effects of high energy, quasi-free photohadronic interactions on single nucleons, as discussed in Sect. 1.2, on the surrounding nuclear environment. In refsec Sect. 1.3.3 we discuss the physical processes of nuclear photodisintegration. Finally, in Sect. 1.3.4 we develop astrophysical efficiency functions for nuclear photodisintegration, in the same way as in Sect. 1.2.2.

Basic principles of nuclear physics are taken from the books of EVANS [Eva55], BLATT & WEISSKOPF [BW52], and MAYER-KUCKUK [May92]. An overview about the physics of nuclear photodisintegration is given in a book of LEVINGER [Lev60], and in several review articles [BW57, DF65].

Notation: We try to comply with the usual notation of nuclear physics throughout this section, as found in the literature listed above. In Sect. 1.3.4 we refer to the notations of Sect. 1.1.3.3 and Sect. 1.2.2. The reader should be warned that the symbol N mostly denotes the neutron number, but is also used as a symbol for “nucleon” (p or n) in some cases, which should always be clear from the context.

1.3.1 Low energy nuclear reactions

1.3.1.1 Binding energy and shell structure

Binding energy in the liquid drop model: In the simplest model the atomic nucleus is treated as a fluid of protons and neutrons, which are bound together by short range forces similar to fluid dynamics. This is called the *liquid drop model* of the nucleus. We will denote a nucleus of an element X , consisting of Z protons and N neutrons, with ${}^N_Z X_A$; $A = N + Z$ is called the nuclear mass number.¹⁰ The *binding energy* $B(Z, N)$ of a nucleus ${}^N_Z X$ is given by its *mass defect*

$$\frac{B}{c^2} \equiv \Delta M_X = Zm_p + Nm_n - M_X \quad .$$

In the liquid drop model, the binding energy can be split into terms representing the *volume energy* $B_V \propto A$, the *surface energy* $B_S \propto A^{2/3}$, and the *Coulomb energy* $B_C \propto Z^2/A^{1/3}$ of the charged fluid drop. Quantum-mechanical effects add terms for the *asymmetry energy* $B_A \propto (N - Z)^2/A$, taking into account the different behavior of protons and neutrons in the nucleus, and the *pairing energy*, which is $B_P \propto (-1)^Z A^{-1/2}$ for A even, and $B_P = 0$ for A odd. The average binding energy $b \equiv B/A$ can then be written as a function of A using the semi-empirical *Weizsäcker mass formula*

$$\begin{aligned} \frac{b(A)}{\text{MeV}} \approx & 15.85 - 18.34 A^{-1/3} - 0.18 A^{2/3} \\ & + 1.3 \times 10^{-3} A^{4/3} - 6.4 \times 10^{-6} A^2 \pm \delta(A) \quad . \end{aligned} \quad (1.3.1a)$$

Here we have applied the relation between Z and A for the β -stable nuclei, given in the liquid drop model as

¹⁰We will only write the indices Z , N or A as far they contain non-redundant information. In particular, Z is implicitly determined by the element name, and it is then sufficient to note either of the numbers N or A to give full information. Hence, Fe_{56} is equivalent to ${}^{56}_{26}\text{Fe}$ or ${}^{56}_{26}X$. We use X for a variable element name.

$$\bar{Z}_{\text{Id}}(A) = \frac{A}{1.98 + 0.015 A^{-1/3}} \approx \frac{A}{2} - 0.003 A^{5/3} \quad , \quad (1.3.1b)$$

neglecting terms contributing only about 1% or less for $1 < A \lesssim 200$. The δ term in Eq. (1.3.1a) expresses corrections due to the pairing energy, and vanishes for odd A . Omitting this term, Eq. (1.3.1a) still describes the average binding energy for nuclei with a mass number around A in a good approximation and is so far useful for our purposes; we will denote the average isobar binding energy per nucleon without the δ -term with $\bar{b}(A)$.

Separation energy: The *separation energy* $S(z, a)$, necessary to separate a nuclear fragment ${}^n_z f$, i.e. a nucleus of proton number z and neutron number n , from a nucleus ${}^N_Z X$, is

$$S_f \equiv S(z, n) = B(Z, N) - B(z, n) - B(Z - z, N - n) \quad .$$

Note that this equation simply bases on energy conservation and does not depend on any properties of the potential, e.g. the charge of f .

The threshold energy of an endoergic nuclear reaction $X(a, b)Y$ is generally expressed as $E_{\text{th}} = -Q_{\alpha\beta}$, where the *Q-value* of the reaction given by

$$Q_{\alpha\beta} = S_a - S_b + (E_a^* + E_X^*) - (E_b^* + E_Y^*) \quad .$$

α and β denote the reaction channels, consisting of the particles (X, a) and (Y, b) , respectively, the separation energies refer to the compound nucleus formed in during the reaction, and the E_{\dots}^* denote the excitation energies of the respective particles. However, if we consider (γ, f) reactions and ask just for the threshold energy for emission of a fragment f , we can set all $E^* = 0$ and simply get

$$E_{\text{th}}(\gamma, {}^n_z f) = S(z, n) \quad .$$

The separation energy strongly depends on the involved nucleus and the emitted fragment. This is particularly the case for light nuclei, where changes occur very rapidly due to the rapid changes in the binding energy per nucleon f . However, for heavy nuclei f can be expressed as a rather smooth function of A ; if we only consider the separation of ν unbound nucleons, we can furthermore omit the binding energy of the fragment and write

$$S_\nu(A) \simeq \nu \bar{b}(A) + \nu(A - \nu) \frac{d\bar{b}}{dA} \quad . \quad (1.3.1c)$$

Clearly, this equation is of limited applicability in light nuclei, and may be regarded as a useful approximation only for $\nu = 1, 2$.

Charge dependent effects and branching ratios: The separation energy S is the energy necessary to remove a fragment ${}^n_z f_a$ from the nucleus to a very large distance. For a charged particle, however, this is not equal to the energy required to move it out of the potential well, because of the existence of the Coulomb force. We can write $S = S^* - S^c$, where

$$S^c(z, n) \simeq \frac{z(Z - z)e^2}{R_{A-a}} \approx \frac{z(Z - z)}{(A - a)^{1/3}} \text{ MeV} \quad (1.3.1d)$$

is the height of the *Coulomb barrier* in the potential function, R_{A-a} is the radius of the residual nucleus. Hence, even though S_f is still the physical reaction threshold, S_f^* is the energy necessary in a classical sense to remove

the fragment from the nucleus. The quantum mechanical transmission effect and the only approximative validity of Eq. (1.3.1d), however, lead to emission spectra of protons peaking at somewhat lower energy.

The effect of the Coulomb force has a strong impact on the branching ratios for different particles in photodisintegration, especially the ratios for proton and neutron emission. For light nuclei with $Z = N$, we find $S_p^c \lesssim S_n - S_p$, and hence $S_p^* \lesssim S_n$, showing that proton emission is favored compared to neutron emission. For beta-stable heavy nuclei, where we generally have $N > Z$, we rather find $S_p^* > S_p$ with $S_p \simeq S_n$, due to the strong Coulomb potential for large Z , making neutron emission more favorable. It plays also a role for the evaporation of composite fragments in very heavy nuclei: For $A > 200$ we have $S_\alpha \simeq 0$, but because of the Coulomb wall $S_\alpha^* \gg S_n$, making the evaporation of α particles very unlikely.

Shell structure and excitation levels: The liquid drop model disregards the quantum mechanical selection rules governing the energy distribution of the nucleons. In the *nuclear shell model*, the nucleons occupy discrete energy states in a collective potential well, connected to the quantum numbers of the radial wave function n , orbital angular momentum l and total angular momentum j . Each level can be populated by four nucleons, two protons and two neutrons with different spin orientation. In contrast to baryon resonances, this is not just a spectroscopic classification for certain scattering channels, but rather resembles the atomic shell model of electrons. The difference of nuclear and atomic shell models is mainly that the LS coupling leads to energy differences comparable to that between radial excitation numbers, and increasing with l . For low l , n can still be considered as the major quantum number as in atomic physics, and big gaps in the level structure occur at the closure of the $1s$, $1p$ and $1d$ shells, where in the latter one the $2s$ level is embedded. This leads to closed shell nuclei with $N, Z = 2, 8, 20$, which are the lowest *magic numbers*. These light nuclei are therefore classified as s -shell ($Z \leq 2$), p -shell ($3 \leq Z \leq 8$), and sd -shell ($9 \leq Z \leq 20$) nuclei. For larger l , however, one finds major level gaps rather between the $j = l - \frac{1}{2}$ and the corresponding $j = l + \frac{1}{2}$ state for $n = 1$, while levels for $n = 2, 3, \dots$ are mixed in between them. This leads to the higher magic numbers $N, Z = 28, 50, 82, 126$. At the magic numbers, the separation energy has a local maximum and drops sharply by about 1 MeV for $N \rightarrow N + 1$ or $Z \rightarrow Z + 1$. Nuclei where both N and Z are magic numbers are called *double magic nuclei*, and have particularly high separation energies; the only stable double magic nuclei are ${}^2_2\text{He}_4$, ${}^8_8\text{O}_{16}$, ${}^{20}_{20}\text{Ca}_{40}$, ${}^{28}_{28}\text{Ca}_{48}$, and ${}^{126}_{82}\text{Pb}_{208}$.

Every level has well defined quantum numbers of angular momentum, l and $J = l \pm \frac{1}{2}$, parity, $P = (-1)^l$, and isospin, T .¹¹ The 3-component of the nuclear isospin is given by $T_z = \frac{1}{2}(N - Z)$, and T can take the values $\frac{1}{2}A, \frac{1}{2}A - 1, \dots, |T_z|$. The symmetry constraints set by the Pauli principle determine the possible isospin configurations of every level, because the nuclei belonging to the same isospin multiplet are required to have the same j_z : in particular, for light nuclei with $|T_z| \leq 1$, one can easily show that the ground state has $T = 0$ for $A = 4n$, $T = \frac{1}{2}$ for $A = 4n \pm 1$, and $T = 0, 1$ for $A = 4n + 2$ ($n = 0, 1, \dots$). In the same way as in particle physics, the shell model sets up selection rules for specific excitation modes, which will be discussed below.

The nuclear shell model cannot account for distinct predictions of the magnitudes of binding energies and separation energies; actually, it just assumes the existence of a self-consistent binding potential and treats the nucleons as non-interacting particles in this potential. If the nucleus is excited in a nuclear reactions, this leads in general to a change of the potential; so, the excitation levels and nucleon transition have to be considered as between two *different nuclei* rather than between energy levels of the same nucleus. Thus, the excitation levels of nuclei vary strongly from one nuclide to the next, and have to be taken from tables collecting empirical results (e.g. [AGL⁺61]).

¹¹The isospin is generally denoted as T in nuclear physics.

1.3.1.2 Electromagnetic excitation of nuclei

Excitation modes: Complex atomic nuclei show, as we have seen above, a behavior which is somewhere in between a classical and a quantum-mechanical description. This affects also their interaction with electromagnetic radiation: For low interaction energies, the shell structure of the nucleus determines possible transitions, which obey the quantum mechanical selection rules. For larger photon energies ϵ , the level density becomes so high that even in small intervals $d\epsilon$ almost every multipole finds a suitable level for transition. However, there are some general rules which determine the probability of excitation by a specific electromagnetic multipole independent on shell selection rules, just on the basis of classical electrodynamics; one finds the approximate proportionality relation

$$\sigma_l \propto \epsilon^{2l-1} \sum_{m=\pm 1} \left[|Q_{lm}|^2 + |M_{lm}|^2 \right] \quad (1.3.2)$$

for the absorption cross section for 2^l pole radiation, where Q_{lm} and M_{lm} are the electric and magnetic multipole moments of the nucleus, respectively. One can show that the magnitudes of these moments follow the relations $Q_{lm} \propto ZR^l$ and $M_{lm}/Q_{lm} \sim \hbar/MRc$; separating the cross section into electric and magnetic parts, $\sigma_l = \sigma_{El} + \sigma_{Ml}$, according to the contributions of Q_{lm} and M_{lm} in Eq.(1.3.2), we find the order of magnitude estimates

$$\frac{\sigma_{l+1}}{\sigma_l} \sim 10^{-4} A^{1/3} \left[\frac{\epsilon}{\text{MeV}} \right] \quad (1.3.2a)$$

$$\frac{\sigma_{Ml}}{\sigma_{El}} \sim 0.16 A^{-4/3} \quad . \quad (1.3.2b)$$

Following this, in medium mass nuclei ($A \gtrsim 10$) magnetic transitions are suppressed compared to electric transitions of the same order by more than two orders of magnitude, and for energies $\epsilon \lesssim 100$ MeV the same suppression occurs by increasing the multipole order, $l \rightarrow l + 1$. Thus we can expect that *electric dipole transition* is the dominant mode of the electromagnetic excitation of nuclei. We will see in Sect. 1.3.3.2 that this transition occurs in form of the *giant resonance* at $\epsilon \sim 20$ MeV, while *E1* transitions at lower energies are mostly forbidden due to selection rules. Because of the high level density at excitation energies of about 20 MeV, electric dipole absorption of nuclei can be treated as a quasi-classical process.

The TRK sum rule for nuclei: Before discussing the photonuclear cross section in detail in Sect. 1.3.3, we may discuss some relations for the most inclusive information about photonuclear reactions, the total integrated cross section for photon absorption. Since we have to deal mainly with dipole absorption, we can apply the sum-rule relation Eq. (1.1.43) to the nucleus; assigning the *effective charges*

$$e_p = \frac{eN}{A} \quad \text{and} \quad e_n = \frac{eZ}{A}$$

to the protons and neutrons in the nucleus, we find

$$\int_0^\infty \sigma_{E1}(\epsilon) d\epsilon \equiv \Sigma_{\text{TRK}} = \frac{2\pi^2 e^2 \hbar}{m_N c} \frac{NZ}{A} \simeq \left[60.0 \text{ MeV mbarn} \right] \frac{NZ}{A} \quad , \quad (1.3.3)$$

which is known as the *Thomas-Reiche-Kuhn (TRK) sum rule* for nuclei. It makes use of the assumption that the dipole moment of the nucleus can be completely described in terms of the coordinates of the single nucleons in a common potential well, under neglect of direct exchange forces between nucleons — an assumption known

in nuclear physics as *Siebert's theorem*. A correction of Eq. (1.3.3) by inclusion of nuclear exchange forces was done by LEVINGER AND BETHE [LB50], who found

$$\Sigma_{\text{LB}} = (1 + C_{\text{LB}}\xi_{\text{a}}) \Sigma_{\text{TRK}} \quad \text{with} \quad 0 \leq \xi_{\text{a}} \leq 1; \quad (1.3.3a)$$

C_{LB} is a constant depending on empirical nuclear parameters which was evaluated by the authors to $C_{\text{LB}} = 0.8 \pm 0.1$, and ξ_{a} is the fraction of the *attractive* exchange force in the neutron-proton interaction. Eq. (1.3.3a) is still a dipole sum rule, therefore neglects absorption cross sections of higher multipoles; however, LEVINGER [Lev60] argues that magnetic dipole and electric quadrupole transitions essentially cancel each other by interference, and from the discussion in the last paragraph we can expect that higher multipoles can be neglected altogether. Therefore, Eq. (1.3.3a) implies that the total integrated photoabsorption cross section of nuclei lies about a factor of 1.5–2 above the TRK value, depending on the fraction of attractive forces in nucleon interactions.

Causality and the GGT sum rule: A different approach to express integrated photonuclear cross sections was introduced by GELL-MANN, GOLDBERGER & THIRRING (GGT) [MGT54], who derived an expression known as the *GGT sum rule*. It is based on the principles of dispersion theory, using the following assumptions: (i) In the low energy limit, $\epsilon \rightarrow 0$, the elastic photon scattering cross sections of the nucleus and the proton are given by the respective Thomson cross sections,

$$\sigma_{\text{el}}^{(p)}(0) = \sigma_{\text{T}p} \quad , \quad \sigma_{\text{el}}(0; Z, A) = \sigma_{\text{T}}(Z, A) = \frac{Z^4}{A^2} \hat{\sigma}_{\text{T}} \quad , \quad (1.3.4a)$$

and $\sigma_{\text{el}}^{(n)}(0) = 0$; (ii) in the high energy limit, photon scattering by the nucleons in the nucleus is identical to the total scattering of the same number of free nucleons,

$$\lim_{\epsilon \rightarrow \infty} [\sigma_A(\epsilon) - Z\sigma_p(\epsilon) - N\sigma_n(\epsilon)] = 0 \quad , \quad (1.3.4b)$$

where we can assume that the total cross section is completely dominated by photomeson production; (iii) the photon absorption cross section of free nucleons vanish in the low energy limit

$$\sigma_{\text{ab}}^{(p)}(0) = \sigma_{\text{ab}}^{(n)}(0) = 0 \quad . \quad (1.3.4c)$$

From this, one can derive the photon absorption cross section integrated up to the pion production threshold ϵ_{π} as

$$\begin{aligned} \int_0^{\epsilon_{\pi}} \sigma_{\text{ab}}(A, \epsilon) d\epsilon &\equiv \Sigma_{\text{GGT}} = \Sigma_{\text{TRK}} + \int_{\epsilon_{\pi}}^{\infty} d\epsilon \left(Z\sigma_{\text{ab}}^{(p)}(\epsilon) + N\sigma_{\text{ab}}^{(n)}(\epsilon) - \sigma_{\text{ab}}(A, \epsilon) \right) \\ &= \Sigma_{\text{TRK}}(Z, A) \left[1 + \xi_{\text{GGT}} \right] \quad . \end{aligned} \quad (1.3.4)$$

The integral in Eq. (1.3.4) must be evaluated on the basis of experimental data; in their original work, GGT found a value $\xi_{\text{GGT}} \simeq 0.4$; but it was clear very soon that this value is exceeded by the experimental integrated cross sections in heavy nuclei. On the basis of the vector dominance model for the hadronic photon, WEISE [Wei74] argued that assumption Eq. (1.3.4b) has to be abandoned: Because of the virtual appearance of photons as vector mesons there occurs a shadowing effect in photonuclear scattering, leading to $\sigma_A < Z\sigma_p + N\sigma_n$ at high energies. Setting $\hat{\sigma} = (Z/A)\sigma_p + (N/A)\sigma_n$ and

$$\sigma_A(\epsilon) = A_{\text{eff}}(\epsilon)\hat{\sigma}(\epsilon) \quad ,$$

Weise developed a modified GGT sum rule, in which ξ_{GGT} is replaced by a function $\xi(Z, A)$ slightly increasing with A . He used $\langle A_{\text{eff}} \rangle_{\epsilon} \simeq A^{0.8}$ in the baryon resonance region, $\epsilon_{\pi} < \epsilon < 2 \text{ GeV}$, and $\langle A_{\text{eff}} \rangle \approx A^{0.91}$ for $2 \text{ GeV} < \epsilon < 20 \text{ GeV}$, which was known from experiment. His scaling rule in the resonance region was, however, not confirmed in the Δ -resonance region in high precision photoabsorption experiments, which rather suggest $A_{\text{eff}} = A$, but there is a tendency of a decrease of A_{eff}/A reported in the second resonance region, confirming Weise's assumption qualitatively [Ahr85].

We may briefly summarize the basic idea behind the GGT approach to the total integrated cross section for photon absorption: The GGT sum rule does not make any assumptions on the detailed photon absorption mechanism of the nucleus; it just uses the principles of unitarity and causality in the transition from coherent scattering of the nucleus to quasi-free scattering on single nucleons. The suppression of the Thomson cross section in the transition from the bound to the free system of nucleons gives immediately the TRK dipole sum rule, and the suppression of real meson production above ϵ_{π} due to Pauli blocking effects in the bound nucleus introduces the additional contribution $\xi(Z, A)\Sigma_{\text{TRK}}(Z, A)$. We may interpret the latter contribution physically as the reabsorption of the produced pions in the nucleus; since such exchange pions are virtual and therefore can have masses below m_{π} , the process can contribute below the real pion threshold.

Experimental results: The TRK sum rule in the formulation of Levinger and Bethe did not predict an upper energy limit for the integral over the cross section; the progress introduced by the GGT approach was to fix it to the pion production threshold. Therefore, it is useful to compare with experimental cross sections only up to this limit, where real meson production does not occur. In early experiments, it were mostly the limited experimental maximum photon energies which founded the belief that the original proposal of GGT, $\Sigma_{\text{tot}} \approx 1.4\Sigma_{\text{TRK}}$, indeed expresses the total absorption cross section. In modern experiments, it turned out that $\Sigma_{\text{tot}} \approx 2\Sigma_{\text{TRK}}$ for $A > 10$, and slightly decreases to lower A , matching the GGT enhancement factor, $\xi = 0.4$, for the deuteron (see [Ahr85], and references therein). This behavior is essentially reproduced by Weise's extension of the GGT sum rule.

The most complete collection of integrated cross sections of all elements up to Fe_{56} has been published by PUGET, STECKER & BREDEKAMP (PSB) [PSB76], on the basis of data tables from the National Bureau of Standards. They have distinguished between one and two nucleon emission cross section for $\epsilon < 30 \text{ MeV}$, and the contribution for $30 \text{ MeV} < \epsilon < 140 \text{ MeV}$, i.e. up to the pion threshold. Their method of data reduction has been quite crude, and also extrapolations have been included in the analysis, therefore their results cannot be considered as more accurate than to about 10%. Their integrated cross sections exceed $2\Sigma_{\text{TRK}}$ for almost all nuclei, which is at the upper limit of the results published by experimental groups [Ahr85]. Thus, even though the PSB results are basically consistent with other publications, the possibility of a systematic error has to be taken into account.

1.3.1.3 Statistics of nucleon emission

Selection rules of the shell model: In the shell model, quantum mechanical selection rules also determine both the excitation of a nucleus and its decay by particle emission. For radiative excitation, it can be shown that the most effective $E1$ transitions lead to $\Delta J = \pm 1, 0$ and $\Delta T = \pm 1, 0$, and require a change of parity. The latter condition implies that transitions between $J = 0$ and $T = 0$ states are forbidden. One finds that for low energy excitation levels these conditions are almost never met; thus, low energy excitations will proceed mainly over higher multipoles, and have therefore a low transition strength. For excitation energies in the range 10–20 MeV, however, some transitions allowed for $E1$ excitations exist.

An important consequence is that the electromagnetic excitation of nuclei mostly leads to states with $T \neq 0$. For the decay of the particle by emission of composite fragments with $T = 0$, i.e. deuterons or α -particles, this means that also the final state must have $T \neq 0$. For light $4n$ nuclei, we know that the ground state has $T = 0$; an state excited by an $E1$ transition then must have $T = 1$. Hence, an α particle can only be emitted by a transition to an *excited state* of the final nucleus (which is also a $4n$ nucleus and has a ground state with $T = 0$). This is particularly important because one finds that the separation energies of α particles are in light $4n$ nuclei mostly below the separation energies for single nucleons. In contrast to the situation in heavy nuclei, where the Coulomb barrier suppresses the emission of α particles, this would — without effect of selection rules — imply that α emission is energetically favored over nucleon emission. However, since the lowest $T = 1$ level in such nuclei has generally an excitation energy of ~ 10 MeV, the effective α separation energy is shifted to about 20 MeV, far above the threshold for nucleon emission. In odd nuclei, the effect of the selection rule is less strict, because $E1$ transitions with $\Delta T = 0$ are allowed, but it still applies partially by ruling out certain transitions. For single nucleon emission, isospin selection rules hardly set constraints, because the total isospin of the nuclear ground level is changed by a half-integer step in this case, so transitions from all $E1$ excited levels to the ground state are possible.

Thermodynamics of nuclei: In heavy nuclei, and at excitation energies above about 20 MeV, the shell model is only of minor use for the description of nuclear reactions. Rather, due to the high density of quantum states, it can be replaced by a statistical description of the nucleus as a thermodynamical fluid, which is commonly called the *statistical model of nuclei*. It assigns a *nuclear temperature* Θ to the excited nucleus,

$$\Theta(E^*) = \frac{1}{dS/dE^*} = \sqrt{\frac{E^*}{\ell}} \quad , \quad (1.3.5a)$$

where E^* is the excitation energy and ℓ is the *level density parameter*, that is connected with the *nuclear entropy* $S = 2\sqrt{\ell E^*}$. ℓ may depend on the details of nuclear structure, but is for heavy nuclei well approximated by

$$\ell \simeq \frac{A}{[8 \text{ MeV}]} \quad . \quad (1.3.5b)$$

The proportionality to $\ell \propto A$ reflects the takeover from the shell description (individual levels) to the statistical description (continuous level density) with increasing nuclear mass.

The emission of nucleons from the “heated” nucleus can now be considered as an evaporation process, leading to a modified Maxwell distribution

$$W_f(\epsilon) = C_0 \check{\sigma}_f(\epsilon) \epsilon \exp\left(-\frac{\epsilon}{\Theta_f}\right) \quad (1.3.6)$$

for the emission probability of a fragment f with an energy ϵ , where the normalization constant is chosen in a way that $\sum_f \int W_f(\epsilon) d\epsilon = 1$ and $\Theta_f \equiv \Theta(E^* - S_f)$ for an excitation energy E^* . $\check{\sigma}_x(\epsilon)$ is the cross section for the inverse process, i.e. the formation of the incident nucleus in a reaction of f with the residual nucleus.

Nucleon evaporation and multiplicities: The statistical model also allows an estimate on the nucleon multiplicity, ν , as a function of the excitation energy, E^* . If we assume that all emitted nucleons are neutrons, we obtain

$$\frac{\sigma_{\nu+1}}{\sigma_\nu} = 1 - \left(1 + \frac{E^* - S_{\nu+1}}{\Theta_\nu}\right) \exp\left(-\frac{E^* - S_{\nu+1}}{\Theta_\nu}\right) \quad , \quad (1.3.7)$$

where σ_ν is the cross section for the emission of ν or more neutrons, S_ν is the separation energy for ν neutrons, and $\Theta_\nu = \Theta(E^* - S_\nu)$ is the nuclear temperature of the ν -th compound nucleus (after the emission of the ν -th neutron). Successive application of Eq. (1.3.7) over all ν with $S_\nu < E^*$ gives the average neutron multiplicity at the excitation energy E^* ; this calculation has been performed by LEVINGER & BETHE [LB52] for five heavy elements, and they found that the result can in all cases be well approximated by the simple linear relation

$$\bar{\nu}(E^*) \approx \frac{2E^*}{S_1 + S_2} . \quad (1.3.8)$$

So far, we only have considered multi-neutron emission, which might be a good approximation for heavy nuclei. For charged particles, the Maxwell distribution of emitted particles is distorted and Eq. (1.3.7) is no longer valid. However, if we ask for the *total nucleon multiplicity*, we can apply the following argumentation to keep Eq. (1.3.7) and Eq. (1.3.8) as useful approximations: For $\Theta_n \approx \Theta_p > S_p^c$, protons and neutrons behave similar; this is almost always the case in light nuclei, where proton emission plays a role. On the other hand, if $\Theta_n \approx \Theta_p < S_p^c$, proton emission is suppressed, and their contribution to the *total distribution* of emitted nucleons is not bigger than the distortions of the Maxwellian by quantum mechanical effects. In any case, the assumptions leading to Eq. (1.3.7) can still be used, and Eq. (1.3.8) remains valid within the limits of application of the statistical model, with $\nu(E)$ now being the function for the total nucleon multiplicity.

Branching ratios of evaporated particles: Eq. (1.3.6) allows a crude estimate of the proton to neutron branching ratio $R_{p/n}$ in photodisintegration. Since $\check{\sigma}_n$ is constant in good approximation and the difference between protons and neutrons in nuclear reactions is only the electric charge, we can set

$$\check{\sigma}_p(\epsilon) = \begin{cases} \check{\sigma}_n , & \epsilon > S_p^c \\ 0 , & \epsilon \leq S_p^c \end{cases} ,$$

and get for $E^* - S_{n,p} \gg \Theta_{n,p}$

$$R_{p/n}(E^*) = \frac{\int W_p(\epsilon) d\epsilon}{\int W_n(\epsilon) d\epsilon} \sim \frac{\Theta_p^2}{\Theta_n^2} \left(\frac{S_p^c}{\Theta_p} + 1 \right) \exp\left(-\frac{S_p^c}{\Theta_p}\right) . \quad (1.3.9)$$

This formula reproduces the gross behavior of the observed p/n branching ratios with nuclear mass, if we set $E^* = 20$ MeV (the energy of the giant resonance) and evaluate the nuclear temperature from Eqs. (1.3.5). Levinger has calculated the *proton* branching ratio within the statistical model (with probably much less crude simplifications) for a bremsstrahlungs photon spectrum and found good agreement with the experimental values; these fall from more than 50% for light nuclei ($Z \lesssim 10$) to less than 1% for $Z > 45$. For light nuclei the statistical model overestimates the proton ratio a bit, while for very heavy nuclei the experimental values fall off much less rapid than the prediction, due to direct disintegration processes.

1.3.2 High energy nuclear reactions

1.3.2.1 Nuclear fragmentation and the abrasion-ablation approximation

The abrasion-ablation model: In Sect. 1.3.1.3 we discussed the evaporation of particles from an excited state of the nucleus within a thermodynamical approach. We have not yet considered, however, how this excitation exactly happens in nuclear interactions. Also, we may ask whether there are limits of applicability of the simple description of the nucleus as an idealized Fermi gas.

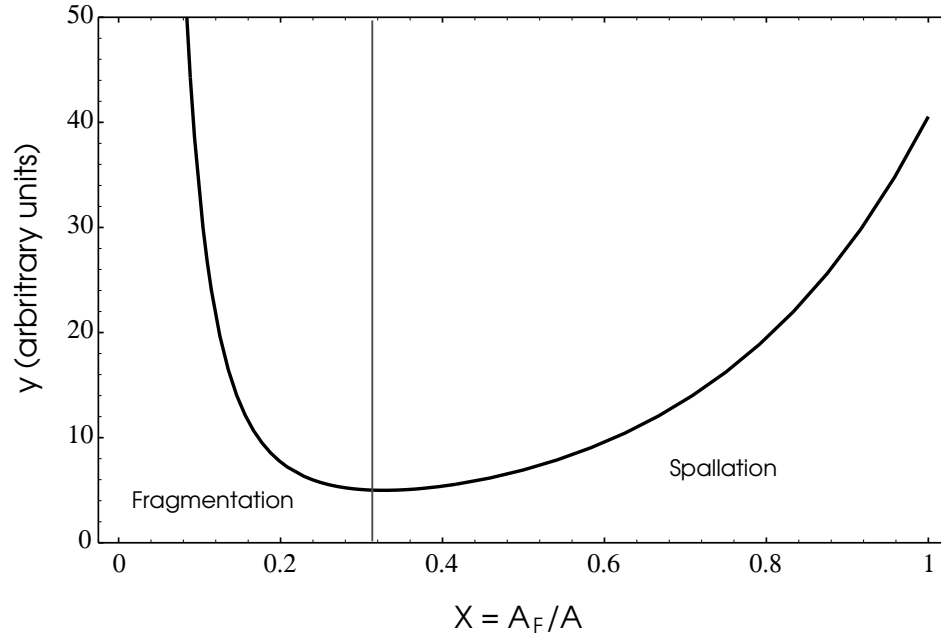


Figure 1.18: Mass yield distribution function for high energy proton induced fragmentation of heavy ions.

The main subject of this section is the estimation of the excitation energy transformed to the nuclear system in direct reactions of its constituents. The *abrasion-ablation model* (see, e.g. [ODR79, Hüf85]), which was designed to describe nucleus-nucleus reactions at high energy, divides the nucleons in both reaction partners into *participants* and *spectators*. The participants are those nucleons which immediately interact and are swept away with the “fireball” of the reaction process (abrasion), while the spectators, i.e. the nucleons outside the interaction zone, take part only peripherally by being excited by some participants or secondary reaction products recoiling through the spectator matter, and by surface deformation energy of the spectator pieces. This highly excited spectator piece, which will be called the *prefragment* in the following, may have a mass $A_{\text{PF}} \lesssim A$, where A is the original mass of the interacting nucleus. Subsequently it will lose further nucleons by evaporation, or even may break up into little pieces (ablation). In astrophysics, we are most interested in what we may call the *surviving nucleus*, i.e. the heaviest fragment being produced in a particle-stable state.

Evaporation vs. fragmentation: It is a matter of debate how the fragmentation of the excited prefragment proceeds. The thermodynamical idealization predicts the successive emission of light nuclear pieces, mainly single nucleons, until the heavy fragment becomes particle stable at some mass A_{F} . This is what we called “evaporation”, and which is more generally called *spallation* in nuclear physics. However, in particular for very heavy ions excited in collisions, this is in contrast to the observation, which shows rather a break-up into several pieces with $A_{\text{F}} > 10$. This is generally called *multifragmentation*, and is most beautifully explained as a phase-transition process: The heated prefragment nucleus transforms into a gaseous state, and then condensates out into fragments; for a condensating Van der Waals gas one predicts a fragment mass distribution $\sigma(A_{\text{F}}) \propto A_{\text{F}}^{-7/3}$.

Empirically, spallation is distinguished from multifragmentation by the mass of the heaviest fragment relative to the incident nucleus, X_{max} , with $X = A_{\text{F}}/A$. The distinction is most evidently seen in the empirical

mass yield distribution formula

$$y(X) \lesssim 0.1X^{-2.5} + \exp(3.7X) \quad , \quad (1.3.10)$$

which is found to be valid for proton induced reactions on targets with $A > 60$, and plotted in Fig. 1.18[Hüf85]. The curve shows two branches, divided by the minimum at $X \approx \frac{1}{3}$: The lower one ($X < \frac{1}{3}$) can be called the multifragmentation branch, and follows a power law similar to this expected for a Van der Waals gas condensation, the higher one is the spallation branch, where only one heavy fragment is produced and all other fragments have $A_F < 10$. Obviously, this difference does no longer exist for $A < 30$; it is reasonable to assume that multifragmentation for lighter nuclei leads to a complete shattering of the nucleus into pieces with $A_F < 10$.

Excitation mechanism for the prefragment: In the abrasion phase, there exist two possibilities to excite the spectator prefragment; *surface deformation* and collision with recoiling participants, called *frictional spectator interaction* (FSI) [ODR79]. The excitation energy per deformed surface area is about 1 MeV fm^{-2} , and was first proposed as the dominant excitation mechanism of the nuclear fragments. However, numerical simulations show that the FSI process leads to an energy deposit of about 7 MeV per nucleon in an Fe-N collision, which is considerably higher than the surface deformation value in this case.

The FSI energy deposit for a single recoiling participant nucleon is here assumed to be described by a simple energy loss equation

$$\frac{dE_{\text{kin}}}{dx} = -K_{\text{NN}}\rho\sigma_{\text{NN}}(E)E \approx 13 \text{ MeV fm}^{-1}, \quad (1.3.11)$$

where $\sigma_{\text{NN}}(E) \approx [300 \text{ MeV fm}^2]E^{-1}$ is the elastic nucleon-nucleon cross section, $\rho \simeq 0.17 \text{ fm}^{-3}$ is the nuclear density and $K_{\text{NN}} \approx 0.25$ is the average inelasticity of a elastic nucleon-nucleon reaction. Consequently, over an average distance of a nuclear radius an energy

$$\langle \Delta E \rangle_{\text{FSI}} = 17 \text{ MeV} \times A^{1/3} \quad (1.3.11a)$$

is thermalized in the nuclear matter. Thus the maximal energy which can be thermalized by a single nucleon is of the order of the Fermi energy $E_F \approx 30 \text{ MeV}$ for medium mass nuclei, but can be much larger in very heavy nuclei.

We must note, however, that the FSI approach does no longer apply if the energy of the crossing participant nucleon is smaller than E_F ; this would correspond to the situation that the “participant gas” is cooler than the “spectator gas”, and a net energy transfer to the spectators would violate the law of entropy. For $E_{\text{kin}} \sim E_F$, we may estimate the excitation energy of the residual nucleus from the Fermi gas picture, under the assumption that the participant is removed. Since this nucleon may have been on any shell level in the nucleus, the excitation energy of the nucleus can range from zero to E_F , and we can estimate from the Fermi distribution, $n(E) \propto \sqrt{E}$, that $\langle E^* \rangle = \frac{2}{5}E_F$. If $E_{\text{kin}} \ll E_F$, some nucleons may be too deep in the potential to be removed; in this case, $\langle E^* \rangle \sim \frac{1}{2}E_{\text{kin}}$ may serve as a crude estimate.

Excitation energy distribution at very high reaction energies: At very high energies, one finds experimentally that the distribution of fragments is almost independent of energy. This leads to the reasonable assumption that the ability of the nucleus to absorb energy saturates. From data on proton-ion reactions at 5 GeV proton energy one can derive the excitation energy distribution [Hüf85]

$$W_{\text{FF}}(E^*) = \frac{1}{\langle E^* \rangle} \exp \left[\frac{-3.7E^*}{\overline{E}_{\text{ev}} A} \right] \quad , \quad (1.3.12)$$

where $\overline{E}_{\text{ev}} \approx 12 \text{ MeV}$ is the mean energy removed by evaporation of one nucleon, and $\langle E^* \rangle = \overline{E}_{\text{ev}} A / 3.7 \approx [3 \text{ MeV}] A$; assuming that the number of participant nucleons is small compared to the number of spectators, thus $A_{\text{PF}} \approx A$, we can say that in the high energy limit the prefragment gets an average excitation energy of 3 MeV per nucleon, corresponding to a nuclear temperature $\langle \Theta_{\text{PF}} \rangle \sim 5 \text{ MeV}$. Clearly, we have to demand that the energy released in the interaction $E_{\text{int}} \gg A \langle E^* \rangle$. There is an obvious discrepancy between the average excitation energy derived from Eq. (1.3.12), $\sim 3 \text{ MeV}$, and the value of 7 MeV derived from Eq. (1.3.11) in numerical simulations [EGLS92]; this is in correspondence to our expectation that Eq. (1.3.11) tends to overestimate the thermalized energy if the Fermi-motion of the spectator nucleons is neglected.

1.3.2.2 High energy interactions of photons and nucleons

Baryon resonances in nuclei: At photon energies of order 100 MeV and above, we can expect that the photon starts to interact with single nucleons. We know from Sect. 1.2.1 that the most effective mechanism of photon-nucleon interaction is the excitation of baryon resonances, in particular the $\Delta(1232)$ resonance, which is also called *isobar excitation* in nuclear physics. Isobar excitation in nuclei is basically a *quasi-free process*, which means that the excitation and decay of the baryon resonance is widely unaffected by the other nucleons. However, this is not exactly true: the possible coupling of the Δ with other nucleons, called the *Δ -hole-system*, shows some decay channels which cannot be observed in free Δ excitation; in particular there is the possibility of quasi-elastic π^0 production, equivalent to vector-meson production at higher energies. This gives an additional contribution to the coherent production of pions at nuclei, as discussed below. While the total excitation strength of the Δ -resonance is approximately independent of A , there is some evidence that the excitation strength of the higher resonances decreases with nuclear mass; but data are sparse for $\epsilon' \gtrsim 400 \text{ MeV}$ [Ahr85].

In any case, the total photoabsorption cross section of bound nucleons in the baryon resonance region is different from that of free nucleons; however, it can be obtained to first approximation from the photoabsorption cross section of the deuteron, which is known in great detail. Due to the Fermi motion of the nucleons, the apparent widths of the baryon resonances in the NRF are broadened by about 50 MeV; the same applies to the pion production threshold, which is smeared out by the Fermi motion. But even below the pion production threshold at about 145 MeV in the *nucleon rest system*, the wings of the Δ resonance may influence the photonuclear cross section also at lower energy, since it can decay also by virtual pion exchange in the nuclear matter.

Considering quasi-free resonance excitation, we may generally assume that the resonance is produced with the interaction mass of the process, given in the *nucleon rest frame*. Therefore, we may completely neglect the quantum mechanical properties of the resonances, and apply isotropic two-particle kinematics over the whole resonance region. Then, the momentum change of the baryon resonance in the rest frame of the nucleus is $p_N^* = \epsilon'/c \sim p_F$; the short lifetime of the resonance, corresponding to a propagation length of 0.5 fm, does not allow an escape from the nucleus before decay. Thus, proton and pion are emitted inside the nucleus, and we have to consider final state interactions with surrounding nucleons. Clearly, for heavier resonances we may expect also other decay channels, but we cannot expect that the detailed properties of free baryon resonances found are exactly reproduced in the nucleus. We therefore confine ourselves to considering only the $N\pi$ decay.

Coherent meson production: Even though meson-production is generally understood as an interaction of photons with single nucleons, and although the energies involved are much greater than the nuclear binding energy, there exist meson production channels which do not disintegrate the nucleus. This kind of process is called *coherent meson production*. It is most easily understood when we consider the 3-momentum transfer to the proton and apply the uncertainty principle: if a momentum q is exchanged in a reaction with a nucleon, the position of the nucleon cannot be located more accurate than $\Delta r = \hbar/q$, which gives $\Delta r > 1 \text{ fm}$ for $q < 200 \text{ MeV}/c$.

Thus, for small exchange momenta the interaction happens on the scale which is larger than required to locate a nucleon in the nucleus, and therefore the momentum is transferred to the nucleus as a whole. Moreover, the kinetic energy transferred to the nucleus this way is only a about few MeV, therefore we can expect that the nucleus remains on a particle stable state, if it is excited at all. In such reactions, we can generally not assume that the cross section simply scales with the number of nucleons, because the nucleus appears here as a unit, not just as a collection of nucleons.¹²

Clearly, small momentum transfers are expected mainly for t -channel reactions which do not involve nucleon excitation. We already have noted that there are some differences between the possible quasi-elastic interactions at bound and free nucleons; the main difference appears in the energy region of the baryon resonances, where we have observed a considerable contribution of direct charged pion production in free γN interactions. This process is almost completely suppressed in nuclei, mainly because of Pauli blocking; it may still occur as a “surface effect” at the nucleus, but is observed as a coherent process only with a very low cross section. On the other hand, the coherent production of neutral pions makes up about $\frac{1}{3}$ of the total effective π^0 production cross section at C_{12} , where “effective” means that the π^0 appears in the final state; we have to consider that there is a reaction cross section of the same magnitude for π^0 production with reabsorption. Quantitatively we may state that coherent π^0 production off nuclei takes about the same fraction of the total photonuclear cross section as direct charged pion production off free nucleons.

At higher energies, diffractive vector meson production will take over the main part of the coherent photonuclear cross section. Clearly, the momentum transfer in this reaction is not always small, in particular not close to threshold, because of the large mass of the ρ^0 . More important than the coherent (γ, ρ^0) cross section, however, is the effect of the VMD contribution of the vector mesons to the hadronic structure of the photon: because the transparency of nuclear matter to vector mesons is much lower than to photons, the VMD contribution causes a *shadowing effect* for high energy photonuclear interactions, due to mutual obscuration of the nucleons. Accordingly, the mass scaling of high energy nuclear reactions is $\sigma(A, \epsilon') \propto A^\alpha$ with $\alpha < 1$; from experiment one finds $\alpha \simeq 0.91$. This shadowing affects coherent and incoherent reactions in the high energy region in the same way.

Pion fireballs: At very high energies, $\epsilon \gtrsim 700$ MeV, a process corresponding to multipion production is expected to dominate the cross section. In the free nucleon case, multipion production was interpreted as the fragmentation of a “fireball” into quark-antiquark pairs. In the vicinity of other nucleons, however, we can expect that there exist other channels to deposit the energy of the fireball. Thus, even though the production mechanism happening sub-nucleon scale can be assumed to be quasi-free, the pion fragmentation process might be not. There exist little work on the absorption of pion-fireballs in nuclear matter, so we have to apply a simple argument by analogy: From the general similarity of photonic and hadronic processes at high energy we may justify the assumption that photonuclear interactions in the “fireball-region” follow the same laws as interactions between nuclei and protons. Thus, we assume that a small number of nucleons are immediately swept out of the nucleus by the fireball, while the remaining prefragment gets an excitation energy close to its saturation limit. We can then use empirical formulae, e.g. Eq. (1.3.10) or Eq. (1.3.12), to derive the further fragmentation of the residual nucleus.

¹²The best example for this property of coherent reactions is Thomson scattering, which scales with Z^2 rather than Z

1.3.3 Photodisintegration processes

1.3.3.1 Photon absorption by bound nucleons

The Bethe-Peierls cross section formula: The electromagnetic behavior of bound nucleons in complex systems is difficult to treat theoretically because of the complicated nature of the nuclear binding forces and the quantum-mechanical effects governing them. However, for the two-nucleon system, a complete theory has been developed already in 1935 by BETHE & PEIERLS [BP35]. For a zero range nuclear force they derived the photoabsorption cross section of the dinucleon as

$$\sigma_{\text{BP}}(\epsilon, B) = \frac{\sigma_{\text{Tp}}}{\alpha_e} \frac{m_p c^2}{B} \frac{(x-1)^{3/2}}{x^3}, \quad (1.3.13)$$

where $x = \epsilon/B$ and B is the binding energy of the dinucleon. For the free dinucleon, e.g. the deuteron, this is $B_d = 2.227$ MeV. We note that, due to the division by two small numbers, α_e and $(B/m_p c^2)$, $\sigma_{\text{BP}} \gg \sigma_{\text{Tp}}$ for $x \gtrsim 1$; the maximum is reached for $x = 2$. We will call σ_{BP} the *Bethe-Peierls cross section* henceforth.

Comparison with the experimental cross section for photodisintegration of the deuteron, σ_d , gives a discrepancy to Eq. (1.3.13) by about a factor of 1.7; this was corrected by BETHE & LONGMIRE [BL50] by considering the effective range r_{eff} of the nuclear force, leading to

$$\sigma_d(\epsilon) = \frac{\sigma_{\text{BP}}(\epsilon, B_d)}{1 - ar_{\text{eff}}} \quad (1.3.13a)$$

with

$$a = \frac{\sqrt{m_p B_d}}{\hbar}; \quad (1.3.13b)$$

this removes the discrepancy to the experiment completely for $r_{\text{eff}} = 1.79$ fm, which is close to the range for virtual pion exchange, $\hbar/m_\pi c^2$. Applying this picture to photodisintegration, we might say that the corrected Bethe-Peierls formula describes photon absorption in a proton-neutron system by virtual pion production and reabsorption. This gives rise to the expectation that a similar process may work in heavier nuclei *below* the threshold for real pion production.

Collective excitation and the Giant Dipole Resonance: In large systems of nucleons, and for high excitation energies, we have already pointed out that a detailed quantum-mechanical description can be replaced by statistical descriptions oriented at thermodynamics and hydrodynamics. A set of models of this kind, which was aimed to explain the main mode of electromagnetic dipole absorption by heavy nuclei, has been proposed by GOLDHABER & TELLER in 1948 [GT48]: They considered each the protons and the neutrons in the nucleus as two penetrating fluids with effective charges, and described their interaction in terms of hydrodynamics. Dipole absorption of electromagnetic radiation leads then, obviously, to a *collective vibration* of the proton fluid against the neutron fluid, and therefore are expected to have a resonance shaped cross section with $\int \sigma(\epsilon) d\epsilon = \Sigma_{\text{TRK}}$. In fact, this *Giant Dipole Resonance (GDR)* is observed in nuclei and is indeed the dominant feature in the photonuclear absorption cross section. It is often treated as a benchmark in the cross section curve, so that any other processes are classified relative to the GDR cross section. The propositions of the Goldhaber-Teller model are further discussed in Sect. 1.3.3.2

In the hydrodynamical model also other multipole excitations can be expected, as the magnetic dipole ($M1$) or electric quadrupole ($E2$) excitation. For both the resonance energy would have about twice the value of the

dipole resonance energy; however, as argued before on a general basis, both excitation modes have small cross sections compared to the GDR, and we will see that they are not necessary to explain the total integrated cross section for photoabsorption.

Discrete level excitations: Well separated discrete excitation levels exist in the nucleus mostly below 10 MeV, thus below the separation energy for a single nucleon. However, also for energies $10 \text{ MeV} < \epsilon' < 20 \text{ MeV}$ discrete levels can be observed as sharp peaks in the cross section, in particular those which are allowed by $E1$ excitation, but their total contribution to the cross section is of order of a few percent. They can be regarded as a structure in the background, set by the low energy wing of the GDR, rather than as an additional contribution. Most level transitions are not allowed for $E1$ excitation and therefore contribute little.

However, the situation is different in very light p -shell nuclei, $A \leq 16$, in particular in those with very low separation energies. The two most striking examples here are Be_9 and C_{13} , with $S_n \approx 1.67 \text{ MeV}$ and $S_n \approx 4.1 \text{ MeV}$, respectively. Both show strong $p - sd$ transitions, forming broad resonances at about 10–15 MeV. Similar low energy features are seen in most odd- A p -shell nuclei, but less pronounced; they merge with the giant resonance and just cause a very broad shape of the cross section down to threshold. Only the $4n$ nucleus C_{12} shows a very clear and sharp GDR, due to its high separation energy for single protons or neutrons. The low energy phenomena disappear mostly in the sd shell nuclei beyond the CNO group, where the shell structure becomes apparent as a substructure of the GDR.

As we have already seen in the discussion of isospin selection rules, discrete levels also govern the emission of composite daughter nuclei, mostly α -particles, trinucleons and deuterons. These reactions have generally a very low cross section compared to single nucleon emission, and appear mostly in the giant resonance region. We will disregard them in the following.

Direct processes and nucleon evaporation: In the same manner as for photohadronic interactions, one can expect that for higher photon energies, or wavelengths smaller or comparable with the size of the nucleus, the interaction will take place with single nucleons or nuclear substructures rather than with the nucleus as a whole. This is essentially equivalent to a breakdown of Siegert's theorem; the nucleon does no longer behave as a part of a system which is excited in total, but rather as an independent particle. The simplest form of a direct interaction would be the Compton scattering of a photon on a proton in the nucleus; however, this interaction has a very small cross section. We have already seen that the photon absorption cross section by a nucleon pair is larger by many orders of magnitudes, and therefore one can expect that the nucleon pair is the smallest structure which can considerably contribute to the photoabsorption cross section of nuclei. In fact, this process is really observed and is called the *quasi-deuteron process*, and was proposed by LEVINGER [Lev51]; we will discuss this process in Sect. 1.3.3.3.

At still higher energies the substructure of the nucleon itself becomes apparent, and baryon resonances can be excited. The physics of this process, as well as of other processes in the high energy region, has already been discussed in Sect. 1.2. In contrast to there, however, we are here not interested in the fate of the interacting nucleon — it is generally removed from the nucleus in the interaction — but rather in the side effects the interaction has on the neighbor nucleons. This is, to a certain grade, also true for the quasi-deuteron process. As we already discussed in Sect. 1.3.1.3, energy deposition in a nucleus can be treated as heating, followed by nucleon evaporation from the Maxwell-tail of the energy distribution, or by fragmentation of the nucleus into small pieces.

1.3.3.2 The giant dipole resonance

Resonance frequency in collective excitation models: Goldhaber and Teller suggested three different hydrodynamical approaches to describe nuclear vibrations: In the first model they assumed that the protons vibrate collectively around their original position in an oscillator potential, which is assumed to be the same in all nuclei, leading to a resonance energy E_{GDR} independent of A . In their second model (hereafter referred to as GT-II), they treated both protons and neutrons as compressible fluids vibrating against each other within a rigid sphere of radius $R = A^{1/3}R_0$; the restoring force is then given by the gradient of the density change of the nuclear fluids, which is proportional to R^{-2} , leading to a dependence

$$E_{\text{GDR}} \propto A^{-1/3} \quad (\text{GT - II}) . \quad (1.3.14)$$

In their third model (GT-III) they assumed that protons and neutrons vibrate as incompressible fluids bound together by a flexible surface. The restoring force per nucleon is then proportional to the ratio of surface and volume, i.e. R^{-1} , yielding

$$E_{\text{GDR}} \propto A^{-1/6} \quad (\text{GT - III}) . \quad (1.3.15)$$

On the basis of photodisintegration data available in 1949, Goldhaber and Teller themselves preferred their model III and gave a more detailed description, expressing the resonance energy for self-conjugated nuclei ($Z = N$) as

$$E_{\text{GDR}} = \sqrt{\frac{3\varphi\hbar^2}{r_{\text{eff}}\hat{m}R}} , \quad (1.3.15a)$$

where \hat{m} is the mass of the bound nucleon and φ is the potential energy due to neutron-proton forces. An improved version of GT-II was proposed by STEINWEDEL & JENSEN [SJ50], who connected E_{GDR} to the constant term of the nuclear binding energy given in the Weizsäcker mass formula Eq. (1.3.1a), $b_v = 15.85$ MeV, as

$$E_{\text{GDR}} = \sqrt{34.6b_v \frac{NZ}{A^2} \frac{\hbar^2}{\hat{m}R^2}} , \quad (1.3.14a)$$

yielding $E_{\text{GDR}} \approx [60 \text{ MeV}]A^{-1/3}$.

Experimental mass-dependence of E_{GDR} and Γ_{GDR} : An early investigation of the mass-dependence of the shape and energy of giant dipole resonance was performed by MONTALBETTI, KATZ & GOLDEMBERG (MKG) [MKG53]. They give results for the (γ, n) cross section of 22 elements between Be_9 and Bi_{209} . They found an overall dependence $E_{\text{GDR}} \approx [37 \text{ MeV}]A^{-0.19}$, favoring the GT-III model. In contrast, in elastic scattering experiments FULLER & HAYWARD [FH56] found a dependence rather consistent with $E_{\text{GDR}} \propto A^{-1/3}$ for $A > 20$; however, their results for light nuclei contradict the high precision results obtained at the Mainz linear accelerator [ABC⁺75], which are rather consistent with the earlier results of MKG.

MKG also published results on the half-width of the giant resonance; they found $\langle \Gamma \rangle \approx 6$ MeV for medium mass nuclei, slightly decreasing for heavier nuclei. For $A > 50$, they found that $\Gamma_{\text{GDR}}/E_{\text{GDR}}$ is roughly constant, while for $A < 50$ the scattering is large and no clear dependence is visible. A more thorough investigation of the mass dependence of the GDR width was performed by OKAMOTO [Oka58] for nuclei with $A \gtrsim 50$; he found a correlation of the GDR width with the nuclear eccentricity ε , and stated that $\Gamma_{\text{GDR}} = \Gamma_0 + \Delta\Gamma$ with $\Gamma_0 = 4.2$ MeV and $\Delta\Gamma/E_{\text{GDR}} \propto n\varepsilon$ for $E_{\text{GDR}} \propto A^{-n/3}$. Noting that nuclei with $A < 50$ have mostly small

eccentricities, one would therefore expect a constant width in light nuclei, and $\Gamma_{\text{GDR}} \propto E_{\text{GDR}}$ in heavy nuclei, which is consistent with the results of MKG. One result predicted by Okamoto's model which is also reflected in the data is that Γ_{GDR} takes local minima for double magic nuclei.

Fine structure of the GDR and shell model predictions: A different approach to explain the giant resonance follows the shell model of the nucleus, and describes the GDR as a the coherent superposition of discrete one particle excitation states. The model is much less successful in determining the gross A dependence of E_{GDR} and Γ_{GDR} ; on the other hand, it can account for the observed fine structure of the giant resonance for intermediate mass nuclei. This fine structure is observed generally on energy resolution scales below $\Delta\epsilon = 1$ MeV, on which the giant resonance peak can be resolved in a sequence of many sub-peaks. It occurs mainly in sd -shell nuclei and is most pronounced in the self-conjugate double magic nuclei O_{16} and Ca_{40} . A good discussion of shell model approaches to the GDR is given in the review by DANOS AND FULLER [DF65].

The fine structure of the giant resonance may be completely disregarded for the determination of average properties of the photonuclear cross section. Principally, the underlying structure for these nuclei still fits in the overall behavior of the GDR. Important for our considerations is rather the description of the GDR as a collective *one-particle* excitation state, which gives rise to the expectation that the GDR is mainly de-excited by the emission of a single nucleon. This will be checked in comparison to data in Sect. 1.3.4.3.

1.3.3.3 The quasi-deuteron process

Classical theory and the Levinger parameter: In its original form, the quasi-deuteron process has been proposed as a photon absorption process for $\epsilon > 150$ MeV, i.e. in above the pion production threshold. The limitation to high energies was applied because at low energies the wave functions of a proton-neutron pair inside the nucleus differs too much from that of a bound deuteron; for high energies, however, the wave functions converge, and from $\sigma_{\text{QD}}/\sigma_{\text{d}} = (\psi_{\text{QD}}/\psi_{\text{d}})^2$ Levinger derived the expression

$$\frac{\sigma_{\text{QD}}}{\sigma_{\text{d}}} = \frac{3}{2AR_0^3} \frac{1 - ar_{\text{eff}}}{a(a^2 + k^2)} \quad , \quad (1.3.16)$$

where k is the wavenumber of the relative motion of the proton-neutron system and a is the scattering length, which is identified with the same parameter used by Bethe and Peierls in their calculation for the free deuteron, Eqs.(1.3.13). This result is now multiplied with the possible number of proton-neutron combinations in the nucleus, NZ , and averaged over all possible wavenumbers, yielding

$$\sigma_{\text{QD}} = L \frac{NZ}{A} \sigma_{\text{d}} \quad (1.3.17)$$

with

$$L = \frac{3}{2R_0^3} \frac{1 - ar_{\text{eff}}}{a} \left\langle \frac{1}{a^2 + k^2} \right\rangle \quad . \quad (1.3.17a)$$

The expectation value of $(a^2 + k^2)^{-1}$ can be evaluated within a Fermi distribution of protons and neutrons with the same maximum wavenumber $k_{\text{max}} = p_{\text{F}}/\hbar$, where p_{F} is the Fermi momentum; Levinger originally used $k = 1.0 \text{ fm}^{-1}$ and adopted the value $a = 0.23 \text{ fm}^{-1}$ as found for the free deuteron, and found $L = 6.4$ for $R_0 = 1.4 \text{ fm}$, which was later corrected to $L = 8$ for $R_0 = 1.2 \text{ fm}$. The parameter L is now known in the literature as the *Levinger parameter*, or *Levinger constant*.

The quasi-deuteron process is now mostly accepted to give the correct description of the high energy photon absorption in nuclei; in contrast to Levinger's original idea, however, it is rather used for energies *below* the pion threshold, where the quasi-deuteron process fills the gap between the giant dipole resonance and the baryon resonance region. To allow a consistent extension of his model to lower energies LEVINGER [Lev79] introduced a *quenching factor*, $\exp(-D/\epsilon)$, into Eq. (1.3.17), which reduces the cross section for low energies expected due to phase-space reduction (i.e. Pauli blocking) of the quasi-deuteron final state. From experimental data for Pb_{208} , he determined $D = 60 \text{ MeV}$. Later, a thorough investigation of the quasi-deuteron cross section for various nuclei, obtained D as a function of A as

$$D = 0.72 A^{0.81} \text{ MeV} , \quad (1.3.18)$$

which is consistent with Levinger's result for lead [TDP89], but gives $D \lesssim 10 \text{ MeV}$ for light nuclei, which is below the GDR regime. Hence, the heuristical introduction of the quenching factor does not seem to give a consistent description of the quasi-deuteron contribution over the whole photon energy and nuclear mass range, and the model is still only used for photon energies above 60 MeV.

The determination of the Levinger parameter has been subject to many experiments, and also to refined calculations. The experimental results prefer consistently a value of $L \approx 6 \pm 2$, hence somewhat lower than the Levinger's result, but still consistent.¹³ TAVERES & TERRANOVA [TT92] recalculated L as a function of A , using the new results on the behavior of the nuclear radius, which they identified with the root mean square of the nuclear charge distribution; they derived L as a function showing the correct behavior in the low-mass limit, i.e. $L = 2$ for the real deuteron. However, it is surprising that apparently the value $a = 0.23 \text{ fm}^{-1}$, used for the scattering length and adopted from the free deuteron calculation, has never been questioned, even though Levinger already mentioned that the classical binding energy of the deuteron, connected to a over Eq. (1.3.13b), cannot be applied to the quasi-deuteron.

Interpretation and modification of the quasi-deuteron process: We may try to give an interpretation of the quasi-deuteron process, in particular in view of its role for the total integrated cross section. As implied by the GGT sum rule, the integrated photonuclear cross section below the pion threshold consists of two components, both contributing about the same fraction: The first is the classical dipole absorption due to collective vibrations of protons and neutrons, leading to the giant dipole resonance. The second is, in the GGT approach, the *reflection* of the missing pion production cross section at $\epsilon > \epsilon_\pi$, due to Pauli blocking of final states, into the low energy regime. The physical process representing this "reflection" is the virtual pion production and absorption by a nucleon pair — restriction to charged pionic currents allows only proton-neutron pairs as interaction partners, which is therefore exactly equivalent to the basic idea of the quasi-deuteron process. In this way, we may expect that $\int \sigma_{\text{QD}} d\epsilon = \Sigma_{\text{GGT}} - \Sigma_{\text{TRK}} \approx \Sigma_{\text{TRK}}$; this, however, forces a low energy restriction of the process, since $\int \sigma_{\text{d}} d\epsilon = \Sigma_{\text{TRK}}$ *without* the multiplication with $L \simeq 6$.

Since the nuclear force is generally explained in terms of pionic currents, this interpretation is nothing really new; it only gives an imaginary explanation what happens when a photon is absorbed by a nucleon pair. However, in comparison to the free deuteron we may expect for the quasi-deuteron that the nucleon pair is much stronger bound, to be separable from the rest of the nucleus. To give a quantitative estimate of the binding energy of the quasi-deuteron, we may use the *separation energy of an np pair*, S_{np} . This estimate is motivated by the

¹³AHRENS ET AL. [ABC⁺75] stated that $L = 8$ gives best correspondence to their experimental results. However, they erroneously used the Bethe-Peierls cross section rather than the effective range corrected value σ_{d} , which differ by a factor of about 1.7. This is inconsistent with LEVINGER'S ansatz, therefore their finding must be corrected to $L \approx 5$, which is consistent with the results of other work (for a comparison and discussion of recent data see [TT92]).

demand that the disintegration products of the quasi-deuteron must be separable from the nucleus to identify it as a substructure of the nucleus. Using the Bethe-Peierls formalism consistently, we now have to write the scattering length as $a = \sqrt{m_p S_{np}}/\hbar$, which gives $a \approx 0.65$ for nuclei with $A > 10$ and influences *both* the shape of the cross section and the value of the Levinger parameter.

To quantify this, it is advisable to reformulate the parameters in Levinger's formula, Eq. (1.3.17), in the way

$$\sigma_{\text{QD}}(\epsilon, A) = \tilde{L} \frac{NZ}{A} \frac{\sigma_{\text{BP}}(\epsilon, B_{\text{QD}})}{a_{\text{QD}}} \quad (1.3.19)$$

with

$$\tilde{L} = \frac{3}{2R_0^3} \left\langle \frac{1}{a^2 + k^2} \right\rangle, \quad (1.3.19a)$$

which now has the dimension of a wave number and will be called the *normalized Levinger parameter*. Here we have used that the effective range correction factor enters in both the classical Levinger parameter and into the deuteron cross section, and cancels in the final expression. Normalizing all energies to the binding energy of the free deuteron, $x = \epsilon/B_d$ and $\xi_{\text{QD}} = B_{\text{QD}}/B_d$, we can write

$$\frac{\sigma_{\text{BP}}(\epsilon, B_{\text{QD}})}{a_{\text{QD}}} = [1.66 \text{ fm}^3] \frac{(x - \xi_{\text{QD}})^{3/2}}{x^3}. \quad (1.3.19b)$$

From comparison with the Bethe-Peierls formula, we note that

$$\frac{\sigma_{\text{BP}}(\epsilon, B_{\text{QD}})}{a_{\text{QD}}} \rightarrow \frac{\sigma_{\text{BP}}(\epsilon, B_d)}{a} \quad \text{for } \epsilon \rightarrow \infty,$$

i.e. the predictions of the classical Levinger formula are not changed in the high energy regime, where it is conventionally applied. This means that the Levinger parameter, which is found in experiments for $\epsilon > 60$ MeV, should still apply to our modification; we obtain from $L \sim 5-7$ that $\tilde{L} \approx 2-2.7 \text{ fm}^{-1}$ for $B_{\text{QD}} = B_d$. If we evaluate Eq. (1.3.19a) for with $a_{\text{QD}} = 0.65$, using Levinger's expression for $\langle (a^2 + k^2)^{-1} \rangle$ [Lev51], we get $\tilde{L} = 1.2-1.5 \text{ fm}^{-1}$ for $k_{\text{max}} = 0.8-1.2 \text{ fm}^{-1}$ and $R_0 = 1.2 \text{ fm}$. For $R_0 = 1.1 \text{ fm}$ the discrepancy can be almost removed; however, we will not put too much emphasis on the determination of the Levinger parameter, noting that Levinger's ansatz contains many simplified assumptions and may be subject to reconsideration on a better founded level than applied here; we note *heuristically* from comparison with the $\text{He}_4(\gamma, pn)d$ cross section, that our modified quasi-deuteron model gives an excellent representation of the shape of the data. We may therefore use Eq. (1.3.19) as a cross section formula for the *np-emission cross section* over the whole energy range, and apply the Levinger parameter which is empirically found at high energies.

Nucleon emission in the quasi-deuteron process: Essentially, the quasi-deuteron process is a *two-nucleon emission process*, which has been emphasized in our modified model. Moreover, it is a *direct process*, because the quasi-deuteron interacts as an independent particle pair. Therefore, the two nucleons can be emitted from any shell level, and the residual nucleus is likely to be in a highly excited, possibly particle unstable state. The kinetic energy of each of the emitted nucleons is approximately half the photon energy, reduced by the quasi-deuteron binding energy; thus, $E_{\text{kin}} \lesssim E_F$ for $\epsilon' \lesssim 80 \text{ MeV}$. Up to this energy, we can assume that the mean excitation energy is about $\frac{1}{2}(\epsilon' - B_{\text{QD}})$. For higher photon energies the emitted nucleons have $E_{\text{kin}} > E_F$, which allows energy transfer by the FSI process. From Eq. (1.3.11) we see that the maximum excitation energy per

emitted nucleon in a medium mass nucleus is about 40 MeV; assuming that the particle cannot be emitted (on average) with less than the Fermi energy, we can assume that this maximum is reached for about $\epsilon \gtrsim 140$ MeV, thus above the pion threshold. The thermalized energy at this point would be about 80 MeV, which gives rise to the assumption that $E^* \approx \frac{1}{2}(\epsilon' - B_{\text{QD}})$ holds up to the pion threshold in first approximation, and is likely to remain constant above.

1.3.3.4 Photodisintegration in the baryon resonance region and beyond

The cross section of complex nuclei in the baryon resonance region: In the energy region above the pion production threshold, $\epsilon' \gtrsim 150$ MeV, the photonuclear cross section is dominated by the excitation of baryon resonances. The total photoabsorption cross section in this region scales linearly with nuclear mass, but the cross section per *bound* nucleon is different from the photohadronic cross section for free nucleons. It is best estimated from the empirical photoabsorption cross section for the deuteron, thus we may write

$$\sigma(A, \epsilon') = A \hat{\sigma}(\epsilon') \quad \text{with} \quad \hat{\sigma}(\epsilon') = \frac{1}{2} \sigma_d(\epsilon') \quad \text{for} \quad \epsilon_\pi < \epsilon' \lesssim 2 \text{ GeV} . \quad (1.3.20)$$

We will give an empirical expression for $\hat{\sigma}(\epsilon')$ in the next section. Since the excitation of baryon resonances is strongly coupled to the $N\pi$ system, the cross section is strongly reduced due to the decrease of the available phase space below the threshold for real pion production; it is, however, not zero as in the free case, because the pion may be emitted as a virtual particle and reabsorbed by another nucleon. We have already interpreted the quasi-deuteron effect as the realization of this process. Hence, we can expect that the low energy wings of the $\Delta(1232)$ resonance have some influence on the quasi-deuteron cross section, which cannot be predicted by the classical theory, treating the nucleon as structureless. Also, the production cross section threshold of real pions will be somewhat diffuse due to the Fermi motion of the nucleons.

Kinematics of quasi-free pion production: Above the pion threshold, the excitation and decay of baryon resonance can be considered as quasi-free scattering of photons on nucleons. The decay of the resonances will mainly proceed in the $N\pi$ channel; the kinematical range for kinetic energy of the outgoing nucleon and pion are shown in Fig. 1.19. We see that in most cases the nucleon has enough energy to be separated from the nucleus, but there is some probability left that the nucleon remains bound. However, we have neglected Pauli blocking effects here, which may change this result by reducing the probability for a small momentum transfer in a quasi-free reaction; in the following, we will assume that the *participant nucleon will be removed from the nucleus*. In the peak of the $\Delta(1232)$ resonance, $\epsilon' \approx 340$ MeV, the energy of the emitted nucleon is hardly larger than the Fermi energy; this has to be considered when final state interactions are to be taken into account. The simple FSI treatment, guided by Eq. (1.3.11), may give inadequate results here; rather we should apply the Fermi gas model with $E_{\text{kin}} \sim E_{\text{F}}$, leading to $\langle E^* \rangle \sim \frac{2}{5} E_{\text{F}}$. This can be certainly only considered as a lower limit for the average thermalized energy; from experiment it is known that particularly the emitted pions lose a considerable fraction of their energy in final state interactions.

Pion reabsorption: An important secondary process connected to pion production in nuclei is the reabsorption of the emitted pion by the surrounding nuclear matter. Real pions cannot be absorbed by single nucleons; the smallest substructure responsible for pion reabsorption is thus a pair of nucleons, similar to the quasi-deuteron absorption of photons; one may therefore call this process the *pionic quasi-deuteron effect* [VG94]. Since the energy transferred to the nucleon pair is of the order of a few hundred MeV (pion mass plus kinetic energy), we can assume that the reabsorbing nucleon pair is always removed from the nucleus; we will call them *secondary participants*, because they are more directly connected to the pion production process than the other,

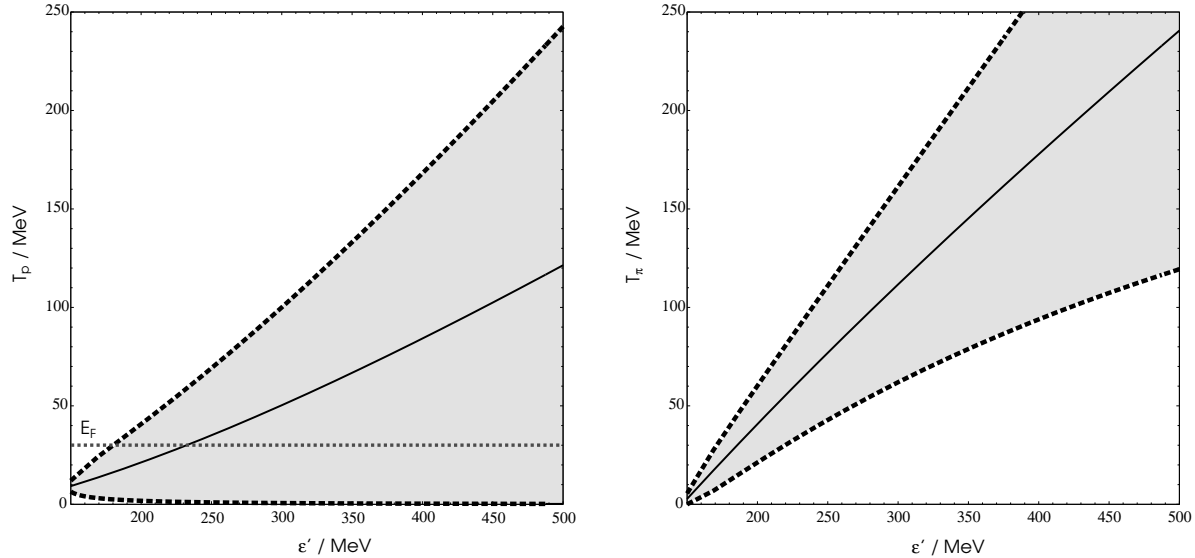


Figure 1.19: The kinematical range allowed for decay nucleons (left panel) and pions (right panel) from the $\gamma N \rightarrow N^* \rightarrow N\pi$ reaction in the NRF, as a function of photon energy ϵ' . Solid lines indicate average values; in the left panel, the approximate Fermi energy of nucleons is indicated.

spectator nucleons. Experimental results obtained at the Bonn synchrotron [AEH⁺81] for C_{12} suggest that the transparency of nuclear matter to charged pions, i.e. the fraction of the charged pion production cross section to the total photoabsorption cross section, is about 50%; naively we would expect that it scales approximately with $A^{1/3}$, since the probability of reabsorption should be proportional to the nuclear radius. Comparison of data obtained on C_{12} , Al_{27} and Pb_{208} seem to indicate that the total pion transparency changes from $\sim 70\%$ for carbon to $\sim 30\%$ for lead, confirming basically the scaling assumption [VG94].

Photonuclear reactions at the highest energies: Considering resonances above the $\Delta(1232)$, we have already noted that a detailed treatment of their excitation and decay, as in the free case, is barely possible. Neither their excitation strength nor their decay modes are sufficiently known in the nuclear environment. However, we may discard this problem, noting that at energies above about 700 MeV photonuclear reactions are dominated by fireball processes, leading to the saturated excitation of the residual nucleus. A detailed treatment of primary and secondary processes would therefore barely make sense, and we have to switch to an empirical description of the excitation of the residual (prefragment) nucleus, as given by Eq. (1.3.12). Since the number of evaporated nucleons in this energy range is generally much larger than the number of participant nucleons, it is justified to neglect the primary interactions altogether and treat high energy photodisintegration as an entirely thermodynamical process.

The problem occurring here is the possibility of multifragmentation. So far we have understood photodisintegration as a process removing *some* nucleons from a nucleus, and leaving over a residual nucleus with its mass close to the incident one. In multifragmentation, this treatment is no longer justified, because the fragments will have masses much below the incident mass, and it may be not possible to choose the heaviest fragment unambiguously. We may therefore distinguish two ways to treat highest energy photodisintegration, marking the extreme limits of possibilities: (i) the nucleus is shattered into little pieces *at once*, thus more or less destroyed in a single interaction; (ii) the nucleus behaves as in the usual thermodynamical approximation, and

evaporates nucleons following Eq. (1.3.8). Taking $\langle E^* \rangle \approx [3 \text{ MeV}]A$ from Eq. (1.3.12), possibility (ii) would mean $\bar{\nu}(A) \sim \frac{1}{4}A$, while possibility (i) always sets $\bar{\nu}(A) \sim A$. Reality is supposed to be somewhere in between; to stress the difference between high and low energy photonuclear reactions, we will use the term *photodisintegration* only for small step spallation processes, and the term *fragmentation* for processes proceeding in Giant Steps [Col59].

1.3.4 Photodisintegration of cosmic ray nuclei

1.3.4.1 Inverse photodisintegration in astrophysics

The continuous mass loss approximation: When we consider UHE cosmic ray protons propagating through a photon background, the basic idea is that we can treat the proton as *one particle* all the time, which loses its energy in subsequent interactions. In some approximation, we can consider the energy loss process as continuous, and determine the loss time scale as the time over which the proton loses a considerable part, $1 - e^{-1} \approx 63\%$, of its energy. When considering heavy nuclei, it seems at first that this idea is no longer applicable: The nucleus changes its “identity”, expressed in proton and neutron number in every reaction. However, in the preceding section we have worked out some features of photodisintegration, which allow to see also the nucleus as *one particle* evolving in a *photodisintegration chain*, regarding its mass number A as a *quasi-continuous* quantity of state. The facts justifying this approach are the following:

1. Most photodisintegration reactions remove only one or two nucleons from the nucleus; thus, the mass evolution proceeds mostly in small steps, $\Delta A \ll A$.
2. The *average* properties of the photonuclear cross section change sufficiently smooth with mass.
3. The Lorentz factor of the nucleus is almost unchanged in a disintegration interaction.

The latter statement arises from the fact that the energy and momentum transfer of the photon to the nucleus in the NRF is negligible compared to the nuclear mass; in its usual meaning, we may therefore say that the inelasticity of a nuclear interaction, with respect to the Lorentz factor of the surviving heavy fragment, vanishes. However, if we consider the mass loss due to photodisintegration, the energy loss in the LF is $\Delta E = \gamma_{\text{CR}} \Delta M$, and we can define the *inelasticity of photodisintegration* as

$$K_A(\epsilon', A) \equiv \left[\frac{\Delta E}{E} \right]_{\text{LF}, \epsilon'} = \left. \frac{\Delta A}{A} \right|_{\epsilon'} , \quad (1.3.21a)$$

and accordingly the efficiency function

$$\eta_A(\epsilon', A) \equiv K_A(\epsilon', A) \sigma(\epsilon', A) \quad (1.3.21b)$$

and the *nucleon yield function*

$$y(\epsilon', A) \equiv \bar{\nu}(\epsilon', A) \sigma(\epsilon', A) = A \eta_A(\epsilon', A) , \quad (1.3.21c)$$

where $\bar{\nu}(\epsilon', A)$ is the average nucleon multiplicity as a function of photon NRF energy and mass number. From $\Delta A \ll A$ follows $K_A(\epsilon', A) \ll 1$, which allows us to consider the evolution of the nucleus as a *continuous mass loss*. The *disintegration loss function*, τ_{dis}^{-1} , can then be defined as in Eq. (1.1.45), and analogously we define here the *nucleon yield rate*

$$v(\epsilon', A) = A \tau_{\text{dis}}^{-1}(\epsilon', A) \quad . \quad (1.3.21d)$$

As in particle physics, we will investigate different disintegration processes separately, and determine the total efficiency or yield rate as the sum of all partial rates.

In contrast to the photohadronic energy loss of a single proton, which is not limited in time, the mass evolution of a nucleus has a well defined end. This is, however, not the disintegration down to the proton, which would make problems because $\Delta A \ll A$ is no longer valid for $A < 10$. Fortunately, nature has drawn a well defined separation line between light and heavy nuclei, by the instability of nuclides with $A = 8$ and $A = 5$; at $A \simeq 10$, the photodisintegration chain drops almost instantaneously to $A = 4$, thus the relic nucleus has to compete with *primary* α particles, which have a cosmic abundance about 10 times larger than that of all heavy nuclei together. Therefore, we may neglect nuclear masses of $A < 10$ in disintegration chains and consider the interesting mass range for astrophysically relevant *heavy nuclei* $10 \leq A \leq 60$; for heavier elements, the abundance drops again by about three orders of magnitude. The assumption of small step mass losses is generally not true in the fragmentation region, i.e. for very high energy interactions: here, we may apply the limiting case of complete destruction of the nucleus at once, and treat this process as a *quasi-absorption process* acting parallel to photodisintegration. The absorption time scale is then easily given by Eq.(1.1.45) with replacing the efficiency function by the interaction cross section for fragmentation.

Even though our main interest is directed to heavy nuclei, we will briefly discuss the photodisintegration cross sections of light nuclei. In particular the α -*cascade*, i.e. the subsequent photodisintegration of α -particles into single nucleons, is of great interest in astrophysics due to the high abundance of He_4 .

Rapid and slow disintegration chains: In Sect. 1.3.1.1 we have briefly discussed the branching ratios of proton and neutron emission from excited nuclei, and the influence of the Coulomb barrier in heavy nuclei. This leads to an interesting conclusion: A heavy nucleus, $A \gtrsim 30$, which generally shows a considerable neutron excess, will always be more likely to emit a neutron than a proton in a photodisintegration event. Generally, we can expect that a β^+ -unstable nuclide is produced in such a reaction, which decays after a certain time and moves the nucleus back to the valley of stability; for $A > 40$, we often find the situation that there exist many stable isotopes, and the conclusion is here that the evolution in a photodisintegration chain goes along the isotopes with the lowest neutron number for every Z . If the nucleus moves into the β^+ unstable region, we have to compare the lifetimes for beta decay, which are mostly of the order of minutes, hours or even days ($\sim 10^2 - 10^5$ sec), with the disintegration rate. For a nucleus with UHECR Lorentz factors, $\gamma_{\text{CR}} \gtrsim 10^9$, a β^+ -unstable isotope may travel distances of order kpc-to-Mpc before decay; if the mean free path for photodisintegration is shorter than this, additional neutrons can be removed, drawing the particle deeper into β^+ -instability. A rough inspection of β^+ -lifetimes and p/n -emission branching ratios shows, that in this case the neutron excess of the nucleus can be fully removed, before proton emission can compete or β^+ lifetimes become sufficiently short. We will call this situation *rapid photodisintegration*, allowing to set $Z = N$ even for heavy nuclei in a photodisintegration chain. In extragalactic transport, however, photon densities are mostly so low that interim β^+ decay is allowed; we call this *slow photodisintegration*, with $Z \approx \bar{Z}_{\text{ld}}(A)$ over the whole range.

Clearly, the difference is only important if we want to consider very heavy nuclei with $A \gtrsim 50$; except the nuclei around Fe_{56} , these play almost no role in astrophysics because of their very low abundances. Nevertheless the possibility for the nucleus to evolve off the valley of stability is important to note: it shows that there is little sense in emphasizing the specific features of photonuclear cross sections of individual nuclides, because we generally have to average over a broad range of partially unstable isobars for any given mass number.

Mass scaling functions: From preceding discussion we may draw the conclusion that a nucleus evolving in a photodisintegration chain can be completely described by its mass number A and its Lorentz factor γ_{CR} . We have also seen that photodisintegration only changes A , not γ_{CR} ; the relevant functions determining dA/dt are, however, dependent on γ_{CR} and A . The loss time scale can therefore be written as a two-parameter function, $\tau_{\text{dis}}(A, \gamma_{\text{CR}})$. The situation can be even reduced to a one dimensional problem, if the nucleon yield function obeys a *mass scaling law*

$$\eta_A^{(c)}(A, \epsilon') = g_0^{(c)}(A) \hat{\eta}_c[\epsilon' g_\epsilon^{(c)}(A)] \quad , \quad (1.3.22)$$

where $g_0^{(c)}(A)$ and $g_\epsilon^{(c)}(A)$ are called the *mass scaling functions* for the disintegration process c , and $\hat{\eta}_c(x)$ is called the *normalized efficiency function*. Inserting in Eq. (1.1.45) and Eq. (1.3.21d), and using the scaling properties of Eq. (1.1.49) in the limit $\gamma_{\text{CR}}\epsilon' \rightarrow \infty$, we immediately obtain

$$\tau_{\text{dis}}(A, \gamma_{\text{CR}}) = g_0^{(c)}(A) \hat{\tau}_{\text{dis}}[\gamma_{\text{CR}} g_\epsilon^{(c)}(A)] \quad . \quad (1.3.22a)$$

This scaling law generally requires the scaling of all relevant energy scales in the NRF with $[g_\epsilon^{(c)}(A)]^{-1}$, e.g. threshold energy, resonance energy and width. Writing the threshold energy as $\epsilon'_{\text{th}} = \hat{\epsilon}_{\text{th}}/g_\epsilon^{(c)}(A)$, and defining the reference Lorentz factor as in Eq. (1.2.31a) by $\gamma_0 = 2\epsilon_0/\hat{\epsilon}_{\text{th}}$, we can write the loss time scale and in power law backgrounds as

$$\tau_{\text{dis}}(A, \gamma_{\text{CR}}) = cN_0 \left[\sum_c \hat{H}_{ab}^{(c)} g_a^{(c)}(A) \right] \hat{\gamma}_{\text{CR}}^{a-1} \quad , \quad (1.3.23)$$

where the efficiency coefficients $\hat{H}_{ab}^{(c)}$ are defined as in Eqs. (1.2.31) with using the normalized efficiency function, $\hat{\eta}_c(x\hat{\epsilon}_{\text{th}})$ in the integral. $g_a^{(c)}(A)$ is called the *power law mass scaling function* with index a , given by

$$g_a^{(c)}(A) \equiv g_0^{(c)}(A) [g_\epsilon^{(c)}(A)]^{a-1} \quad . \quad (1.3.23a)$$

For the special case of power law type scaling functions $g_0^{(c)}(A) = A^\alpha$ and $g_\epsilon^{(c)}(A) = A^\beta$, $g_a^{(c)}(A, a)$ is a power law in A with index $\alpha - \beta + a\beta$.

1.3.4.2 Photodisintegration cross sections of light nuclei

Stability gaps and the breakdown of scaling: In heavy nuclei, a lot of degrees of freedom are given to distribute the energy absorbed from an incoming photon; it is mainly for this reason, that they can readily be described in simple, quasi-classical models obeying elementary scaling rules. This method breaks down for nuclei with $A < 10$, because their structure is essentially quantum-mechanical.

Empirically, one of the main features occurring for light nuclei are the *stability gaps* at $A = 8$ and $A = 5$. No stable nucleus exists there: the nuclei Li_8 and B_8 are both β -unstable with decay times of about a second, transforming to Be_8 which is unstable against spontaneous fission into two α -particles. All nuclides with $A = 5$ are unstable against spontaneous nucleon emission. In between, there exist the stable nuclides Li_6 and Li_7 ; however, they are unlikely to be produced by photodisintegration of a heavier nucleus, for the following reason: The only stable nucleus with $A = 9$ is Be_9 , which has the lowest neutron separation energy of all stable nuclei, $S_n = 1.667 \text{ MeV}$. The Be_9 nucleus may be considered as consisting of a Be_8 core with one loosely bound valence neutron, keeping the whole system together. Since the separation energy for the emission of two nucleons off Be_9 is about 10 times higher, the only considerable disintegration channel is $\text{Be}_9(\gamma, n)2\alpha$. The Be_9 nucleus itself has a unusually large cross section for $\epsilon' \sim 10 \text{ MeV}$, more than a factor of two below the giant

resonance; it can therefore be expected to be disintegrated much faster than other nuclei in astrophysical photon spectra with strongly decreasing number density for increasing energy.

We will here present empirical fits to the cross sections for photodisintegration of the deuteron (D_2), the trinucleon ($T_3 \equiv H_3$ and He_3), the α particle (He_4), and the Be_9 nucleus. We will not consider nucleon yield functions, because they only make sense in the scaling region; rather, we briefly discuss the possible disintegration channels for every nucleus and their quantitative contribution. We only give the cross sections below the pion threshold here; for $\epsilon > \epsilon_\pi$, light nuclei obey the same scaling rules as heavy nuclei, which are discussed in the Sect. 1.3.4.3.

The deuteron and the trinucleon: The deuteron is the only nucleus where an adequate theoretical description of its dipole photodisintegration cross section exists; it is well described by the Bethe-Peierls formula corrected for effective range, Eq. (1.3.13a). The cross section is shown in Fig. 1.20; obviously there exists only one reaction channel, $d(\gamma, np)$.

For the trinucleon, we have the situation that there are additional degrees of freedom which could cause deviations from a simple Bethe-Peierls behavior, but on the other hand there is still a strong similarity to the deuteron structure. We use the results obtained at the LINAC accelerator in Stanford [FBMO81], to model an empirical cross section expression. The trinucleon has two channels for disintegration, one with a deuteron and a nucleon, and one with three nucleons in the final state. The data show that both channels contribute almost equally; moreover, their cross sections seem to be acceptably described by a simple scaling of the Bethe-Peierls cross section, if the binding energy of the deuteron in Eq. (1.3.13) is replaced by the threshold energy for the respective process. We have applied the same modification to explain the low energy behavior of the quasi-deuteron process, so we may interpret the disintegration of the trinucleon *entirely* as due to a similar effect, for both the two-body and the three-body decay. We find a good fit with

$$\sigma_1^T(\epsilon') = 1.4 \sigma_{BP}(\epsilon', 5.8 \text{ MeV}) \quad \text{for } T_3(\gamma, N)D_2 \quad (1.3.24a)$$

$$\sigma_2^T(\epsilon') = 1.7 \sigma_{BP}(\epsilon', 7.3 \text{ MeV}) \quad \text{for } T_3(\gamma, 3N) \quad , \quad (1.3.24b)$$

which represents the total integrated cross section, $\Sigma_{1/2}^{(30)}$, and the position and absolute value of the maximum cross section found from the data. These equations apply to both H_3 and He_3 disintegration; these nuclei are mirror nuclei belonging to the same iso-multiplet, and indeed behave quite similar also in photodisintegration. The small differences due to the different Coulomb field, which causes the differences in binding energy, will be disregarded in our treatment. The binding energy values inserted in Eqs. (1.3.24) are averages for the respective channels over both isobars.

The α particle: The He_4 nucleus, i.e. the α particle, is the lightest double magic nucleus, and has the highest separation energy for single nucleon emission of all nuclei, $S_n \approx S_p \approx 20 \text{ MeV}$. Its structure has to be considered as fundamentally different from the deuteron; in fact, in contrast to the trinucleon we find a quite different behavior of one and two nucleon emission in $\gamma\alpha$ reactions, the latter contributing only about 10%. Using the data for He_4 photodisintegration obtained in cloud chamber experiments [GS58], we find the fit functions

$$\sigma_1^\alpha(\epsilon') = [3.6 \text{ mbarn}] \text{Pl}(\epsilon'; S_n^\alpha, 27 \text{ MeV}, 5) \quad (1.3.25a)$$

$$\sigma_2^\alpha(\epsilon') = 1.4 \sigma_{BP}(\epsilon', S_{pn}^\alpha) \quad , \quad (1.3.25b)$$

where $S_n^\alpha = 19.8 \text{ MeV}$ and $S_{pn}^\alpha = 26.1 \text{ MeV}$. $\sigma_2^\alpha(\epsilon')$ has been obtained assuming the validity of our modified quasi-deuteron model. We stress that the energy dependence of the $He_4(\gamma, np)d$ data is well represented by

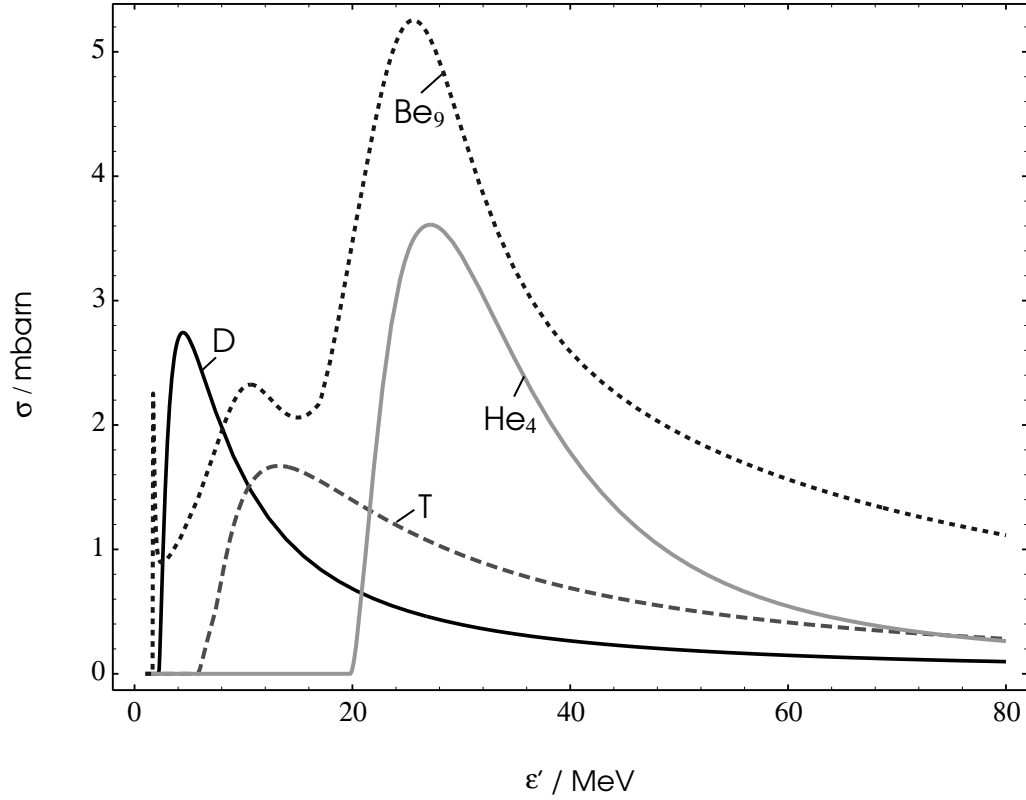


Figure 1.20: Total photodisintegration cross sections of light nuclei with $A < 10$.

the model over the whole energy range, suggesting that the quasi-deuteron process entirely triggers photo- np -emission off He_4 . For the Levinger parameter we find empirically $\tilde{L} \approx 1.1 \text{ fm}^{-1}$, which is much below the empirical value found for heavy nuclei, but fairly consistent with the prediction of our modified model applying Levinger's theoretical formula.

The Be_9 nucleus: The photodisintegration cross section of Be_9 shows essentially three peaks at low energy: one, very sharp just above threshold at about 1.7 MeV, one broad resonance around 10 MeV and the giant resonance at about 25 MeV. The central energy of the giant resonance fits well into the smooth A -dependence observed for nuclei with higher mass numbers (see below), but the width of about 15 MeV is exceptionally large. The lower energy peaks are also exceptional and are observed in only a few nuclides, and in none of them with a strength relative to the giant resonance as in Be_9 . They are readily explained by $p \rightarrow s$ and $p \rightarrow d$ shell transitions of the valence neutron. The low energy part of the cross section can be fitted by

$$\begin{aligned} \sigma_1^{\text{Be}_9}(\epsilon') = & [1.5 \text{ mbarn}] \hat{\sigma}_L(\epsilon'; 1.7 \text{ MeV}, 0.3 \text{ MeV}) + [1.6 \text{ mbarn}] \hat{\sigma}_L(\epsilon'; 10 \text{ MeV}, 10 \text{ MeV}) \\ & + [3.5 \text{ mbarn}] \hat{\sigma}_L(\epsilon'; 25 \text{ MeV}, 15 \text{ MeV}) \quad . \end{aligned} \quad (1.3.26a)$$

The peak around 25 MeV is attributed to the GDR of the Be_8 core nucleons. At higher energies, we adopt the quasi-deuteron cross section as predicted by our modified model, using $B_{\text{QD}} = S_{pn} = 16.9 \text{ MeV}$, and obtain

$$\sigma_2^{\text{Be}_9}(\epsilon') = 9 \sigma_{\text{BP}}(x, 16.9 \text{ MeV}) \quad , \quad (1.3.26b)$$

assuming a normalized Levinger parameter of $\tilde{L} \approx 2.6 \text{ fm}^{-1}$, as found empirically for heavy nuclei. Summing up low and high energy contributions, we obtain a total integrated cross section of about $235 \text{ MeV mbarn} \approx 1.75 \Sigma_{\text{TRK}}$ up to the pion threshold. We may expect that quasi-deuteron disintegration will remove 2 nucleons from Be_9 , and may therefore produce Li_7 nuclei; however, it is not clear whether this general statement applies in loosely bound systems like Be_9 , and moreover the reaction products are likely to be produced in an excited state and can further decay down to He_4 ; thus, we may treat all reaction channels of Be_9 as quasi-absorption. The total photoabsorption data of Be_9 at high energies [ABC⁺75], and the data for neutron emission at low energies [NH53] are reproduced fairly well by our parametrization.

Fig. 1.20 compares the total photodisintegration cross section of Be_9 with that of other light nuclei; we see, that despite of its exceptional low energy behavior, Be_9 marks the transition to heavy nuclei, with a cross section dominated by the giant resonance and continued to high energies by quasi-deuteron photodisintegration.

1.3.4.3 Photodisintegration yield functions in the mass scaling regime

Threshold energy and evaporation scaling laws: Eq.(1.3.1c) for the nucleon separation energy is only approximately valid for nuclei with $A < 50$, in particular we note that it tends to underestimate S_n and S_{np} systematically. Its mass scaling behavior is quite complicated; thus, it may be advisable to find an empirical law with simpler scaling properties to parametrize the threshold energies as a function of A ; in view of the scaling properties of the GDR, we may try to find an expression which complies with the empirically well confirmed GT-III model, proposing a scaling with $A^{-1/6}$. We find a satisfactory fit for the threshold energies S_1 and S_2 with

$$\tilde{S}_1(A) = \hat{S}_1 A^{-1/6} \quad \text{with} \quad \hat{S}_1 = 16.6 \text{ MeV} \quad (1.3.27a)$$

$$\tilde{S}_2(A) = \hat{S}_2 A^{-1/6} \quad \text{with} \quad \hat{S}_2 = 33.3 \text{ MeV} . \quad (1.3.27b)$$

This affects obviously also the mean energy per nucleon removed in an evaporation process, which is now $[25 \text{ MeV}] A^{-1/6}$, leading to

$$\bar{\nu}(A, E^*) = A^{1/6} E_{25}^* \quad , \quad (1.3.27c)$$

where E_{25}^* is the excitation energy in units of 25 MeV.

The giant dipole resonance: It has been shown that the GT-III model of the giant dipole resonance, predicting a mass scaling of the GDR maximum energy with $A^{-1/6}$, fits the data much better than any other GDR model; we therefore adopt it here and fit the available data on GDR maximum energies [MKG53, Oka58] with the functions

$$E_{\text{GDR}}(A) = \hat{E}_{\text{GDR}} A^{-1/6} \quad \text{with} \quad \hat{E}_{\text{GDR}} = 35.3 \text{ MeV} \quad (1.3.28a)$$

$$\Gamma_{\text{GDR}}(A) = \hat{\Gamma}_{\text{GDR}} A^{-1/6} \quad \text{with} \quad \hat{\Gamma}_{\text{GDR}} = 15.1 \text{ MeV} . \quad (1.3.28b)$$

Clearly, for medium mass nuclei there is no empirical evidence for a scaling of Γ_{GDR} in this way, but on the other hand Eq. (1.3.28b) is not in contrast to the data either. We apply this scaling because we have seen above

that the possibility of the general scaling laws, Eqs. (1.3.22), requires scaling of all relevant energy quantities in the same way.

The photoabsorption cross section of the GDR will be assumed to have a Lorentzian shape in the NRF; we neglect the small deviations from the exact Breit-Wigner shape, because we know that the *empirical* cross sections are in any case only approximately described by a single resonance peak. For the normalization we use Eq. (1.1.56b), noting that $D_{\text{th}} = 2.48$ independent of A , and write

$$\Sigma_{\text{GDR}} = \xi_1 \Sigma_{\text{TRK}} = 1.38 \sigma_0 \Gamma_{\text{GDR}} \quad ,$$

where ξ_1 denotes the fraction of the total dipole absorption strength due to GDR. We determine ξ_1 empirically under the assumption that the GDR excitation is *the generic one-nucleon emission process*. We can then take the fractions $\xi_1^{(30)}$, obtained by PSB by integration the observed one-nucleon emission cross sections up to 30 MeV, and find an acceptable parametrization by $\xi_1^{(30)} \approx 0.68 + 0.007A$; the dependence on A is expected by the mass scaling of the resonance position, and comparing with $\Sigma_{\text{GDR}}^{(30)}/\Sigma_{\text{GDR}}$ as a function of A , yields consistency with $\xi_1 = 1$ for all A , confirming beautifully our assumption that the GDR is the *only* relevant process governing classical dipole absorption in nuclei. Thus we have

$$\sigma_0(A) = \hat{\sigma}_0 A^{7/6} \quad \text{with} \quad \hat{\sigma}_0 = 0.72 \text{ mbarn} \quad , \quad (1.3.28c)$$

and with $\nu(A) \equiv 1$ we can write

$$y_{\text{GDR}}(\epsilon', A) = \sigma_{\text{GDR}}(\epsilon', A) = \hat{\sigma}_0 A^{7/6} \hat{\sigma}_L(\epsilon' A^{1/6}; \hat{E}_{\text{GDR}}, \hat{\Gamma}_{\text{GDR}}) \quad . \quad (1.3.29)$$

Hence, Eq. (1.3.29) complies with the scaling condition, Eq. (1.3.22), and we obtain

$$g_0^{\text{GDR}}(A) = g_\epsilon^{\text{GDR}}(A) = A^{1/6} \quad \text{and} \quad g_a^{\text{GDR}}(A, a) = A^{a/6} \quad . \quad (1.3.29a)$$

We do not take into account discrete level excitations. We note that they are expected to contribute only for nuclei with $A \leq 16$, and with a total strength of a few percent of Σ_{TRK} , which is equivalent to the background set at low energies by the wing of the GDR.

The quasi-deuteron regime: In the same way we have treated GDR photoabsorption as a generic one-nucleon emission process, we can treat the quasi-deuteron process as a *generic two-nucleon emission process*. The cross section predicted by our modified quasi-deuteron model, which is proposed to give an approximate description of this process down the two-nucleon emission threshold, can then be compared with the PSB values for two-nucleon emission below 30 MeV, as well as with their total integrated cross sections in the range 30–150 MeV. The latter range will be taken as the more important one, because there the quasi-deuteron effect dominates the total photoabsorption cross section, while it is only a 10% contribution below 30 MeV.

We have found in our modified quasi-deuteron theory an approximately constant value for the Levinger parameter in the mass range $10 \leq A \leq 56$, $\bar{L} \approx 6.5$. Adopting this value, which is quite consistent with all available data sets, and inserting $B_{\text{QD}} = \tilde{S}_2(A)$ from Eq. (1.3.27b) in Eq. (1.3.19), we find

$$\sigma_{\text{QD}}(\epsilon', A) = [0.55 \text{ mbarn}] A^{5/4} \frac{(x_{\text{QD}} - 1)^{3/2}}{x_{\text{QD}}^3} \quad \text{with} \quad x_{\text{QD}} = \frac{\epsilon' A^{1/6}}{\hat{S}_2} \quad . \quad (1.3.30a)$$

To check the absolute normalization, we integrate Eq. (1.3.30) over energy and compare with the PSB results (Fig. 1.21). In the range between 30 MeV and the pion threshold we have to consider that there is a contribution of the high energy GDR wing, which we find by integration of Eq. (1.3.29). The sum of GDR and QD

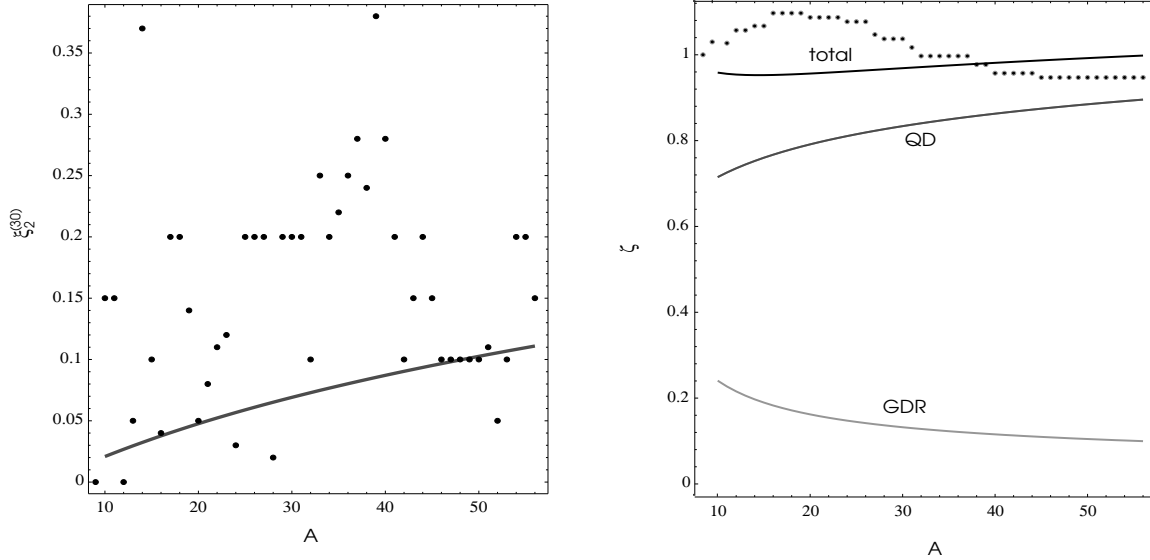


Figure 1.21: Total integrated cross sections for two-nucleon emission below 30 MeV (left panel), and for total photoabsorption in the range 30–150 MeV. Data are taken from [PSB76], the curves represent results from our parametrization (see text).

contribution in this energy range is in good correspondence with the PSB results, but below 30 MeV the QD contribution seems to be insufficient to explain the data for $A < 40$. However, in view of the neglect of shell effects in our treatment, and the reduction of the GDR to a pure one-nucleon emission process, this discrepancy is not really surprising; assuming a 5–10% branching ratio for two-nucleon decay of the GDR would suffice to explain the data; also a slight modification of the assumption $B_{\text{QD}} = \tilde{S}_2(A)$ can change a lot on this result. We simply discard this problem noting the uncertainties contained in the PSB data, and that the sum of Eq. (1.3.29) and Eq. (1.3.30), integrated up to the pion threshold, is in beautiful correspondence with the general trend and magnitude of the modified GGT sum rule, slightly increasing from $1.6 \Sigma_{\text{TRK}}$ for $A = 10$ to $\approx 2 \Sigma_{\text{TRK}}$ for $A = 56$. We note that we did not include any quenching factor into our calculation; this would deteriorate the correspondence with the data a lot, unless we would increase the Levinger parameter *ad hoc* by a factor of 2, in contrast to all experimental results. We conclude that our low energy modification of the quasi-deuteron model, does sufficiently consider the low energy cross section reduction in light nuclei. In heavy nuclei, however, this might no longer be true; the effect of Levinger’s heuristic quenching factor in lead can hardly be reproduced by our model, so that an application of Eq. (1.3.19) with $B_{\text{QD}} = \tilde{S}_2(A)$ to masses $A \gtrsim 100$ would overestimate the quasi-deuteron cross section.

Important for our considerations is, that Eq. (1.3.30a) obviously complies with the scaling condition. To obtain the nucleon yield rate, we note that the quasi-deuteron process leads *by assumption* to a direct emission of two nucleons; additionally, it deposits an excitation energy $E^* \approx \frac{1}{2}(\epsilon' - \tilde{S}_2(A))$ in the nucleus, leading to an average nucleon emission multiplicity of the quasi-deuteron process $\bar{\nu}_{\text{QD}}(\epsilon', A) = 2 + \frac{2}{3}(x_{\text{QD}} - 1)$ with $x_{\text{QD}} = \epsilon' / \tilde{S}_2(A)$. Obviously, this has the same scaling properties as Eq. (1.3.30a), and we get

$$g_0^{\text{QD}}(A) = A^{1/4} \quad , \quad g_\epsilon^{\text{QD}}(A) = A^{1/6} \quad \text{and} \quad g_a^{\text{QD}} = A^{1/12+a/6} \quad , \quad (1.3.30b)$$

with the normalized efficiency yield function

$$\hat{\eta}_{\text{QD}}(x_{\text{QD}}) = [0.55 \text{ mbarn}] \frac{6(x_{\text{QD}} - 1)^{3/2} + 2(x_{\text{QD}} - 1)^{5/2}}{3x_{\text{QD}}^3} \quad . \quad (1.3.30)$$

At high energies, this scaling breaks down because of the saturation of the excitation energy deposition. However, this occurs mainly for $\epsilon > \epsilon_\pi$, where the quasi-deuteron process contributes little, so we discard this problem.

The baryon resonance regime: In the baryon resonance region, we obtain the cross section from an empirical fit of the total γd cross section. We have noted that a detailed treatment of all baryon resonances barely makes sense, and that Fermi-broadening of the resonances has to be considered. We therefore divide up the baryon resonances from Tab. 1.2 into four groups, and approximate them by Lorentz functions in the NRF, writing the total cross section as

$$\sigma_{\text{BR}}(\epsilon', A) = A \sum_i \sigma_i \hat{\sigma}_L(\epsilon'; E_i, \Gamma_i) \quad . \quad (1.3.31)$$

The data express the total photoabsorption cross section; to obtain the photodisintegration cross section, we must first subtract the coherent pion production part. Guided by the fraction of t -channel interactions in free γN interactions, and considering Fermi-broadening, we use the estimate

$$\frac{\sigma_{\text{coh}}(\epsilon', A)}{[\mu\text{barn}]} \sim 65 A \hat{\sigma}_L(\epsilon'; 450 \text{ MeV}, 500 \text{ MeV}) + 22 A \text{ Ef}(\epsilon'; 500 \text{ MeV}, 1 \text{ GeV}) \quad ;$$

comparison with the data obtained at the Bonn synchrotron for C_{12} basically confirms this estimate in the resonance region [AEH⁺82]; the high energy part assumed here is due to diffractive vector meson production. We discard the problem of the mass scaling of coherent interactions, and apply “natural” scaling with A , noting that the contribution of these processes is not strong. The residual data for the γd reaction are fitted by Eq. (1.3.31) with the following parameters:

$$\begin{aligned} E_1 &= 340 \text{ MeV} \quad , \quad \Gamma_1 = 170 \text{ MeV} \quad , \quad \sigma_1 = 351 \mu\text{barn} \quad , \\ E_2 &= 750 \text{ MeV} \quad , \quad \Gamma_2 = 500 \text{ MeV} \quad , \quad \sigma_2 = 159 \mu\text{barn} \quad , \\ E_3 &= 1 \text{ GeV} \quad , \quad \Gamma_3 = 600 \text{ MeV} \quad , \quad \sigma_3 = 21 \mu\text{barn} \quad , \\ E_4 &= 1.5 \text{ GeV} \quad , \quad \Gamma_4 = 800 \text{ MeV} \quad , \quad \sigma_4 = 26 \mu\text{barn} \quad . \end{aligned}$$

We stress that these parameters cannot be considered as more as a rough approximation, in particular when visualizing the problems of mass scaling in the second resonance region.

To obtain the nucleon yield rate, we consider three kinds of nucleon emission processes: (i) emission of the primary participant nucleon with probability 1; (ii) reabsorption of the pion by a nucleon pair with probability $0.13A^{1/3}$; (iii) deposition of an excitation energy $E^* \approx 40 \text{ MeV}$ per emitted participant nucleon, primary and secondary. The latter value is set to the approximate saturation found for medium mass nuclei. Then we have

$$\bar{\nu}_{\text{BR}}(A) = \left[1 + 0.13A^{1/3}\right] \left[1 + 1.6A^{1/6}\right] \quad , \quad (1.3.31a)$$

independent on ϵ' , leading to the scaling functions

$$g_a^{\text{BR}}(A) = g_0^{\text{BR}}(A) = \overline{\nu}_{\text{BR}}(A) \quad \text{with} \quad g_\epsilon^{\text{BR}}(A) = 1 \quad . \quad (1.3.31\text{b})$$

The independence on ϵ' is, of course, just a result of the approximations we used. However, noting that baryon resonance excitation will probably not play a dominant role in astrophysical applications due to the large required excitation energies, the introduced error can be assumed to be small.

The high energy regime: Photodisintegration and photo-fragmentation at highest energies is treated as the result of multipion production at single nucleons. We can therefore adopt the multipion cross section for photohadronic interactions, and the empirical mass scaling law known for high energy photonuclear reactions, $\sigma_A \propto A^{0.91}$, considering shadowing effects due to the VDM structure of the photon. Since the difference between fragmentation and spallation reactions in this energy regime is difficult to treat exactly, we will confine ourselves to discuss the maximum effect of fragmentation, the instantaneous destruction (absorption) of the nucleus, $\overline{\nu}(A) = A$; we note that therefore all our results have to be considered as upper limits. Thus we can write

$$\hat{\eta}_{\text{frag}}(\epsilon) = [1 \mu\text{barn}] \tilde{\zeta}_{(\pi)}(\epsilon/[\text{GeV}]) \quad , \quad (1.3.32)$$

with $\tilde{\zeta}_{(\pi)}(x)$ given by Eq. (1.2.30), and find the scaling functions

$$g_a^{\text{frag}}(A) = g_0^{\text{frag}}(A) = A^{0.91} \quad \text{and} \quad g_\epsilon^{\text{frag}}(A) = 1 \quad . \quad (1.3.32\text{a})$$

The efficiency is here obviously proportional to the cross section, because the destruction of the nucleus is assumed to proceed in one reaction.

1.3.4.4 Total efficiency and astrophysical applications

Comparison of disintegration processes: In astrophysics, we are mainly interested in the total efficiency for photodisintegration in a given photon spectrum, and in the contribution of the different disintegration processes. Fig. 1.22 shows the total photodisintegration cross section, as obtained for the method described above, for $A = 56$. We realize the typical two-bump structure, connected by the slowly decreasing quasi-deuteron cross section, and extended to high energies by the constant cross section for fragmentation. In comparison, the nucleon yield function shows an even more constant behavior, because the high energy reactions are favored by higher emission multiplicities; now, baryon resonance excitation is the most efficient disintegration process, comparable to instantaneous fragmentation. For different nuclear masses, these functions scale both in energy and absolute value, as shown in Fig. 1.23 for $A = 12, 28, 56$ and 208 . The scaling up to the heaviest stable nucleus, Pb_{208} , has to be considered as only approximative, because many of our simple assumptions do no longer apply for very heavy nuclei; it is done here only for comparison, and we note that nuclei with $A > 60$ play almost no role in astrophysics.

Loss time scales in anisotropic power laws: Although the baryon resonances mark the highest peak in the photodisintegration efficiency, they occur at photon energies which are about one order of magnitude above the giant resonance, and are therefore generally assumed to be negligible in astrophysical photon spectra. We check this for isotropic power law spectra calculating the normalized efficiency coefficients, $\hat{H}_{ab}^{(\epsilon)}$, as to be used with the specific mass scaling functions for the different processes (Fig. 1.24). The scaled coefficients for $A = 12$ and $A = 56$ are shown in Fig. 1.25: we see that quasi-deuteron disintegration (QD), and in particular isobar

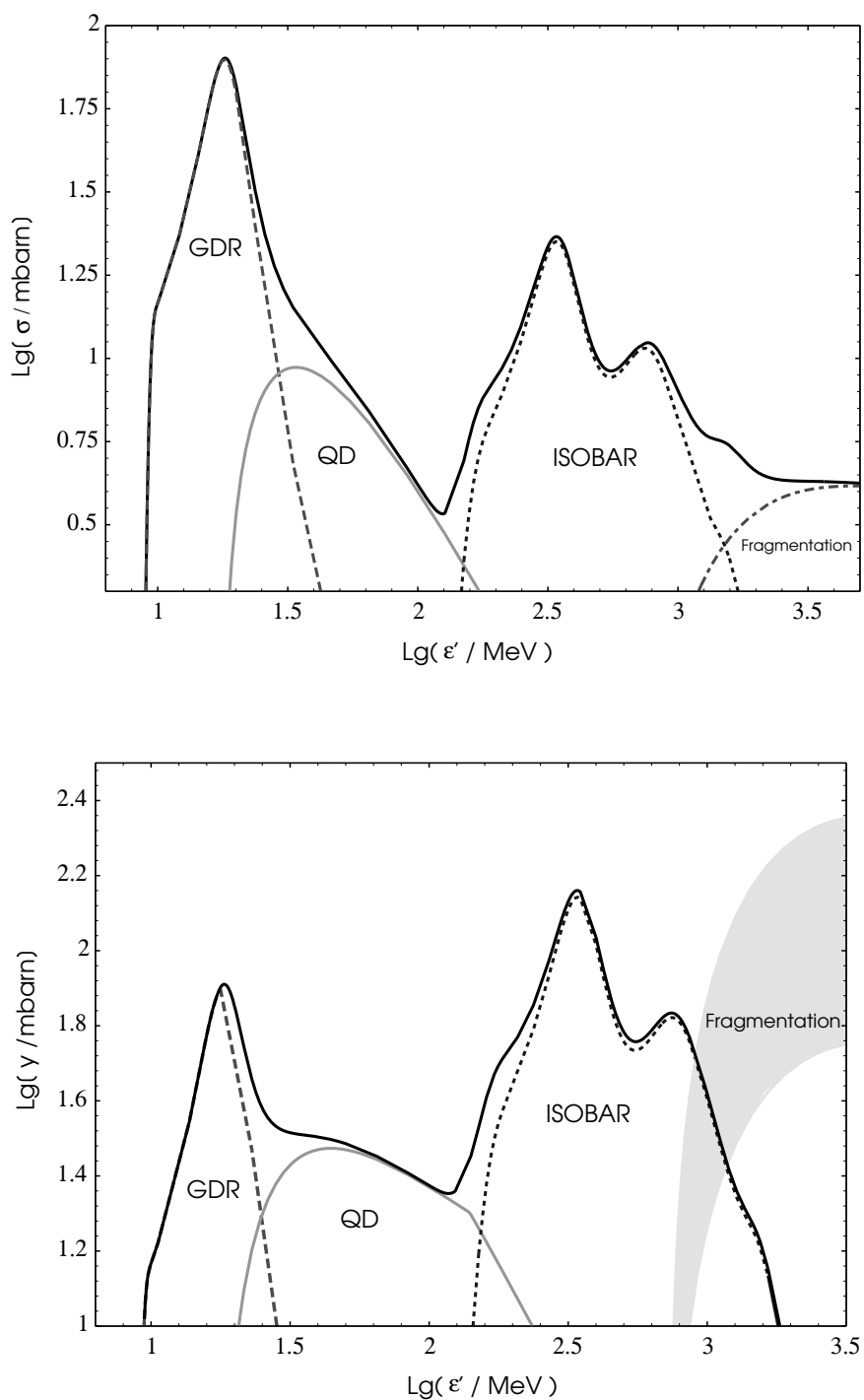


Figure 1.22: Total cross section (upper panel) and nucleon yield function (lower panel) for photodisintegration of an $A = 56$ nucleus, as calculated from the scaling model, with the contributions of the GDR, the quasi-deuteron process (QD), baryon resonance excitation (ISOBAR) and fragmentation. The shadowed region for the nucleon yield of fragmentation corresponds to the range between ordinary evaporation and the instantaneous absorption approximation.

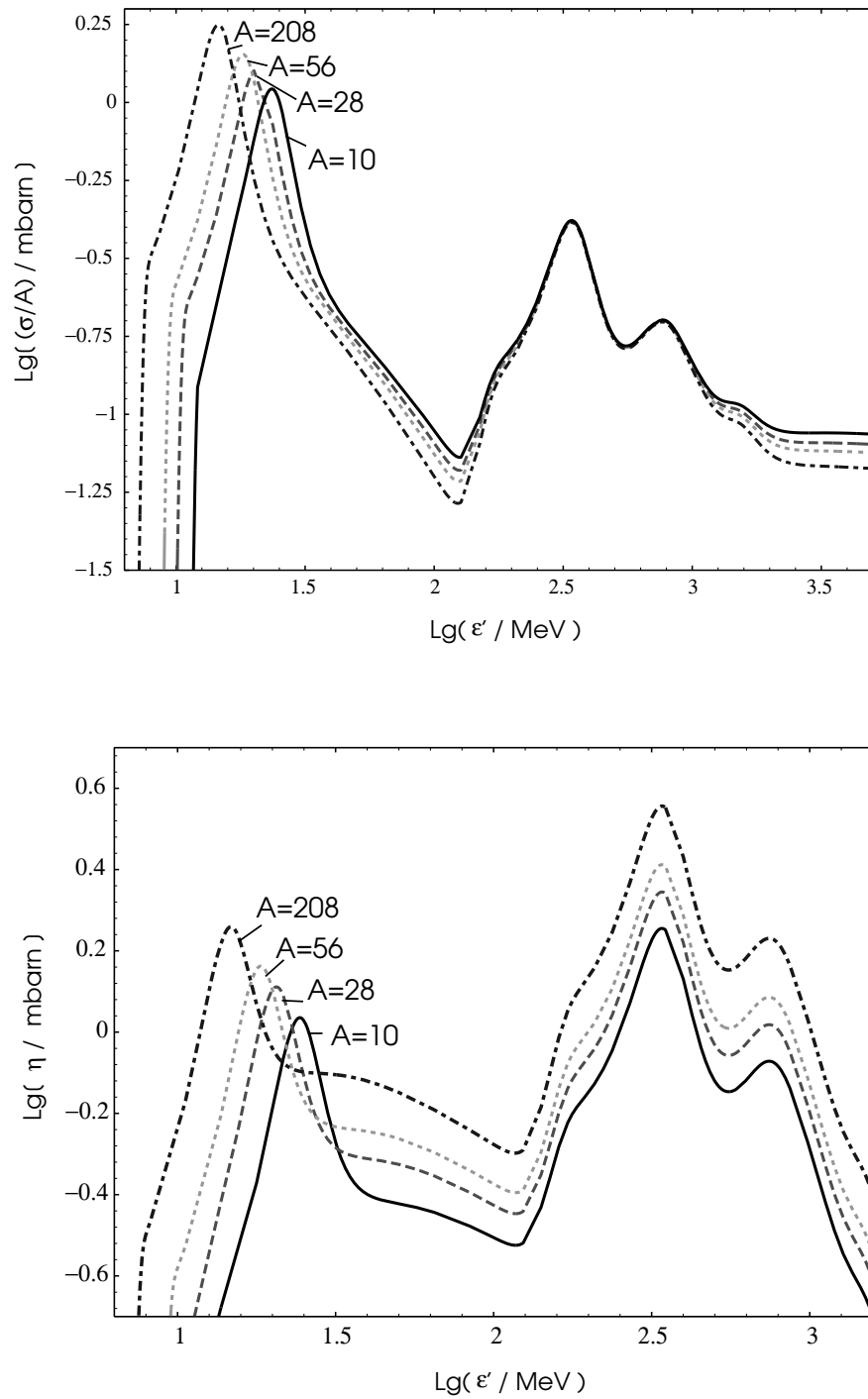


Figure 1.23: Mass scaling of total cross section per nucleon (upper panel) and efficiency function (lower panel) for photodisintegration.

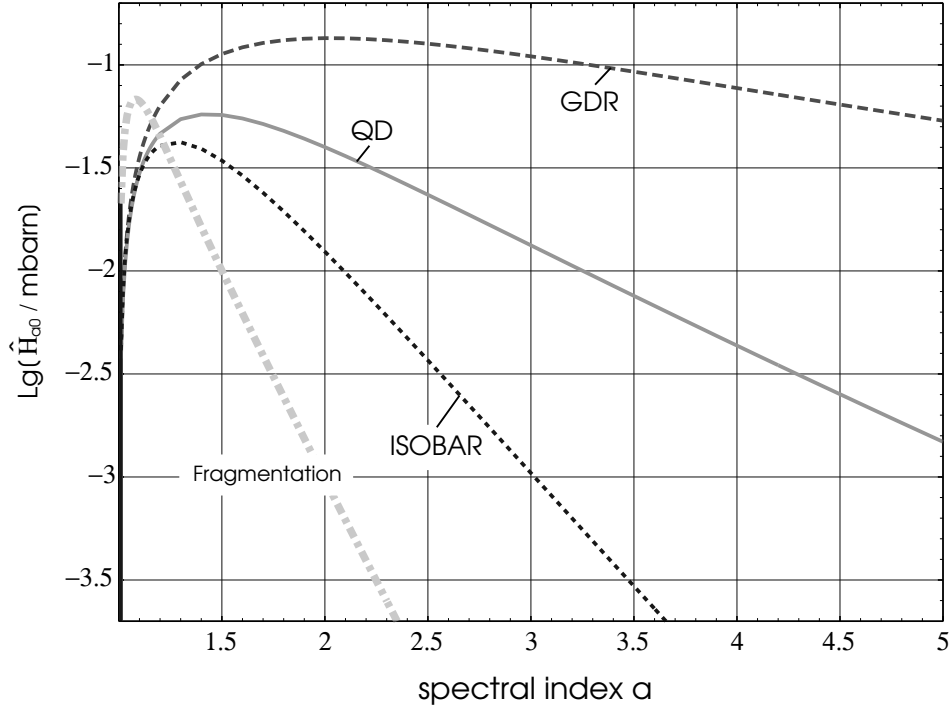


Figure 1.24: Normalized total efficiency coefficients $\hat{H}_{ab}^{(e)}$ for the photodisintegration processes GDR, QD and ISOBAR in isotropic power law photon spectra, to be used in Eq. (1.3.23). The curve for instantaneous fragmentation marks an upper limit for the absorption efficiency of nuclei.

excitation and fragmentation play only a role in inverse spectra, where their contribution may be diminished by cutoff effects. We note that for both masses the total efficiency coefficient is roughly constant over a .

We also determine the total weighted cross sections, Σ_{a0} , of light nuclei in power law photon spectra. The only difference of Σ_{a0} and H_{a0} is that in the former case the nucleon yield is not considered; Σ_{a0} expresses the cross section for the first interaction rather than for total disintegration. If we want to consider disintegration chains, we have to calculate secondary injection functions for all light nuclei from the disintegration of heavier ones, and perform a full transport calculation with emission and absorption. Of course, we will not do this here; here we just note from Fig. 1.26 that Be_9 has the largest effective cross section of all light nuclei in power law spectra, while its disintegration product, the α particle, has the smallest. We also see that in flat spectra the time scale for α photodisintegration is about two times larger than for the trinucleon, and about one order of magnitude longer than for the deuteron; we can estimate the time scale for *total disintegration* of α particles to $\tau_{\text{dis}}^\alpha \approx 1.5\tau_{\text{int}}^\alpha$, when τ_{int}^α is the time scale for the first interaction. In steeper spectra, τ_{dis}^α approaches τ_{int}^α , because the further disintegration of T_3 and D_2 proceeds very much faster.

We may compare the total efficiency coefficients of C_{12} and Fe_{56} with the Σ_{a0} coefficients for light nuclei, noting the difference in their definition described above. In particular, the reference threshold which determines the Lorentz factor scale is here taken as 1 MeV rather than $\hat{\epsilon}_{\text{th}} = 16.6$ MeV. Applying Eq. (1.2.31) uses then for the same Lorentz factor γ_{CR} different scaled values $\hat{\gamma}_{\text{CR}}$; to compensate this, we also plot $\check{\Sigma}_{a0} = 16.6^a \Sigma_{a0}$ in Fig. 1.26, which is then directly comparable to Fig. 1.25. We see that indeed Be_9 disintegrates much faster than

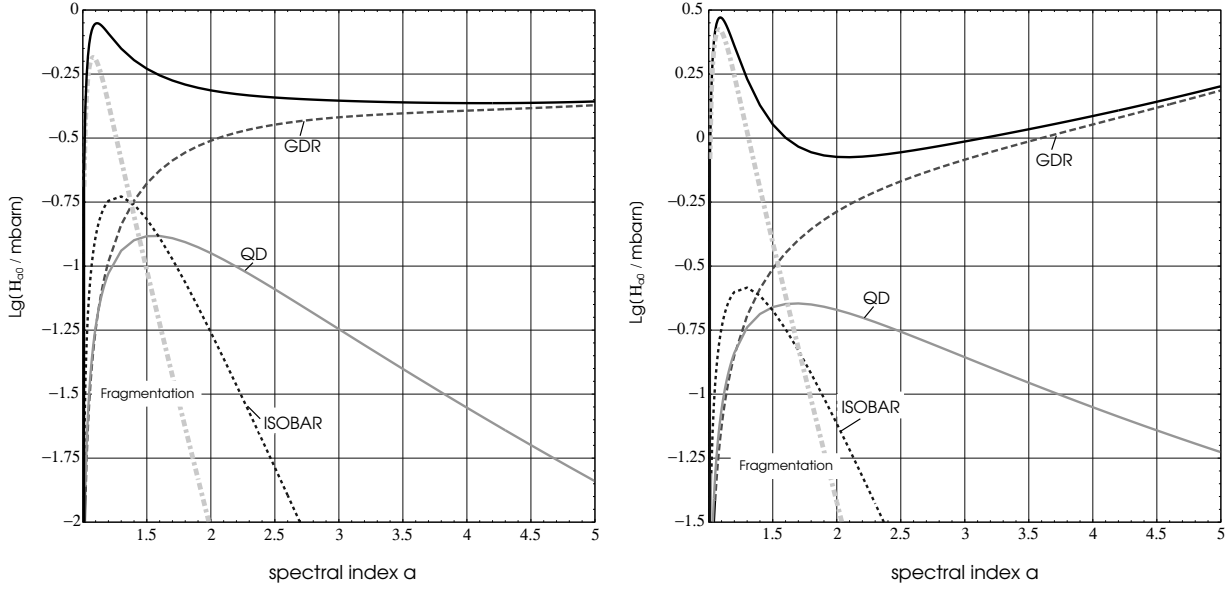


Figure 1.25: Scaled total efficiency coefficients for $A = 12$ (C_{12} , left panel) and $A = 56$ (Fe_{56} , right panel).

heavier nuclei, which justifies to leave it out of consideration for heavy nuclei mass evolution.

Rigidity conservation and the acceleration of nuclei in photon backgrounds: Finally, we want to note one important feature of photodisintegration in connection to particle acceleration by large scale magnetic scattering, i.e. the Fermi-process. We see from Eqs. (1.1.18) that the acceleration time scale in the Fermi process is only dependent on the gyration radius, r_g , of the particle. Introducing the particle *rigidity*, $R = (pc/ZeB)$, we can write for ultrarelativistic nuclei

$$\tau_{\text{acc}} \propto R \propto \frac{A\gamma}{Z} . \quad (1.3.33)$$

Now, for nuclei with $A < 30$ we have $Z \simeq \frac{1}{2}A$; for heavier nuclei, we recall our discussion from above and note that, during subsequent photodisintegration, the number of neutrons approaches the number of protons in the nucleus, if the interactions occur fast enough to prevent interim β^+ decay. In any case, we can use $R \propto \gamma$ for all astrophysically relevant nuclei *while photodisintegration is in action*. We have already noted that γ remains constant in photodisintegration interactions, so also R and τ_{acc} . This means that the *Fermi acceleration of nuclei is unaffected by photodisintegration*; the acceleration process just sees a particle with *constant rigidity*.

We can use this property to make a simple estimate of the maximum Lorentz factor a complex nucleus can gain in the Fermi process, before it is completely disintegrated. As before, we set the end point to $A_{\text{min}} = 10$, so ruling out light nuclei from the treatment, which is reasonable because the heavy nuclei are only important if they have a favorable E/γ ratio over the much more abundant primary α -particles. From Eq. (1.1.18a), assuming $\theta = 0$ for simplicity, we combine all quantities determining the acceleration rate in one parameter, $\hat{\tau}_{\text{acc}}$, and write the acceleration time as a function of the scaled Lorentz factor, $\hat{\gamma}_{\text{CR}} = 2\epsilon_0\gamma/\hat{\epsilon}_{\text{th}}$, which reads

$$\tau_{\text{acc}} = \hat{\tau}_{\text{acc}} \hat{\gamma}_{\text{CR}}^\alpha \quad \text{with} \quad \hat{\tau}_{\text{acc}} = \frac{r_c(r_c + 1)}{r_c - 1} \frac{\hat{\eta}_B \hat{m} c^3 \gamma_0}{2V_s e B} , \quad (1.3.34a)$$

where $\eta_B = \hat{\eta}_B \hat{\gamma}_{\text{CR}}^{\alpha-1}$, corresponding to an index of the turbulence spectrum $\beta = 2 - \alpha$ (cf. [BS87, Rac92]), and

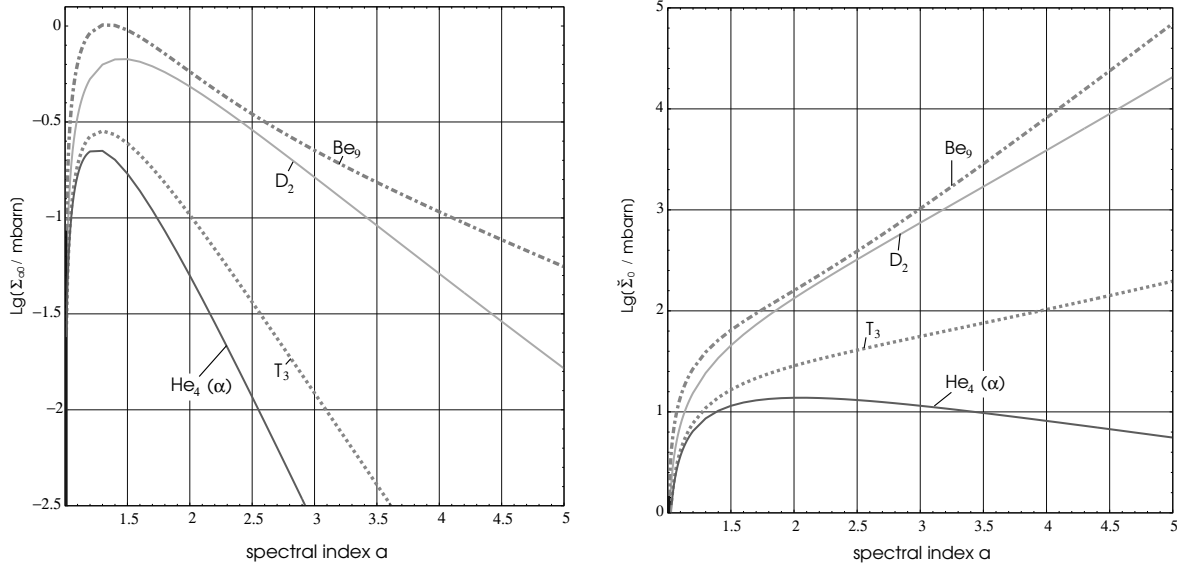


Figure 1.26: Total effective cross section in power law spectra for light nuclei with reference threshold $\epsilon_{\text{th}} = 1$ MeV (left panel), and scaled to the standard reference threshold for heavy nuclei (right panel, see text).

V_S is the shock velocity; for diffusion with energy-independent η_B (i.e. Bohm diffusion), we have $\alpha = 1$. Now we can write a differential equation for the total acceleration time

$$\frac{dt}{d\hat{\gamma}_{\text{CR}}} = \hat{\tau}_{\text{acc}} \hat{\gamma}_{\text{CR}}^{\alpha-1}, \quad (1.3.34b)$$

which allows now to express the nuclear mass as a direct function of the Lorentz factor

$$\frac{dA}{d\gamma} = \frac{dA}{dt} \frac{dt}{d\gamma} = \hat{\tau}_{\text{acc}} v(\gamma, A) \hat{\gamma}_{\text{CR}}^{\alpha-1}. \quad (1.3.34c)$$

Integrating out, we finally find the maximum Lorentz factor, γ_{max} , defined by the time where $A = A_{\text{min}}$ is reached as the result of photodisintegration, as

$$\hat{\gamma}_{\text{max}} = \left[\frac{a + \alpha - 1}{c \hat{\tau}_{\text{acc}} N_0} \int_{A_{\text{min}}}^{A_0} dA \left(A \sum_c \hat{H}_{ab}^{(c)} g_a^{(c)}(A) \right)^{-1} \right]^{\frac{1}{a+\alpha-1}}. \quad (1.3.35)$$

Multiplying with the mass of the final nucleus, $10\hat{m}$, we also find the maximum energy reached in the acceleration process. Clearly, we may also apply the classical gain-loss balance, $\tau_{\text{dis}} = \tau_{\text{acc}}$, to obtain a maximum energy, E_{max} ; but this works only if the Lorentz factor $\tilde{\gamma}_{\text{max}}$ for which this balance is given is *smaller or equal* to γ_{max} . If $\tilde{\gamma}_{\text{max}} < \gamma_{\text{max}}$, we will find the maximum energy nuclei for nuclei with $A > A_{\text{min}}$; otherwise, the highest energy nuclei have $A \approx 10$. $\tilde{\gamma}_{\text{max}} > \gamma_{\text{max}}$ obviously means, that the culminated photodisintegration, integrated up from the injection of the particle, leads to its final destruction before $|\Delta A/A| > |\Delta\gamma/\gamma|$ in a given time interval.

We may give a numerical example: We consider a system with equipartition of magnetic and radiation energy density, $U_B = U_\gamma = 2 \text{ keV/cm}^3$. The photon spectrum may be given by a power law with $a = 2.5$, extending

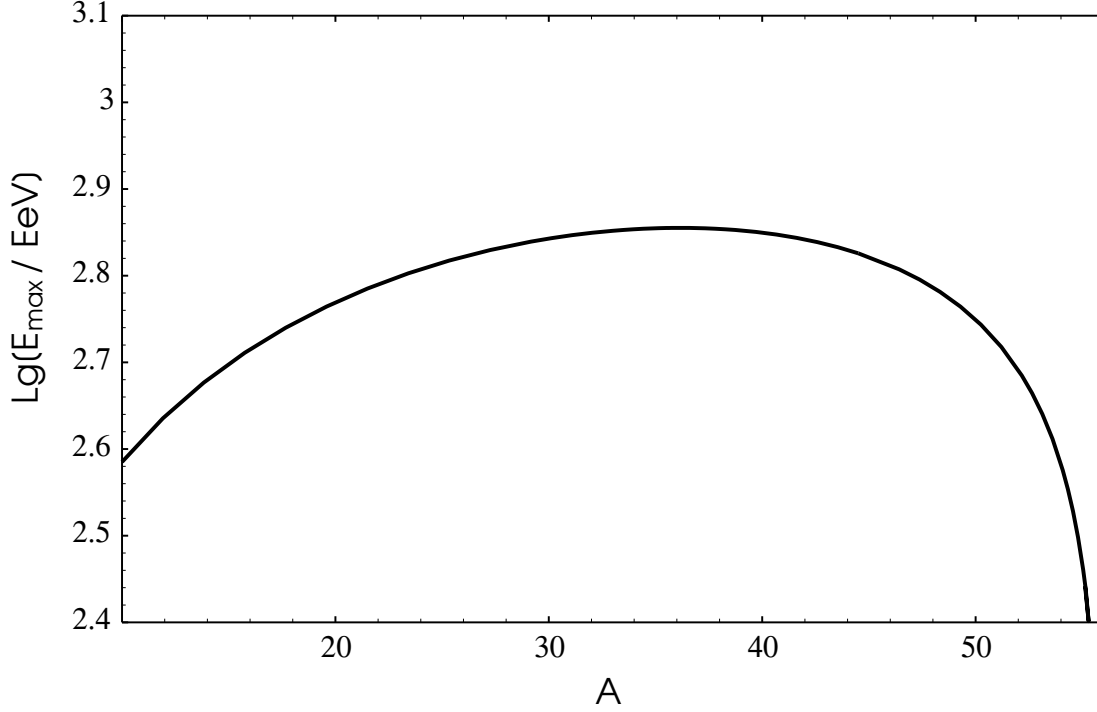


Figure 1.27: Maximum energy achievable with heavy nuclei by shock acceleration under the example conditions discussed in the text.

from $\epsilon_0 = 10^{-5}$ eV (equivalent to 2.4 GHz) to infinity. With $\hat{\epsilon}_{\text{th}} = 16.6$ MeV we then have the scaling Lorentz factor $\gamma_0 = 8.3 \times 10^{11}$. We assume Bohm diffusion, and acceleration at a strong shock ($r_c = 4$) with velocity $\frac{1}{3}c$, giving $\hat{\tau}_{\text{acc}} = 8.6 \times 10^{12}$ sec and $\alpha = 1$. For the photon spectrum we find $N_0 = 6.7 \times 10^7 \text{ cm}^{-3}$; since we see from Fig. 1.25 that for a power law index $a = 2.5$ the GDR dominates photodisintegration, we neglect all other channels and have $\hat{H}_{ab} \equiv \hat{H}_{ab}^{\text{GDR}} = 126 \mu\text{barn}$ and $g_a(A) = A^{-5/12}$. Injecting Fe_{56} nuclei, we then find for $A_{\text{min}} = 10$ the value of the integral as 3.75 mbarn^{-1} . Multiplying with the constants, and noting the the power index on the right side of Eq. (1.3.35) is $\frac{2}{5}$, we finally have $\hat{\gamma}_{\text{max}} \approx 0.047$, or $\gamma_{\text{max}} \approx 4 \times 10^{10}$. This maximum Lorentz factor is achieved with for the minimal possible mass, $A_{\text{min}} = 10$, thus the corresponding energy is $E_{\text{max}} \approx 380 \text{ EeV}$, which of the order of the highest cosmic ray energies. If we consider the ejection of heavier nuclei, i.e. set A_{min} variable between 10 and 56, we obtain maximum energies as shown in Fig. 1.27. We see that the highest energies are emitted in nuclei with $A \sim 35$, giving $E_{\text{max}} \approx 660 \text{ EeV}$. We note that the numbers we have used in this example are quite close to the conditions in radio galaxy hot spots; thus, even though a more thorough calculation is required to obtain reliable quantitative results, this example already shows that acceleration of UHECR heavy nuclei in radio galaxy hot spots is possible.

Chapter 2

Statistics of cosmic ray interactions

Abstract: Cosmic ray transport through photon backgrounds is a classical example for that what is called a *random point process* in mathematics; the energy of the particles is changed discontinuously in randomly steps, with a randomly distributed step size. Historically, it is even the case that cosmic ray physics has largely motivated the development of the mathematical theory of random processes. The most developed part of the theory of random processes is the theory of *Markov processes*, which are processes requiring that the future propagation of a particle is only determined by its present state — a situation which can be assumed to apply generally in physics. In fact, it can be shown that the most general problem of particle transport, the description of the evolution of spectra governed by the *Boltzmann equation*, can be completely transformed into a description in terms of Markov processes.

However, in contemporary astrophysics the treatment of the transport of cosmic rays splits up into mainly two groups: On the one side there are simple, but mostly qualitative approaches, which are useful to understand the basic phenomena, but clearly overburdened when used for detailed predictions; on the other side some Monte Carlo or other numerical results can be found in the literature, which may give a quantitatively correct answer to some specific questions, but are barely transportable to other problems. Understanding the differences between the results of the first and second approach remains a task for physical intuition.

In this chapter we develop a method which is proposed to close the gap between both extremes, based on the theory of discontinuous Markov processes. Unfortunately, we cannot avoid to introduce a “statistical language” which is probably not common for many physicists. Therefore, Sect. 2.1 gives an overview about the basic formal terms and concepts of probability theory. Then, Sect. 2.2 introduces the basic concepts of the theory of Markov processes and random point processes, which is applied to cosmic ray physics in some simple examples. The main result is the derivation of a set of differential equations, which propose to give a simple solution to *some* physical transport problems, which may be described as processes with a weak *autocorrelation*; we call them the *perturbative equations* for the description of Markovian point processes. These equations are applied in a simple example in the end of this chapter, but their full range of applicability has to be further investigated.

2.1 Notes on probability theory and Markov chains

This section gives a general overview about the mathematical foundations of probability theory in the context of this work. It is thought as a reference for the discussion of random processes in the next section. We introduce some mathematical terms which will be used in the following, more physical section.

Since most of this section covers subjects which can be found in textbooks, we do not give detailed references. For general reading about probability theory we recommend the books of CRAMER [Cra46] and FISZ [Fis80]; the latter also gives a very good introduction to random processes. Many specific formulae and relations can be found in the compendium of ABRAMOWITZ & STEGUN [AS65]. The theory of generalized functions is described in the book of KANWAL [Kan83].

Notation: The symbol “ \doteq ” is used for implicit definitions. Open and closed intervals are written as $]a, b[$ and $[a, b]$, respectively. If we consider multidimensional objects, $\mathbf{x}, \mathbf{y}, \dots$, the ordinary product \mathbf{xy} is generally understood as a *tensor product*, i.e. \mathbf{xy} is a tensor of rank 2 if \mathbf{x} and \mathbf{y} are vectors. The *generalized scalar product* is denoted as $\mathbf{X} \cdot \mathbf{Y} \equiv X_{ij\dots k} Y^{ij\dots k}$. The ordinary matrix product as $\mathbf{A} \bullet \mathbf{B}$; powers of matrices are written as $(\mathbf{A} \bullet)^k$. In Sect. 2.1.2 we use a special notation for subspaces of n -dimensional probability (vector) spaces: $\mathbb{IP}_{\leq k} \equiv \{\xi_1, \dots, \xi_k\}$ is a k -dimensional hyper-surface of $\mathbb{IP}^n \equiv \{\xi_1, \dots, \xi_n\}$; accordingly we use, e.g. $\mathbb{IP}_{\setminus k} \equiv \{\xi_1, \dots, \xi_{k-1}, \xi_{k+1}, \dots, \xi_n\}$ and $\mathbb{IP}]_{j,k}[\equiv \{\xi_{j+1}, \dots, \xi_{k-1}\}$, etc.; the same notation is used for vectors and related quantities. The Dirac delta function is denoted as $\delta(x)$, the Heaviside step function with $\text{Hs}(x)$. We use the Kronecker symbol, $\delta_{kj} = 1$ for $k = j$ and 0 otherwise, and the abbreviation $\hat{\delta}_{kj} \equiv 1 - \delta_{kj}$. The symbol “ \circ ” is used for the formal concatenation of functions, $(f \circ g)(x) \doteq f(g(x))$; $\mathbb{I}(x) \equiv 1$ is the unit function. The power of a function, $f \circ g$ with $f(x) = x^k$, is denoted as $g^k(x)$ (as in trigonometry, e.g. $\sin^2 x$); to avoid confusion, we write the inverse function as g^\ominus rather than g^{-1} . Derivatives are abbreviated as $f^{(k)}(x) \doteq (d^k f/dx^k)$. The important propagator product “ \triangleright_x ” is introduced in Eq. (2.1.63). Other symbols are introduced in the text or used in their common meaning.

2.1.1 Probability distribution functions

2.1.1.1 Random variables and distributions

Continuous and discrete random variables: The basic concept of the theory of probability is expressed by the terms “random event”, “random variable” and “probability”. A *random event* \mathcal{E} is a non-mathematical (i.e. physical) entity which is related to a number $0 \leq \mathcal{P}(\mathcal{E}) \leq 1$, called its *probability*. We will not try to discuss the axiomatic approaches to the definition of the terms “probability” and “randomness”, but use the heuristic approach to these terms common in natural sciences: *Randomness* of an event means, that, in a specific situation, we are not able to give a definite prediction whether a specific event will happen or not. The *probability* of a specific event \mathcal{E}_k is given as the limit of the ratio of the *actual* number of occurrences of \mathcal{E}_k , N , to the *maximally possible* number of occurrences of \mathcal{E}_k , M , for a large number M . It is the law of *statistical regularity* which guarantees that the limit of this ratio for $M \rightarrow \infty$ always exists and is well defined; for practical use, the methodological rule that an *empirically given* ratio of this kind for an ensemble of size M may be assigned to a single event of the same kind as its approximative probability $\mathcal{P}(\mathcal{E})$.

A random variable ξ is a representation of a random event in a set of numbers \mathcal{M} . For discrete sets, i.e. $\mathcal{M} \cong \mathbb{N}$, ξ is called a *discrete random variable*, while for continuous sets we, i.e. $\mathcal{M} \cong \mathbb{R}$, ξ is called a *continuous random variable*. There is an important difference between both cases: In the discrete case, a random event is expressed by simple numbers, $\mathcal{E}: \xi = x$, thus a probability value $\mathcal{P}(\xi = x)$ can be given; in the continuous case, a random event is only connected to number intervals, $\mathcal{E}: \xi \in [a, b]$, and only probabilities $\mathcal{P}(\xi \in [a, b])$ are defined. Equality to simple numbers, $\xi = x$, is only connected to a *probability density*.

Cumulative Probability distribution and probability density: The probability of a continuous random variable $\xi \in \mathbb{R}$ to be found in an interval $]a, b]$ can be expressed as

$$\mathcal{P}(\xi \in]a, b]) \doteq F(b) - F(a) \quad , \quad (2.1.1)$$

where F is called the *cumulative distribution function* of ξ . Obviously, $F(x)$ may be written as

$$F(x) = \int_{-\infty}^x f(\xi) d\xi \quad , \quad (2.1.2)$$

with $f(\xi)$ defining the *probability density function* of ξ . Since $f(\xi)$ is non-negative, F is a non-decreasing function; assuming that $f(\xi)$ is a simple function, F is also continuous. f is not necessarily continuous and has at least one maximum, which is called the *mode* of the distribution.

For a discrete random variable, $\nu \in \mathbb{N}_0$, the probability density function is replaced by a series of probabilities p_ν , normalized to $\sum_\nu p_\nu = 1$. Obviously, the cumulative distribution function is now given by

$$F(n) = \sum_{\nu=0}^n p_\nu \quad . \quad (2.1.3)$$

The continuous representation $F(x)$ of a discrete distribution function is a non-decreasing *step function*, and we will see later in Sect. 2.1.1.3 that Eq. (2.1.2) can be generalized to describe discrete distribution functions by introducing the Dirac- δ function as a probability density.

Obviously we have $F(x) \rightarrow 0$ for $x \rightarrow -\infty$ and $F(x) \rightarrow 1$ for $x \rightarrow +\infty$, both in the continuous and the discrete case. Any point $x_{\frac{1}{2}}$ satisfying $F(x) \geq \frac{1}{2}$ for $x \geq x_{\frac{1}{2}}$ and $F(x) \leq \frac{1}{2}$ for $x \leq x_{\frac{1}{2}}$ is called a *median* of the distribution. The median is generally defined as a real number; for a strictly increasing cumulative probability function, it is uniquely given by the equation $F(x_{\frac{1}{2}}) = \frac{1}{2}$; otherwise, we can find an interval with all points $x_{\frac{1}{2}} \in [a_{\frac{1}{2}}, b_{\frac{1}{2}}]$ being a median, which in particular occurs for all discrete distributions. By convention, we will always take the lower bound of this interval, which is always an allowed discrete value for ξ , as the median of a discrete distribution.

Probability density and cumulative probability distribution are obviously equivalent for expressing the properties of a random variable ξ , because they are uniquely related. We will therefore use the expression “distribution of ξ ” as the sample of all its properties, and we may use either a cumulative or a density function as its representation. It should be noted that the terms “random variable ξ ” and “distribution $f(\xi)$ ” express practically the same: A random variable is *defined* by its distribution. In practice this means that *any empirically or theoretically given distribution of events* — may it be count rates, energy or particle spectra, luminosity functions, or whatever — *can be used for the definition of a random variable describing the physical process which produced those distributions by means of statistical theory.*

Expectation values and moments: The *expectation value* $\langle f(\xi) | g(\xi) \rangle \equiv \langle g \rangle_\xi$ of a function ψ of a random variable ξ distributed with a density function $f(\xi)$ is defined by

$$\langle f(\xi) | \psi(\xi) \rangle = \int_{-\infty}^{\infty} \psi(\xi) f(\xi) d\xi = \int_{-\infty}^{\infty} \psi(\xi) dF(\xi) \quad . \quad (2.1.4)$$

The expectation value¹ of ξ itself, $m = \langle \xi \rangle$ is called the *mean* of the distribution, the expectation value of its k -th power, $\mu_k = \langle \xi^k \rangle$, is called its *k-th total moment*.² It should be noted that the moments are not defined for

¹In the following, the explicit notation of ξ as the random variable over which the expectation value is taken will be omitted if there is no danger of confusion. The same method will be applied to any other function related to ξ . On the other hand, the full notation $\langle f | g \rangle$ will be used if the functional properties of f are important.

²Lacking any better word, we use “total moment” as a short form of “moment about the origin”.

every distribution; to guarantee the existence of μ_k for all $k \in \mathbb{N}$, we have to require that either $f(\xi)$ vanishes outside some finite interval, or decreases at least as $e^{-|\xi|}$ for $\xi \rightarrow \infty$. Of particular meaning for the description of a distribution function are their *central moments*

$$\tilde{\mu}_k \equiv \langle (\xi - m)^k \rangle . \quad (2.1.5)$$

The connection between total and central moments is given by the equation

$$\tilde{\mu}_k = \sum_{j=0}^k \binom{k}{j} (-1)^{k-j} \mu_j m^{k-j} . \quad (2.1.6)$$

This formula also gives the transformation of the total moments of a distribution under a linear transformation of the random variable, $\xi' = a\xi + b$, if we replace μ_j by $a^j \mu_j$ and m by b . Obviously, the central moments transform just by $\tilde{\mu}'_k = a^k \tilde{\mu}_k$.

If $\psi(\xi)$ is a function of a random variable with distribution function $F(\xi)$, we will call $\langle \psi^k(\xi) \rangle_\xi$ the k -th moment of the random function ψ . Obviously, this notation is motivated by the fact that $v = \psi(\xi)$ is a random variable distributed by $G(v) = (F \circ \psi^\ominus)(v)$, if ψ is invertible. Differentiation of $G(v)$ and substitution of variables gives

$$\langle v^k \rangle_v = \langle \psi^k(\xi) \rangle_\xi . \quad (2.1.7)$$

It can be shown that this relation also holds if ψ is not invertible.

Dispersion and shape parameters: In general, a distribution function is fully described by the set of its moments. The second central moment is the *variance* $\tilde{\mu}_2 = \sigma^2$, where σ gives a measure of the *width* of $f(\xi)$ is called the *standard deviation* of ξ about m . Of the higher order moments, μ_3 and μ_4 are of specific importance and are usually expressed as the quantities

$$\gamma_1 = \frac{\mu_3}{\sigma^3} \quad \text{and} \quad \gamma_2 = \frac{\mu_4}{\sigma^4} - 3 ,$$

which are called *skewness* and *excess* of the distribution, respectively. A positive (negative) skewness expresses an asymmetric displacement of probability in favor of the positive (negative) wing of the distribution. The excess expresses the symmetrical displacement of probability between the center and to the wings of the distribution relative to the “normal”. However, for an asymmetric distribution this “degree of peaking” is determined by γ_1 as well as by γ_2 (see Sect. 2.1.2.4). Skewness and excess are the first members of a family of invariant parameters describing a distribution (see Sect. 2.1.1.2). In general discussions, the scaling dependent parameters m and σ are usually absorbed in the definition of the *standard variable*

$$\zeta = \frac{\xi - m}{\sigma} . \quad (2.1.8)$$

We will denote the *standardized distribution functions* by $\hat{f}(\zeta) \equiv f(\xi)$ and $\hat{F}(\zeta) \equiv F(\xi)$. Since ζ gives the deviation of ξ from its mean in terms of σ , ζ may be used as the quantum and σ as the unit of dispersion. The meaning of the higher order parameters γ_i is discussed in the next section.

Quantiles and confidence intervals: The median $x_{\frac{1}{2}}$ of a random distribution belongs to a class of parameters, which are called *quantiles*. The *standard p -quantile* ζ_p is defined by

$$\mathcal{P}(\zeta \leq \zeta_p) = \hat{F}(\zeta_p) \doteq p \quad , \quad (2.1.9)$$

where p expresses a specific probability value. In physics it is common to call $\xi_p = m + \zeta_p \sigma$ the *p confidence limit*³, and accordingly the interval $[\xi_c^+, \xi_c^-]$, $\xi_c^\pm \equiv m \pm \zeta_c \sigma$, is called a *p -confidence interval* if $\mathcal{P}(|\zeta| \leq \zeta_c) = p$. Quantiles give therefore the connection between dispersion and probability: for a distribution with known mean and variance, we can express any cumulative probability (confidence) limit by its according dispersion limit, which is expressed as $\zeta_p \sigma$.

Clearly, the connection between p and ζ_p is dependent on the shape of the distribution. The requirement of the existence of a finite σ , however, sets an upper limit on ζ_p , which is expressed by the Chebyshev-inequality

$$\mathcal{P}(|\zeta| \geq \zeta_p) \leq \frac{1}{p^2} \quad \text{for all } p \quad . \quad (2.1.10)$$

From this we can easily derive the limit $\zeta_p \leq 1/\sqrt{1-p}$. As long we do not know more about a distribution than its mean and variance, no better restrictions can be given for its confidence limits. To give a numerical example: If confidence of 99% is required, a random variable with arbitrary distribution (but finite dispersion) can only be restricted to values $\xi < m + 10\sigma$. If we require the existence of all moments, the exponential function $e^{-|\xi|}$ sets an asymptotic limit to the probability density, which leads to the upper limit estimate

$$\zeta_p \lesssim \ln \left(\frac{1}{1-p} \right) \quad , \quad (2.1.11)$$

which, however, is only asymptotically correct and can therefore only be used for estimates of the allowed dispersion. In the above example of a 99% confidence limit this leads to the estimate $\xi \lesssim m + 4.5\sigma$. We will return to the discussion of confidence limits and dispersion measure at the end of Sect. 2.1.1.3.

2.1.1.2 Generating functions and the cumulants

The moment generating function $M_\xi(s)$: The set of moments of a theoretically defined distribution can be expressed in a single function, called the *moment generating function (m.g.f)* of the random variable ξ . It is defined by

$$M_\xi(s) = \langle e^{\xi s} \rangle \quad , \quad (2.1.12)$$

with the k -th derivative $\langle \xi^k e^{\xi s} \rangle$, and therefore

$$\mu_k = M_\xi^{(k)}(0) = \left. \frac{\partial^k M_\xi(s)}{\partial s^k} \right|_{s=0} \quad . \quad (2.1.12a)$$

In the literature, many variations of generating functions are used. The most common one is the complex valued counterpart $C_\xi(s) = M_\xi(is)$, which is called the *characteristic function* of ξ . Other than $M(s)$, $C(s)$ is bounded for all real ξ ; in the applications relevant here, $C(s)$ and $M(s)$ are equally useful, only that $M(s)$ allows for a simpler notation. For discrete distributions, the *probability generating function* $G_\xi(z) = \langle z^\xi \rangle_\xi = M_\xi(\ln z)$ is often used. Here, the moments are simple functions of the derivatives $G^{(k)}(1)$, but not given as directly as in Eq. (2.1.12a). Obviously we have $M(0) = C(0) = G(1) = 1$. We also note the simple relation of $M_\xi(s)$ to the Laplace transform of f , f^* , by $M_\xi(s) = f^*(-s)$, and that $C(s)$ is nothing but its Fourier transform.

³ p is usually expressed in percent, i.e., we say “ $(p \times 100)\%$ confidence limit”.

The cumulants and the invariant parameters: Of particular interest for the description of probability distribution functions is the *cumulant generating function* (c.g.f.)

$$\chi_\xi(s) = \ln M_\xi(s) \quad ; \quad (2.1.13)$$

its j -th derivative, taken at the origin,

$$\kappa_j \equiv \chi_\xi^{(j)}(0) = \left. \frac{\partial^j \ln M_\xi(s)}{\partial s^j} \right|_{s=0} \quad (2.1.13a)$$

is called the j -th *cumulant* κ_j of the distribution $F(\xi)$. The cumulants are also called the *semi-invariants* of a distribution; for a linear transformation of the random variable $\xi' = a\xi + b$, we have $\kappa'_j = a^j \kappa_j + b\delta_{1j}$, where δ_{1j} is the Kronecker-Symbol. In particular, we find for the standard variable ζ that $\hat{\kappa}_1 = 0$, $\hat{\kappa}_2 = 1$ and $\hat{\kappa}_j = \kappa_j/\sigma^j$. This gives rise to the definition

$$\gamma_i \equiv \hat{\kappa}_{i+2} = \frac{\kappa_{i+2}}{\sigma^{i+2}} \quad (2.1.14)$$

The parameters γ_i are obviously invariant under linear transformations of the random variable, and they give the cumulants of $\hat{F}(\zeta)$, $\hat{\kappa}_j$, for $j \geq 3$. From Eqs. (2.1.15c) and (2.1.15d) in the next paragraph we see that γ_1 and γ_2 defined by Eq. (2.1.14) are the earlier defined coefficients for skewness and excess. The parameters γ_i determine the shape of a distribution independent of scaling.

Relations between cumulants and moments: If a distribution is not analytically given, the cumulants cannot be calculated using Eq. (2.1.13a). However, an explicit calculation of the moments, $\mu_k = \langle \xi^k \rangle$, allows a determination of the cumulants. The relation of the cumulants to the moments of $F(\xi)$ is given by

$$\kappa_1 = \mu_1 = m \quad (2.1.15a)$$

$$\kappa_2 = \mu_2 - \mu_1^2 = \sigma^2 \quad (2.1.15b)$$

$$\kappa_3 = \mu_3 - 3\mu_2\mu_1 + 2\mu_1^3 = \tilde{\mu}_3 \quad (2.1.15c)$$

$$\kappa_4 = \mu_4 - 4\mu_3\mu_1 - 3\mu_2^2 + 12\mu_2\mu_1^2 - 6\mu_1^4 = \tilde{\mu}_4 - 3\sigma^4 \quad (2.1.15d)$$

$$\kappa_5 = \mu_5 - 5\mu_4\mu_1 - 10\mu_3\mu_2 + 20\mu_3\mu_1^2 + 30\mu_2^2\mu_1 - 60\mu_2\mu_1^3 + 24\mu_1^5 \quad (2.1.15e)$$

The inverse relations to the total moments can be important for theoretical considerations and are given by

$$\mu_1 = \kappa_1 \quad (2.1.16a)$$

$$\mu_2 = \kappa_2 + \kappa_1^2 \quad (2.1.16b)$$

$$\mu_3 = \kappa_3 + 3\kappa_2\kappa_1 + \kappa_1^3 \quad (2.1.16c)$$

$$\mu_4 = \kappa_4 + 4\kappa_3\kappa_1 + 2\kappa_2^2 + 6\kappa_2\kappa_1^2 + \kappa_1^4 \quad (2.1.16d)$$

$$\mu_5 = \kappa_5 + 5\kappa_4\kappa_1 + 10\kappa_3\kappa_2 + 10\kappa_3\kappa_1^2 + 15\kappa_2^2\kappa_1 + 10\kappa_2\kappa_1^3 + \kappa_1^5 \quad (2.1.16e)$$

There is barely a reason to include higher order moments or cumulants in the description of a distribution, which will become clear in Sect. 2.1.2.4.

2.1.1.3 Some special distributions

The Dirac- δ distribution: The simplest possible distribution is also the most abstract one: It is the distribution function of a random variable which has *certainly* a specific value a — i.e. it is the degenerate case of a “probability” distribution function with $\mathcal{P}(\xi = a) = 1$. Obviously, according to Eq. (2.1.1) the cumulative distribution is a step function, $F(x) = \text{Hs}(x - a)$; the corresponding probability density function satisfying Eq. (2.1.2) is the *Dirac- δ* function, defined by

$$\int_{-\infty}^{\infty} d\xi \delta(\xi - a)\varphi(\xi) = \varphi(a) \quad (2.1.17)$$

for any smooth function φ . Setting $\varphi(\xi) = e^{\xi s}$, we find the m.g.f., $M_\delta(s) = e^{as}$, yielding $\mu_k = a^k$. Obviously, all central moments vanish, and therefore $\sigma = 0$ and all $\gamma_i = 0$.

The great relevance of the Dirac-function in distribution theory arises not only from being the density function expressing “certainty”, but also from its property to transform continuous distributions into discrete distributions. Inserting the density function

$$f(\xi) = \sum_k p_k \delta(\xi - k) \quad (2.1.18)$$

into Eq. (2.1.2) yields Eq. (2.1.3); thus, Eq. (2.1.18) is a discrete probability density function defined on a continuous random variable.

The uniform distribution: The δ distribution expresses that a continuous random variable is certainly (or with some weighting probability p_k) identical to a specific value a . In reality, however, we will be rather confronted with the case that ξ is certainly inside an interval $[a, b]$. Lacking better knowledge about the distribution of ξ , the first order estimate will generally be a *uniform distribution* over this interval. Transforming to a unified random variable, $v = (\xi - a)/(b - a)$, the unified probability density function is

$$\check{f}_u(v) = \begin{cases} 1 & : 0 \leq v \leq 1 \\ 0 & : \text{otherwise} \end{cases}, \quad (2.1.19a)$$

and the unified cumulative distribution function is⁴

$$\check{F}_u(v) = \begin{cases} 0 & : v < 0 \\ x & : 0 \leq v \leq 1 \\ 1 & : v > 1 \end{cases}. \quad (2.1.19b)$$

For the unified m.g.f. we find

$$\check{M}_u(s) = \frac{e^s - 1}{s}, \quad (2.1.19c)$$

leading to the unified moments $\check{\mu}_k = (1 + k)^{-1}$. With Eq. (2.1.6) we find $\check{\mu}_k = \check{\mu}_k/2^k$ for k even, and $\check{\mu}_k = 0$ for k odd. The cumulants are given by $\kappa_k = B_k/k$ for $k > 1$, where B_k are the *Bernoulli numbers*; the first non-vanishing cumulants are $\kappa_2 = \frac{1}{12}$ and $\kappa_4 = -\frac{1}{120}$, leading to the basic parameters

$$\check{m} = \frac{1}{2}; \quad \check{\sigma} = \frac{1}{2\sqrt{3}}; \quad \gamma_2 = -\frac{6}{5}.$$

and $\gamma_1 = \gamma_3 = 0$. We immediately see that the standard deviation the non-unified random variable ξ , which is uniformly distributed over a width $2h = b - a$, is $\sigma = h/\sqrt{3}$. We also note that the absolute value of γ_i increases with i . Since the uniform distribution is symmetric, its median is equal to its mean.

⁴Note the difference to the standardized distributions, \hat{f} and \hat{F} .

The saw-tooth distribution: The uniform distribution is symmetrical about its mean, all odd central moments vanish. For some applications we may ask for the “we-don’t-know-better” form of a *maximally asymmetric* distribution. This is obviously realized by a saw-tooth density function, whose unified form is given by

$$\check{f}_s(v) = 2v\check{f}_u(v) \quad ; \quad (2.1.20a)$$

the corresponding unified cumulative distribution function is $\check{F}_s(v) = v^2$ in the interval $[0, 1]$, and $\check{F}_s(v) = \check{F}_u(v)$ otherwise. For the unified m.g.f. we find

$$\check{M}_s(s) = \frac{2}{s^2}[(s-1)e^s + 1] = 2\check{M}'_u(s) \quad . \quad (2.1.20b)$$

From the simple connection to the uniform distribution, the unified total moments are easily found as $\check{\mu}_k = 2(k+2)^{-1}$, but there is no simple general expression for $\check{\mu}_k$ and κ_k ; the low-order parameters are here

$$\check{m} = \frac{2}{3} \quad ; \quad \check{\sigma} = \frac{1}{3\sqrt{2}} \quad ; \quad \gamma_1 = -\frac{2\sqrt{2}}{5} \quad ; \quad \gamma_2 = -\frac{3}{5} \quad ; \quad \gamma_3 = -\frac{12\sqrt{2}}{7} \quad .$$

We note that the even γ_i are smaller in absolute value than the odd and seem to decrease; however, for larger i there is a general tendency of $|\gamma_i|$ to increase. The median of the saw-tooth distribution can be found as $\check{x}_{\frac{1}{2}} = 1/\sqrt{2}$. Turning back to the non-unified random variable ξ and dividing the interval $[a, b]$ into three parts, $3h = b - a$, we have $m = a + 2h$ and $\sigma = h/\sqrt{2}$, and the median satisfies $x_{\frac{1}{2}} = a + 3\sigma$.

The exponential distribution: As the last form of a continuous distribution of a particularly simple shape we discuss the exponential distribution, which is defined by the density function

$$f_e(\xi; a, b) = \frac{1}{b} \exp\left(\frac{\xi - a}{b}\right), \quad \text{for } \xi \geq a, \quad (2.1.21a)$$

and $f_e(\xi; a, b) = 0$ for $\xi < a$. We easily derive its mean and standard deviation as $m = a + b$ and $\sigma = b$; introducing the standard variable ζ as defined in Eq. (2.1.8), we find for $\zeta \geq -1$

$$\hat{f}_e(\zeta) = \exp(-\zeta - 1) \quad (2.1.21b)$$

$$\hat{F}_e(\zeta) = 1 - \exp(-\zeta - 1) \quad (2.1.21c)$$

and $\hat{f}_e(\zeta) = \hat{F}_e(\zeta) = 0$ for $\zeta < -1$. From this we find for the standardized median $\zeta_{\frac{1}{2}} = \ln 2 - 1$, giving the approximate relation $x_{\frac{1}{2}} \approx m - 0.3\sigma$. The c.g.f. is easily found as

$$\chi(s) = (m - \sigma)s - \ln(1 - \sigma s) \quad , \quad (2.1.21d)$$

leading to the simple expression

$$\gamma_i = (i + 1)! \quad . \quad (2.1.21e)$$

Since the invariant parameters γ_i determine uniquely the shape of a distribution, we can use Eq. (2.1.21e) as a signature for the exponential distribution, and the ratio $\gamma_i/(i + 1)!$ may be used as measure of the convergence of a given distribution to the exponential.

The binomial distribution: A simple case where a theoretical distribution can be derived is the *counting statistics* problem: If we consider a limited number of N trials, and assume that p is the probability in each trial to give a desired result and set $q = 1 - p$ as probability that the trial fails, then the probability to find this result k times is given by the probability density of the *binomial distribution*

$$f_B(k; N, p) = \binom{N}{k} p^k q^{N-k} . \quad (2.1.22a)$$

There is no closed form for the cumulative distribution function, which is obtained by inserting Eq. (2.1.22a) into Eq. (2.1.3). The m.g.f. is

$$M_B(s; N, p) = [1 + p(e^s - 1)]^N . \quad (2.1.22b)$$

Mean and variance of the binomial distribution are $m = Np$ and $\sigma^2 = Npq$, and the lowest order parameters are given by

$$\gamma_1 = \frac{1 - 2p}{\sqrt{Npq}} ; \quad \gamma_2 = \frac{1 - 6pq}{Npq} ; \quad \gamma_3 = \frac{(1 - 2p)(1 - 12pq)}{\sqrt{Npq}^3} .$$

As the uniform distribution in the continuous case, the binomial distribution is the generic discrete distribution. It only expresses the combinatorial possibilities of a counting experiment for a *limited number of trials*. The extension to an unlimited for the number of trials is discussed in the next paragraph.

The Poisson distribution and the Gamma distribution: We consider a binomial distribution in the limit $N \rightarrow \infty$, $p \rightarrow 0$, but $Np \rightarrow r \neq 0$; we get the case where in principle an unlimited number of occurrences is possible, but only a small value r (not necessarily an integer) is expected; the binomial distribution transforms into the *Poisson distribution*, for which the probability density reads

$$f_P(k; r) = \frac{r^k}{k!} e^{-r} . \quad (2.1.23a)$$

Obviously we have $f_P(n, r) \approx 0$ for $n \gg r$. We may point out the interesting fact that both $\sum_n f_P(n; r) = 1$ for fixed r , and $\int f_P(n; r) dr = 1$ for fixed n ; hence, we may define two kinds of cumulative probabilities for the Poisson distribution: The probability of up to k occurrences for a *given* expectation of r

$$F_P(k; r) = e^{-r} \sum_{j=0}^k \frac{r^j}{j!} = Q(k+1, r) , \quad (2.1.23b)$$

and the probability of an expectation less than r for k *known* occurrences

$$\tilde{F}_P(r; k) = \frac{1}{k!} \int_0^r e^{-t} t^k dt = P(k+1, r) , \quad (2.1.23c)$$

where P and Q are the *incomplete Gamma functions* defined by

$$P(a, x) \equiv \frac{1}{\Gamma(a)} \int_0^x e^{-t} t^{a-1} dt$$

$$Q(a, x) \equiv \frac{1}{\Gamma(a)} \int_x^\infty e^{-t} t^{a-1} dt = 1 - P(a, x) .$$

Each F_P and \tilde{F}_P correspond to a different question about a counting experiment; the former is a distribution of occurrences, the latter a distribution of expectations. We immediately see that there seems to be a simple

connection between both questions, because we have $F_P(k; r) + \tilde{F}_P(r; k) = 1$, in other words, F_P and \tilde{F}_P express complementary probabilities. We will return to this point in Sect. 2.2.1.3. When we speak of the Poisson distribution, we will always mean $F_P(k; r)$, i.e. we take k as the random variable and r as a fixed parameter. The distribution $F_T(r; a) = P(r, a)$ is called the *Gamma distribution*, which is also defined for non-integer a .

The m.g.f. of the Poisson distribution is

$$M_P(s) = e^{-r} \exp(re^s) \quad . \quad (2.1.23d)$$

We find that $\mu_1 = r$ and $\mu_2 = r(r + 1)$, but no simple general formula for the moments. However, $\chi_P(s) = r(e^s - 1)$ has a particularly simple form, and we find that the cumulants are

$$\kappa_j = r \quad \text{for all } j \text{ .}$$

This leads to the basic parameters

$$m = r \quad ; \quad \sigma = \sqrt{r} \quad ; \quad \gamma_i = r^{-i/2} \quad .$$

The Poisson distribution is a discrete distribution; nevertheless, the cumulative probability distribution functions, Eqs. (2.1.23), and the probability density function, Eq. (2.1.23a), can be principally defined as continuous functions by the transition $k! \rightsquigarrow \Gamma(k + 1)$. However, integrating over the continuized Poisson density function does *not* give the correct cumulative probability, $\int_0^n f_P(a; r) da \neq Q(n + 1, r)$; rather, we find

$$\int_0^{n+\frac{1}{2}} da f_P(a; r) \approx F_P(n; r) \quad .$$

Thus, continuous and discrete probability functions behave quite different and have to be carefully distinguished, which turns out to be a problem when compound continuous and discontinuous distributions have to be considered.

In contrast to the Poisson distribution, the Gamma distribution, $F_T(r, a)$, is continuously defined, both for its random variable and its parameter. Its c.g.f. is

$$\chi_T(s) = -a \ln(1 - s) \quad , \quad (2.1.24)$$

leading to $\kappa_j = a(j - 1)!$ and $\gamma_i = a^{-i/2}(i + 1)!$. Obviously, the Gamma distribution is closely connected to the exponential distribution.

The Gaussian distribution: The *Gaussian normal* or simply *normal* probability density function is given as

$$f_G(\xi, m, \sigma) = \frac{1}{\sigma\sqrt{2\pi}} \exp\left\{-\frac{(\xi - m)^2}{2\sigma^2}\right\} \quad , \quad (2.1.25a)$$

leading to the cumulative distribution function

$$F_G(\xi, m, \sigma) = \frac{1}{2} \left\{ 1 + \operatorname{erf}\left(\frac{\xi - m}{\sigma\sqrt{2}}\right) \right\} \quad , \quad (2.1.25b)$$

where the *error function*, $\operatorname{erf}(x)$, is defined by

$$\operatorname{erf}(x) = \frac{2}{\sqrt{\pi}} \int_0^x \exp(-t^2) dt \quad .$$

For the m.g.f. we find

$$M_G(s) = \exp \left\{ ms + \frac{1}{2} \sigma^2 s^2 \right\} . \quad (2.1.25c)$$

From this we immediately find that $\mu_1 = m$ and $\tilde{\mu}_2 = \sigma^2$; m and σ are the mean and standard deviation of the normal distribution. We also see from $\chi(s) = ms + \frac{1}{2} \sigma^2 s^2$ that all cumulants κ_j for $j > 2$ vanish; therefore we have $\gamma_i = 0$ for all i . This property makes the normal distribution to a “simple” distribution of a particular kind: *it is the generic distribution of a random variable with mean m and standard deviation σ .*

In Sect. 2.1.2 we will discuss the specific role of the Gaussian distribution for theoretical and applied statistics. Because of its importance, we introduce a special notation for the distribution functions of the standard variable ζ :

$$\Phi(\zeta) = \frac{1}{2} \left\{ 1 + \operatorname{erf} \left(\frac{\zeta}{\sqrt{2}} \right) \right\} \quad (2.1.26a)$$

$$\phi(\zeta) = \frac{1}{\sqrt{2\pi}} \exp \left(-\frac{\zeta^2}{2} \right) . \quad (2.1.26b)$$

The derivatives of $\phi(\zeta)$ are given by the simple relation

$$\phi^{(n)}(\zeta) = (-1)^n \phi(\zeta) H_n(x) , \quad (2.1.27)$$

where $H_k(x)$ are the *Hermite polynomials* defined by⁵

$$H_n(x) = n! \sum_{k=0}^{[n/2]} \frac{(-1)^k x^{n-2k}}{2^k k! (n-2k)!} . \quad (2.1.27a)$$

The Hermite polynomials for $k \leq 5$ are $H_1(x) = x$, $H_2(x) = x^2 - 1$, $H_3(x) = x^3 - 3x$, $H_4(x) = x^4 - 6x^2 + 3$ and $H_5(x) = x^5 - 10x^3 + 15x$.

Normal dispersion and confidence limits: The property of the normal distribution to be the “generic m - σ ” distribution gives it a special role in the discussion of confidence limits. We call the “normal standard p -quantile” ς_p , defined by $\Phi(\varsigma_p) = p$; in a normal distribution, it gives the upper limit in dispersion, $\xi_p = m + \varsigma_p \sigma$ corresponding to the confidence level p . Since the correspondence of quantiles to confidence values is unique, ς_p can be used as the *normal measure for confidence*, and is expressed in units of normal standard deviation, called *Gaussian Sigmas*.⁶ The numerical values of confidence the first integer normal standard quantiles, $p_n = \Phi(n)$ for $n \leq 4$, are 84.13%, 97.72%, 99.87 and 99.997%; the values of ς_p for the frequently used confidence levels 90%, 99% and 99.9% are 1.282, 2.326 and 3.09, respectively. If deviation from the mean should be restricted in both directions, the normal confidence intervals $[-\varsigma_c, \varsigma_c]$ with $C = \mathcal{P}(|\zeta| \leq \varsigma_c) = \Phi(\varsigma_c) - \Phi(-\varsigma_c)$ are used. The well known numerical values of confidence C_n for integer $\varsigma_c \leq 4$ are 68.29%, 95.45%, 99.73% and 99.99%.

In physics it is common to use the “Gaussian Sigmas” as a measure for confidence estimation; this is justified by the Central Limit Theorem, which states that the distribution of a large sample of independent observations

⁵In the literature different definitions of the Hermite polynomials may be used. A collection of all possible definitions is given by Abramowitz and Stegun [AS65], who denote the definition used here with $He_n(z)$.

⁶To be compatible with the usual language of physicists, we will use the notation *Sigma* for the Gaussian standard deviation measure, used as a *unit* for confidence levels. It has to be strictly distinguished from the symbol “ σ ”, which denotes the standard deviation of any distribution under consideration.

tends to be normal (see Sect. 2.1.2.3). In the general case, however, the normal dispersion ς_p for a given p is rather a *minimum estimate*. The upper limits are given by Chebyshev's inequality Eq. (2.1.10), and the exponential estimate derived from the requirement of the existence of all moments gives also much weaker restrictions to the allowed dispersion, and is for many distributions a better estimate than the normal dispersion.

2.1.1.4 Operational definition of distributions

Probability distributions, operators and generalized functions: In Sect. 2.1.1.1 we have introduced the notation $\langle f | \varphi \rangle$ alternatively to $\langle \varphi \rangle_\xi$ for the expectation value of a function φ of a random variable ξ with distribution f . We also have noticed that (as long only one random variable is considered) the usage of f and ξ is synonym, because f gives the definition of ξ as a random variable; this property distinguishes f from any other function of ξ . Thus, $f(\xi)$ has rather the meaning of a functional operating on functions of ξ , which is expressed by the notation $\langle f(\xi) | \varphi(\xi) \rangle$. Even if f can generally be written as a locally defined function of ξ , it is rather defined by global properties. The theory of *generalized distributions*⁷ uses only global operations of distributions to define their properties. For probability distributions, the moments or cumulants are examples for their global properties. Distributions which can be written as ordinary functions are called regular distributions; the general algebraic and analytic relations which can be found for them are then used for the definition of *non-regular* distributions, as, i.e. the Dirac- δ function.

In the theory of generalized functions, some special restrictions are applied to the set of functions on which a generalized function acts: the *test-functions* $\varphi(\xi)$ must be (i) infinitely differentiable, and (ii) vanish identically outside a finite interval. The latter restriction, called the requirement of *compact support*, guarantees that the integral Eq. (2.1.4) always exists for locally integrable distributions $f(\xi)$. However, we may use the notation $\langle f | \psi \rangle$ also for functions which do not have a compact support and may not even be convergent, as we already did in the definition of the moments. Here, we apply special requirements to the distribution f to guarantee that $\langle f | \psi \rangle$ exists. A generalized function, which should be interpreted as a probability density function, must obviously satisfy the relation $\langle f | \mathbb{1} \rangle = 1$. Moreover, a probability density function expressing the distribution of a physical parameter will always have a compact support itself, because no physical quantity can be distributed over infinite intervals. When mathematical distributions are considered, we will force the existence of the moment generating function $\langle f | e^{\xi s} \rangle$. The only non-regular distribution of practical importance, the Dirac- δ distribution, even has a singular support. Therefore, we can completely reject the requirement of a compact support of the test-function, and restrict ourselves to the requirement of infinite smoothness.

Calculus of abstract distributions: A generalized distribution is defined as a real-valued, linear functional $\langle f | \cdot \rangle$, operating on set of test functions D . Linearity is expressed by the relation

$$\langle f | \sum_i c_i \varphi_i \rangle = \sum_i c_i \langle f | \varphi_i \rangle \quad .$$

In the context of probability theory, we will always require that any distribution f is uniquely connected to a random variable ξ ; if required for unambiguity, we use the functional notation $f(\xi)$. Other functions which depend on ξ are treated as regular, infinitely differentiable functions. Any functions which are not dependent on ξ can be treated as constants in the distribution calculus. We will not assume that test functions have a compact support, but only that $\varphi(\xi)e^{-|\xi|} \rightarrow 0$ for $|\xi| \rightarrow \infty$. Distributions will generally be understood as probability

⁷One usually says *generalized functions* or *distributions* in this context. Since we want to use (random) distributions in the sense of generalized functions, we say *generalized distributions*.

density functions with finite moments to arbitrary order, i.e. $\langle f | \mathbb{1} \rangle = 1$ and $\langle f(\xi) | e^{\xi s} \rangle < \infty$; this is in particular the case when f has compact support. In the following, the integer indexed symbols f_i will denote distributions of a random variable ξ ; $\varphi_i \equiv \varphi_i(\xi_i)$ denote test functions, $\psi_i = \psi_i(\xi_i)$ other functions which are not distributions, and c_i constants; the index may be omitted in all cases, if only one symbol of a certain kind is used.

The following relations are all motivated by Eq. (2.1.4), which is valid for regular distributions; for non-regular distributions, these relations *define* their properties. Usually, a random variable is uniquely connected to its distribution; however, it can be sensible to speak of sums of distributions of the *same random variable* ξ , if its properties are itself subject of a random distribution. In this case, one may have a sequence of mutually excluding distributions $f_i(\xi)$, which satisfy the linearity relation

$$\langle \sum_i f_i | \varphi \rangle = \sum_i \langle f_i | \varphi \rangle \quad . \quad (2.1.28a)$$

There is no general definition for the product of distributions of the *same* random variable; however, there is also no meaning attached to it, because there is no factorization rule for the distribution of a random variable. Multiplication with numbers and other functions are defined by

$$\langle cf | \varphi \rangle = c \langle f | \varphi \rangle \quad (2.1.28b)$$

$$\langle \psi f | \varphi \rangle = \langle f | \psi \varphi \rangle \quad . \quad (2.1.28c)$$

For Eq. (2.1.28c) we have to set some additional requirements on the function ψ , if neither f nor φ have a compact support; obviously, $\psi \varphi$ must be a test function in the same manner as φ itself. The transformation of random variables is expressed in the relation

$$\langle f \circ \psi^\ominus | \varphi \rangle = \langle |\psi'| f | \varphi \circ \psi \rangle \quad (2.1.28d)$$

for any function ψ which is invertible over the support of f . From this relation, by setting $\varphi = \mathbb{1}$ we can easily see that the probability density function of a random variable $v = \psi(\xi)$, $g(v)$, is given by $g = (f \circ \psi^\ominus) / |\psi'|$, when $f(\xi)$ is the probability density function of ξ ; inserting this result into Eq. (2.1.28d) we find

$$\langle g(v) | \varphi \rangle = \langle f(\xi) | \varphi \circ \psi \rangle \quad \text{for } v = \psi(\xi) ,$$

which is nothing but the operational formulation of Eq. (2.1.7) for $\varphi(v) = v^k$.

Applying the rule of partial integration to Eq. (2.1.4) we find that the n -th derivation of a distribution can be defined by

$$\langle f^{(n)} | \varphi \rangle = (-1)^n \langle f | \varphi^{(n)} \rangle \quad . \quad (2.1.28e)$$

It should be noted that Eq. (2.1.28e) relates the derivation of the left side of a functional to the derivation of its right side; in particular it is $\langle \psi f^{(n)} | \varphi \rangle = (-1)^n \langle f | (\psi \varphi)^{(n)} \rangle$, and *not* $(-1)^n \langle f | \psi \varphi^{(n)} \rangle$. Of course, if f can be represented by a regular function, its derivative is much easier derived in the usual way than by applying Eq. (2.1.28e); this equation is only of practical use when non-regular distributions like δ functions are involved.

Properties of the Dirac-function: From Eq. (2.1.28) we can derive some useful properties of the Dirac- δ function, which we have introduced in Sect. 2.1.1.3 as the probability density function of the one-point distribution; its general definition reads

$$\langle \delta | \varphi \rangle \equiv \varphi(0) \quad .$$

Using the functional notation $\delta(\psi(x)) \equiv (\delta \circ \psi)(\xi)$ and choosing $\psi(\xi) = \xi - a$, Eq. (2.1.28d) yields the well known relation $\langle \delta(\xi - a) | \varphi(\xi) \rangle = \varphi(a)$, which is equivalent to the definition Eq. (2.1.17) used before. We can easily confirm the relations

$$\delta(-\xi) = \delta(\xi) \quad (2.1.29a)$$

$$\psi(\xi) \delta(\xi - a) = \psi(a) \delta(\xi - a) \quad (2.1.29b)$$

Eq. (2.1.28e) yields for the derivatives of the δ function

$$\langle \delta^{(n)}(\xi - a) | \varphi \rangle = (-1)^n \varphi^{(n)}(a) \quad (2.1.29c)$$

$$\psi(\xi) \delta^{(n)}(\xi - a) = (-1)^n \sum_{i=0}^n \binom{n}{i} \psi^{(n-i)}(a) \delta^{(i)}(\xi - a) \quad ; \quad (2.1.29d)$$

if ψ has m simple zeros a_1, \dots, a_m , we have

$$\delta(\psi(\xi)) = \sum_{i=1}^m \frac{\delta(\xi - a_i)}{|\psi'(a_i)|} \quad , \quad (2.1.29e)$$

which is a simple result of Eq. (2.1.28d). There is no consistent definition for $\delta(\psi(x))$ if $\psi(x)$ has higher order zeros.

2.1.2 Multidimensional probability spaces and joint distributions

2.1.2.1 Uncorrelated random variables and the probability space

Connected, correlated and independent random events: Up to now, we only dealt with *one* random variable. It is obvious that many practical problems involve more than one random characteristic. Consider two events \mathcal{E}_1 and \mathcal{E}_2 , and assume that \mathcal{E}_1 precedes \mathcal{E}_2 : In the simplest case, \mathcal{E}_1 and \mathcal{E}_2 are *connected*, what means that we *know the result* of \mathcal{E}_2 in the moment we get knowledge about \mathcal{E}_1 ; here \mathcal{E}_1 might *imply* \mathcal{E}_2 ($\mathcal{E}_1 \rightsquigarrow \mathcal{E}_2$), or *exclude* it ($\mathcal{E}_1 \wr \mathcal{E}_2$). If we call $\mathcal{P}(\mathcal{E}_1 \cap \mathcal{E}_2)$ the *joint probability* of \mathcal{E}_1 and \mathcal{E}_2 (i.e. the probability that both events occur), and $\mathcal{P}(\mathcal{E}_1 \cup \mathcal{E}_2)$ the *total probability* of \mathcal{E}_1 and \mathcal{E}_2 (i.e. the probability that either one of them occurs), we get the well-known relations

$$\begin{aligned} \mathcal{E}_1 \rightsquigarrow \mathcal{E}_2 &: \mathcal{P}(\mathcal{E}_1 \cap \mathcal{E}_2) = \mathcal{P}(\mathcal{E}_1) \quad ; \quad \mathcal{P}(\mathcal{E}_1 \cup \mathcal{E}_2) = \mathcal{P}(\mathcal{E}_2) \\ \mathcal{E}_1 \wr \mathcal{E}_2 &: \mathcal{P}(\mathcal{E}_1 \cap \mathcal{E}_2) = 0 \quad ; \quad \mathcal{P}(\mathcal{E}_1 \cup \mathcal{E}_2) = \mathcal{P}(\mathcal{E}_1) + \mathcal{P}(\mathcal{E}_2) \end{aligned}$$

These equations apply to different events related to *the same random variable*. If we relate the events to different random variables ξ_1 and ξ_2 , and find that *all* events $\mathcal{E}_1: \xi_1 \in]a_1, b_1]$ and $\mathcal{E}_2: \xi_2 \in]a_2, b_2]$ are connected, we can find a relation $\psi(\xi_1, \xi_2) = 0$. This case has already be treated in the last section.

A more interesting case is given if \mathcal{E}_1 does not tell us the result of \mathcal{E}_2 , but gives us additional information about the *probability of* \mathcal{E}_2 ; in this case, we will call the events *correlated* ($\mathcal{E}_1 \prec \mathcal{E}_2$). If not even this is the case, i.e. if the probability for \mathcal{E}_2 is unaffected by the occurrence of \mathcal{E}_1 , we will call them *independent* random events

$(\mathcal{E}_1 \parallel \mathcal{E}_2)$. In both cases, it is obviously not possible to reduce the problem to one random variable; rather, ξ_1 and ξ_2 span up a two-dimensional *probability space* \mathbb{P}^2 . This is easily generalized to the n -dimensional case: We will call the random variables ξ_1, \dots, ξ_n unconnected, if there exist n events $\mathcal{E}_1: \xi \in]a_1, b_1]$, \dots , $\mathcal{E}_n: \xi \in]a_n, b_n]$, which are pairwise unconnected. In this case, the random vectors $\mathbf{x} = (\xi_1, \dots, \xi_n)$ span up an n -dimensional probability space \mathbb{P}^n . The n -dimensional *joint distribution function* is defined as

$$F(\mathbf{a}) \equiv \mathcal{P}(\xi_1 \leq a_1 \cap \dots \cap \xi_n \leq a_n) \doteq \mathcal{P}(\mathbf{x} < \mathbf{a}) \quad . \quad (2.1.30)$$

We may formally speak of a m -dimensional space of random variables v_1, \dots, v_m , for which are restricted by k independent connection relations $\psi_k(v_1, \dots, v_m) = 0$; in this case, the probability space \mathbb{P}^n is a hypersurface of \mathbb{R}^m with dimension $n = m - k$.

Conditional probabilities and Bayes' theorem: If we consider a two-dimensional probability space $\mathbb{P}_2 = \{\xi_1, \xi_2\}$, it is useful to define for any two events, $\mathcal{E}_1: \xi_1 \in]a_1, x_1]$ and $\mathcal{E}_2: v \in]a_2, b_2]$, the *conditional probability* of \mathcal{E}_2 under the condition that \mathcal{E}_1 , by

$$\mathcal{P}(\mathcal{E}_2|\mathcal{E}_1) \equiv \frac{\mathcal{P}(\mathcal{E}_1 \cap \mathcal{E}_2)}{\mathcal{P}(\mathcal{E}_1)} \quad . \quad (2.1.31)$$

The requirement that \mathcal{E}_1 and \mathcal{E}_2 are unconnected is equivalent to $0 < \mathcal{P}(\mathcal{E}_2|\mathcal{E}_1) < 1$, while $\mathcal{P}(\mathcal{E}_2|\mathcal{E}_1) = 1$ means $\mathcal{E}_1 \rightsquigarrow \mathcal{E}_2$, and $\mathcal{P}(\mathcal{E}_2|\mathcal{E}_1) = 0$ is equivalent to $\mathcal{E}_1 \wr \mathcal{E}_2$. Since \mathcal{E}_1 and \mathcal{E}_2 can be interchanged in this Eq. (2.1.31), we get the relation

$$\mathcal{P}(\mathcal{E}_2 \cap \mathcal{E}_1) = \mathcal{P}(\mathcal{E}_2|\mathcal{E}_1)\mathcal{P}(\mathcal{E}_1) = \mathcal{P}(\mathcal{E}_1|\mathcal{E}_2)\mathcal{P}(\mathcal{E}_2) \quad . \quad (2.1.31a)$$

If we consider k events, $\mathcal{E}_{11}, \dots, \mathcal{E}_{1k}$, all related to ξ_1 , with $\mathcal{E}_{1i} \wr \mathcal{E}_{1j}$ for all pairs (i, j) and $\mathcal{P}(\bigcup_i \mathcal{E}_{1i}) = 1$, the *law of total probability*

$$\mathcal{P}(\mathcal{E}_2) = \sum_{i=1}^k \mathcal{P}(\mathcal{E}_2|\mathcal{E}_{1i}) \mathcal{P}(\mathcal{E}_{1i}) \quad (2.1.32)$$

relates the probability of \mathcal{E}_2 to that of the events \mathcal{E}_{1i} , and we can immediately derive from Eq. (2.1.31a)

$$\mathcal{P}(\mathcal{E}_{1j}|\mathcal{E}_2) = \frac{\mathcal{P}(\mathcal{E}_{1j})\mathcal{P}(\mathcal{E}_2|\mathcal{E}_{1j})}{\sum_i \mathcal{P}(\mathcal{E}_{1i})\mathcal{P}(\mathcal{E}_2|\mathcal{E}_{1i})} \quad . \quad (2.1.33)$$

This is known as *Bayes' theorem*, which proves to be a particularly useful tool for the reversion of conditional probabilities.

The idea of the conditional probability is easily extended to a n dimensional probability space. The joint probability of n unconnected events is then given by

$$\mathcal{P}(\mathcal{E}_1 \cap \dots \cap \mathcal{E}_n) = \mathcal{P}(\mathcal{E}_n | \mathcal{E}_{n-1} \cap \dots \cap \mathcal{E}_1) \dots \mathcal{P}(\mathcal{E}_2|\mathcal{E}_1)\mathcal{P}(\mathcal{E}_1) \quad . \quad (2.1.34)$$

Since the \mathcal{E}_i are principally interchangeable, the *conditional chain* Eq. (2.1.34) may be started with any \mathcal{E}_i and be continued over any path through all other events. However, the probabilities in the chain are generally different in all such permutations. In physical application, conditional probabilities often connect events occurring in a fixed time order, which then gives in any case a natural order to the conditional chain. If orderliness of this kind is given, we will say that the random variables ξ_1, \dots, ξ_n , related to $\mathcal{E}_1, \dots, \mathcal{E}_n$, span up an *orderly probability space* \mathbb{P}^n .

Independent random variables: Two random variables ξ_1 and ξ_2 are called *independent* if any two events $\mathcal{E}_1: \xi_1 \in]a_1, b_1]$ and $\mathcal{E}_2: \xi_2 \in]a_2, b_2]$ are independent. From our earlier characterization of independence of events and the definition of conditional probability, it is clear that two events \mathcal{E}_1 and \mathcal{E}_2 are independent if $\mathcal{P}(\mathcal{E}_2|\mathcal{E}_1) = \mathcal{P}(\mathcal{E}_2)$, which means that the joint probability satisfies the relation

$$\mathcal{P}(\mathcal{E}_1 \cap \mathcal{E}_2) = \mathcal{P}(\mathcal{E}_1)\mathcal{P}(\mathcal{E}_2) \quad . \quad (2.1.35)$$

This immediately leads to the following relation: The joint distribution function of n *independent random variables*, $F(\xi_1, \dots, \xi_n)$, and the corresponding probability density function $f(\xi_1, \dots, \xi_n)$ are related to the distribution and density functions of the single random variables as

$$F(\xi_1, \dots, \xi_n) = \prod_{i=1}^n F_i(\xi_i) \quad (2.1.35a)$$

$$f(\xi_1, \dots, \xi_n) = \prod_{i=1}^n f_i(\xi_i) \quad . \quad (2.1.35b)$$

In the simplest case all F_i are identical, i.e. we have n *identically distributed, independent random variables* and can write $F(\xi_1, \dots, \xi_n) = F^n(\xi)$. Obviously, the case of independent random variables is in so far related to the case of connected random variables that both cases can be reduced to the consideration of one-dimensional probability distributions. Interesting new aspects arise from the consideration of correlated random variables, which can be expressed as combinations of independent random variables (Sect. 2.1.2.3).

2.1.2.2 Random vectors and probability propagation

Multivariate distribution functions: There are two reasons to consider multidimensional distribution functions: First, a random event may be specified by an n -dimensional random vector in a physical space (e.g. a random point in space or phase space), or second, to describe the joint distribution of random variables in an n -dimensional probability space. The former case leads to the general discussion of multidimensional random variables, the latter emphasizes the connection to the one-dimensional distributions describing multivariate random functions defined on a probability space \mathbb{P}^n , which we may assume as orderly.

The probability density function of a vector of n unconnected random variables, $\mathbf{x} = (\xi_1, \dots, \xi_n)$, is given by

$$f(\mathbf{x}) = \frac{dF(\mathbf{x})}{d\mathbf{x}} \equiv \frac{\partial^n F(\mathbf{x})}{\partial \xi_1 \dots \partial \xi_n} \quad , \quad (2.1.36)$$

where the cumulative probability distribution function $F(\mathbf{a})$ is defined as in Eq. (2.1.30). The probability element $f(\mathbf{a}) d\mathbf{a}$ is the joint probability $\mathcal{P}(\mathcal{E}_1 \cap \dots \cap \mathcal{E}_n)$ of the events $\mathcal{E}_i: a_i \leq \xi_i \leq a_i + da_i$ for $i = 1, \dots, n$. The k -th moment of an n -dimensional random variable is a tensor of rank k defined by $\boldsymbol{\mu}_k = \langle f | \mathbf{x}^k \rangle$; in principle, all relations for the moments and the cumulants can be transformed straightforwardly to the multidimensional case by interpreting ordinary products as tensor products. Of specific importance are the *mean vector* $\mathbf{m} \equiv \boldsymbol{\mu}_1$ and the *covariance matrix* $\mathbf{A} \equiv \boldsymbol{\mu}_2$; the elements of \mathbf{A} can be written as $\lambda_{ii} = \sigma_i^2$ and $\lambda_{ij} = \sigma_i \sigma_j \rho_{ij}$ for $i \neq j$, where ρ_{ij} is known as the *correlation coefficient* of ξ_i and ξ_j ; for independent variables we have $\rho_{ij} = 0$ for all $i \neq j$, thus \mathbf{A} is diagonal. The change of variables by n relations $\xi_j = \psi_j(\mathbf{y})$ is performed by

$$g(\mathbf{y}) = f(\mathbf{x}) |\mathbf{J}| \quad , \quad (2.1.37)$$

where

$$\mathbf{J} = \det \left(\nabla_{\mathbf{y}} \mathbf{x} \right) \quad (2.1.37a)$$

is the *Jacobian* of the transformation.⁸

The expectation value of a real-valued function $\psi(\mathbf{x})$ is, according to Eq. (2.1.4), defined by

$$\langle f(\mathbf{x}) | \psi(\mathbf{x}) \rangle = \langle \psi \rangle_{\mathbf{x}} = \int_{\mathbb{P}} d\mathbf{x} f(\mathbf{x}) \psi(\mathbf{x}) \quad , \quad (2.1.38)$$

and in the same way one can define the moments of ψ by $\langle \psi^k \rangle_{\mathbf{x}}$. Obviously the function ψ defines a one-dimensional random variable $v = \psi(\mathbf{x})$ with a distribution function $G(y) = \int g(v) dv$ and the moments $\langle g | v^k \rangle = \langle \psi^k \rangle_{\mathbf{x}}$. Since the random variation of v is connected to the random variations of n variables ξ_i , we call $\psi(\mathbf{x})$ a *multivariate random function*. If there is a function connecting one dimension of the probability space \mathbb{P} uniquely with v , i.e. $\xi_j = \psi_j^{\ominus}(v, \mathbf{x}_{\setminus j})$, $g(v)$ can be derived from $f(\mathbf{x})$ by

$$g(v) = \int_{\mathbb{P}_{\setminus j}} d\mathbf{x}_{\setminus j} \left(\left| \frac{\partial \psi}{\partial \xi_j} \right|^{-1} f(\mathbf{x}) \right)_{\xi_j = \psi_j^{\ominus}(v, \mathbf{x}_{\setminus j})} \quad . \quad (2.1.39)$$

Even if ψ is not invertible in any dimension, one can get $g(v)$ by splitting of the probability space in pieces where ψ^{\ominus} locally exists and use the law of total probability. However, in many cases it may be advisable to calculate the moments of $g(v)$ by explicit integration of $\langle f(\mathbf{x}) | \psi^k(\mathbf{x}) \rangle$ and construct $g(v)$ in the way described in Sect. 2.1.2.4.

Marginal and conditional distributions: The joint probability of k events assigned to a random vector, $\mathbf{x}_{\leq k} = (\xi_1, \dots, \xi_k)$, in a probability subspace $\mathbb{P}_{\leq k} \subset \mathbb{P}^n$, is described by the *k-dimensional marginal probability density*

$$f_{\leq k}(\mathbf{x}_{\leq k}) \equiv \int_{\mathbb{P}_{> k}} d\mathbf{x}_{> k} f(\mathbf{x}) \quad , \quad (2.1.40)$$

which integrates over all dimensions of probability on which $f_{\leq k}$ does not depend; we will say that the dimensions with index $j > k$ are *reduced* in $f_{\leq k}$. Analogously we define the marginal probability density of one dimension

$$f_k(\xi_k) \equiv \int_{\mathbb{P}_{\setminus k}} d\mathbf{x}_{\setminus k} f(\mathbf{x}) \quad ; \quad (2.1.40a)$$

the corresponding distribution function $F_k(a) = \int^a f_k(\xi_k) d\xi_k$ gives the probability $\mathcal{P}(\xi_k \leq a)$ unaffected by the other dimensions of \mathbb{P} .

Reduction is one possibility to remove dimensions; the other is fixing certain ξ_k to specific values, which we will call *restriction*. The *conditional probability density*

$$f(\mathbf{x}_{\geq k} | \mathbf{c}_{< k}) = \frac{f(\mathbf{x})}{f_{< k}(\mathbf{c}_{< k})} \quad (2.1.41)$$

gives the joint probability $f(\mathbf{a}_{\geq k} | \mathbf{c}_{< k}) d\mathbf{a}_{> k} = \mathcal{P}(\mathcal{E}_k \cap \dots \cap \mathcal{E}_n | \mathcal{E}_1 \cap \dots \cap \mathcal{E}_{k-1})$ of the events $\mathcal{E}_i : a_i \leq \xi_i \leq a_i + da_i$ for $i \geq k$ after k events $\mathcal{E}_j : \xi_j = c_j$ have been fixed.

⁸In our notation, it is indeed $\nabla_{\mathbf{y}} \mathbf{x} \equiv (\partial x_i / \partial y_j)_{ij}$, because we understand the product between multidimensional objects as tensor products!

Propagators and Markov chains: We define the *restricted marginal probability density* by

$$f_{\leq k}(\xi_k | \mathbf{c}_{<k}) = \int_{\mathbb{P}_{>k}} d\mathbf{x}_{>k} f(\mathbf{x}_{\geq k} | \mathbf{c}_{<k}) \quad , \quad (2.1.42)$$

which corresponds to the distribution of the random variable ξ_k , restricted by fixing all ξ_i for $i < k$, and reduced for all ξ_j for $j > k$. The *conditional chain* given in Eq. (2.1.34) can then be written as

$$f(\mathbf{x}) = \prod_{k=1}^n f_{\leq k}(\xi_k | \mathbf{x}_{<k}) \quad , \quad (2.1.43)$$

setting $f_{<1}(\xi_1 | \mathbf{x}_{<1}) \equiv f_1(\xi_1)$. Eq. (2.1.43) can also be called a *prospective propagator chain* through \mathbb{P}^n , because every factor $f(\xi_k | \mathbf{x}_{<k})$ acts as a propagator of probability from subspace $\mathbb{P}_{<k}^n$ to $\mathbb{P}_{\leq k}^n$. The term “prospective” refers here to the assumption of a natural (time) order of the dimensions of \mathbb{P}^n . The propagators in Eq. (2.1.43) connect every state ξ_k of a propagating random system to its *history* c_1, \dots, c_{k-1} . A substantial simplification occurs if $f_{\leq k}(\xi_k | \mathbf{c}_{<k}) = f_{[k-1,k]}(\xi_k | c_{k-1})$; in this case, the conditional chain Eq. (2.1.43) is called a *Markov chain*, and we can define the *transition* or *Markov propagator*

$$\vec{f}(\xi_j, \xi_k) \equiv \int_{\mathbb{P}_{]j,k[}} d\xi_{j+1} \dots d\xi_{k-1} \prod_{j < i \leq k} f_{[i-1,i]}(\xi_i | \xi_{i-1}) \quad , \quad (2.1.44)$$

which connects uniquely the dimensions j and k of \mathbb{P}^n , and transforms one-dimensional marginal distributions as

$$f_k(\xi_k) = \int_{-\infty}^{\infty} d\xi_j f_j(\xi_j) \vec{f}(\xi_j, \xi_k) = \langle f_j(\xi_j) | \vec{f}(\xi_j, \xi_k) \rangle \quad . \quad (2.1.45)$$

Eq. (2.1.44) satisfies the symmetry relation

$$\vec{f}(\xi_j, \xi_k) = \langle \vec{f}(\xi_j, \xi_i) \vec{f}(\xi_i, \xi_k) \rangle_{\xi_i} \quad , \quad (2.1.46)$$

which is called the *Markov equation*. Since in a Markov chain there is no influence of the history on the propagation from ξ_j to ξ_k , the direction of time can be reversed and we can define a *retrospective propagator chain*. Prospective and retrospective propagators are connected by Bayes’ theorem

$$\vec{f}(\xi_k, \xi_j) = \frac{f_j(\xi_j) \vec{f}(\xi_j, \xi_k)}{\langle f_j(\xi_j) | \vec{f}(\xi_j, \xi_k) \rangle} \quad . \quad (2.1.47)$$

In a *homogeneous Markov chain* all one-step propagators $\vec{f}(\xi_k, \xi_{k+1})$ are identical, thus the general propagator $\vec{f}(\xi_j, \xi_k)$ is only dependent on the “jump-size”, $k - j$.

Formally, the Markov equation is a matrix multiplication chain, which becomes clear when we assume that the ξ_k are discrete random variables which can take only a finite number of states. We may therefore formally write the propagator $\vec{f}(\xi_j, \xi_k)$ as a transition matrix $\mathbf{T}_x(j, k)$, and use the simplified notation $\mathbf{T}_x(j) \equiv \vec{f}(\xi_{j-1}, \xi_j)$, the Markov equation reads $\mathbf{T}_x(j, k) = \mathbf{T}_x(j+1) \bullet \dots \bullet \mathbf{T}_x(i)$. In a homogeneous Markov chain is $\mathbf{T}_x(j) = \mathbf{T}_x$ for all j , and we have $\mathbf{T}_x(j, k) = (\mathbf{T}_x \bullet)^{k-j}$. One-dimensional marginal distribution functions are represented by vectors $\mathbf{f}_x(j) \equiv f_j(\mathbf{x})$ in the matrix-language, and Eq. (2.1.45) looks like $\mathbf{f}_x(k) = \mathbf{T}_x(j, k) \bullet \mathbf{f}_x(j)$. We will not use the matrix language for the description of Markov chains; instead, we define a more general language on the basis of propagators in Sect. 2.1.2.5.

2.1.2.3 Markov chains with independent increments

The convolution product: Any Markov chain can be written as a sequence of n random variables

$$v_k = \sum_{i=1}^k \xi_i \quad \text{for } k = 1, \dots, n \quad , \quad (2.1.48)$$

where the ξ_i are called the sequence of *increments*. We may call v_k the *accumulating random variable* of the increments ξ_i . If the ξ_i are independent random variables with distributions $f_i(\xi_i)$, we will call the sequence v_k a *Markov chain with independent increments*, which has the propagators $\vec{g}(v_{j-1}, v_j) = f_j(v_j - v_{j-1})$. Inserting this into Eq. (2.1.45) gives

$$g_{j+1}(v_{j+1}) = \int_{-\infty}^{\infty} dv_j g_j(v_j) f_j(v_{j+1} - v_j) \equiv (g_j * f_j)(v_{j+1}) \quad , \quad (2.1.49)$$

and the operation $g * f$ is called the *convolution product* of distributions. One easily verifies that the convolution product is commutative and associative⁹ and that finally

$$g_n(v_n) = (f_1 * \dots * f_n)(v_n) \quad ; \quad (2.1.50)$$

the distribution of the sum of independent random variables is given by the convolution product of the individual distributions. Eq. (2.1.49) could also have been obtained by applying Eq. (2.1.39) with $\psi(v_j, \xi_{j+1}) = v_j + \xi_{j+1} = v_{j+1}$.

Moments, cumulants and error propagation: We temporarily generalize our discussion to a random variable $\check{\xi}$ defined by the linear combination

$$\check{\xi} = \sum_{i=1}^n a_i \xi_i \quad , \quad (2.1.51)$$

where a_i are constants and ξ_i independent random variables. Denoting the m.g.f. and c.g.f. of each ξ_i with $M_i(t)$ and $\chi_i(t)$, respectively, we obtain

$$\check{M}(t) = \prod_{i=1}^n M_i(a_i t) \quad (2.1.51a)$$

$$\check{\chi}(t) = \sum_{i=1}^n \chi_i(a_i t) \quad . \quad (2.1.51b)$$

Calling $\kappa_{i;j} = \chi_i^{(j)}(0)$, Eq. (2.1.51b) leads immediately to

$$\check{\kappa}_j = \sum_{i=1}^n a_i^j \kappa_{i;j} \quad . \quad (2.1.51c)$$

For $j = 2$ this reads $\check{\sigma}^2 = \sum_i a_i^2 \sigma_i^2$, which is known as the *law of error-propagation*. We may therefore consider Eq. (2.1.51c) as a generalization of this law, covering also the higher order properties of the error distribution.

⁹Associativity of the convolution product presupposes certain restrictions on the support of the distributions, which are always verified for probability density functions.

For the compound moments $\check{\mu}_k$ there is no such simple formula in the general case; however, for two independent random variables we have the relation

$$\check{\mu}_k = \sum_{i=0}^k \binom{k}{i} a_1^i \mu_{1;i} a_2^{k-i} \mu_{2;k-i} \quad (2.1.52)$$

which can be straightforwardly (but also laboriously) extended to more variables.

The Central Limit Theorem: A particularly simple situation occurs when we consider a Markov chain $\check{\xi}_n$ with independent increments ξ_i , which are *identically distributed* by $f(\xi_i)$. Denoting the generating functions of the individual ξ_i by $M(t)$ and $\chi(t)$, and setting all $a_i = 1$, Eqs. (2.1.51) simplify to

$$\check{M}_n(t) = M^n(t) \quad (2.1.53a)$$

$$\check{\chi}_n(t) = n\chi(t) \quad , \quad (2.1.53b)$$

and for the cumulants we find $\check{\kappa}_{n;j} = n\kappa_j$. With Eq. (2.1.14) this leads to the interesting relation

$$\check{\gamma}_{n;i} = \frac{\gamma_i}{n^{i/2}} \quad . \quad (2.1.54a)$$

Therefore we have for all $i \in \mathbb{N}$

$$\lim_{n \rightarrow \infty} \check{\gamma}_{n;i} = 0 \quad (2.1.54)$$

It is easy to verify that Eq. (2.1.54) also holds for independent random variables which are not identically distributed.

We have seen in Sect. 2.1.1.3 that the distribution with $\gamma_i = 0$ for all i is the *Gaussian normal distribution*. Eq. (2.1.54) expresses that the accumulating random variable of a Markov chain with independent increments, $\check{\xi}_n = \xi_1 + \dots + \xi_n$, tends to be distributed normally for sufficiently large n , independent of the distribution of the individual ξ_i , with

$$\check{m}_n = \sum_{i=1}^n m_i \quad \text{and} \quad \check{\sigma}_n^2 = \sum_{i=1}^n \sigma_i^2 \quad .$$

Eq. (2.1.54) is known as the *Central Limit Theorem (CLT)* of statistics.

Sampling statistics and the CLT: Another formulation of the CLT is immediately obtained if we consider that the arithmetic mean \bar{x}_n of n random values ξ_i distributed about a mean m with a standard deviation σ is $\bar{x}_n = \sum_i \xi_i/n$: Obviously, the sample mean \bar{x}_n is also a random variable. The CLT claims that for sufficiently large sample sizes n the sample means are distributed normally about the theoretical mean $\bar{m} = m$ with a standard deviation $\bar{\sigma} = \sigma/\sqrt{n}$. What “sufficiently large” means, depends on the distributions of the ξ_i and on the requirements of accuracy. Quantitatively, we may set some small number $\varepsilon \ll 1$, and the CLT guarantees that we can find for any parameters an n_0 such that $F(\xi)$ is “sufficiently normal” for $n > n_0$, in the sense that all $\bar{\gamma}_i < \varepsilon$; this case will be called the “*rich statistics*” case in the following, the case where the theoretical distributions of $F(\xi)$ have to be considered will be called the “*poor statistics*” case.

Clearly, the simplest example of sampling is counting; we can see immediately from Eq. (2.1.22b) ff. that the binomial distribution for large N , and from Eq. (2.1.23d) ff. that the Poisson distribution for large r , are approximated by Gaussian distributions. In the latter case, we find the well known relation

$$F_P(k, r) \approx F_G(k; r, \sqrt{r}) \quad .$$

This approximation is generally considered as good for $r \gtrsim 10$, which we may call a “rich” counting statistics. It should be pointed out, however, that we only consider the counting of independent incidents; if the occurrence of counts influences the probability of subsequent counts, the CLT does not apply and the asymptotic distribution may strongly differ from the normal, as we will see in Sect. 2.2.1.3.

2.1.2.4 Asymptotic expansion of compound distributions

Practical use of the CLT: The central limit theorem states that any sum of *independent* random variables, $\check{\xi}_n = \xi_1 + \dots + \xi_n$, is asymptotically normal distributed for $n \rightarrow \infty$. In practice, we will be interested in the question *how fast* this convergence proceeds, and how the remaining difference depends on the invariant parameters γ_i . In particular: Is there a way to find a function $\check{R}_n(z; \gamma_1, \dots, \gamma_k)$, expressing the deviation of \hat{F} from the normal distribution? The usefulness of such a remainder function is obvious: The combination of different random variables with different distribution functions can be reduced to finding relations for the combined moments or cumulants, from which we can then reconstruct the final distribution. For a sum of n independent variables and a sufficiently large n , the CLT guarantees that for any desired accuracy, $\|\check{R}_n(z)\| < \varepsilon$, there exists a number k such that all γ_i for $i > k$ can be neglected.

From Eq. (2.1.54a), the CLT applied to a sum of n independent random variables, may be expressed in the form

$$\hat{F}(z) = \Phi(z) + \check{R}_n(z; \gamma_1, \dots, \gamma_k) + O(n^{-(k+1)/2}) \quad . \quad (2.1.55)$$

Considering Eq. (2.1.55) as the k -th approximation, we may call the Gaussian $\Phi(z)$ as the 0-th order approximation of any combined distribution function, giving $\hat{F}(z)$ to order $1/\sqrt{n}$. For a Poisson distribution, this has even a direct interpretation: If we say that a Poisson distribution about a parameter $r \approx 10$ is sufficiently well approximated by a Gaussian with $\sigma = \sqrt{10}$, knowledge of the remainder function up to γ_3 would enable us to describe a Poisson distribution about $r \approx 2$ to the same accuracy.

The Gram-Charlier expansion in orthogonal polynomials: We consider the standardized probability density function, $\hat{f}(\check{\zeta}_n)$, where $\check{\zeta}_n$ is the standard variable related to the accumulating sequence $\check{\xi}_n = \xi_1 + \dots + \xi_n$ of independent random variables. For simplicity, we assume that all ξ_i are identically distributed, so that the parameters $\check{\gamma}_i$ of the distribution f are connected to the parameters γ_i of the distribution of the individual ξ_i by Eq. (2.1.54a). Because of the connection of the derivatives of the standardized normal distribution $\phi(z)$ to the orthogonal Hermite polynomials, the *Gram-Charlier* expansion,

$$\hat{f}(\check{\zeta}_n) = \sum_{k=0}^{\infty} \frac{c_k}{k!} \phi^{(k)}(\check{\zeta}_n) = \phi(\check{\zeta}_n) \sum_{k=0}^{\infty} \frac{c_k}{k!} H_k(\check{\zeta}_n) \quad , \quad (2.1.56)$$

is an orthogonal expansion of \hat{f} , and the coefficients are given as $c_k = \langle \hat{f} | H_k \rangle$, so they are a functions of the standardized moments of $\hat{f}(\zeta)$; in particular we find we find $c_0 = 1$, $c_1 = c_2 = 0$, $c_3 = -\check{\gamma}_1$, $c_4 = \check{\gamma}_2$, $c_5 = -\check{\gamma}_3$ and $c_6 = \check{\gamma}_4 + 10\check{\gamma}_1^2$. We have indicated the coefficient c_6 not only to show that the simple relations between the c_k and the $\check{\gamma}_i$ up to $k = 5$ do not hold for higher orders; more important is the fact that, replacing the $\check{\gamma}_i$ by γ_i using relation Eq. (2.1.54a), we find that $c_k \propto n^{1-k/2}$ for $k \leq 5$, but only $c_6 \propto n^{-1}$. Hence, even though the Gram-Charlier expansion gives us the desired relation of the deviation of \hat{f} from the normal to its basic parameters, but it does not easily allow to find the cut the expansion at a specified order in n . For the following considerations it is important to point out that the asymptotic dependence of the coefficients c_k on n is independent on the assumption that the ξ_i are identically distributed.

The Edgeworth and Cornish-Fisher asymptotic expansions: The problem is obviously solved by ordering the terms in Eq. (2.1.56) by powers of $n^{-1/2}$, considering Eq. (2.1.54a). This *asymptotic expansion* of the probability density function is called the *Edgeworth-expansion* and can be written as

$$\hat{f}(\check{\zeta}_n) = \phi(\check{\zeta}_n) \left(1 + \sum_{i=1}^k R_i(\check{\zeta}_n; \gamma_1, \dots, \gamma_i) \right) + O(n^{-(k+1)/2}) \quad , \quad (2.1.57)$$

where each R_i introduces a correction of order $n^{-i/2}$. Up to third order, the correction factors are

$$R_1(x) = \frac{\gamma_1}{6} H_3(x) \quad (2.1.57a)$$

$$R_2(x) = \frac{\gamma_2}{24} H_4(x) + \frac{\gamma_1^2}{72} H_6(x) \quad (2.1.57b)$$

$$R_3(x) = \frac{\gamma_3}{120} H_5(x) + \frac{\gamma_2\gamma_1}{144} H_7(x) + \frac{\gamma_1^3}{1296} H_9(x) \quad . \quad (2.1.57c)$$

We see here very clearly that the odd γ_i (i.e. all odd combinations of γ_i) are connected to asymmetric polynomials, thus express the asymmetric parts of the deviation of the distribution to the normal, while the even combinations of γ_i express the symmetric parts. We also see why the denotation “excess” for γ_2 is misleading: For any skew distribution ($\gamma_1 \neq 0$) the “excess” of a distribution relative to the normal is affected by γ_1^2 to the same order as by γ_2 .

It is obvious from $\Phi'(z) = \phi(z)$, that a similar expansion for the cumulative distribution function can be found as

$$\hat{F}(z) = \Phi(z) + \phi(z) \sum_{i=1}^k \hat{R}_i(z; \gamma_1, \dots, \gamma_i) + O(n^{-(k+1)/2}) \quad , \quad (2.1.58)$$

where the \hat{R}_i are simply obtained by replacing all H_k by H_{k-1} in Eqs. (2.1.57). A more interesting problem connected to the cumulative distribution function is, however, to give an expression for the standard variable ζ_p connected to a specific probability p , $\hat{F}(\zeta_p) = p$. This is provided by the Cornish-Fisher expansion: using the Gaussian standard quantile ς_p , given by $\Phi(\varsigma_p) \doteq p$, we can write

$$\zeta_p = \varsigma_p + \sum_{i=1}^k \omega_i(\varsigma_p; \gamma_1, \dots, \gamma_i) + O(n^{-k/2}) \quad (2.1.59)$$

with

$$\omega_1(x) = \frac{\gamma_1}{6} H_2(x) \quad (2.1.59a)$$

$$\omega_2(x) = \frac{\gamma_2}{24} H_3(x) - \frac{\gamma_1^2}{36} \{ 2H_3(x) + H_1(x) \} \quad (2.1.59b)$$

$$\omega_3(x) = \frac{\gamma_3}{120} H_4(x) - \frac{\gamma_2\gamma_1}{24} \{ H_4(x) + H_2(x) \} + \frac{\gamma_1^3}{324} \{ 12H_4(x) + 19H_2(x) \} \quad . \quad (2.1.59c)$$

Since ς_p expresses the probability p in units of Gaussian Sigmas, we may say that Eqs. (2.1.59) allow to transform Gaussian Sigmas into “real” σ 's, which means to multiples of the actual standard deviation. We also obtain an approximate expression for the standardized median of a distribution (the “0-Sigma” confidence limit), which is to third order

$$\zeta_{\frac{1}{2}} = -\frac{\gamma_1}{6} + \frac{17\gamma_1^3}{324} - \frac{\gamma_1\gamma_2}{12} + \frac{\gamma_3}{40} \quad . \quad (2.1.60)$$

Note that the second order term is zero, because even orders do not influence the skewness of a distribution.

Applicability of asymptotic expansion: Eqs. (2.1.57) and (2.1.59) approach asymptotically the real distributions or quantiles, respectively, only if ξ_n is a Markov chain with independent increments. However, we may use them as approximative expressions for general distributions; the only real requirement is that the invariant parameters γ_i asymptotically decrease with i . We see from Eqs. (2.1.57) and (2.1.59) that a decreasing influence of higher order terms is given even when γ_i keeps its order of magnitude with increasing i . We will set this as the minimum requirement on the applicability of asymptotic expansion formulae. If this is not fulfilled, it may be that the inclusion of successive higher orders of γ_i diminishes the quality of the approximation, it may even yield in completely useless results. One may verify this by trying an expansion of the exponential or the uniform distribution!

Therefore, the applicability of this formulae is not restricted to Markov chains with independent increments, but may be generalized to other accumulating sequences. However, we have to make sure that the γ_i which are included in the expansion tend to decrease, and that we have reasons to assume that the neglected parameters do not contribute substantially. In many physical applications, the first condition can be examined empirically, while the second may just be assumed on the basis of general arguments. It is generally not advisable to expand to orders much higher than γ_3 , because the result will rarely be improved; for this reason we have restricted all formulae given here to this order. The reason to choose an *odd* order as the highest one is, of course, that the asymmetric redistribution of probability generally has the more important consequences. Even if the minimum condition for an asymptotic expansion is not fulfilled, it is often possible to improve the approximation — compared to the frequently used normal approximation — just by including the skewness coefficient γ_1 .

2.1.2.5 Products of distributions

Multidimensional distributions in abstract notation: According to the abstract notation of distribution operations introduced in Sect. 2.1.1.4 we give here the abstract operations dealing with multidimensional distributions. Since abstract distributions are rather defined by their operational properties than by their functional form, we again understand the explicit notation of variables only as a indication of the action of a distribution, and will be omitted as far as possible. We will use an ordered notation in the sense that in any combination ξ_j occurs on the left side of ξ_k if $j < k$; this does not generally lead to the requirement of an orderly probability space. We use the convention that $f \equiv f(\xi_1, \dots, \xi_n)$ is the multivariate distribution defined on \mathbb{IP}^n and $\varphi(\xi_1, \dots, \xi_n)$ the according test function, while $f_k \equiv f_k(\xi_k)$ are marginal distributions with the related test functions $\varphi_k \equiv \varphi_k(\xi_k)$; this convention is accordingly used for ordinary functions ψ and ψ_k .

The *direct product* of two distributions f_1 and f_2 is defined by

$$\langle f_1 \otimes f_2 | \varphi_{12} \rangle \doteq \langle f_1 | \langle f_2 | \varphi_{12} \rangle \rangle. \quad (2.1.61)$$

It satisfies the relation of associativity and commutativity, and can therefore be expanded to a chain $f_1 \otimes \dots \otimes f_n$. A set of one-dimensional distributions f_j related to the dimensions $j = 1, \dots, n$ of \mathbb{IP}^n is combined to the joint distribution function f of \mathbb{IP}^n by

$$f \doteq f_1 \sqcap \dots \sqcap f_n. \quad (2.1.62)$$

Comparing with Eq. (2.1.34), we obviously have to understand the f_i occurring in a \sqcap -product as restricted marginal distributions, where all random variables of the distributions occurring at the left side of f_i act as conditional restrictions, while the random dimensions on the left side are integrated out. We call Eq. (2.1.62) the *conditional outer product*. Therefore, the meaning of the “factors” in a conditional outer product depend on their position in the product. If f_1, \dots, f_n are independent random distributions, we clearly have

$$f_1 \sqcap \dots \sqcap f_n = f_1 \otimes \dots \otimes f_n \quad . \quad (2.1.62a)$$

Introducing the notations $\vec{f}_{jk} \equiv \vec{f}(\xi_j, \xi_k)$, $\vec{f}_k = \vec{f}(\xi_{k-1}, \xi_k)$ and $\vec{f}_1 \equiv f_1$, we can give the abstract description of a *Markov chain* f_1, \dots, f_n as

$$f_1 \sqcap \dots \sqcap f_n = \vec{f}_1 \otimes \dots \otimes \vec{f}_n \quad . \quad (2.1.62b)$$

The conditional outer product may be written in any order, expression that we have in general the freedom to express every random variable as conditionally dependent on the others. Nevertheless, the operation is not commutative in a common sense, because different orders of the product contain different terms; in orderly probability spaces (i.e. if a natural or time-order is applied to the random dimensions), we can assume that only one order of the product contains well-defined terms.¹⁰ In the general case for conditional chains with memory, it is not associative. For Markov chains and independent random distributions, associativity of the conditional outer product follows from the associativity of the direct product. In the following, we will only consider Markov chains.

The propagator product: Marginal distributions connected to random variables in a Markov chain are mapped onto each other by use of propagators; in abstract notation, Eq. (2.1.45) can be written as

$$\langle f_k | \varphi_k \rangle = \langle f_j | \langle \vec{f}_{jk} | \varphi_k \rangle \rangle \quad .$$

We introduce the *propagator product*

$$\langle f(x) \triangleright_x g(x, y) | \varphi(y) \rangle \doteq \langle f(x) | \langle g(x, y) | \varphi(y) \rangle_y \rangle_x \quad , \quad (2.1.63)$$

which may in this sense applied to any kind of functions f and g , and call x the conditional variable of $g(x, y)$, which is reduced by the operation $f \triangleright_x g$. For propagator chains, the conditional variable is just identical to the free variable of the left hand propagator, so that its explicit notation can be omitted and we can write

$$\langle f_k | \varphi_k \rangle = \langle f_i \triangleright f_{j_1} \triangleright \dots \triangleright f_{j_n} \triangleright f_k | \varphi(\xi_k) \rangle \quad , \quad (2.1.64)$$

which we call a *propagator chain*. Here, we implicitly understand every f_j occurring on the right side of an operator, $\triangleright f_j$, as a propagator, where the conditional variable is set to the free variable of its left neighbor, and reduced in the operation. The first distribution in the propagator chain f_i is an unconditional marginal distribution and is called the initial distribution. Obviously, the number of terms in a propagator chain is arbitrary, because from the Markov equation Eq. (2.1.46) we see that

$$f_i \triangleright f_k = f_i \triangleright f_j \triangleright f_k$$

for any combination of dimensions f_i , f_j and f_k ; this also guarantees the associativity of the propagator product. It is obviously an ordered operation and therefore not commutative, even though it may be written in different orders yielding the same result; in the same sense as the conditional outer product, the meaning of the terms changes by changing the order. In a time-ordered probability space, we may say that the propagator product

¹⁰This corresponds to the problem of time-reversibility; see Sect. 2.2.2.1.

unfolds the generation history of the final distribution f_k . Writing more or less terms into the product means looking more or less detailed on this history.

To write propagators explicitly, we note that a propagator is nothing but the unconditional marginal distribution obtained from a propagator chain which starts from an initial one-point distribution δ_i , and we define

$$\vec{f}_{jk} \doteq \delta_j \triangleright f_k \quad (2.1.65a)$$

$$f_j \doteq \delta_j \triangleright f_j \quad (2.1.65b)$$

The notation of the Dirac-function on the left side of the propagator product can be understood from the explicit definition Eq. (2.1.63) by writing

$$\delta_i \triangleright f_k \leftrightarrow \delta(\xi' - \xi_i) \triangleright_{\xi'} \vec{f}(\xi', \xi_k) \quad .$$

For the combination of propagator products with ordinary functions of random variables we use the convention that

$$(f_i \triangleright f_k) \psi_j \doteq f_i \triangleright (f_j \psi_j) \triangleright f_k \quad ; \quad (2.1.66)$$

clearly, we can insert $f_j \psi_j$ at any place of the product. The meaning of Eq. (2.1.66) is, of course, that since we are interested in a specific marginal distribution of a random variable ξ_k , functions of other random variables are averaged over their random dimension. This becomes particularly clear if we assume that ξ_j and ξ_k are independent random variables; Eq. (2.1.66) becomes then

$$(f_i \triangleright f_k) \psi_j = \langle \psi_j \rangle f_k \quad . \quad (2.1.66a)$$

It is clear that the propagator chain Eq. (2.1.64) can be formally written also for independent distributions; however, it does not contain any additional information about f_k .

Properties of the convolution product: Let now v_j , $j = 1, \dots, n$, be a Markov chain with independent increments, $\xi_i = v_i - v_{i-1}$, $v_1 \equiv \xi_1$. Denoting the distributions with $g_i(v_i)$ and $f_i(\xi_i)$, we can generalize Eq. (2.1.50) as

$$g_i \triangleright g_k = g_i * f_{i+1} * \dots * f_k \quad , \quad (2.1.67)$$

where the initial distribution g_i can be freely chosen.

The convolution product has some useful properties, which simplify the treatment of Markov chains with independent increments. The abstract definition of the convolution product is

$$\begin{aligned} \langle f_1 * f_2 | \varphi \rangle &= \langle (f_1 \otimes f_2)(\xi_1, \xi_2) | \varphi(\xi_1 + \xi_2) \rangle \\ &= \langle f_1(\xi_1) | \langle f_2(\xi_2) | \varphi(\xi_1 + \xi_2) \rangle \rangle \quad , \end{aligned} \quad (2.1.68)$$

and we have already mentioned that it is commutative, and associative for normalized distributions. The Dirac-function acts as the unit element in the convolution,

$$\delta_i * f_j = f_j \quad , \quad (2.1.69a)$$

and the multiplication rule with ordinary functions $\psi_j(\xi_j)$ is

$$(f_i * f_j)\psi_j = f_i * (f_j\psi_j) \quad (2.1.69b)$$

From this relations and Eq. (2.1.67) we can find the propagator rules

$$\delta_i \triangleright g_k = f_{i+1} * \dots * f_k \quad (2.1.70a)$$

$$\delta_i \triangleright g_k = (\delta_i \triangleright g_j) * (\delta_j \triangleright g_k) \quad (2.1.70b)$$

$$\psi_j(\delta_i \triangleright g_k) = (\delta_i \triangleright g_{j-1}) * (f_j\psi_j) * (\delta_j \triangleright g_k) \quad (2.1.70c)$$

The derivative of a convolution product satisfies for any combination $i + j = k$

$$(f_1 * f_2)^{(k)} = f_1^{(i)} * f_2^{(j)} \quad , \quad (2.1.71a)$$

from which follows that

$$\delta^{(k)} * f = f^{(k)} \quad . \quad (2.1.71b)$$

The relation for the moments of the sum of two independent random variables, Eq. (2.1.52), can be rewritten in abstract notation as

$$\langle (f_1 * f_2)(\xi) \mid \xi^k \rangle = \sum_{j=0}^k \binom{k}{j} \langle f_1 \mid \xi^j \rangle \langle f_2 \mid \xi^{k-j} \rangle \quad , \quad (2.1.72)$$

which proves to be particularly useful for the investigation of propagators in connection to Eqs. (2.1.70).

2.2 The point process approach to cosmic ray transport

In this section we develop a new approach to the treatment of cosmic ray transport, which is founded on the theory of Markov processes, in particular discontinuous Markov processes, called *point processes*. In Sect. 2.2.1 we give a mathematical introduction to this theory, under reference to the general discussion of probability theory in the last section. The concept of the perturbative treatment of Markov processes is developed, which reduces the description of an evolving distribution function (propagator) by its moments. In the following section, Sect. 2.2.2, we establish the connection to classical transport theory, and show the general method as well as a simple example for the application to cosmic ray transport. A detailed application to specific questions of cosmic ray physics is, however, postponed to future work.

The theory of Markov processes is described in the book of FISZ [Fis80]. Specific discussions of point processes can be found in the books of COX & ISHAM [CI80], a rather mathematical discussion is given by SNYDER [Sny75]. Other references are given in the text.

Notation: We use the notation introduced in the last section and in Chapter 1, in particular Sect. 1.2.2 and Sect. 1.3.4. Please read carefully the em Notation-paragraph on page 96! The author apologizes that more detailed information cannot be given here; it is just necessary to read the other sections *before* reading this one.

2.2.1 Random point processes

2.2.1.1 Definition and classification of point processes

Random processes and propagator chains: In the last section we have discussed probability spaces of finite dimension, in which it was possible to define sequences of random variables and relations describing them. The next generalization is obviously the extension to probability spaces of infinite, in general even uncountable dimension. The theory arising from this is the theory of *random processes*. A *random process* is a random function $\Xi(t)$, depending on a real parameter t , which can in general be identified with *time*. Therefore we might say that a random process is a random quantity changing in time. The realization of a random process is a function on \mathbb{R} , called a *path*. The properties of this path function classify the random processes, where the most basic distinction is between *continuous* and *discontinuous* random processes; the latter are called *point processes*.

At any fixed time t_0 , $\Xi(t_0)$ is a random variable with a distribution $F_{\Xi}(t_0, \mathbf{x}) = \mathcal{P}(\Xi(t_0) < \mathbf{x})$, following Eq. (2.1.30). The corresponding probability density function will be denoted with $f_{\Xi}(t_0, \mathbf{x})$. If we select an arbitrary number of instances t_1, \dots, t_n , the random sequence $\Xi(t_i)$ forms a propagator chain

$$f_{\Xi}(t_n) = f_{\Xi}(t_1) \triangleright \dots \triangleright f_{\Xi}(t_n) \quad . \quad (2.2.1)$$

We might say that a random process is a *family of propagator chains*. In the most general case, the distribution $f_{\Xi}(t_k)$ will be conditionally restricted by all $\Xi_k(t_i)$ with $t_i < t_k$. If $f_{\Xi}(t_1), \dots, f_{\Xi}(t_n)$ is a Markov chain for *any selection of* t_1, \dots, t_n , the process $\Xi(t)$ is called a *Markov process*. Markov processes are the random processes with the lowest reasonable autocorrelation; a random process which maps to *independent random variables* $\Xi(t_i)$ for any sequence of instances t_1, \dots, t_n could just be used as a definition for *complete chaos*, in the sense that there is no way to determinate the behavior at a specific time t_j from the knowledge we have for times $t < t_j$.¹¹ We may alternatively repeat what we have stated in the discussion of the propagator product — a propagator chain connecting independent distributions does not contain additional information about the final distribution. Therefore, the simplest random processes are represented as Markov chains with *independent increments*.

¹¹This is a nice, but not very useful definition of “chaos”. In contemporary non-linear physics, one attempts to define this term on the basis of determinate behavior [Hak83].

Point processes: Pure *point processes* are random processes which are realized by step-functions in time. A realization path of a point process over a finite period of time can therefore be described by a finite, but randomly given number of quantities expressing the discontinuous changes of the random functions; we might say that point processes are entities defined in probability spaces of *random dimension*. In the simplest case, the step quantities are all identical (in absolute value *and* sign), and the randomness is completely reduced to the number of counts accumulated over time; we call such processes *counting processes*. A counting process with independent increments, i.e. where the numbers of counts occurring in a fixed sequence of time intervals are independent, is called a *Poisson process*. A counting process of Markov type is called a *birth process*. The simplest case of a birth process is the *Yule-Furry process*, in which the count rate is proportional to the accumulated number of counts. An important property which we will always assume for counting processes is *orderliness*, which means that only single counts occur at single instants, i.e. the probability that more than one count occurs in an infinitesimal time interval, vanishes.

A point processes, $\Xi(t)$, in which the amounts of change, $\Delta(t_i)$, contributed by single steps occurring at t_1, \dots, t_n , are not identical, is called *compound* or *marked point process*. Every purely discontinuous random process can be written as a marked point process. A marked point process can always be separated into a counting process, $\Xi_c(t)$, and a mark distribution, $f_m(\Delta; t)$. We might look at a marked point process as a counting process which *drives* the accumulation of random variables Δ distributed by f_m . The marks are in general m -dimensional realizations of an n -dimensional probability space \mathbb{P}_m^n , which we call the *mark space*; in many cases, marks are just real-valued physical quantities. Clearly, the dimension of the mark space must be larger than or equal to the dimension of the mark variable, $n \geq m$; if $n > m$, the mark is described by a multivariate random function defined on \mathbb{P}_m^n . The relations between Ξ_c and f_m can be various, and are used to classify marked point processes in Sect. 2.2.1.4.

2.2.1.2 Markov processes

Markov property in continuous time: If a conditional chain Eq. (2.2.1) is a Markov chain, it enjoys associativity, which means that any subchain $\Xi(t_j) \triangleright \Xi(t_k)$ can be treated separately. In particular, it makes sense to define the for any $t_j < t_k$ the propagator

$$\vec{f}_{\Xi}(t_j; t_k) \equiv \delta_{\Xi}(t_j) \triangleright f_{\Xi}(t_k) \quad , \quad (2.2.1a)$$

which is independent of the distribution of $\Xi(t)$ at any other time $t \neq t_j, t_k$. In an ordered time sequence $t_1 < \dots < t_n$, the Markov equation Eq. (2.1.46) can be applied to any propagator $\vec{f}_{\Xi}(t_j, t_k)$ with $k - j > 1$; since the choice of time instants is arbitrary in a Markov process with continuous time, we can generalize this equation and obtain *for any* t

$$\delta_{\Xi}(t_j) \triangleright f_{\Xi}(t_k) = \delta_{\Xi}(t_j) \triangleright f_{\Xi}(t) \triangleright f_{\Xi}(t_k) \quad ; \quad (2.2.2)$$

this is known as the *Chapman-Kolmogorov equation*. A *homogeneous Markov process* is defined by

$$\delta_{\Xi}(t) \triangleright f_{\Xi}(t + \Delta t) \doteq \delta_{\Xi}(0) \triangleright f_{\Xi}(\Delta t) \quad \text{for all } t, \Delta t \quad . \quad (2.2.3)$$

The Kolmogorov equations: The Chapman-Kolmogorov equation can be transformed into a differential equation; we consider the propagator of Ξ from an instant t to $t + \Delta t$ in the limit $\Delta t \rightarrow 0$, and we can write

$$\lim_{\Delta t \rightarrow 0} [\delta_{\Xi}(t, \mathbf{x}) \triangleright f_{\Xi}(t + \Delta t, \mathbf{y})] \doteq \tau(t, \mathbf{x}, \mathbf{y}) + [1 - \rho(t, \mathbf{x})] \delta(\mathbf{y} - \mathbf{x}) \quad (2.2.4)$$

with

$$\rho(t, \mathbf{x}) \equiv \int_{\mathbb{P}_{\Xi}} d\mathbf{y} \tau(t, \mathbf{x}, \mathbf{y}) \quad . \quad (2.2.4a)$$

τ and ρ are called *intensity functions* of the random process. $\tau(t, \mathbf{x}, \mathbf{y})$ expresses the probability per unit time of a change of $\Xi(t)$ at a time t from a state \mathbf{x} to a state $\mathbf{y} \neq \mathbf{x}$, and $1 - \rho(t, \mathbf{x})$ is the probability per unit time that nothing happens. Applying the Chapman-Kolmogorov equation, we immediately obtain

$$\left. \frac{\partial}{\partial t} \vec{f}_{\Xi}(t_0; t) \right|_{\Xi(t)=\mathbf{y}} = \vec{f}_{\Xi}(t_0; t) \triangleright_{\mathbf{x}} \tau(t, \mathbf{x}, \mathbf{y}) - \delta_{\Xi}(t_0) \triangleright \rho(t, \mathbf{y}) f_{\Xi}(t, \mathbf{y}) \quad , \quad (2.2.5a)$$

which is called the *prospective Kolmogorov equation* describing the Markov process $\Xi(t)$. Analogously, the *retrospective Kolmogorov equation* can be found as

$$\left. \frac{\partial}{\partial t_0} \vec{f}_{\Xi}(t_0; t) \right|_{\Xi(t_0)=\mathbf{y}} = \rho(t_0, \mathbf{y}) \delta_{\Xi}(t_0, \mathbf{y}) \triangleright f_{\Xi}(t) - \tau(t_0, \mathbf{y}, \mathbf{x}) \triangleright_{\mathbf{x}} f_{\Xi}(t) \quad . \quad (2.2.5b)$$

Note that the term “retrospective” refers here to the variation of the *condition* rather than the *result* of a process $\Xi(t)$. Both Eq. (2.2.5a) and Eq. (2.2.5b) give a complete description of a Markov process.

The Kolmogorov equation for strictly continuous Markov processes: In the general case, the Kolmogorov equations are integro-differential equations. However, in the case of a *strictly continuous Markov process*, which satisfies for any $\varepsilon > 0$ the condition

$$\lim_{\Delta t \rightarrow 0} \left\{ \frac{1}{\Delta t} \mathcal{P} \left(|\Xi(t + \Delta t) - \Xi(t)| > \varepsilon \right) \right\} = 0 \quad , \quad (2.2.6)$$

the Kolmogorov equations reduce to a parabolic partial differential equation. Expanding to second order in $\mathbf{q} = \mathbf{y} - \mathbf{x}$, we obtain

$$\begin{aligned} f_{\Xi}(t) \triangleright_{\mathbf{x}} \tau(t, \mathbf{x}, \mathbf{y}) &= f_{\Xi}(t, \mathbf{y}) \rho(t, \mathbf{y}) + \nabla_{\mathbf{y}} \cdot \left(f_{\Xi}(t, \mathbf{y}) \langle \tau(t, \mathbf{y}, \mathbf{y} - \mathbf{q}) | \mathbf{q} \rangle \right) \\ &\quad + \nabla_{\mathbf{y}}^2 \cdot \left(f_{\Xi}(t, \mathbf{y}) \langle \tau(t, \mathbf{y}, \mathbf{y} - \mathbf{q}) | \mathbf{q}^2 \rangle \right) \quad , \end{aligned}$$

and it can be inferred from the continuity condition, Eq. (2.2.6), that all higher order terms vanish identically, so that the prospective Kolmogorov equation for the continuous Markov process is

$$\left. \frac{\partial}{\partial t} \vec{f}_{\Xi}(t_0; t) \right|_{\Xi(t)=\mathbf{y}} = -\nabla_{\mathbf{y}} \cdot \left[\vec{f}_{\Xi}(t_0; t, \mathbf{y}) \mathbf{b}(t, \mathbf{y}) \right] + \nabla_{\mathbf{y}}^2 \cdot \left[\vec{f}_{\Xi}(t_0; t, \mathbf{y}) \mathbf{D}(t, \mathbf{y}) \right] \quad , \quad (2.2.7)$$

with

$$\mathbf{b}(t, \mathbf{y}) = \left\langle \tau(t, \mathbf{y}, \mathbf{y} + \mathbf{q}) \middle| \mathbf{q} \right\rangle_{\mathbf{q}} \quad (2.2.7a)$$

$$\mathbf{D}(t, \mathbf{y}) = \left\langle \tau(t, \mathbf{y}, \mathbf{y} + \mathbf{q}) \middle| \mathbf{q}^2 \right\rangle_{\mathbf{q}} \quad . \quad (2.2.7b)$$

The coefficients \mathbf{b} and \mathbf{D} are called *drift vector* and *diffusion tensor*, respectively. In the general case, they are of the same order; for a strictly increasing (or decreasing) random process, however, the drift \mathbf{b} dominates and \mathbf{D} may be neglected to first order. The continuous Markov process with independent increments, i.e. if drift and diffusion coefficients do not depend on Ξ , is called a *Wiener process*. We can easily see that the random variables $\Xi(t)$ of a Wiener process have Gaussian distributions for all t ; we should note that this is not true in the general case.

2.2.1.3 Counting processes

The Poisson process: The simplest discontinuous random process is given by a counting process with independent increments, which is called a *Poisson process*. This process is completely described by its *rate function* $\rho(t)$; in fact, ρ has the same meaning here as in Sect. 2.2.1.2, only that $\tau(t, x, y) = \rho(t)\delta(y-x-1)$ for all y, x and t , expressing that only positive integer steps (counts) are possible. The Kolmogorov equation for the Poisson process reads

$$\frac{\partial}{\partial t} \vec{f}(t_0; t, k) = \hat{\delta}_{k0} \rho(t) \vec{f}(t_0; t, k-1) - \rho(t) \vec{f}(t_0; t, k) \quad . \quad (2.2.8)$$

With the initial condition $\vec{f}(t_0; t_0, k) = \delta_{0k}$ we find the solution

$$\vec{f}(t_0; t, k) = \frac{r^k}{k!} e^{-r} \quad \text{with} \quad r = \int_{t_0}^t dt' \rho(t') \quad ; \quad (2.2.8a)$$

this is the Poisson distribution, which was already discussed in Sect. 2.1.1.3, and r is the Poisson parameter. For the homogeneous Poisson process we simply have $r = \rho t$.

We may now discuss the finding about the complementary character of the expectation and occurrence probability,

$$\tilde{F}_P(k, r) = 1 - F_P(k, r) \quad ,$$

as expressed in the symmetry of Eqs. (2.1.23b) and (2.1.23c). In a Poisson process, the expectation r is an increasing function of time, therefore we may introduce a uniquely determined time t_r according to a given r . Then, the symmetry of Eqs. (2.1.23b) and (2.1.23c) expresses that the probability that an arbitrary realization of a Poisson process has k counts at a time $t < t_r$ is equal to the probability that it has *more than* k counts at $t = t_r$. This is obviously an immediate consequence of the increasing character of a Poisson process, and we can conclude that this symmetry holds for any distribution arising from a purely increasing random process.

The Yule-Furry process: The general case of a Markovian counting process, where the rate of increments ρ depends on the number of accumulated counts, is called a *birth process*; the naming arises from its application to self-reproducing populations. With the initial condition $\vec{f}(t_0; t_0, k) = \delta_{ki}$, $i \geq 1$, the Kolmogorov equation for the birth process reads

$$\frac{\partial}{\partial t} \vec{f}(t_0; t, k) = \hat{\delta}_{ki} \rho(t, k-1) \vec{f}(t_0; t, k-1) - \rho(t, k) \vec{f}(t_0; t, k) \quad . \quad (2.2.9)$$

In the simplest case, we have $\rho(t, k) \doteq k\rho_1(t)$, where $\rho_1(t)$ can be called the birth rate of one ‘‘individual’’ in the process. This process is called the *Yule-Furry process*, whose solution is easily found as

$$\vec{f}(t_0; t, k) = f_{YF}(t, k) \equiv \binom{k-1}{k-i} e^{-ir} (1 - e^{-r})^{k-i} \quad \text{with} \quad r = \int_{t_0}^t dt' \rho_1(t') \quad . \quad (2.2.9a)$$

Introducing the notations $N \equiv N(t) = \exp\{\int^t dt' \rho_1(t')\}$, $q = 1/N$ and $p = 1 - q$ this can be rewritten as a generalization of the binomial distribution,

$$f_{YF}(t, k) = \binom{k-1}{k-i} q^i p^{k-i} = \frac{1}{k} f_B(k-i, k, p) \quad . \quad (2.2.9b)$$

Note that $i \geq 1$ is required; in the following we briefly discuss the properties of the *Yule-Furry distribution*, Eq. (2.2.9a), for $i = 1$. The cumulant generating function is

$$\chi_{YF}(s) = s + \ln q - \ln(1 - pe^s) \quad , \quad (2.2.10)$$

from which we find the lowest order cumulants as

$$\kappa_1 = N \quad (2.2.10a)$$

$$\kappa_2 = N^2 - N \quad (2.2.10b)$$

$$\kappa_3 = 2N^3 - 3N^2 + N \quad (2.2.10c)$$

$$\kappa_4 = 6N^4 - 12N^3 + 7N^2 - N \quad (2.2.10d)$$

$$\kappa_5 = 24N^5 - 60N^4 + 50N^3 - 15N^2 + N \quad (2.2.10e)$$

The expressions for the invariant parameters γ_i of the Yule-Furry distribution are easily found from Eqs. (2.2.10), and one can verify the asymptotic expression

$$\lim_{N \rightarrow \infty} \gamma_i = (i+1)! \quad ,$$

which shows that the Yule-Furry distribution converges against the exponential distribution for large N . For the Yule-Furry process we have $N \propto e^t$, therefore we can expect that the distribution of $\Xi_{\text{YF}}(t)$ converges very fast against an exponential shape with time.

Birth process with polynomial rate function: We now assume that the rate function $\rho(k, t)$ of a general birth process can be written as a polynomial of degree m in k ,

$$\rho(k, t) = \sum_{l=0}^m \hat{\rho}_l k^l \quad . \quad (2.2.11a)$$

With this formulation, it is possible to reduce the integro-differential equation Eq. (2.2.9) to a coupled set of ordinary first order differential equations, which describe the *moments* $\mu_j(t)$ of $\vec{f}(t_0; t, k)$ as functions of time. Applying both the left and the right side of Eq. (2.2.9) on k^j , we obtain

$$\frac{\partial \mu_j}{\partial t} = \sum_{l=0}^m \sum_{i=0}^{j-1} \binom{j}{i} \hat{\rho}_l \mu_{l+i} \quad . \quad (2.2.11)$$

Hence, only in the case of independent increments, $m = 0$, the moments μ_j are completely described by all *lower order moments*, μ_i with $i < j$. The case $m = 1$ includes a ‘‘Yule-Furry-component’’ into $\rho(k, t)$, and the moments become self-coupled, which results in the exponential time-evolution of the Yule-Furry process. For $m > 1$ the equation system becomes upward-coupled, and higher order moments influence the evolution of each μ_j . We may therefore consider the degree m as the *coupling strength* of a birth process, which describes its degree of autocorrelation; $m = 0$ means that the process has independent increments, and that therefore the distribution of $\vec{f}(t_0; t, k)$ obeys the CLT. Of course, the quantities $\hat{\rho}_i$ have also to be considered there: if the sequence of absolute values $|\hat{\rho}_i|$ strongly decreases with i , it may be possible to choose a limited coupling strength \tilde{m} by neglecting all $\hat{\rho}_i$ for $i > \tilde{m}$. Since, by assumption, the $\hat{\rho}_i$ are dominated by $\hat{\rho}_0$, we can furthermore assume that the CLT holds *approximately* for such processes, which means that the γ_i decrease with time, and that an Edgeworth expansion to limited order n is possible for at least some accuracy $\varepsilon(\tilde{m}, n)$. This treatment we will call the *perturbative description* of birth processes, which is below extended to the general Markov process.

2.2.1.4 Marked point processes

Definition and classification: The general discontinuous Markov process which accumulates m quantities y_i over time in a random number N of non-identical steps, can be written as $\mathcal{Y}(t) \equiv (N(t), y_1(t), \dots, y_m(t))$, and is called a *marked point process*.¹² It is described by Eqs. (2.2.5) by setting

$$\tau(t, N, \mathbf{y}, \mathbf{y} + \Delta) = \rho(t, N, \mathbf{y}) f_m(\Delta | t, \mathbf{y}) \quad . \quad (2.2.12)$$

Since ρ and τ are connected by Eq. (2.2.4a) we have $\int f_m d\Delta = 1$, thus f_m is a probability density function, called the *mark distribution*, conditionally depending on t and \mathbf{y} . $\rho(t, N, \mathbf{y})$ itself describes, according to Sect. 2.2.1.3, a counting process $\Xi_c(t)$, which we will call the *driving process* of $\mathcal{Y}(t)$, accumulating the interaction number $N(t)$. We have assumed that f_m is not dependent on N ; this assumption arises from the physical interpretation of the functions τ and f_m , namely that f_m is completely described by the local physical state (see Sect. 2.2.2.4). For the same reason we will assume that f_m cannot depend on parameters which do not influence ρ . With these restrictions, we can give the following classification to marked point processes:

1. The *compound Poisson process* is given when $\rho \equiv \rho(t)$ and $f_m \equiv f_m(t)$; we then have a point process with independent increments, which are, however, *not* identical. If both ρ and f_m are constant, we have a homogeneous compound Poisson process.
2. The *compound birth process* allows the dependences $\rho \equiv \rho(t, N)$ and $f_m \equiv f_m(t)$. In this case, the *driving process alone* shows autocorrelation, while the mark distribution is uncorrelated to the process. A typical example for this is a idealized cascade process, in which a single interaction is not dependent on the physical state of the interacting particle.
3. The *Markov point process with uncorrelated marks*, $\rho \equiv \rho(t, N, \mathbf{y})$ and $f_m \equiv f_m(t)$. Here the complete state of the process determines the interaction rate, but not the mark distribution. In most cases, this situation is not exactly realized, but can be used as an approximation.
4. The *general Markov point process* with the highest possible autocorrelation, as assumed in Eq. (2.2.12).

The first two cases will be called *compound counting processes*, because here uncorrelated marks are just superposed to a counting process. The latter cases are combined as *Markov point processes*.

Compound counting processes with homogeneous increments: If a counting process is superposed by uncorrelated marks, which are all distributed identically, we can find for any given instant t a simple connection between the cumulant generating functions of the distributions $f_y(y, t) \equiv \vec{f}_y(t_0; t, y)$, $f_c(N, t)$ and $f_m(\Delta)$, which we will denote $\chi_y(s, t)$, $\chi_c(s, t)$ and $\chi_m(s)$, respectively.¹³ In this case, the state y of the point process can at any t be written as a sum

$$y = \sum_{i=1}^{N(t)} \Delta_i \quad ,$$

with a random number N of terms Δ_i , which are all identically distributed random variables. Since for any fixed number n of increments Δ_i the multivariate m.g.f. of f_y is given by $M_y(s, n) = M_m^n(s)$, we can write

$$\chi_y(s, t) = \ln \left\langle f_c(N, t) \left| M_m^N(s) \right\rangle_N = \ln G_c(M_m(s), t) = \ln M_c(\chi_m(s), t) \quad ,$$

¹²Marked point processes are not generally restricted to Markov processes, but we will apply this restriction here.

¹³We will restrict our considerations to one-dimensional marks here, because the specific case discussed here is only of didactical importance. The generalization to multidimensional marks is straightforward.

and therefore formally

$$\chi_y(s, t) = (\chi_c \circ \chi_m)(s, t) \quad . \quad (2.2.13)$$

In other words, we just have to replace the parameter s in the cumulant generating function of the driving process by the c.g.f. of the mark distribution. For this reason, point processes are often formally described by generating *functionals* instead of generating functions. Eq.(2.2.13) can be used to give the general relation for the cumulants $\check{\kappa}_j$, and thus for the invariant parameters of the distribution $f_y(y, t)$; denoting $\lambda_j \equiv \chi_c^{(j)}(0; t)$ for fixed t , and $\kappa_j \equiv \chi_m^{(j)}(0)$, we find

$$\check{\kappa}_1 = \lambda_1 \kappa_1 \quad (2.2.13a)$$

$$\check{\kappa}_2 = \lambda_2 \kappa_1^2 + \lambda_1 \kappa_2 \quad (2.2.13b)$$

$$\check{\kappa}_3 = \lambda_3 \kappa_1^3 + 3\lambda_2 \kappa_2 \kappa_1 + \lambda_1 \kappa_3 \quad (2.2.13c)$$

$$\check{\kappa}_4 = \lambda_4 \kappa_1^4 + 6\lambda_3 \kappa_2 \kappa_1^2 + 3\lambda_2 \kappa_2^2 + 4\lambda_2 \kappa_3 \kappa_1 + \lambda_1 \kappa_4 \quad (2.2.13d)$$

$$\begin{aligned} \check{\kappa}_5 = & \lambda_5 \kappa_1^5 + 10\lambda_4 \kappa_2 \kappa_1^3 + 10\lambda_3 \kappa_3 \kappa_1^2 + 15\lambda_3 \kappa_2^2 \kappa_1 + 10\lambda_2 \kappa_2 \kappa_3 \\ & + 5\lambda_2 \kappa_4 \kappa_1 + \lambda_1 \kappa_5 \quad . \end{aligned} \quad (2.2.13e)$$

Following Eqs.(2.1.15), the κ_j can be calculated from the moments μ_j of the mark distribution, which in turn may be found by direct integration. The λ_j can be found from the Kolmogorov equation of the driving process Eq.(2.2.11), if the rate function can be expressed or approximated by a low order polynomial. In the special case of the compound Poisson process we find from Eq.(2.2.13) the very simple expression

$$\chi_y(s, t) = r(t) M_m(s) \quad , \quad (2.2.14)$$

where the $r(t)$ is the accumulated Poisson parameter, which leads to

$$\check{\kappa}_j = r \mu_j \quad , \quad (2.2.14a)$$

when μ_j are the moments of the mark distribution. For the compound Yule-Furry process, with initial condition $\vec{f}(t_0; t_0, k) = \delta_{k1}$, we obtain

$$\chi_y(s, t) = \chi_m(s) + \ln q(t) - \ln(1 - p(t) M_m(s)) \quad , \quad (2.2.15)$$

and by successive differentiation we may explicitly verify Eqs.(2.2.13) with the λ_j replaced by the cumulants of the Yule-Furry process given in Eq.(2.2.10).

Markov point processes: The compound counting process allows a very simple treatment of marked point processes, but has also a very restricted applicability: it can be used only if (i) the driving process is self-correlated, and not affected by the marks, (ii) the marks are independent of the state of the process, and (iii) the marks are homogeneous in time. If one of these restrictions is not given, the general Kolmogorov equation for the marked point process has to be considered. Applying Eq.(2.2.12), and ordering the functions in the propagator product according to their dependence on random variables, we can rewrite Eq.(2.2.5a) as

$$\left. \frac{\partial}{\partial t} \vec{f}_r(t_0; t) \right|_{\mathbf{r}(t)=\mathbf{y}} = \delta_r(t_0) \triangleright \left[f_r(t) \rho(t) \triangleright_x f_m(\mathbf{y} - \mathbf{x} | t, \mathbf{x}) - \rho(t, \mathbf{y}) f_r(t, \mathbf{y}) \right] \quad . \quad (2.2.16a)$$

In the general case, this equation cannot be easily simplified. However, in the case if *uncorrelated marks*, which means that condition (ii) of the list above still applies and f_m does not depend on the process state, and restricting to one-dimensional random processes, this transforms into a simple convolution

$$\frac{\partial}{\partial t} \vec{f}_r(t_0; t) \Big|_{\Gamma(t)=y} = \delta_r(t_0) \triangleright \left[[\rho f_r * f_m](t, y) - \rho(t, y) f_r(t, y) \right] . \quad (2.2.16b)$$

Considering Eq. (2.1.72), this can now be applied to y^k , and yields

$$\frac{\partial}{\partial t} \langle \vec{f}(t_0; t) | y^k \rangle = \sum_{j=0}^{k-1} \binom{k}{j} \langle \vec{f}(t_0; t) \rho(t) | y^j \rangle \langle f_m(t) | y^{k-j} \rangle . \quad (2.2.17)$$

For a polynomial representation of the rate function ρ ,

$$\rho(t, y) = \sum_{l=0}^m \hat{\rho}_l y^l ,$$

we obtain the set of coupled differential equations for the moments,

$$\frac{\partial \check{\mu}_k}{\partial t} = \sum_{l=0}^m \sum_{j=0}^{k-1} \binom{k}{j} \hat{\rho}_l \check{\mu}_{j+l} \mu_{k-j} , \quad (2.2.18)$$

in analogy to Eq. (2.2.11), where here $\check{\mu}_j$ denote the total moments of the propagator \vec{f}_r , and μ_j are the moments of the mark distribution f_m . Noting that any rate function can be represented as a polynomial by means of a Taylor expansion, we can generally write

$$\hat{\rho}_l = \frac{1}{l!} \frac{d^l \rho}{dy^l} ; \quad (2.2.18a)$$

depending on the magnitude of the derivatives of ρ and the desired accuracy, we can then find a suitable degree m determining the coupling strength of the system. When evaluating propagators, Eq. (2.2.18) has to be solved with the initial values $\check{\mu}_k(0) = \check{\mu}_1^k(0)$, corresponding to an initial δ -function at the position $\check{\mu}_1(0)$.

We may finish the mathematical discussion of marked point processes with some remarks about the applicability of Eq. (2.2.18): As already noted for Eq. (2.2.11), the differential equation system is upward coupled if the dependence of the rate function ρ on the Markov parameter is higher than linear. We therefore have to rely on the assumption that $|\hat{\rho}_l|$ decreases with l fast enough to allow an upper cut in the equation system. This problem is unchanged when mark distributions are considered: We note that the lowest order moments of the mark distribution introduce in the highest order upward coupling degree; it doesn't help to assume "close-to-the-normal" distributions in the mark space to make the equations better handable. We note that this problem does not depend on how many moments we want to include in the Edgeworth expansion of the propagator; rather, it is the *evolution of the lower order moments* which might be uncontrollable influenced by the higher order moments. Finally, we will expect that a thorough *mathematical and empirical investigation* of the results of Eq. (2.2.18) in specific applications is required to find to which processes it can be applied and to which not; we will, however, not do this within this work, and just state that at least for weakly coupled problems ($m \leq 1$) Eq. (2.2.11) proposed to be useful, and that in other cases it may help to explain more detailed why too simple minded transport approximations give wrong results.

2.2.2 Random processes and particle transport

2.2.2.1 Transport theory: the physical language of random processes

Random variables, distributions and propagators in physics: A random process describes the evolution of a probability distribution with time; this is the easiest and most general way to speak of random processes in physics, even though “time” may be replaced by any continuous parameter, or even a set of parameters. We will call this parameter vector \mathbf{t} in the following, noting that in many cases we may simply replace it by the time t .

In physics, a distribution function is usually related to an ensemble of identical entities, which are distributed over a, possibly multidimensional, quantity of state, \mathbf{y} ; in case of a distribution of particles over energy, it is also called a *spectrum*. With respect to an *individual particle*, the spectrum becomes a *probability distribution of a random variable* \mathbf{y} . The mathematical terms *probability density* and *cumulative distribution* correspond to the physical terms *differential spectrum* and *integral spectrum*, respectively. Thus, a physical *random variable* is nothing but a quantity connected to a particle distribution or spectrum, but related to an individual particle, for which it is not fixed by any initial conditions. This is what we meant before when we said that a random variable is *defined* by its distribution: the distribution describes the range of possibilities given by the physical laws governing the problem.

A physical *propagator* is a distribution which arises from a well defined state at a time \mathbf{t}_0 , as a function of time. It describes the *transport* of the particle, and is connected to a physical process which we may characterize as an *interaction process* in the widest sense. Since the process generates a distribution from a well defined state, it must have the property of randomness. Hence, it must have some internal degrees of freedom, which are not fixed by initial conditions, and are described by a random vector \mathbf{x} , with a joint distribution function $f(\mathbf{x})$ determined by the physical laws of the interaction process. The change of the random variable \mathbf{y} is a random function $\Delta\mathbf{y}(\mathbf{x})$, their distribution is the *intensity function* of the interaction process, $\tau(\mathbf{t}, \mathbf{y}, \mathbf{y} + \Delta\mathbf{y}(\mathbf{x}))$, as given in Eqs. (2.2.4). The integral rate function $\rho(\mathbf{t}, \mathbf{y})$ is obviously equivalent with the interaction rate, thus connected to the interaction time scale by $\tau_{\text{int}}^{-1} = \rho(\mathbf{t}, \mathbf{y})$. We may distinguish between continuous and discontinuous interaction processes; the former are well known in transport theory and are called *diffusion processes*, the latter are those which we are most interested in: they describe the transport of a particle which undergoes well separable interactions with background particles. There is no common term for this in physics, except the mathematical term *Markov process*, or, more precise, *Markov point process*.

Markov processes and the Boltzmann equation: The aim of transport theory is the description of the evolution of spectra in time under the influence of interaction processes. The aim of the theory of random processes is the description of propagators. Obviously, both are equivalent, which becomes mathematically clear from our notation of a propagator as $\delta_{\Xi}(t_0) \triangleright f_{\Xi}(t)$ in Sect. 2.2.1.2: the Kolmogorov equations, describing the evolution of propagators, do not really depend on the restriction to random processes starting at a specific initial state. We may readily apply an initial spectrum, $f(t_0) \triangleright$, to the left side of Eqs. (2.2.5) or (2.2.7), and they transform to equations describing a propagating spectrum $f(t)$. Writing the integrated form of Eq. (2.2.5a) in full notation, we have

$$\frac{\partial f(t, \mathbf{y})}{\partial t} = \int d\mathbf{x} \left\{ f(t, \mathbf{x}) \tau(t, \mathbf{x}, \mathbf{y}) - f(t, \mathbf{y}) \tau(t, \mathbf{y}, \mathbf{x}) \right\} \quad , \quad (2.2.19)$$

which is known as the *Boltzmann equation* from kinetic theory¹⁴, or as the *master equation* in a more general context of transport phenomena.

¹⁴Written this way, it is the Boltzmann equation in a comoving volume element.

Analogously, the reader may have already verified that the continuous Kolmogorov equation, Eq. (2.2.7), is nothing but the *Fokker-Planck equation* known as the transport equation for diffusion processes. For this equation, an equivalent formulation in terms of stochastic processes was given by ITÔ [Itô51], which has been found to allow a fast simulation of diffusion transport problems [KA94]. The perturbative equations, Eq. (2.2.18), propose an approximative description for the discontinuous Kolmogorov equation, and thus for the Boltzmann equation in its most general form, if the coupling of the system to its higher moments is not too large. We will give brief examples how to use these equations in the end of this section; a thorough investigation of their applicability in general physical and astrophysical problems remains a task for future work.

The continuous loss approximation and meaning of the loss time scale: After we have discussed the connection of the mathematical theory of point processes to the most general tasks of transport theory, we return to the physical treatment of photonuclear interaction processes we have performed in Chapter 1, and investigate the meaning of the concepts derived there.

In Chapter 1 we have been guided by a principle we may call the *leading particle concept of cosmic ray transport*: it expresses the fact that, at least over a certain time, protons and heavy nuclei can be treated as *individual particles*, to which a evolving quantity of state is attached. In the most general view this is the energy, but we have already noted that it falls apart into a description of the Lorentz factor and the nuclear mass, which are essentially independent. The relevant quantity which we have used to describe the evolution of the variables of state was the *loss time scale*. But what does the time scale tell us with respect to particle transport, independent of their property of being comparable to other time scales (e.g. of acceleration processes)?

The loss time scale describes over which time the *average* of the quantity of state changes considerably. We may therefore expect that, in terms of random processes, the loss rate, τ_{loss}^{-1} , is the expectation value over the energy change per time, or the first moment of the intensity function

$$\tau_{\text{loss}}^{-1} \stackrel{!}{=} \langle \tau(t, y, y + \Delta y) \mid \Delta y \rangle \quad . \quad (2.2.20a)$$

It is obviously equivalent to the parameter b used in the continuous Kolmogorov equation, Eq. (2.2.7). But is the way we have defined τ_{loss} in Chapter 1, resp. Eq. (1.1.45), really equivalent with Eq. (2.2.20)? Obviously, we may write Eq. (1.1.45) as

$$\tau_{\text{loss}}^{-1} \equiv \left\langle \left[\frac{dN_{\epsilon'}}{d\epsilon'} \right]_E \cap \left[\frac{d^n \sigma(\epsilon', \varphi)}{d\varphi_1 \dots d\varphi_n} \right] \mid \frac{\Delta E(\epsilon', \varphi)}{E} \right\rangle \quad , \quad (2.2.20b)$$

using the conditional outer product introduced in Sect. 2.1.2.5. The intensity function is thus the product distribution of photon NRF spectrum and interaction final state distribution applied to a random function $\Delta y(\epsilon', \varphi) = \Delta \phi(E)$, describing the change of a function $\phi(E)$ of the random variable E ; however, the inelasticity $K = -(\Delta E/E)$ cannot be identified with the change of a random function, $\Delta \phi(E)$, in the general case. Only for *infinitesimal steps* we can set $y = \ln E$ and have

$$dy = d \ln E = \frac{dE}{E} = -K \quad , \quad (2.2.21)$$

or $\phi(E) = \ln E$. This we may interpret as that the classical loss rate describes the *mean loss* of the *logarithm of energy* per time, if the single steps in energy loss are infinitesimally small.

In the general case of non-infinitesimal steps, however, τ_{loss}^{-1} does not describe the mean evolution of *any* random quantity. We may visualize the problem in an example: Assume a process through which a particle loses many orders of magnitude of energy in every interaction, i.e. $E_f \ll E_i$. Then, we obviously have $\Delta E \approx E$ or

$K \approx 1$, and consequently $\tau_{\text{loss}}^{-1} = \rho(t, E)$, which is the interaction rate function and thus independent from the magnitude of energy loss in every reaction. It is clear that this cannot be correct, if we assume that the evolution of the quantity of state, E , is described. In the limit of strong losses per interaction, the classical loss time scale turns into the interaction time scale, $\tau_{\text{loss}} \rightarrow \tau_{\text{int}}$, which gives a description of number of interactions rather than the mean energy loss.

Prospective and retrospective views on cosmic rays: Before considering transport processes in greater detail, we may add some remarks on the problem of time reversibility in stochastic processes. In practice we are often confronted with two different views on a physical problem: The first, which we may regard as the theoretician's point of view, follows a physical process as it happens in reality, i.e. in positive time direction. Here, the physical system can straightforwardly be described by application of physical laws to the present state of the system. On the other hand, the experimentalist is often interested to draw conclusions from his experimental results without referring to theories, which means a description of a physical system backward in time, starting from the current observation and proceeding to earlier states. This approach will be called the *retrospective*, the former the *prospective* description of the system. In determinate problems, both views are obviously equivalent, because of the time reversibility of the fundamental laws of physics; however, we know from the entropy law in thermodynamics that, as soon stochastic effects play a role, time reversibility does no longer hold.

Considering the transport of a cosmic ray particle, the problem of reversibility can be discussed at the following example: Consider an interaction type of cosmic ray particles with a background field, which sets in instantaneously at a certain threshold of cosmic ray energy, E_{th} , and leads to a certain, discontinuous energy loss of the particle. Now consider a particle with an energy $E_0 \gtrsim E_{\text{th}}$ hardly above threshold, which will move to an energy E_1 below threshold in the next interaction. In the prospective view, we will determine a certain non-vanishing probability of the particle to interact, and therefore end up with an energy below $E_1 < E_{\text{th}}$. In the retrospective view, if we start with an observed energy E_1 , we find that the probability for a jump up to E_0 , is zero, as far as we use only the *present state* of the particle for its description; a result which is obviously incorrect. The reason is, of course, that the properties of the interaction which took place were determined by the physical initial state, which is the *final state* in the retrospective view. Therefore, the total probability of an interaction is given by the distribution of final states in the retrospective view, which cannot be derived solely by the knowledge drawn from the observation. This problem is mathematically expressed by *Bayes theorem*, Eq. (2.1.33), which makes clear that we need knowledge — or at least assumptions — of the initial state distribution of the particle to draw retrospective probabilistic conclusions. The importance of *Bayesian methods* in statistical inference and data interpretation has recently been emphasized by PRESS [Pre96]. We will not discuss these methods in detail here, but point out their importance in particular for the interpretation of highest energy cosmic ray data and the discussion of possible models for their origin, and refer to, e.g., the book of MARITZ [Mar70].

The retrospective view on cosmic ray transport is obviously possible if stochastic effects are not considered, and has been extensively used in our previous work [Rac92, RB93]. However, we will see below that these *quasi-continuous* approaches do not produce useful results in the vicinity of the GZK cutoff, and hence *both* the quasi-continuous approach and the retrospective view has to be abandoned for further considerations.

2.2.2.2 Classification of transport processes

The Markov parameter: The transport of cosmic rays protons and nuclei through photon background fields is a classical example for a — generally discontinuous — Markov process. It is described by the Kolmogorov equations, Eqs. (2.2.5), and the task of the description of the interaction process is finding the intensity function

$\tau(\mathbf{t}, \mathbf{y}, \mathbf{y} + \Delta \mathbf{y}(\mathbf{x}))$, where the variable of state, \mathbf{y} , is called the the *Markov parameter* of the transport problem. We distinguish the Markov parameter from other quantities of state which are described by *determinate* processes, which we combine in the parameter vector \mathbf{t} .

Even though the physical quantity which is subject to random changes may be given unambiguously, the choice of the Markov parameter bears a degree of freedom: we obviously may take any unique function of the variable of state as a Markov parameter. In our choice, we will be guided by the separation of astrophysics and interaction physics; we require, that the dependence of the interaction physics can be described *as far as possible* independently from the astrophysical state. Since the interaction physics shall give the change of the Markov parameter in every single step, $\Delta \mathbf{y}(\mathbf{x})$, we thus require that the *changes in y* do not depend on \mathbf{y} itself; in other words, we try to describe cosmic ray transport as a *point process with uncorrelated marks*, i.e. we can write

$$\tau(t, \mathbf{y}, \mathbf{y} + \Delta) = \rho(t, \mathbf{y}) f_m(\Delta) \quad . \quad (2.2.22a)$$

If we restrict ourselves to the description of one-dimensional random processes, this relation is required to allow a description by means of the perturbative equations Eq. (2.2.18). To make sure that this description works, we also have to require that the rate function is not violently dependent on the Markov parameter, i.e.

$$\frac{d^k \rho}{dy^k} \lesssim \rho \quad \text{for } k > 1 \quad . \quad (2.2.22b)$$

Then, Eq. (2.2.18a) shows that $\rho_l \propto 1/l!$, which we will assume as a minimal condition for the perturbative approach to work.

The variables of state describing cosmic ray nuclei are the *Lorentz factor*, γ_{CR} , and the nuclear mass number, A_{CR} . Considering protons, it is the Lorentz factor which is subject to random changes due to photomeson production; from Sect. 1.2 we know that the relative change of the Lorentz factor in a photopion production is essentially given by the pion/proton mass ratio, $\Delta \gamma_{\text{CR}}/\gamma_{\text{CR}} \sim m_\pi/m_p$; thus it is natural to choose

$$y_L \equiv \ln \gamma_{\text{CR}} \quad (2.2.23a)$$

as the Markov parameter; as we have already stated in Sect. 1.2.2.4 (see also Fig. 1.13), $\langle \Delta y_L \rangle \approx 0.2$ over the whole range of γ_{CR} . The mass number is obviously constant for protons, i.e. $A_{\text{CR}} \equiv 1$. For heavy nuclei, the mass number is the quantity which is subject to random changes; from Sect. 1.3.3 we know that the change of A_{CR} in a photodisintegration reaction, which was expressed by the nucleon multiplicity $\nu(A)$, is independent of A for the most important process, the *giant dipole resonance excitation* ($\nu \equiv 1$); consequently we set

$$y_A \equiv A_{\text{CR}} \quad , \quad (2.2.23b)$$

and identify the Markov parameter for photodisintegration with the mass number. The Lorentz factor is, as we have seen, approximately conserved in photodisintegration; it is nevertheless an important parameter of state determining the intensity function, and it is subject to change due to other interaction processes, mainly inverse Bethe-Heitler losses. We will see below that these processes are *determinate* in good approximation, thus γ_{CR} is *not* a Markov parameter in the transport of heavy nuclei and can be included in the parameter vector \mathbf{t} .

The properties of cosmic ray transport, i.e. that a quantity of state undergoes to first approximation either constant *absolute* or constant *fractional* changes may give rise to a general distinction of marked point processes: we write the evolution chain of a random variable X alternatively as

$$X_n = X_0 + \sum_{i=1}^n \Delta_i = X_0 \prod_{i=1}^n f_i \quad .$$

Particularly simple cases are given when either the increments Δ_i or the increment fractions f_i are equally distributed. We will call the first case the elementary *arithmetic step process*, the second the elementary *geometric step process*. Both are represented by Markov chains with independent increments, which is obvious for arithmetic processes with $y = X$, and for geometric with $y = \ln X$ leading to

$$\ln y_n = \ln y_0 + \sum_{i=1}^n \ln f_i \quad .$$

The mark distribution for geometric step processes is therefore given by the distribution of the random function $\ln f$. In most cases there are simple physical reasons to decide which process rather describes the physical system under consideration, and we can take this distinction as a first step to reduce the coupling of the system. In special cases, of course, other suitable functions to define Markov parameters from given quantities of state may be chosen.

Quasicontinuous processes: Principally, photonuclear interaction processes are *discontinuous*, i.e. their statistical treatment leads to a point process, because changes of the particle state are invoked by single photon hits. However, we have described in Sect. 1.1.2 some processes which have a fairly large cross section, therefore a large interaction rate, but lead only to very small energy changes in each single interaction, i.e. a small inelasticity $K_i = -(\Delta E)_i/E_i$. Then, the energy loss rate can be written as

$$-\left(\frac{1}{E} \frac{dE}{dt}\right) = \langle K \rangle(E) \rho(t, E) \quad , \quad (2.2.24)$$

where $\rho(t, E)$ is the interaction rate of the process, and $\langle K \rangle \ll 1$. Since $\rho(t, E)$ is given by the interaction physics, Eq.(2.2.24) is a differential equation describing the energy evolution of the particle. This is a well known classical approach to cosmic ray transport, called the *continuous approximation*.

If we turn back to the discussion of Sect. 2.2.1.2, we could classify such processes as approximately continuous Markov processes, because Eq. (2.2.7) holds for all $\varepsilon > \|\Delta E\|$, where $\|\Delta E\|$ expresses the maximum step size and is still a very small quantity. So, we will expect that Eq. (2.2.7) gives the description of the process in good approximation, with $\mathbf{b} \equiv \eta$ and $|\mathbf{q}| \sim K$. In a pure loss process as considered here, we can now easily see that the diffusion coefficient is of order $D \sim K^2$, and can therefore be neglected because $\langle K \rangle \ll 1$ by assumption. Then, it is easy to show that Eq. (2.2.7) is equivalent to Eq. (2.2.24), which can be called the *drift approximation of quasi-continuous loss processes* [BG88, Rac92].

It should be pointed out that the diffusion coefficient D in Eq. (2.2.7) cannot be neglected when the transport problem allows for *energy gains* as well as energy losses. This is generally the fact when we consider system in which Fermi acceleration takes place; it will be principally possible to describe Fermi acceleration in the framework of random processes developed here; however, this would be beyond the scope of this work, and we will generally restrict our consideration to pure loss processes. Therefore, all quasi-continuous processes can be treated in drift approximation, and will be called *drift processes* henceforth. It is obvious from Eq. (2.2.24) that drift processes are strictly determinate, they are *not* random processes.

Adiabatic processes: A process which is generally treated as determinate is the *adiabatic cooling and heating* of the “cosmic ray gas” enclosed in some expanding or contracting “cosmic box”. The change of energy density of an ultrarelativistic gas in an adiabatic process is expressed by $u \propto R^{-4}$, when $R \equiv V^{1/3}$ is the characteristic length scale of the box with volume V . Since the energy change is equally distributed over all particles, we have

$$E_{\text{CR}} \propto R^{-1} \quad (2.2.25)$$

for the energy of a cosmic ray particle captured in the volume V . The application of this is various for cosmic rays which are magnetically confined; the first order Fermi acceleration process principally bases on this equation, because it describes the acceleration of particles which are captured between permanently approaching magnetic mirrors. The application important in the transport of cosmic rays over cosmological distances is, of course, connected to the expansion of the universe itself: Inserting for R the characteristic length scale of the universe (see, e.g., [Wei72]), Eq. (2.2.25) results in the *redshift relation* $E \propto 1+z$, where the redshift z is related to time by

$$\frac{dz}{dt} = -H_0(1+z)^2 \sqrt{1+2q_0z} \quad . \quad (2.2.26)$$

We note that this relation applies to any ultrarelativistic gas, not just to photons to which it is usually applied. In the nonrelativistic case, Eq. (2.2.25) still applies to the momentum of a particle.

Adiabatic losses are strictly determinate with respect to the energy loss of a single particle, if the “binding” of the particle to the expanding system is due to permanently acting force; in the cosmological case, it expresses the expansion of the gravitational field. It applies as well in systems where the particle is bound by frequent scattering, i.e. in a system of expanding magnetic clouds. Then however, it describes the evolution of the *average* energy of the particle distribution, while the energy change of a single particle is subject to fluctuations. In this case, the determinate concept will certainly break down in the small statistics limit, i.e. when $\tau_{\text{scat}} \sim T_{\text{esc}}$, where τ_{scat} is the scattering time as defined in Eq. (1.1.11) and T_{esc} the time scale for the escape of the particle from the system; adiabatic losses can then be treated as an inverse first order Fermi process by means of a statistical evaluation of Eq. (1.1.13).

2.2.2.3 Simplified approaches to cosmic ray transport

Absorption processes: The simplest random process is one which allows only one kind of event, and only one event per particle: it is the *pure absorption process*. Such processes may be applied in the transport of energetic photons, if the subsequent cascade is neglected, or to light nuclei which are destroyed in the first interaction (see Sect. 1.3.4.2). For other cosmic ray transport problems, they may serve as a first order approximation: We just assume that a particle is absorbed with a time scale τ_{int} . This was the original approach performed by GREISEN, ZATSEPIN & KUZMIN [Gre66, ZK66] to propose the UHE cutoff in the extragalactic cosmic ray spectrum. It was later corrected by STECKER [Ste68] by replacing τ_{int} by τ_{loss} , which gives a more accurate estimate of the extinction of cosmic rays by the microwave background; nevertheless it is only a first order approximation.

To show how the absorption approach works, and how it compares with other approximations, we divide the energy axis into logarithmic intervals with a constant bin size, $\Delta y_L = D$, starting from an arbitrary energy, E_1 , corresponding to the bin number $k = 1$, and assume a power law particle energy spectrum, i.e. $N_0(E) \propto E^{-a}$, corresponding to $N_0(k) \propto \exp(-\alpha k)$ with $\alpha = aD$. The interaction rate will be given by a function $\rho(k)$, for which we make two simple assumptions: (a) a constant interaction rate, $\rho_a(k) = \rho_0$, and (b) a linearly increasing rate, $\rho_b(k) = \rho_1 k$. We define the *modification factor* by $\mathcal{M}(k, t) = N(k, t)/N_0(k)$, where $N(k, t)$ is the spectrum we find after a propagation time t . We easily get

$$\mathcal{M}_a(k, t) = \exp(-r) \quad (2.2.27a)$$

$$\mathcal{M}_b(k, t) = \exp(-r'k) \quad , \quad (2.2.27b)$$

with $r = \rho_0 t$ and $r' = \rho_1 t$. Case (a) yields a constant reduction, while case (b) results in a steepening of the spectrum, $\alpha \rightsquigarrow \alpha + r'$. In principle, this behavior should be reproduced by all transport approaches.

Continuous loss approximation: A different, although just as simple approach to cosmic ray transport has been introduced by BEREZINSKY & GRIGOR' EVA (BG) [BG88]; they assumed that all particles propagate equally, with a relative energy loss $\tau_{\text{loss}}^{-1}(\gamma_{\text{CR}})$. This is an application of the quasi-continuous loss approximation to UHE cosmic ray transport; we have already noted that this cannot give an exact description of the transport of cosmic rays, because we have finite steps of considerable size, and random fluctuations cannot be neglected. Moreover, we have noted that the inelasticity as defined in Sect. 1.1.3.3, which was also used by BG, does not give an exact description of the mean energy loss of a single particle when finite steps are considered. We refer to Sect. 2.2.2.4 how this problem can be removed; the main drawback of the method, however, will become clear from applying it to our simple example described above: The loss rate in our example is obviously given by $\rho(k)$, because $\Delta k = 1$ in every interaction. The process we consider now is not stochastic; rather, after a time $t = \rho(k)^{-1}$ all particles in bin k move to bin $(k - 1)$, and we get the modification factors

$$\mathcal{M}_a(k, t) = \exp(-\alpha \lfloor r \rfloor) \quad (2.2.28a)$$

$$\mathcal{M}_b(k, t) = \begin{cases} 1 & \text{for } k < \lfloor 1/r' \rfloor \\ [1 - \exp(-\alpha)]^{-1} & \text{for } k = \lfloor 1/r' \rfloor \\ 0 & \text{for } k > \lfloor 1/r' \rfloor \end{cases}, \quad (2.2.28b)$$

where $\lfloor x \rfloor$ denotes the largest integer $n \leq x$. The modification in case (a) corresponds to a spectrum moved by $\lfloor r \rfloor$ bins to the left; it therefore depends on the spectral index and on the bin size. $\mathcal{M}_b(k)$ shows the typical ‘‘Berezinsky-Grigor’eva-spike’’, followed by an abrupt cutoff. It shows the advantage and the disadvantage of this method immediately: The advantage over the absorption approach is, that the method conserves particle number; in calculations where one sums up over many spectra with different modification factors, where the ‘‘spikes’’ are smoothed out by superposition, the method will give a correct result concerning total flux far off from the cutoff, while the absorption approach will underestimate the flux. For single sources, and in particular near to the maximum energies, however, the continuous loss approach does not give useful results, because it proposes a total cutoff of the spectrum. In a correct statistical treatment, the particle flux can obviously not be diminished stronger than in the absorption approach.

Counting processes: We now try to introduce a statistical treatment which considers both fluctuations and particle conservation. In our simple example, we assume that all steps are equal; thus, the random process we have to consider is a pure point process, or *counting process*. From Sect. 2.2.1.3 we know that our case (a) corresponds to a *Poisson process*, which means that we find the particles of bin k Poisson distributed, i.e.

$$f_a(j; k, t) = \frac{r^{k-j}}{(k-j)!} e^{-r} \quad \text{with } r = \rho_0 t,$$

over the bins $j = 1, \dots, k$. The integral over the spectrum is obviously conserving particle number; however, some particles are moved out of the energy range. Summing up, we find after a little algebra

$$\mathcal{M}_a = \exp \{ -r (1 - e^{-\alpha}) \} \quad (2.2.29a)$$

For case (b), we note that the counting process falls into the class of *birth processes*; however, the interaction rate *falls* linearly with the number of interactions (because the particle loses energy). We may therefore call it the *inverse Yule-Furry process*; we could actually transform it into a Yule-Furry process if we would consider it *retrospectively*, but we also noted that random processes are not time-reversible and we would have to use

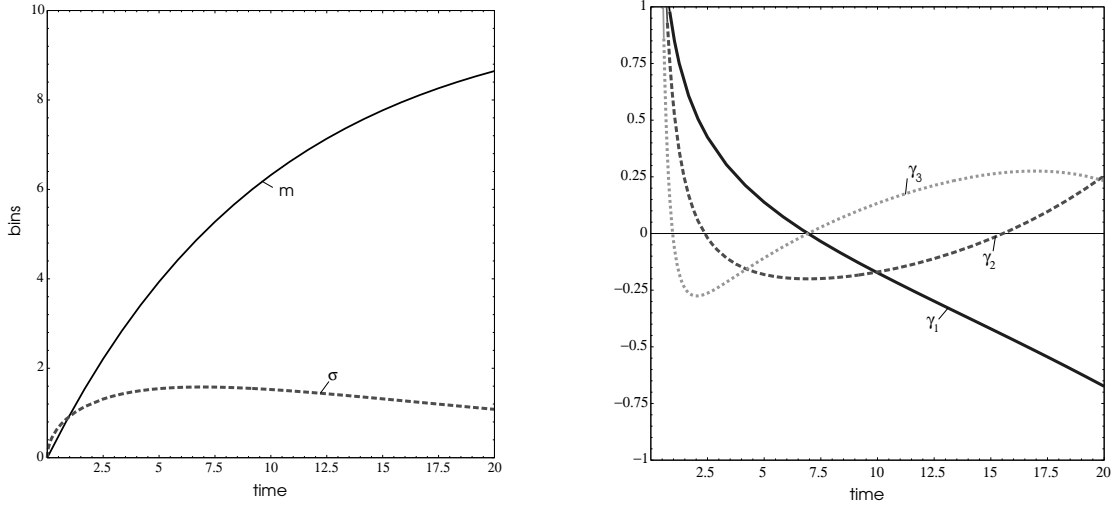


Figure 2.1: Evolution of dispersion and shape parameters of the inverse Yule-Furry distribution with time, for propagators starting from bin $j_0 = 10$. Left panel: mean distance from starting bin, m , and standard deviation σ . Right panel: shape parameters γ_i .

Bayesian methods. We could, of course, try to solve the Kolmogorov equation for the birth process with falling birth rate and starting bin j , which is

$$\frac{\partial}{\partial t} f(t, k) = \hat{\delta}_{kj} \rho_1 (k+1) f(t, k+1) - \rho_1 k f(t, k) \quad . \quad (2.2.30)$$

Instead of doing this work — which is analytically possible, but quite laborious and tricky, because it is a differential equation system which has to be solved successively — we will go the easier way and describe the system perturbatively, using Eq.(2.2.11) with $m = 1$, $\hat{\rho}_0 = \rho_1 j$ and $\hat{\rho}_1 = -\rho_1$. We can solve Eq.(2.2.11) analytically for $j = 1, \dots, 5$; however, we abstain from giving the lengthy expressions for the solutions here, and rather show a graphical example for the time evolution of the dispersion and shape parameters (m , σ and γ_{1-3}), from which we model the distribution arising from particles starting in a bin $j_0 = 10$, using the Edgeworth expansion, Eq. (2.1.57). Fig. 2.2 shows the resulting distributions at $t = 5$ for different starting bins.

Comparison of the approaches and their applicability to cosmic ray transport: Let us first study the case of an energy independent interaction rate; here we have only to compare simple numbers, and we see that the counting process treatment gives generally the “smallest” modification of the spectrum (i.e. M closest to 1). The continuous energy loss predicts a modification dependent on the product of spectral index and step-bin-size, $\alpha = aD$; for $\alpha > 1$, it predicts a stronger drop of the flux in each bin than the absorption approach, which certainly cannot be true: there is no way to reduce the flux more than by removing the particles entirely in the first interaction. The simple factor given in Eq. (2.2.29a), predicted by the evaluation of the Poisson process, considers *both* the statistical fluctuations and the “refill” of particles into every bin coming from higher bins.

We have assumed initial spectra without cutoff so far; if we have a cutoff, the action of the absorption approach is unchanged, and the continuous loss approach moves the cutoff steadily to the left. The point process approach predicts that the absorption approach applies in the highest bin, where no particles can be refilled; therefore, we have to expect that the factor $(1 - e^{-\alpha})$ in the exponent of Eq. (2.2.29a) will slowly increase to 1 close to the cutoff.

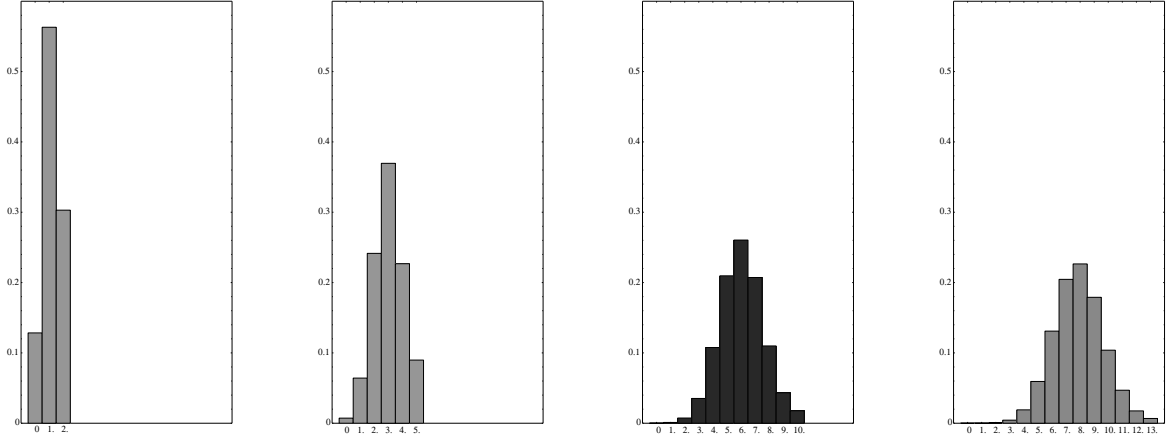


Figure 2.2: Inverse Yule-Furry propagators for $t = 5$ in natural units; bins are counted up to the starting bin in all cases.

For the comparison of the approaches in case of an increasing interaction rate it is best to insert numbers for our parameters and to compare numerically. We set $\Delta y_L = \Delta \ln \gamma_{\text{CR}} = 0.2$, i.e. $\Delta \log \gamma_{\text{CR}} \approx 0.09$; thus, eleven bins cover approximately one decade of energy. We set $\rho_1 = 0.1$, which defines the natural time unit; after a time $t = 1$ we expect one interaction per particle in the tenth bin. Furthermore, we set $a = 2$, thus $\alpha = 0.4$. We compare the modification factors for the three approaches discussed here in Fig. 2.3 for $t = 5$; because of our simple assumption of proportionality, $\rho(k) \propto k$, both the absorption approach and the point process approach predict a steepening of the spectrum. However, the point process approach leads to a much smaller increase of the spectral index than pure absorption, and includes a small bump at low energies to account for particle conservation. In contrast, the continuous loss approximation predicts a pronounced bump and a “razor blade” cutoff, which strongly deviates from the predictions of both other methods. Hence, it cannot be considered as a suitable method to describe single cosmic ray sources, it is just useful for integrated calculations because of its property of particle number conservation and its simplicity. The right panel of Fig. 2.3 shows the dependence of the spectral steepening on the number of time steps in the inverse Yule-Furry process. Here, we have taken into account a possible cutoff in the source spectrum, by limiting our summation to bins up to $k = 15$. We clearly see the turnover to an exponential decline, but we do not quite approach the limit set by the absorption approach in the last bin; this indicates numerical inaccuracies of our perturbative approach for small probabilities (i.e. the regions of the propagator far from the mean), which we certainly have to expect.

To which extent does our discussion apply to cosmic ray transport? Clearly, it is not a quantitatively reliable calculation, but it already shows some spectral features we will expect in the vicinity of the GZK cutoff: Close to the maximum of the interaction rate of protons in the cosmic microwave background, at $\gamma_{\text{CR}} \lesssim 10^{12}$, we can approximate the interaction rate as proportional to $\ln \gamma_{\text{CR}}$, which turns into a constant rate for $\gamma_{\text{CR}} > 10^{12}$. Thus we expect a steepening of the spectrum, as shown in Fig. 2.3, for $\gamma_{\text{CR}} \gtrsim 3 \times 10^{10}$, and a constant reduction (thus a continuation with the initial spectral index) for $\gamma_{\text{CR}} > 10^{12}$. Comparing to our example, we may assign the tenth bin to $\gamma_{\text{CR}} = 3 \times 10^{11}$, where $\lambda_{\text{int}} \sim 6 \text{ Mpc}$, thus $t = 5$ corresponds to 30 Mpc. Since the steepening of the spectrum in this case is about $\Delta a \approx 0.75$, we expect a “flat” cosmic ray spectrum in the conventional $E^{2.75}(dN/dE)$ representation between 30 and 300 EeV; which will be probably followed by an exponential decline due to cutoff effects in the source. Even though our statement is not quantitatively reliable,

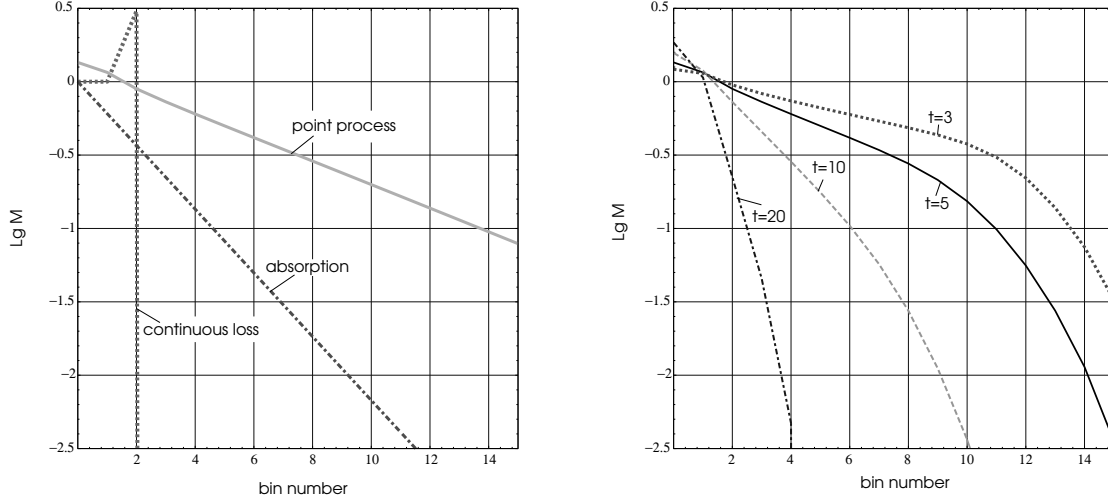


Figure 2.3: Left panel: Modification factors for an E^{-2} power law spectrum without cutoff, arising from the different transport approaches discussed in the text, for $t = 5$. Right panel: Modification factor resulting from the point process approach for an E^{-2} power law spectrum with an abrupt cutoff after the 15th bin, for different t .

and more thorough investigations are required, it already shows that there may be need to reconsider some of the strong statements done after the the detection of the 200–300 EeV cosmic ray events at Fly’s Eye and AGASA experiments [BCD⁺95, HHH⁺94, ES95, SSB94].

2.2.2.4 Cosmic ray transport as a marked point process

Separation of the probability space: In the previous section, we discussed the statistical properties of cosmic ray transport using estimated numbers for the interaction inelasticity, and neglecting its distribution. A full calculation would require to consider a marked point process, i.e. determine both the interaction rate, $\rho(t, y)$, and the mark distribution $f_m(t, \Delta y)$, i.e. the energy loss distribution per interaction, directly from the interaction physics, which has been described in Chapter 1.

To determine the intensity function, $\tau(t, y, y + \Delta y)$, we may separate the probability dimensions of the interaction as follows:

1. The initial state probability space, \mathbb{P}_i , given by the energy distribution of the photon in the NRF, folded with the total interaction cross section.
2. The branching ratio, b_c , choosing an interaction channel.
3. The final state probability space, \mathbb{P}_f , given in photomeson production by the final state distribution function, $\Phi_c(\varphi_c)$, of the channel c (see Eq. (1.1.54) and Sect. 1.2.1.4), and in photodisintegration by the nucleon multiplicity function $\nu(\epsilon', A)$.

While the branching ratios and Φ_c are normalized probability distribution functions, the absolute normalization of the initial state determines the rate function,

$$\rho(y) = \tau_{\text{int}}^{-1} = c \int_{\epsilon'_{\text{th}}}^{\infty} d\epsilon' \left[\frac{dN_{\epsilon'}}{d\epsilon'} \right]_{\gamma_{\text{CR}}} \sigma(\epsilon') \quad . \quad (2.2.31a)$$

We can then write formally for the mark space distribution

$$f_{\text{m}} = \tau_{\text{int}} \left[\frac{dN_{\epsilon'}}{d\epsilon'} \right]_y \sigma \sqcap b_c \sqcap \Phi_c \quad , \quad (2.2.31b)$$

where we have used again the conditional outer product (Sect. 2.1.2.5) to emphasize the causal dependence of the distribution functions: every distribution can depend on the random variables given by the distributions to its left. Here it means that the photon NRF energy determines the branching ratio, and both ϵ' and channel number c determine the final state distribution. We may describe the mark distribution by the set of its moments, which are given by $\langle f_{\text{m}} \mid (\Delta y)^k \rangle$; explicitly we can write

$$\mu_k^{(c)} = \tau_{\text{int}} \left\langle \left[\frac{dN_{\epsilon'}}{d\epsilon'} \right]_y \sigma_c \sqcap \Phi_c \mid (\Delta y)^k \right\rangle \quad (2.2.32)$$

and $\mu_k = \sum_c \mu_k^{(c)}$; here we have used the linearity of distributions and the definition of the specific cross section of the channel c , $\sigma_c(\epsilon') = b_c(\epsilon')\sigma(\epsilon')$. We know from our discussion above that for photomeson production we have $\Delta y = \ln(1 - K)$, where K is the inelasticity as used in Sect. 1.1.3.3. We note that the first moment, μ_1 , describes the average change of the Markov parameter in one interaction; $\mu_1 \tau_{\text{int}}^{-1}$ is therefore an expression for the energy loss rate,

$$\mu_1 \tau_{\text{int}}^{-1} = \frac{d \ln y}{dt} = -\frac{1}{E} \frac{dE}{dt} \quad , \quad (2.2.33)$$

which is also correct for non-infinitesimal steps, in contrast to τ_{loss}^{-1} as defined in Eq. (1.1.45). For photodisintegration, we have $\Delta y = \nu(A)$.

Scaling relations and the applicability of the perturbative approach: In the general case, the moments of the mark distribution will depend on the Markov parameter; in some cases, however, this dependence can be removed and the transport process can be described as a point process with uncorrelated marks, which allows a description of the moments of the propagator by Eq. (2.2.18).

In photomeson production, the Markov parameter is connected to the cosmic ray Lorentz factor, $y = \ln \gamma_{\text{CR}}$. We can immediately infer from the discussion in Sect. 1.2.2.4 (cf. that section for the notation used here), that in anisotropic power law spectra, Eq. (1.1.51b), the moments of the mark distribution are given

$$\mu_k = \frac{1}{\Sigma_{ab}^{(c)}} \frac{2(a-1)(b+1)}{a+b+1} \int_1^{\infty} dx x^{-a} \langle \sigma_c \Phi_c \mid \ln^k(1-K) \rangle \quad , \quad (2.2.34a)$$

where the cross section coefficient $\Sigma_{ab}^{(c)}$ is obtained as in Eq. (1.2.31b), by replacing η_c by σ_c . Then, the rate function is obviously given as

$$\rho(\hat{\gamma}_{\text{CR}}) = c N_0 \Sigma_{ab} \hat{\gamma}_{\text{CR}}^{a-1} \quad (2.2.34b)$$

with $\Sigma_{ab} = \sum_c \Sigma_{ab}^{(c)}$. We note that the moments μ_k are indeed independent of $\hat{\gamma}_{\text{CR}} = \gamma_0 \gamma_{\text{CR}}$, and thus of y . Moreover, we find that

$$\hat{\rho}_l = \frac{1}{l!} \frac{d^l \rho}{dy^l} = \frac{(a-1)^l}{l!} \hat{\rho}_0 \quad (2.2.34c)$$

with $\hat{\rho}_0 = \rho(y)$. Hence, for not too large power law indices a , the absolute values of the coefficients $\hat{\rho}_l$ decrease very fast, and the perturbative approach may give reasonable results.

In photodisintegration, the situation is principally more complicated: the Markov parameter is here the nuclear mass, which is essentially connected to the microphysics — in contrast to the Lorentz factor, which acts only indirectly by shifting the NRF photon spectrum relative to the cross section. In fact, we do not find a chance to obtain mark distributions which are *completely* independent of the Markov parameter. On the other hand, we know that the most efficient photodisintegration process is the excitation of the giant dipole resonance, which almost entirely decays by emission of a single nucleon. Thus, we may describe the photodisintegration process by a simple, unmarked point process, as discussed in the last section. To obtain consistency with the average mass evolution, we may set the number of removed nucleons per interaction not to 1, but to the average value obtained from the ratio of efficiency and rate function.

The complete description of cosmic ray transport: Cosmic rays are not only subject to incoherent photonuclear reactions — they are, of course, also affected by quasi-continuous and adiabatic loss processes. These are of particular importance when considering cosmic ray transport over large extragalactic distances, at energies below the GZK cutoff, where cosmological redshift and Bethe-Heitler losses have been proven to have an important effect on the spectral evolution [BG88, Rac92]. Moreover, we might be interested to describe cosmic rays also *inside* their sources, where loss process act parallel to Fermi acceleration processes. Is it possible to consider all these processes, including the Markovian loss processes, in one treatment?

The transport equation describing the most general case of cosmic ray transport, separated into continuous and discontinuous processes, is known as the *Ginzburg-Syrovatskii-Equation* [GS64, HS85]. In the language of random processes, this equation describes the evolution of a random variable which is subject to continuous and discontinuous Markov processes, thus a superposition of the continuous and discontinuous Kolmogorov equation. With respect to our perturbative approach, it just means the inclusion of some additional terms on the right side of the moment evolution equations, Eq. (2.2.18). Since we know that diffusion terms essentially lead to the evolution of Gaussian distributions, we may expect that a continuous diffusion term in our equation even reduce the effects of upward coupling arising from the discontinuous Markovian contributions — it only adds a “harmless” component keeping the propagator closer to a Gaussian shape and thus better handable.

The answer to our question is therefore: Yes — at least in many interesting cases. Even though it remains an unproved statement at this point, we may expect that the transport approach developed here may allow a simple, and numerically fast description of the evolution of cosmic ray spectra in *any* astrophysical system. An investigation of this — and of course the production of many astrophysically relevant results — can be set as a program for the next years.

Outlook — no Conclusion

Contemplations about life, the universe and everything¹⁵

About life: writing and finishing PhD theses

At this point the reader will certainly ask: *Why stopping here?* And all I can say is: *Because there must be a time to stop, and the time is now!*

This work was a — maybe typical — example for a PhD theses which was started with a big, but apparently feasible plan, then worn out between scientific everyday requirements and funding politics, extended due to the insight that life (and in particular physics) is not that simple as it initially appears, and finally finished abruptly as a snapshot of its present state. When the time came to take this snapshot (i.e. writing down and come to an end), it became more and more clear to me that this work would contain — even though it is officially a PhD thesis in astronomy — almost *no* astronomy at all! I just finished developing the toolkit to solve my problems; but now there was no time to solve them any more. However, I realized that the toolkit *itself* may be interesting enough, and before doing some bad work quickly with the good tools, better try to complete the toolkit and sell it; there are enough people who may use it, and, finally: *There is a life after the PhD* — hopefully!

About the universe: the hot questions of cosmic ray astrophysics

Clearly, I *did* also astrophysical work in the last years; the results have been published in a couple of papers listed at the end of this section (there are no distinct references given here). I may briefly summarize what they were about, and how they fit into the “big view” of hadronic astrophysics stated in the beginning:

Analysis of soft X-ray spectra of PG quasars observed by the ROSAT PSPC instrument: We found that the soft X-ray excess in UV-bright quasars is unlikely to be due to a thermal hot bump of a temperature of about 50 eV. Rather, it seems that it is a gradual transition from a flat X-ray power law to a steeper power law towards the UV-region. We found that this behavior is expected if hadronic X-ray generating processes are taken into account. While it would be clearly exaggerated to state that hadronic models are the only ones which can explain such a simple behavior, we may still consider our work as another hint that hadronic processes are important in AGN — when they are probably *necessary* to explain the TeV features of AGN, it would be unreasonable to ignore them at lower energies. This jump over energy regions is, in principle, nothing but a consequent application of Occams razor, even though some “conventionally” thinking astronomers tend to interpret this principle in a different way.

¹⁵The author drops the scientific “We”-form in this section, because it contains some rather personal statements. Nevertheless, the reader may feel free to be included in the argumentation. Of course, “we” is still used in references to work which was done in a collaboration.

The search for the sources of the highest energy cosmic rays: The project to investigate systematically the arrival directions of the highest energy cosmic rays was born during my stay at the Bartol research institute. The first idea was (a) to find common features in the directional distribution of events above a few times 10^{19} eV in different experiments, and (b) to check the correlation with possible source distributions. While we had to realize that the data situation is much too bad to solve the second task, the first part of the program had at least the success to come in touch with various experimental groups. Later, this connection turned out to be fruitful, and lead to the discovery of a correlation of the highest energy cosmic ray arrival directions with the supergalactic plane, i.e. the local large scale structure of the universe. A positive side effect of our source search was also the “discovery” of the FR-II radio galaxy 3C134, which is directionally near to the Fly’s Eye event. Its redshift is unknown, but a simple estimate of its distance can be obtained from its radio size-luminosity ratio, which gives a value in the range 30–300 Mpc; this was meanwhile confirmed by an infrared detection of the obscured central galaxy. Thus, this source may be the closest FR-II galaxy in the sky, and a candidate source for the highest energy cosmic ray event.

Acceleration of cosmic rays at large scale shocks around clusters of galaxies: This model, based on an idea by KANG, RYU & JONES [KRJ96], goes right into the direction I have stated on the basis of very general arguments on large scale magnetic scattering in Sect. 1.1.1.3: The highest energy particles can most easily be accelerated in the largest structures. In this paper we found, however, that an end to this rule can be set by the microwave background: The highest energy cosmic rays become “GZK-limited” already in during their acceleration. If the diffusion is too slow, they are even limited by pair production losses to much lower energies, but for the fastest possible diffusion coefficients they may reach up to 100 EeV and above. One of the most interesting ideas connected with this model is the prediction of a spatial structuring of cosmic rays: since the large scale flow, and thus the accelerated particles, move *inside the cluster*, their only way to escape is through the cosmic matter sheets attached to the clusters. In other words, they are *confined to the large scale structure of matter*. It is immediately clear that this fits perfectly into our finding of a correlation of UHE cosmic ray anisotropy to the supergalactic plane!

At the present state, this work seems to give rise to more questions than it gives answers. But, considering that I am in search for an application of my hadronic-astrophysics toolkit, it is not a bad idea to ask questions — here are some of them:

- If the ultra-high energy cosmic rays are confined in supergalactic sheets, how good is this confinement? Is there a leakage? If so, it will be probably energy dependent, so — is there a spectral modification by an *supergalactic leaky box*? We note that both the sources (galaxy clusters or active galaxies) and we as the observers are inside the box — like in galactic cosmic ray physics. And what about the total flux normalization, if cosmic rays fill only a small fraction of the total space? May it even be that finally a much larger fraction of cosmic rays is of extragalactic origin than we ever thought?
- Considering this possibility, where is the transition point from the galactic to the extragalactic spectrum? Is it really the “ankle” at about 3 EeV? This question is closely connected to the experimental dispute whether there is a change of chemical composition in the spectrum at this point or not. If it is *not*, it is interesting to note that the spectral features around the ankle — a steepening of the spectrum followed by a flattening — which are observed consistently by all experiments [BCD⁺94, YHH⁺95], perfectly fit into the picture of a purely extragalactic modification due to the set-in of pair production losses at the microwave background. And if this is in fact the explanation, we note that these spectral features have a

well defined position in energy, dependent only on the temperature of the microwave background, which is known to a high precision — couldn't we use this to turn the tables and *check the calibration of the experiments* by the position of the ankle?

- If this speculation is wrong, and the ankle is the transition from the galactic to the extragalactic spectrum, i.e. if the composition change at the ankle is confirmed, we have to ask the following question: can we really accelerate heavy nuclei to energies of a few EeV in supernova shocks running into progenitor winds [SBG93], or at other places in the galaxy, *without* disintegrating them in background photon fields? Or, turning the argument around — if we really observe such energetic nuclei from the galaxy, what can we learn about the radiation fields in their sources?
- Leaving the field of cosmic ray physics, and turning to the sources of TeV gamma radiation: If this radiation is of hadronic origin, which contribution to the cosmic ray background do these sources give? Could this even constrain the models for the active radiation processes? How do the cosmic rays escape from the sources — is the isospin-flip mechanism (i.e. the escape as neutrons) the only process, which energies must the particles reach to escape? Which role play adiabatic losses, if we consider particles with gyration radii close to the size of the magnetic system?

These are only some of the questions which come into my mind right now. There may be many more. And, personally, I feel much better now when considering such questions than I did a year ago — because now I feel I have the possibility to solve them, using the tools developed in this theses.

About everything: here in particular about the way of science

There is still one principal question the reader might ask: *For what do we need these parametrizations and mathematical methods, when we have so fast computers now and are able to simulate everything in Monte-Carlo or other numerical codes?*

Here I have a principal answer. In my understanding, science has to fulfill (at least) four principles:

1. Knowledge cannot be gained by pure observations; we understand only on the basis of *theories explaining data*, never on the basis of data themselves.
2. Every prediction must be *testable* by observations; the more independent ways exist to falsify a prediction, the stronger is it.
3. The way a prediction or an explanation of data is gained must be *transparent*; if a prediction cannot be confirmed by observations, it must be possible to determine the exact reason for it.
4. Both data and theories must be *communicable* — and actually *communicated*; every scientist must be able to reproduce exactly the results other scientists have published.

The first two propositions may be called *Popper's principles*; they state that science gains knowledge not in *one direction* — i.e. either purely empirical on the basis of data, nor purely deductive on the basis of theories — but rather in an interplay of prediction, confirmation and falsification. The second two principles are requirements to the form in which predictions are made, or data are explained. There will probably be no scientist who denies the last three principles — in contrast to the first one, which is doubted by some people.

For my part, I believe that all four principles are essential for science, and I will now try to discuss how numerical simulations fit into this picture of science. The first question is: *Are numerical simulations data, or*

theoretical explanations or predictions? The answer is: they can be both and neither of them! They are predictions, but not gained from (physical) theories; if at all, they are extrapolated from data using *mathematically simple functions* without physical foundation. They are never explanations, because they do not connect the data to any more general principles. They may be treated as data, but they cannot replace real observations.

The *empirist* may be very happy with numerical simulations, because they allow to go the *empirist way* — which states that knowledge is gained by extrapolation and abstraction directly from the data — a few steps further than it was possible before fast computers were available. But they do not resolve the principal problem that the empirist way does not lead to a definite end.¹⁶ I do not deny that numerical simulations play an important role in contemporary science, and that they are really a useful technical tool — but it is dangerous to treat them as substitutes for theories; we may be able to simulate the world using numerical techniques, but we will never be able to *understand* it this way.

Less philosophical, but more serious is that for my impression many papers presenting results of numerical simulations do not comply with the last two principles, transparency and communicability. In some cases, Monte-Carlo codes are such obscure that, if there is a deviation in the results of two different simulations, even the authors of the programs themselves cannot exactly tell the reason for this deviation. What is often missing are the in-between steps of a calculation, which allow to analyze a result step by step. And even if this is carefully done, the detailed methods are rarely published — which violates the forth principle, communicability. Or, can any reader tell me a paper presenting Monte-Carlo results where the exact code is printed in the appendix?

Finally, even though I see numerical simulations as a very important tool of science, I still see the need for methods based on exact mathematical and theoretical principles. Without them, we run danger to lose control about our own results. I wouldn't like to see science going this way, because it may probably be the way to its end!

¹⁶The reader may understand that we cannot discuss in detail here the problems of empirism, and is referred to Popper [Pop94].

List of publications

Refereed journal articles

1. J.P. Rachen & P.L. Biermann: *Extragalactic ultra-high energy cosmic rays I: Contribution from hot spots in FR-II radio galaxies*, 1993, *Astronomy & Astrophysics* 272, 161.
2. J.P. Rachen, T. Stanev & P.L. Biermann: *Extragalactic ultra-high energy cosmic rays II: Comparison with experimental data*, 1993, *Astronomy & Astrophysics* 273, 377.
3. T. Stanev, P.L. Biermann, J. Lloyd-Evans, J.P. Rachen & A.A. Watson, *The arrival directions of the most energetic cosmic rays*, 1995, *Phys. Rev. Lett.* 75, 3056.
4. K. Mannheim, M. Schulte & J.P. Rachen: *The origin of soft X-rays in luminous quasars*, 1995, *Astronomy & Astrophysics* 303, L41.
5. J.P. Rachen, K. Mannheim & P.L. Biermann: *ROSAT PSPC observations of six PG quasars and PHL 1657*, 1996, *Astronomy & Astrophysics* 310, 371.
6. H. Kang, J.P. Rachen & P.L. Biermann: *Contributions to the cosmic ray flux above the ankle: Clusters of galaxies*, 1996, *MNRAS*, in press.

Conference proceedings, published

7. J.P. Rachen & P.L. Biermann: *Ultrahigh Energy Cosmic Rays from Fanaroff Riley Class II Radio Galaxies*, in: H.-J. Röser & K. Meisenheimer, *Jets in Extragalactic Radio Sources* (Workshop held at Ringberg Castle, Tegernsee, Germany, September 22-28, 1991). Springer-Verlag, Heidelberg, 1992, p. 287.
8. J.P. Rachen & P.L. Biermann: *Ultrahigh-Energy Cosmic Rays from Fanaroff Riley class II Radio Galaxies*, in: G. Zank & T.K. Gaisser, *Particle Acceleration in Cosmic Plasmas* (Workshop held at the Bartol Research Institute, Newark, Delaware, December 4-6, 1991). AIP, New York, 1992, p. 393.
9. J.P. Rachen: *Possible Extragalactic Sources of the Highest Energy Cosmic Rays*, in: *Seventeenth Texas Symposium on Relativistic Astrophysics* (Conference held at the München Park Hilton, Munich, Germany, December 10-16, 1994). The New York Academy of Sciences, New York, 1995, p. 468.
10. P.L. Biermann, J.P. Rachen & T. Stanev: *The origin of the highest energy cosmic rays and the large scale structure of the universe*, in: *Proc. of the 24th International Cosmic Ray Conference*, Rome, 1995, p. 809.

Conference presentations, unpublished

11. J.P. Rachen: *Propagation of Ultra-High Energy Heavy Nuclei in Extragalactic Space*. Talk presented at the APS meeting: *Particle and Nuclear Astrophysics and Cosmology in the Next Millenium*, Snowmass, Colorado, June 29 – July 14, 1994.

Bibliography

- [ABB68] ABBHHM Collaboration. *Photoproduction of Meson and Baryon Resonances At Energies Up To 5.8 GeV*. Phys. Rev., 175:1669, 1968.
- [ABC⁺75] J. Ahrens, H. Borchert, K.H. Czock, H.B. Eppler, H. Gimm, et al. *Total Nuclear Photon Absorption Cross Section For Some Light Elements*. Nucl. Phys. B, 251:479, 1975.
- [AEH⁺81] J. Arends, J. Eyink, H. Hartmann, B. Hegerath, B. Mecking, G. Nöldecke, and H. Rost. *Inclusive Charged Pion Photoproduction On ^{12}C Using Tagged Photons in the Energy Range 200-390 MeV*. Z. Physik A, 305:205, 1981.
- [AEH⁺82] J. Arends, J. Eyink, H. Hartmann, B. Hegerath, B. Mecking, G. Nöldecke, and H. Rost. *Experimental Investigation of the Reaction $^{12}\text{C}(\gamma, \pi^0)X$ in the Photon Energy Range Between Threshold and 450 MeV*. Z. Physik A, 311:367, 1982.
- [AGL⁺61] F. Ajzenberg-Selove, N.B. Gove, T. Lauritzen, C.L. Mc Ginnis, R. Nakasima, J. Scheer, and K. Way. *Energy Levels of Nuclei*. In A.M. Hellwege and K.H. Hellwege, editors, *Landolt-Börnstein*, volume I/1 of *New Series*. Springer-Verlag, Berlin, 1961.
- [Ahr85] J. Ahrens. *The Total Absorption of Photons by Nuclei*. Nucl. Phys. B, 446:229c, 1985.
- [AS65] M. Abramowitz and I.A. Stegun. *Handbook of Mathematical Functions*. Dover Publications, New York, 1965.
- [BCD⁺94] D. J. Bird, S. C. Corbato, H. Y. Dai, B. R. Dawson, J. W. Elbert, et al. *The Cosmic-Ray Energy Spectrum observed by the Fly's Eye*. ApJ, 424:491, 1994.
- [BCD⁺95] D. J. Bird, S. C. Corbato, H. Y. Dai, J. W. Elbert, K. D. Green, et al. *Detection of a cosmic ray with measured energy well beyond the expected spectral cutoff due to cosmic microwave radiation*. ApJ, 441:144, 1995.
- [BFMM73] A. Baldini, V. Flamino, W.G. Moorhead, and D.R.O. Morrison. *Total Cross-Sections for Reactions of High Energy Particles*. In H. Schopper, editor, *Landolt-Börnstein*, volume I/12b of *New Series*. Springer-Verlag, Berlin, 1973.
- [BG88] V.S. Berezinsky and S.I. Grigor'eva. *A Bump in the Ultra-High Energy Cosmic Ray Spectrum*. A&A, 199:1, 1988.
- [Bie93] P.L. Biermann. *Cosmic Rays I. The Cosmic Ray Spectrum between 10^4 GeV and 3×10^9 GeV*. A&A, 271:649, 1993.
- [BL50] H.A. Bethe and C. Longmire. *The Effective Range of Nuclear Forces: II. Photo-Disintegration of the Deuteron*. Phys. Rev., 77:647, 1950.
- [Blu70] R.G. Blumenthal. *Energy Loss of High-Energy Cosmic Rays in Pair-Producing Collisions with Ambient Photons*. Phys. Rev. D, 1:1596, 1970.
- [BM53] H.A. Bethe and L.C. Maximon. *Theory of Bremsstrahlung and Pair Production. I. Differential Cross Section*. Phys. Rev., 93:768, 1953.

- [BM73] B.H. Bransden and R.G. Moorhouse. *The Pion-Nucleon System*. Princeton University Press, Princeton, New Jersey, 1973.
- [BP35] H. Bethe and R. Peierls. *Quantum Theory of The Dipion*. Proc. Roy. Soc., A 148:146, 1935.
- [BS87] P. L. Biermann and P. A. Strittmatter. *Synchrotron Emission from Shock Waves in Active Galactic Nuclei*. ApJ, 322:643, 1987.
- [BSYP78] T.H. Bauer, R.D. Spital, D.R. Yennie, and F.M. Pipkin. *The Hadronic Properties of the Photon in High-Energy Interactions*. Rev. Mod. Phys., 50(2):261, 1978.
- [BW52] J.M. Blatt and V.F. Weisskopf. *Theoretical Nuclear Physics*. John Wiley & Sons, New York, 1952.
- [BW57] G.R. Bishop and R. Wilson. *The Nuclear Photoeffect*. In *Handbook of Physics*, volume XLII, page 309. Springer-Verlag, Berlin, 1957.
- [Cam67] Cambridge Bubble Chamber Group. *Production of the $N^*(1238)$ Nucleon Isobar by Photons of Energy up to 6 BeV*. Phys. Rev., 163:1510, 1967.
- [CI80] D.R. Cox and V. Isham. *Point Processes*. Chapman and Hall, London, 1980.
- [CO70] J. Cumming and H. Osborn, editors. *Hadronic Interactions of Electrons and Photons*, London, 1971, 1970. Academic Press.
- [CO79] D.C. Cheng and G.K. O'Neill. *Elementary Particle Physics*. Addison Wesley Publ. Company, Reading, Massachusetts, 1979.
- [Col59] J. Coltrane. *Giant Steps*. Atlantic Records 781337-2, 1959.
- [Cra46] H. Cramér. *Mathematical Methods of Statistics*. Princeton University Press, Princeton, New Jersey, 1946.
- [DBM53] H. Davies, H.A. Bethe, and L.C. Maximon. *Theory of Bremsstrahlung and Pair Production. II. Integral Cross Section for Pair Production*. Phys. Rev., 93:788, 1953.
- [DF65] M. Danos and E.G. Fuller. *Photonuclear Reactions*. Ann. Rev. Nucl. Sci., 15:29, 1965.
- [Dru83] L.O'C Drury. *An Introduction to the Theory of Diffusive Shock Acceleration of Energetic Particles in Tenuous Plasmas*. Rep. Prog. Phys., 46:973, 1983.
- [DS72] A.N. Diddens and K. Schlüpmann. *Properties and Production Spectra of Elementary Particles*. In H. Schopper, editor, *Landolt-Börnstein*, volume I/6 of *New Series*, page 53. Springer-Verlag, Berlin, 1972.
- [DW88] A. Donnachie and S. Webb. *Isoscalar diffractive photoproduction: A source of gluonium*. Z. Physik C, 40:111, 1988.
- [EGLS92] J. Engel, T.K. Gaisser, P. Lipari, and T. Stanev. *Nucleus-Nucleus Collisions and Interpretation of Cosmic Ray Cascades*. Phys. Rev. D, 46:5013, 1992.
- [Erw71] A.R. Erwin. *Inelasticity of Multipion Production from a Quark Model*. Phys. Lett. B, 36:489, 1971.
- [ES95] J.W. Elbert and P. Sommers. *In search of a source for the 320 EeV Fly's Eye cosmic ray*. ApJ, 441:151, 1995.
- [Eva55] R.D. Evans. *The Atomic Nucleus*. McGraw-Hill Book Company, New York, 1955.
- [FBMO81] D.D. Faul, B.L. Bermann, P. Meyer, and D.L. Olson. *Photodisintegration of ^3H and ^3He* . Phys. Rev. C, 24:849, 1981.
- [Fer49] E. Fermi. *On the Origin of the Cosmic Radiation*. Phys. Rev., 75:1169, 1949.
- [Fer51] E. Fermi. *Angular Distribution of Pions Produced in High Energy Nuclear Collisions*. Phys. Rev., 81:683, 1951.

- [Fey72] R.P. Feynman. *Photon-Hadron Interactions*. W.A. Benjamin, Inc., Reading, Massachusetts, 1972.
- [FH56] E.G. Fuller and E. Hayward. *Nuclear Elastic Scattering of Photons*. Phys. Rev., 101:692, 1956. also in [FH76].
- [FH76] E.G. Fuller and E.H. Hayward, editors. *Photonuclear Reactions*, Dowdon, Hutchinson & Ross, Stroudsburg, Pennsylvania, 1976.
- [Fis80] M. Fisz. *Wahrscheinlichkeitsrechnung und mathematische Statistik*. VEB Deutscher Verlag der Wissenschaften, Berlin, 1980. Transl. from Polish original, *Rachunek prawdopodobieństwa i statystyka matematyczna*, Warszawa, 1967.
- [Gai90] T.K. Gaisser. *Cosmic Rays and Particle Physics*. Cambridge University Press, Cambridge, UK, 1990.
- [Gre66] K. Greisen. *End to the Cosmic-Ray Spectrum?* Phys. Rev. Lett., 16:748, 1966.
- [GS58] A.N. Gorbunov and V.M. Spiridonov. *Photodisintegration of Helium*. Sovjet Phys. JETP, 33(6):16, 1958. Parts II&III: Vol. 34(7), 596&600.
- [GS64] V.L. Ginzburg and S.I. Syrovatskii. *The Origin of Cosmic Rays*. Pergamon Press, Oxford, UK, 1964.
- [GT48] M. Goldhaber and E. Teller. *On Nuclear Dipole Vibrations*. Phys. Rev., 74:1046, 1948. also in [FH76].
- [Hak83] H. Haken. *Synergetics*. Springer Verlag, Berlin, 3rd edition, 1983.
- [Hay69] S. Hayakawa. *Cosmic Ray Physics*. Wiley Interscience, New York, 1969.
- [HHH⁺94] N. Hayashida, K. Honda, M. Honda, S. Imaizumi, N. Inoue, et al. *Observation of a Very Energetic Cosmic Ray Well Beyond the Predicted 2.7 K Cutoff in the Primary Energy Spectrum*. Phys. Rev. Lett., 73:3491, 1994.
- [HS85] C.T. Hill and D.E. Schramm. *Ultrahigh-Energy Cosmic-Ray Spectrum*. Phys. Rev. D, 31:564, 1985.
- [Hüf85] J. Hüfner. *Heavy Fragments Produced in Proton-Nucleus and Nucleus-Nucleus Collisions at Relativistic Energies*. Phys. Rep., 125:129, 1985.
- [Itô51] K. Itô. *On Stochastic Differential Equations*. Mem. Am. Math. Soc., 4:1, 1951.
- [Jac75] J.D. Jackson. *Classical Electrodynamics*. John Wiley & Sons, Inc., New York, 1975.
- [JLS50] R. Jost, J.M. Luttinger, and M. Slotnik. *Distribution of Recoil Nucleons in Pair Production by Photons*. Phys. Rev., 80:189, 1950.
- [Jok87] J.R. Jokipii. *Rate of energy gain and maximum energy in diffusive shock acceleration*. ApJ, 313:842, 1987.
- [JR76] J.M. Jauch and F. Rohrlich. *The Theory of Electrons and Photons*. Springer-Verlag, New York, 2nd edition, 1976.
- [KA94] W.M. Krülls and A. Achterberg. *Computation Of Cosmic-Ray Acceleration by Ito's Stochastic Differential Equations*. A&A, 286:314, 1994.
- [Kan83] R.P. Kanwal. *Generalized Functions*. Academic Press, New York, 1983.
- [Krü92] W. M. Krülls. *Combined First- and Second-Order Fermi Acceleration in Radio Galaxy Hot Spots*. A&A, 260:49, 1992.
- [KRB96] H. Kang, J. P. Rachen, and P. L. Biermann. *Contributions to the Cosmic Ray Flux above the Ankle: Clusters of Galaxies*. MNRAS, 1996, in press.
- [KRJ96] H. Kang, D. Ryu, and T.W. Jones. *Cluster Accretion Shocks as Possible Acceleration Sites for Ultra-High-Energy Cosmic Rays below the Greisen Cutoff*. ApJ, 456:422, 1996.
- [LAQ89] R. Lieu, W.I. Axford, and J.J. Quenby. *Synchrotron Radiation treated by the Weizsäcker-Williams Method of Virtual Quanta*. A&A, 208:351, 1989.

- [LB50] J.S. Levinger and H.A. Bethe. *Dipole Transitions in the Nuclear Photo-Effect*. Phys. Rev., 78:115, 1950. also in [FH76].
- [LB52] J.S. Levinger and H.A. Bethe. *Neutron Yield from the Nuclear Photoeffect*. Phys. Rev., 85:577, 1952.
- [Lev51] J.S. Levinger. *The High Energy Nuclear Photoeffect*. Phys. Rev., 84:43, 1951. also in [FH76].
- [Lev60] J.S. Levinger. *Nuclear Photodisintegration*. Oxford University Press, London, 1960.
- [Lev79] J.S. Levinger. *Modified Quasi-Deuteron Model*. Phys. Lett. B, 82:181, 1979.
- [Lev93] A. Levy. *Photoproduction in Light of the First HERA Data*. J. Phys. G, 19:1489, 1993.
- [Man93] K. Mannheim. *The proton blazar*. A&A, 269:67–76, 1993.
- [Mar70] J.S. Maritz. *Empirical Bayesian Methods*. Methuen and Co LTD, London, 1970.
- [May92] T. Mayer-Kuckuk. *Kernphysik*. Teubner Studienbücher, Stuttgart, 1992.
- [MGT54] M. Gell-Mann, M.L. Goldberger, and W.E. Thirring. *Use of Causality Conditions in Quantum Theory*. Phys. Rev., 95:1612, 1954.
- [MKB91] K. Mannheim, W. M. Krüßls, and P. L. Biermann. *A Novel Mechanism For Nonthermal X-Ray Emission*. A&A, 251:723, 1991.
- [MKG53] R. Montalbetti, L. Katz, and J. Goldemberg. *Photoneutron Cross Sections*. Phys. Rev., 91:659, 1953.
- [NH53] R. Nathans and J. Halpern. *Excitation Function for the Photodisintegration of Beryllium*. Phys. Rev., 92:940, 1953.
- [ODR79] L.F. Oliveira, R. Donangelo, and J.O. Rasmussen. *Abrasion-Ablation Calculations of Large Fragment Yields from Relativistic Heavy Nuclei Ion Reactions*. Phys. Rev. C, 19:826, 1979.
- [Oka58] K. Okamoto. *Intrinsic Quadrupole Moment and the Resonance Width of Photonuclear Reactions*. Phys. Rev., 110:143, 1958.
- [Par94] Particle Data Group. *Review of Particle Properties*. Phys. Rev. D, 50(3), 1994.
- [PBK⁺96] D. Petry, S.M. Bradbury, A. Konopelko, J. Fernandez, F. Aharonian, et al. *Detection of VHE γ -Rays from Mkn 421 with the HEGRA Cherenkov Telescopes*. A&A, submitted, 1996. Eprint: astro-ph/9606159.
- [Per82] D.H Perkins. *Introduction to High Energy Physics*. Benjamin/Cummings Publ. Company, Inc., Menlo Park, California, 2nd edition, 1982.
- [PK83] R. J. Protheroe and D. Kazanas. *On The Origin Of Relativistic Particles And Gamma-Rays In Quasars*. ApJ, 265:620, 1983.
- [Pop94] K. Popper. *Logik der Forschung*. Mohr, 10th edition, 1994.
- [Pre96] W.H. Press. *Understanding Data Better with Bayesian and Global Statistics Methods*. In J.P. Ostriker, editor, *Unsolved Problems in Astrophysics*, Princeton, NJ, 1996. Princeton University Press. E-print: astro-ph/9604126.
- [PSB76] J. L. Puget, F. W. Stecker, and J. H. Bredekamp. *Photonuclear Interactions of Ultrahigh Energy Cosmic Rays and Their Astrophysical Consequences*. ApJ, 205:638, 1976.
- [Rac92] J.P. Rachen. *Der Beitrag von Hot-Spots in FR-II Radiogalaxien zur Ultrahochenergetischen Komponente der Kosmischen Strahlung*. Master's thesis, Universität Bonn, 1992.
- [RB93] J. P. Rachen and P. L. Biermann. *Extragalactic ultra-high energy cosmic rays. I. Contribution from hot spots in FR-II radio galaxies*. A&A, 272:161, 1993.
- [RL79] G.B. Rybicki and A.P. Lightman. *Radiative Processes in Astrophysics*. John Wiley & Sons, New York, 1979.

- [SBG93] T. Stanev, P.L. Biermann, and T.K. Gaisser. *Cosmic Rays. IV: The chemical composition above 10^4 GeV.* A&A, 274:902, 1993.
- [SJ50] H. Steinwedel and J.H.D. Jensen. *Hydrodynamik von Kerndipol-schwingungen.* Z. Naturforsch., 5a:413, 1950. engl. transl. in [FH76].
- [Sny75] D.L. Snyder. *Random Point Processes.* John-Wiley & Sons, New York, 1975.
- [Sok89] P. Sokolsky. *Introduction to Ultrahigh Energy Cosmic Ray Physics*, volume 76 of *Frontiers in Physics.* Addison-Wesley Publishing Comp., Redwood City, CA, 1989.
- [SSB94] G. Sigl, D.N. Schramm, and P. Bhattacharjee. *On the Origin of Highest Energy Cosmic Rays.* Astropart. Phys., 2:401, 1994.
- [Ste68] F.W. Stecker. *Effect of Photomeson Production by the Universal Radiation Field on High-Energy Cosmic Rays.* Phys. Rev. Lett., 21:1016, 1968.
- [TDP89] M.L. Terranova, D.A. De Lima, and J.D. Pinheiro Filho. *Evaluation of Total Nuclear Photoabsorption Cross-Sections by the Modified Quasi-Deuteron Model.* Europhys. Lett., page 523, 1989.
- [TT92] O.A.P. Tavares and M.L. Terranova. *Nuclear Photoabsorption by Quasi-Deuterons and An Updated Evaluation of Levinger's Constant.* J. Phys. G, page 521, 1992.
- [VG94] V.A. Vartanyan and S.R. Gevorkan. *The Cross Section of Pion-Free Photoabsorption by Nuclei in the Resonance Energy Region.* Phys. Atomic Nuclei (Yad. Fiz.), 57:1330, 1994.
- [Wan69] C.P. Wang. *Regularity of Multiplicity Distribution in NN and πN Collisions and the Structure of the Nucleon.* Phys. Rev., 180:1463, 1969.
- [Wei72] S. Weinberg. *Gravitation and Cosmology.* John Wiley & Sons, Inc., New York, 1972.
- [Wei74] W. Weise. *Hadronic Aspects of Photon-Nucleus Interactions.* Phys. Rep., 13:53, 1974.
- [YHH⁺95] S. Yoshida, N. Hayashida, K. Honda, M. Honda, S. Imaizumi, et al. *The Cosmic-Ray Energy Spectrum above 3×10^{18} eV measured by the Akeno Giant Air Shower Array.* Astropart. Phys., 3:105, 1995.
- [ZK66] G.T. Zatsepin and V.A. Kuzmin. *Upper Limit of the Spectrum of Cosmic Rays.* JETP Lett., 4:78, 1966.

Danksagung

Diese Arbeit wurde zum größten Teil am Max-Planck-Institut für Radioastronomie (MPIfR) in Bonn, und in der Zeit von Februar bis September 1994 auch am Bartol Research Institute (BRI) in Newark, Delaware, U.S.A., angefertigt. Mein besonderer Dank gilt dabei meinen Betreuern, Prof. Dr. P.L. Biermann am MPIfR, sowie Prof. Dr. T. Stanev und Prof. Dr. T.K. Gaisser am BRI, für ihren Rat, ihr Interesse und Ihre Unterstützung in allen Belangen meiner Dissertation und darüber hinaus. Prof. Dr. H.-J. Fahr danke ich für die Durchsicht und die Begutachtung dieser Arbeit, Dipl.-Phys. T. Enßlin für das sorgfältige Korrekturlesen des Manuskripts.

Meine Dissertation wurde unterstützt durch das Max-Planck-Institut für Radioastronomie aus Mitteln des Bundesministeriums für Forschung; mein besonderer Dank gilt hier unserem Direktor, Prof. Dr. G. Weigelt, auch für die großzügige Gewährung von Reisemitteln. Meine Arbeit am Bartol-Research-Institute wurde gefördert durch ein HSP-II Doktorandenstipendium des Deutschen Akademischen Austauschdienstes. Hier sei Prof. Dr. H. Meyer (Uni-GHS Wuppertal) gedankt für sein Referenzschreiben, das diese Förderung ermöglichte. Obwohl letztlich erfolglos, möchte ich auch Prof. Dr. J. Speth (ITKP Bonn und KFA Jülich) für seine Unterstützung bei meinem Antrag auf Graduiertenförderung danken.

Bevor ich den vielen Personen danke, die durch interessante wissenschaftliche Diskussionen diese Arbeit beeinflusst haben, möchte ich an dieser Stelle ganz besonders Dr. Karl Mannheim (Uni Göttingen, ehem. MPIfR) herausheben, der meine Arbeit nicht nur wissenschaftlich, sondern auch darüber hinaus durch seinen freundschaftlichen Rat und seine Unterstützung begleitet hat. Prof. Dr. P. David (ISKP Bonn) danke ich für die einführenden Diskussionen zur photonuklearen Physik, Dr. Klaus Desch (PI Bonn) für interessante Diskussionen über die vergangene, gegenwärtige und zukünftige Elementarteilchenphysik. Dr. Kai Otterbein sei gedankt für seine Hilfe bei meinem "Nebenjob", der Analyse von ROSAT-Daten. Weiterhin seien genannt: Prof. Dr. A.A. Watson (Leeds), Dr. E. Zas (Santiago), Dr. G. Zank (BRI), Dr. P. Sommers (Fly's Eye), Dr. M. Teshima (ICRR Tokyo), Dr. Chr. Spiering und Dr. A. Karle (DESY Zeuthen).

Natürlich darf auch das Umfeld nicht vergessen werden, in dem diese Arbeit entstanden ist. Hier danke ich zuerst allen meinen ehemaligen und gegenwärtigen Gruppenkollegen, Reinhold Schaaf, Wolfram Krülls, Heino Falcke, Martina Niemeyer, Henning Seemann, Torsten Enßlin, Alina und Fanel Donea, sowie Christian Zier. Für das freundschaftliche Klima während meines Aufenthalts am BRI möchte ich außer meinem Betreuer, Todor Stanev, noch Stuart Pittel und Hristofer Vankov danken. Aber auch der technische Teil sei erwähnt: Ich danke allen Mitarbeitern der Rechnerabteilungen am MPIfR und am BRI für ihre Hilfe und Unterstützung, ganz besonders Peter Müller (MPIfR), Perry Gray (BRI), und nicht zuletzt H.G. Girnstein und Ingo Kruhm für ihren schnellen Beistand in den schweren Tagen nach dem plötzlichen Verscheiden meiner getreuen Workstation, der *dec14*, im Januar diesen Jahres.

Nicht zuletzt aber gilt mein Dank meiner Familie; meinem Vater, der mir das Studium ermöglichte, meiner Mutter und meinem Bruder, natürlich meiner Großmutter, die mich immer nach Kräften unterstützte; ganz besonders aber meiner Frau Sabine, die mich über den größten Teil dieser Arbeit begleitete, über die lange Zeit der Trennung und die vielen durchgearbeiteten Wochenenden stets zu mir gehalten hat und mir Antrieb und Motivation war, dieses Werk endlich zu einem Ende zu bringen.

Curriculum vitae

Zur Person

Name: Jörg Paul Rachen
Geburtsdatum: 9. März 1964
Geburtsort: Aldenhoven (bei Jülich, NRW)
Eltern: Rolf Rachen, Dipl.-Mathematiker, und Ingrid Rachen, geb. Baas, Hausfrau.
Geschwister: Marc Rachen, 27 Jahre, Student der Biologie
Familienstand: verheiratet seit dem 3. März 1995
mit Sabine Rachen, geb. Löschmann, Diplom-Übersetzerin
Kinder: keine

Bildungsweg

1970 – 1971 Grundschule Aldenhoven
1971 – 1974 Grundschule Wuppertal-Cronenberg
1974 – 1983 Gymnasium Bayreuther Str., Wuppertal-Elberfeld
Juni 1983 Abitur. Prüfungsfächer: Mathematik, Chemie, Philosophie, Deutsch
1983 – 1986 Grundstudium Physik an der Uni-GHS Wuppertal
April 1986 Vordiplom an der Uni-GHS Wuppertal
1986 – 1989 Hauptstudium Physik / Astronomie an der Universität Bonn
1990 – 1992 Diplomarbeit bei Prof. Biermann am MPIfR Bonn
Thema: *Der Beitrag von Hot Spots in FR-II Radiogalaxien zur ultrahochenergetischen Komponente der kosmischen Strahlung*
März 1992 Physik-Diplom an der Universität Bonn
1992 – 1996 Promotionsstudium in Astronomie / Philosophie an der Universität Bonn
Dissertation bei Prof. Biermann am MPIfR Bonn
September 1996 Abschlußprüfungen der Promotion an der Universität Bonn

Auslandsaufenthalt

1994 8 Monate am Bartol Research Institute, University of Delaware, U.S.A.
Arbeit im Rahmen der Dissertation mit Prof. Stanev und Prof. Gaisser

Weitere wissenschaftliche Tätigkeit

1993 – 1994 Datenauswertung für das ROSAT Beobachtungsprojekt
“Weiche Röntgenstrahlung von Quasaren” (Prof. Biermann / Dr. Mannheim)

Bonn, den 22. August 1996

gez. Jörg Rachen